Proteomic Analysis Identifies Translationally Controlled Tumor Protein as a Potential Novel Mediator of Occlusive Vascular Remodeling in Pulmonary Arterial Hypertension

Jessie Lavoie

Thesis submitted to the

Faculty of Graduate and Postdoctoral Studies

in partial fulfillment of the requirements

for a doctoral degree in Cellular and Molecular Medicine

Department of Cellular and Molecular Medicine

Faculty of Medicine

University of Ottawa

ABSTRACT

Pulmonary arterial hypertension (PAH) is a lethal disease characterized by excessive proliferation of pulmonary vascular cells, such as endothelial cells (ECs). Hereditary (H) PAH is mainly caused by “loss-of-function” mutations in the gene coding for the bone morphogenetic protein type II receptor (*BMPR2*). However, the mechanisms by which these mutations cause PAH remain unclear. The hypothesis of this thesis was that *BMPR2* mutations produce an imbalance in EC protein expression and/or activity that is integrally related to the development of abnormalities in lung vascular function and structure in HPAH. Patient-specific blood-outgrowth endothelial cells (BOECs) expanded *ex vivo* from peripheral blood mononuclear cells from patients with HPAH and healthy subjects were used to examine the consequences of *BMPR2* mutations on the BOEC protein expression profile as well as on their functionality. Functional analyses of the BOECs revealed that HPAH-derived BOECs are more susceptible to apoptosis and more proliferative compared with healthy controls. Protein isolates of BOECs from patients with HPAH and from healthy subjects were subjected to 2-D gel electrophoresis and stained for total proteins and phosphoproteins, and to a quantitative computer-assisted analysis. Differentially regulated proteins were identified by mass spectrometry (LC-MS/MS). Of the 416 total proteins detected under basal conditions, 11 were significantly downregulated in HPAH-derived BOECs and 11, including the translationally controlled tumor protein (TCTP), were upregulated. TCTP has previously been shown to be involved in systemic arteriolar remodeling, inflammation and growth. Therefore, the potential role of TCTP in PAH was studied *in vivo* in the SU5416 rat model of severe angioproliferative PAH. Immunofluorescence staining revealed high expression of TCTP in arteriolar ECs of PAH lungs tightly localized to proliferating cells within occlusive intimal lesions; whereas, only minimal TCTP expression was seen in vascular ECs of

normal lungs. Similarly, abundant TCTP immunostaining was also seen in human PAH lung sections, again associated with complex vascular lesions. In BOECs, TCTP was found to participate in cell growth and survival. These data suggest that TCTP could play an important role in PAH by mediating pro-survival and growth signaling in vascular cells, contributing to occlusive pulmonary vascular remodeling triggered by EC apoptosis.

TABLE OF CONTENTS

LIST OF TABLES

LIST OF FIGURES

LIST OF ILLUSTRATIONS

LIST OF APPENDICES

LIST OF ABBREVIATIONS

2D-PAGE	two dimensional polyacrylamide gel electrophoresis
5'-UTR	5'-untranslated region
6MWD	six minute walk distance
Alk1	activin receptor-like kinase 1
AMHR-II	anti-Müllerian hormone type II
ANOVA	analysis of variance
APAH	associated pulmonary arterial hypertension
BAMBI	BMP and activin membrane-bound inhibitor
BMP	bone morphogenetic protein
BMPR2	bone morphogenetic protein receptor type II
BOEC	blood outgrowth endothelial cell
Brdu	bromodeoxyuridine
CHAPS	3-((3-Cholamidopropyl)dimethylammonium)-1-propanesulfonate
cAMP	adenosine 3',5'-cyclic monophosphate
cGMP	cyclic guanosine monophosphate
EBM	endothelial basal media
EC	endothelial cell
ECM	extracellular matrix
EDTA	ethylenediaminetetraacetic acid
eEF-1	eukaryotic elongation factor-1
ENG	endoglin
EGM-2MV	endothelial growth media 2 microvascular
ELISA	enzyme-linked immunosorbent assay
eNOS	endothelial nitric oxide synthase
ERK1/2	extracellular signal-regulated protein kinases 1 and 2

E-selectin	endothelial selectin
ESI	electrospray ionization
FDA	food and drug administration
GAPDH	glyceraldehyde 3-phosphate dehydrogenase
GFP	green fluorescent protein
HIV	human Immunodeficiency Virus
HPAH	hereditable Pulmonary Arterial Hypertension
HHT	hereditary hemorrhagic telangiectasia
HUVECs	human umbilical vein endothelial cells
IEF	isoelectric focusing
IgE	immunoglobulin E
IPAH	idiopathic Pulmonary Arterial Hypertension
jetPEI	commercial polyethylenimine
kb	kilo-base pair
kDa	kilodalton
LOESS	bivariate local polynomial regression
LTQ	linear Trap Quadrupole
MALDI-TOF	matrix-assisted laser desorption/ionization-time of flight
Mcl-1	myeloid leukemia cell differentiation protein
MCT	monocrotaline
mRNP	messenger ribonucleoprotein
MS	mass spectrometry
NO	nitric oxide
PAH	pulmonary Arterial Hypertension
PAP	pulmonary arterial pressure
PAEC	pulmonary artery endothelial cells

PASMC	pulmonary artery smooth muscle cells
PBS	phosphate-buffered saline
PCNA	proliferating cell nuclear antigen
PE	phycoerythrin
PECAM-1	platelet endothelial cell adhesion molecule-1 (CD31)
PFA	paraformaldehyde
PI	propidium iodide
pRS-X	plasmid containing gene “X” under the control of Rous Sarcoma virus promotor
PVDF	polyvinylidene difluoride
PVR	pulmonary vascular resistance
R-SMAD	receptor-regulated Smads
RV	right ventricle
RV/(LV+S)	weight ratio of right ventricle to left ventricle plus septum
RVSP	right ventricular systolic pressure
RIPA	radioimmunoprecipitation assay
SD	standard deviation
SDS	sodium dodecyl sulfate
SDS-PAGE	sodium dodecyl sulfate polyacrylamide gel electrophoresis
SEM	standard error of the mean
sh	short hairpin
siRNA	small interfering ribonucleotide acid
SMA	smooth muscle actin
Smad	mothers against decapentaplegic
Smurf	smad ubiquitination and regulatory factors
SU5416	3-(3,5-dimethyl-1H-pyrrol-2-ylmethylene)-1,3-dihydroindol-2-one

TCTP	translationally controlled tumor protein
TGF	tumor growth factor
TNF-α	tumor necrosis factor-α
TSAP6	tumor suppressor activated pathway-6
VEGF	vascular endothelial growth factor
VEGFR2	vascular endothelial growth factor receptor - 2
vWF	von Willebrand factor
µA	microampere
Vh	volt hour
WHO	world health organization

LIST OF ORIGINAL PUBLICATIONS

During my PhD studies, I contributed to different collaborations with scientists from my Institute, from the University of Ottawa Heart Institute, from the "Centre National de la Recherche Scientifique" of the University of Nantes, in France, and from the University of Cambridge, in the United Kingdom, that led to the following published and submitted articles, as well as original abstracts. The publications presented in sections A and B are found in Chapter 6.

A. Articles published and accepted in refereed journals

1. Chang, W.Y., **Lavoie, J.R.**, Kwon, S.T., Chen, Z., Manias, J.L., Behbahani, J., Ling, V., Kandel, R.A., Stewart, D.J., and Stanford, W.L. (2012) Feeder-independent derivation of induced-pluripotent stem cells from peripheral blood endothelial progenitor cells. Stem Cell Res. 10(2)195-202.

2. **Lavoie, J.R**., Stewart, D.J. (2012) Genetically modified endothelial progenitor cells in the therapy of cardiovascular disease and pulmonary hypertension. Curr Vasc Pharmacol. 10(3): 289-299.

3. Guevel, L., **Lavoie, J.R.***, Perez-Iratxeta, C.*, Rouger, K., Dubreil, L., Feron, M., Talon, S., Brand, M., and Megeney. L,A. (2011) Quantitative proteomic analysis of dystrophic dog muscle. J Proteome Res. 10(5): 2465-2478. *authors contributted equally

4. Ward, M.R., **Lavoie, J.**, and Stewart, D.J. (2008)"B2 or not B2?": Kinin receptors and endothelial progenitor cell dysfunction. Journal of Circulation Research. 103(11):1202-1203.

B. Articles submitted to refereed journals

1. Hibbert, B., **Lavoie, J.R.**, Ma, X., Seibert, T., Raizman, J., Simard, T., Chen, Y.-X., Stewart D.J., and O'Brien, E.R. Glycogen Synthase Kinase-3β Inhibition Augments Diabetic Endothelial Progenitor Cell Abundance and Functionality via Cathepsin B: Novel Therapeutic Opportunity for Arterial Repair. Submitted to Circulation Research (CIRCRES/2013/301388).

C. Other refereed contributions: Published meeting abstracts

1. **Lavoie, J.R.**; Ormiston, M., Perez-Iratxeta, C., Courtman D.W., Morrell, N.W., and Stewart, D.J. (2012) Paradoxical increase in BMP kinome activity in blood-derived endothelial cells from patients with hereditary pulmonary arterial hypertension Am. J. Respir. Crit. Care Med. 185: A6518

2. **Lavoie, J.R.**; Ormiston, M., Perez-Iratxeta, C., Jiang, B., Courtman D.W., Morrell, N.W., and Stewart, D.J. (2012) Translationally Controlled Tumor Protein (TCTP) Revealed by Proteomic Analysis of Patient-Specific Blood outgrowth Endothelial Cells in Heritable Pulmonary Arterial Hypertension. Canadian Journal of Cardiology Vol. 28, Issue 5, Supplement, Page S284.

3. **Lavoie, J.**; Ormiston, M., Courtman D.W., Morrell, N.W., and Stewart, D.J. (2011) Paradoxical increase in background phosphorylation of bmp-responsive proteins in blood-derived endothelial cells from bmpr2 mutation carriers with hereditary pulmonary arterial hypertension. Circulation Journal. 124: A13520.

CONTRIBUTIONS OF COLLABORATORS

I would like to acknowledge the following contributions from collaborators who participated in the work presented in Chapters 2-5.

From the University of Ottawa Department of Regenerative Medicine, at the Ottawa Hospital Research Institute in Ottawa, Canada:

i) Dr. Duncan J. Stewart: Supervised the project and contributed to revisions.

i) Dr. Carol Perez-Iratxeta: Conducted the statistical analyses of the 2-D proteomic study (Figures 6 and 8).

ii) Dr. Baohua Jiang: Provided the RSVP and RVH data and paraffin-embedded lung tissue sections of the SU5416 rat model of PAH (Figures 18, 22 and Appendix N).

iii) Dr. David W. Courtman: Provided technical guidance.

From the University of Cambridge Department of Medicine, at the Addenbrooke's Hospital in Cambridge, United Kingdom:

i) Dr. Nicholas W. Morrell: Provided technical guidance.

ii) Dr. Mark Ormiston: Generated the blood-outgrowth endothelial cells, performed the stainings for TCTP in the human lung tissues and performed the Id1 Western blot in PAECs (Figures 16, 17 and Appendices A, D and E).

iii) Dr. Elisabet Ferrer: Provided the exosome samples and executed the CD81 Western blot with the exosomes and microparticles (Appendix I, panel A).

ACKNOWLEGMENTS

This study was carried out at the Ottawa Hospital Research Institute (Ontario), in collaboration with the University of Cambridge, at the Addenbrooke's Hospital in Cambridge, United Kingdom. I would like to thank the Fonds de la recherche en santé du Québec (FRSQ) and the University of Ottawa for their financial support. I wish to thank my supervisor, Dr. Duncan J. Stewart, for giving me the opportunity to work on a very challenging project in collaboration with the Morrell group. It was very motivating to design and build the project from the beginning and to share its progress with the collaborators and at conferences. Dr. Stewart's enthousiasm for the use of proteomics to discover new targets in PAH as well as his scientific and clinical insights have been great elements of motivation. I also want to thank Dr. Stewart for having included me in other collaborative work with the Stanford and O'Brien groups, which made my research life more fascinating and enriching.

Special thanks to Drs. Nicholas W. Morrell and Mark Ormiston as well as Drs. Carol Perez-Iratxeta and Elisabet Ferrer for their generous intellectual contributions to the project and for their continuous support. Thanks to my committee members, Drs. Marjorie Brand, Lynn Megeney, Erik Suuronen and Rhian Touyz for their constructive criticism, valuable comments and continuous support. A special thank to Dr. Baohua Jiang, who has generously shared her work with me and provided technical help in the *in vivo* pilot trial to help bring forward this project to a very exciting level. Thank you to Dr. Lawrence Puente, a talented expert in mass spectrometry, for always being enthousiastic towards analyzing my never ending supply of samples. I wish to thank Dr. Laetitia Guével, for giving me the opportunity to collaborate with her and for inviting me to her laboratory to further advance my knowledge in proteomics. Thank you

to Katy Morin, Lacrimioara Comanita, Helen Muleme and Dr. Caryn Ito for their fruitful scientific and personnal discussions that were elements of great motivation. Thank you to Katy Morin for her enthousiasm for proteomics, experimental insight and technical help. Stella Yuen, thank you for your emotional support and for your many words of encouragements. Thank you to those individuals who have provided technical assistance with this work in the *in vivo* pilot trial: Dr. Baohua Jiang, Yupu Deng, Anli Yang and Xiaoxue Wen, who helped perform the shRNA plasmid injections, and Jack Zhang, who prepared the DNA. I wish to thank Mohamad Taha, who generously shared with me his protocols and was always there to provide his help. I have to thank two summer students who contributed to this work: Jennifer Klowak, who helped optimise the BrdU and REC transfection assays, and Annette Ye, who also helped with the REC transfection assay. I would also like to thank Lisa Souliere, Adrienne Szalamin and Melanie Genereaux for supporting me with their incredible administrative skills.

Tremendous thanks to my spouse François Blouin, who has been instrumental to my scientific success by being a wonderful "agent" during the course of my studies and until the end by revising this thesis. Special thanks to my friend Mélanie Martin, who I consider family, for the continuous emotional support, all the many words of encouragements and for celebrating with me even the most miniscule of accomplishments. A special thank to my family, who has been very supportive and encouraging every step of the way by celebrating with me my personal milestones and by giving me the energy and confidence to keep going. I feel very privileged to have had the emotional and scientific support for all these people during the course of my studies, which have enriched my graduate studies. Merci à vous tous.

CHAPTER 1: INTRODUCTION

1.1 Pulmonary Arterial Hypertension (PAH)

1.1.1 General Overview

Pulmonary arterial hypertension (PAH) is a devastating, progressive disease with poor prognostic (Galie et al., 2009b). Characteristic pathophysiologic features of PAH include sustained elevation of pulmonary arterial pressure (mean pulmonary arterial pressure >25 mm Hg), as assessed by right heart catheterization, and increased pulmonary vascular resistance (D'Alonzo et al., 1991; Gaine and Rubin, 1998). Early symptoms of PAH are fatigue, dyspnea, weakness and syncope (Gaine, 2000). Histologically, the disorder is characterized by pathological changes in pre-capillary pulmonary arteries, where endothelial and smooth muscle cells proliferate, leading to vascular remodeling and narrowing of the blood vessels (Tuder et al., 2007). As the pulmonary arterial pressure increases, the right ventricular afterload increases, which progressively leads to right ventricular dysfunction (Gaine and Rubin, 1998). When therapy is not effective, patients succumb to right-sided heart failure within three years from onset of symptoms in adults and within one year in children (D'Alonzo et al., 1991; Gaine and Rubin, 1998; Widlitz and Barst, 2003).

1.1.2 Clinical Classification of Pulmonary Hypertension (PH)

This classification for pulmonary hypertension (PH) has evolved since it was first introduced in 1973, at the first international conference on primary PH in Geneva, Switzerland (Simonneau et al., 2004), and updates were made based on the Second and Third World Symposia on PH in Evian, France, in 1998 and Venice, Italy, in 2004 (Simonneau et al., 2004), and the Fourth World Symposium on PH in Dana Point, California, United States, in 2008 (Simonneau et al., 2009). More recent guidelines for the diagnosis and treatment of PH arose from a joint task force of the European Society

of Cardiology and of the European Respiratory Society (Galie et al., 2009b, c), which are derived from the proceedings of Dana Point (Simonneau et al., 2009). These guidelines provide an updated clinical classification of PH, in which five main clinical groups of PH are described: group 1) pulmonary arterial hypertension (PAH); group 1') pulmonary veno-occlusive disease and/or pulmonary capillary haemangiomatosis; group 2) PH due to left heart disease; group 3) PH due to lung diseases and/or hypoxia; group 4) chronic thromboembolic PH; and group 5) PH with unclear and/or multifactorial mechanisms (Galie et al., 2009b). Table 1 gives an overview of the above-mentioned five main clinical groups of PH and their sub-categories. This thesis focuses on group 1, subcategory 1.2 (heritable PAH).

1.1.3 Epidemiological Profile of PAH

Previous data from the USA National Institutes of Health (NIH) registry (period 1981-1987) showed that the annual incidence of primary PH (now termed IPAH) was 1-2 cases per million population (Rich et al., 1987). A total of 187 patients with primary PH or IPAH were entered in the registry with a mean age of 36 years and a female-to-male ratio of 1.7:1 (Rich et al., 1987). Recent epidemiology studies from specialist centres of PAH management, such as the Scottish Pulmonary Vascular Unit (SPUV) and the French National Registry, were conducted and based on very similar diagnostic criteria than the NIH registry. The prevalence of PAH, including IPAH, connective tissue disease-associated PH and congenital heart disease-associated PH, was 15 and 26 cases per million adult population, based on the French National Registry (period 2002-2003) and the SPVU database (period 1997–2005), respectively (Peacock et al., 2007). The incidence was 2.4 and 7.6 annual cases per million population for the French registry and the SPVU database, respectively (Humbert et al., 2006; Peacock et al., 2007). Regarding the French registry, the female-to-male sex ratio was documented at

1.9 and the mean (± SD) age of patients registered was 50 ± 15 years (Humbert et al., 2006).

Table 1. Updated clinical classification of pulmonary hypertension

1 PAH

- 1.1 Idiopathic (IPAH)
- 1.2 Heritable
  - 1.2.1 BMPR2
  - 1.2.2 ALK-1, endoglin (with or without hereditary haemorrhagic telangiectasia)
  - 1.2.3 Unknown
- 1.3 Drugs and toxins induced
- 1.4 Associated with (APAH)
  - 1.4.1 Connective tissue diseases
  - 1.4.2 HIV infection (HIV)
  - 1.4.3 Portal hypertension
  - 1.4.4 Congenital heart disease
  - 1.4.5 Schistosomiasis
  - 1.4.6 Chronic haemolytic anaemia
- 1.5 Persistent pulmonary hypertension of the newborn

1' Pulmonary veno-occlusive disease and/or pulmonary capillary haemangiomatosis

2 Pulmonary hypertension due to left heart disease

- 2.1 Systolic dysfunction
- 2.2 Diastolic dysfunction
- 2.3 Valvular disease

3 Pulmonary hypertension due to lung diseases and/or hypoxia

- 3.1 Chronic obstructive pulmonary disease
- 3.2 Interstitial lung disease
- 3.3 Other pulmonary diseases with mixed restrictive and obstructive pattern
- 3.4 Sleep-disordered breathing
- 3.5 Alveolar hypoventilation disorders
- 3.6 Chronic exposure to high altitude
- 3.7 Developmental abnormalities

4 Chronic thromboembolic pulmonary hypertension

5 PH with unclear and/or multifactorial mechanisms

- 5.1 Haematological disorders: myeloproliferative disorders, splenectomy
- 5.2 Systemic disorders: sarcoidosis, pulmonary Langerhans cell histiocytosis, lymphangioleiomyomatosis, neurofibromatosis, vasculitis
- 5.3 Metabolic disorders: glycogen storage disease, Gaucher disease, thyroid disorders
- 5.4 Others: tumoural obstruction, fibrosing mediastinitis, chronic renal failure on dialysis

---

Adapted from Galie et al. ERJ 2009

1.1.4 Current PAH Therapies: Targeting Vascular Cell Dysfunction

Conventional PAH therapy included anticoagulants, calcium channel blockers, digoxin and/or supplemental oxygen, which addressed solely the restoration of the imbalance in vasodilator and vasoconstrictor agents (Galie et al., 2002). Since the mid-1990s, advances in understanding the pathobiology of PAH have led to therapies that target multiple mechanistic pathways: prostacyclin, endothelin and nitric oxide. The current PAH therapies are thereby not directed only at restoring the imbalance in pulmonary vasoconstriction/vasodilatation (e.g. endothelin, nitric oxide), but also at reversing or diminishing endothelial cell dysfunction, vascular endothelial and smooth muscle cell proliferation (Boutet et al., 2008). Current approved treatment options include prostanoids, endothelin-receptor antagonists and phosphodiesterase type-5 inhibitors (Galie et al., 2009d).

1.1.4.1 Prostacyclin: Decreased Levels in PAH

Prostacyclin, the principal arachidonic acid metabolite of vascular endothelial and smooth muscle cells, is an important mediator in endothelial homeostasis (Chen and Oparil, 2000; Humbert et al., 2004a). It causes vasodilatation, inhibits platelet aggregation and has anti-proliferative activities (Christman, 1998). A decrease in urinary excretion of the 2.3-*dino*-6-keto prostacyclin $F_{1\alpha}$ ($PGF_{1\alpha}$), a metabolite of prostacyclin, in PAH patients has been documented by Christman et al. (Christman, 1998). Tuder et al. showed by immunohistochemistry studies that PAH patients present a reduction in the number of pulmonary arteries positive for prostaglandin I_2 synthase (PGI2-S) expression and a lack of PGI2-S expression in concentric and plexiform lesions (Tuder et al., 1999). Prostacyclin analogues (epoprostenol, epoprostenol-AM and iloprost) and derivatives (trepostinil) have been tested in clinical trials for patients with PAH (Frumkin, 2012; Ventetuolo and Klinger, 2012). The results published in 1996 from a multi-center

randomized trial with 81 patients suffering from severe IPAH indicated that epoprostenol therapy led to significant improvements in exercise capacity, hemodynamics, quality of life, and survival (Barst et al., 1996). The phase III study that led to the approval of tretrostinil for PAH included 470 patients and resulted in significant improvements in Borg Dysnea Scores, quality of life and hemodynamics (Simonneau et al., 2002). Six different options of prostacyclin therapy for the World Health Organisation (WHO) Group 1 PAH are now approved in the United States and Europe (Ventetuolo and Klinger, 2012).

1.1.4.2 Endothelin-1: Increased Levels in PAH

Endothelin-1 is an endothelial cell-derived polypeptide with an important role in vascular smooth muscle cell contraction (Chen and Oparil, 2000). Endothelin-1 binds to two receptors: endothelial receptor type A (ET-A), which mediates vasoconstriction and has mitogenic activity on vascular smooth muscle cells, and type B (ET-B), which induces endothelial NO synthase and acts to clear endothelin from the circulation (Humbert et al., 2004b; Michel et al., 2003). Our group was the first to demonstrate that patients with PH have increased levels of circulating endothelin-1 (Stewart et al., 1991) and increased expression in pulmonary arteries with medial thickening and intimal fibrosis (Giaid et al., 1993). Bosentan, a dual-endothelin (ET-1A/B) receptor antagonist, was the first endothelin antagonist receptor (ERA) approved by the United States Food and Drug Administration to improve exercise ability and decrease the rate of clinical worsening in patients with PAH in WHO functional classes (Frumkin, 2012). Ambrisentan is an oral selective ET-A-receptor antagonist that has been approved in the United States in 2007 (Jeffery and Morrell, 2002). A recent review published by Liu et al. included 11 randomized trials of 1457 PAH patients treated with ERA. The authors found that patients treated with ERA had an average in improvements in 6 minute walk (6MWD)

distance of 33.7 meters, improvements in functional class and a trend towards reduced mortality (Liu et al., 2009).

1.1.4.3 Phosphodiesterase-type 5 and Nitric Oxide Levels in PAH

Phosphodiesterase-type 5 (PDE-5) is the major enzyme responsible for cyclic guanosine monophosphate (cGMP) metabolism in the lung (Thomas et al., 1990). Increased activity in PDE-5 has been shown to be upregulated in pulmonary vascular disease such as PAH (Maclean et al., 1997; Murray et al., 2007). PDE-5 inhibitors therefore facilitate vasodilatation by inhibiting degradation of cGMP, thereby promoting the activity of the nitric oxide (NO) pathway (Tsai and Kass, 2009). NO is an endothelium-derived relaxing factor which modulates pulmonary and systemic vascular tone by activating soluble guanylate cyclase (sGC) to increase intracellular cGMP levels (Tsai and Kass, 2009). A reduction in pulmonary vascular NO synthesis has been documented in patients with PAH (Giaid and Saleh, 1995), although this finding remains controversial (Xue and Johns, 1995). Two PDE5 inhibitors were approved in the United States for the treatment of PAH following clinical trials: sildenafil and tadalafil. In a double-blind, placebo-controlled study named SUPER-1 (Sildenafil Use in Pulmonary Arterial Hypertension), Galie et al. randomly assigned 278 patients with symptomatic PAH (either idiopathic or associated with connective-tissue disease or with repaired congenital systemic-to-pulmonary shunts) a placebo or sildenafil (20, 40, or 80 mg) administered orally three times daily for 12 weeks. Sildenafil was shown to improve exercise capacity in all treatment groups, WHO functional class, and hemodynamics (all sildenafil doses reduced the mean pulmonary artery pressure) in patients with symptomatic PAH (Galie et al., 2005). A 3-year open-label uncontrolled extension study (SUPER-2) was later conducted by Rubin et al., in which the majority of the patients received sildenafil monotherapy at a 80 mg dose three times daily during the study (Rubin et al., 2011).

After those 3 years, the majority of patients (60%) who entered the SUPER-1 trial improved or maintained their functional status, and 46% maintained or improved 6MWD (Rubin et al., 2011). Tadalafil was approved based on a 16-week, double-blind, placebo-controlled study called PHIRST (Pulmonary Arterial Hypertension and Response to Taladafil). In this trial, 405 patients with PAH (idiopathic or associated) were either treatment-naive or on background therapy with the endothelin receptor antagonist bosentan and were randomized to placebo or tadalafil 2.5, 10, 20 or 40 mg orally once daily. Tadalafil 40 mg was found to significantly improve exercise capacity and quality of life measures and reduced clinical worsening in patients with PAH (Galie et al., 2009a).

1.1.4.4 Need for New Therapies

Meta-analyses on randomized controlled trials (RCTs) performed in PAH with the above-mentioned drugs (prostanoids, ERA and PDE-5 inhibitors) were recently conducted by Macchia et al. (Macchia et al., 2007) and Galie et al. (Galie et al., 2009d). The systematic review conducted by Macchia et al. included 16 randomized clinical trials recruiting over 1900 patients with PH (IPAH and APAH) that have been published over a 15-year period (1990-2005) (Macchia et al., 2007). The main conclusions of this meta-analysis were that new agents were not associated with a statistically significant survival benefit among patients with PH and effect on survival and treatments produced limited significant benefits in dyspnea, exercise tolerance and hemodynamic parameters (Macchia et al., 2007). In the meta-analysis that Galie et al. published two years later, the authors argued that their study included a more appropriate selection of the trials and a larger sample size regarding the number of studies and patients. In Galie's study, 21 trials were included in the primary analysis recruiting over 3140 patients. They found that active treatments were associated with a significant overall reduction of mortality of 43% and statistically significant improvements in the hemodynamic data, including

pulmonary arterial pressures (Galie et al., 2009d). The two above-mentioned meta-analyses essentially disagree over whether survival is improved, which makes it difficult to ascertain current treatments efficacy. Furthermore, it highlights the need for more effective treatment strategies to halt or reverse disease progression.

1.1.5 Pathogenesis of PAH

Regardless of the etiology, common histological features are found in the distal pulmonary arteries (<500 μm of diameter) in lungs from PAH patients (Galie et al., 2009b). The pathological features seen in the small pulmonary arteries and arterioles include medial hypertrophy, intimal proliferative and fibrotic changes (concentric and eccentric), adventitial thickening with moderate perivascular inflammatory infiltrates, complex lesions (plexiform lesions) and thrombotic lesions (Jeffery and Morrell, 2002). These obstructive pathologic changes in the lung microcirculation are the results of genetic susceptibility (mutations in genes such as *BMPR2*) and environmental triggers (toxin, anorexogins, HIV and shear stress) (Jurasz et al., 2010). Emphasis on genetic susceptibility will be addressed in the next sections of this thesis.

1.1.6 Genetic Susceptibility of PAH

Heritable forms of PAH include clinically sporadic idiopathic PAH (IPAH) with germline mutations, mainly of the bone morphogenetic protein receptor 2 gene (*BMPR2*), as well as the activin receptor-like kinase type-1 (*ALK-1*) (Abdalla et al., 2004; Fujiwara et al., 2008; Harrison et al., 2005; Harrison et al., 2003; Trembath et al., 2001) and *ALK-6* genes (Chida et al., 2012), *ENDOGLIN* (*ENG*) gene (Chaouat et al., 2004; Harrison et al., 2005), or the *SMAD8* gene (Shintani et al., 2009), and the clinical familial cases with or without the identified germline mutations (Galie et al., 2009b). BMPR-II, ALK-1/6, ENG and SMAD8 are all components of the transforming growth factor beta (TGFβ) receptor-

mediated signalling system, which highlights the importance of this pathway in inherited vascular diseases such as PAH.

1.1.6.1 Bone Morphogenetic Protein Receptor 2 (BMPR-II)

Genetic studies, published in 2000 by two independent groups of investigators demonstrated an association of PAH with heterozygous germline mutations in the gene encoding bone morphogenetic protein type II receptor (BMPR-II), a member of the TGF receptor superfamily (Lane et al., 2000; Thomson et al., 2000). *BMPR2* gene comprises 13 exons which encode a 4 kb transcript generating a poplypeptide of 1,038 amino acids (Deng et al., 2000; Lane et al., 2000). The BMPR-II receptor protein contains the 4 highly conserved domains that TGFβ type II receptors possess: N-terminal ligand binding domain, a single transmembrane region, a serine/threonine kinase domain and a cytoplasmic domain, with the exception of a particularly long cytoplasmic tail of unknown function (Lane et al., 2000). BMPR-II is essential for BMP signaling pathway in early mouse development, as mice homozygous for a mutation in the kinase domain of *BMPR2* die at day 9.5, whereas the heterozygous for the mutation are morphologically normal and fertile (Beppu et al., 2000). Mutations in the *BMPR2* gene represent the major genetic predisposing factor for PAH: mutations are found in up to 60% of cases, when PAH happens in a familial context, and in 26% of those with sporadic idiopathic PAH (Machado et al., 2001; Thomson et al., 2000). To date, 298 independent mutations in the *BMPR2* gene have been reported (Machado et al., 2009). Hereditary PAH segregates as an autosomal dominant pattern of inheritance of heterozygous mutations in the *BMPR2* gene with incomplete penetrance, in which approximately 20% of family members actually develop the disease (Machado et al., 2009). This incomplete penetrance has lead scientists to search for additional genetic and/or environmental factors that could play a critical role in the development of PAH in *BMPR2* mutation

carriers. Conditional heterozygous or homozygous *BMPR2* deletion in pulmonary endothelial cells predisposes mice to develop PAH (Beppu et al., 2004; Hong et al., 2008) and renders them more susceptible to vascular remodeling (Beppu et al., 2004).

1.1.6.2 Other Genes Belonging to the TGFβ/BMP Signaling: *ALK-1/6*, *ENG* and *SMADs 1, 4, 8 and 9*

Diverse heterozygous mutations in other genes encoding receptor members of the TGFβ signaling superfamily have been shown to be associated with PAH*: ALK-1/6, ENG* (a so-called accessory protein to the ligand receptor complex) and *SMAD8*. Heterozygous mutations in *ALK-1* , a TGFβ type I receptor, were demonstrated in patients with the vascular disorder named "hereditary hemorrhagic telangiectasia" (HHT) in association with PAH (Abdalla et al., 2004; Harrison et al., 2003; Trembath et al., 2001). HTT is an heterogenous autosomal dominant condition characterized by the presence of multiple arteriovenous malformations (McDonald et al., 2011). Mutations have been documented in one IPAH patient without a family history of HHT (Harrison et al., 2005) and children with IPAH and HPAH (Fujiwara et al., 2008). Missense mutations in the BMP type I receptor protein BMPRIB or *ALK-6* gene in pediatric patients with PAH have been reported (Chida et al., 2012). Of significant interest, the authors of this study suggested that mutations in the BMPR1B kinase domain receptor lead to a gain-of-signaling mechanism by strongly inducing SMAD8 phosphorylation and increased transcriptional activity in the presence of SMAD8 (Chida et al., 2012). Although HHT-related PAH cases are predominantly associated with mutations in *ALK-1*, *ENG* germline mutations have also been identified in a patient with HTT and in appetite-suppressant dexfenfluramine-associated PAH (Chaouat et al., 2004) as well as in a child with HHT-related PAH (Harrison et al., 2005). *SMAD8*, another gene part of the BMPR-II signaling pathway (i.e. Smad 1/5/8), has been suggested to be involved in the pathogenesis of PAH. Shintani et

al. screened for mutations in *ENG, SMAD1-6* and *SMAD8* genes in 23 patients with IPAH who had no mutations in *BMPR2* or *ALK-1* and identified a nonsense mutation in one patient (Shintani et al., 2009). Another group reported in the same year that *SMAD8* mutant mice resulted in characteristic changes in distal pulmonary arteries, including medial thickening and smooth muscle hyperplasia, that were observed in patients with PAH (Huang et al., 2009). Nasim et al. screened for gene variants in a cohort of 324 PAH cases and identified four variants in members of the BMP pathway, namely *SMAD1*, *SMAD4*, and *SMAD9* that were absent in 1244 control samples (Nasim et al., 2011).

1.1.7 BMPR-II-mediated Signal Transduction

There are seven known bone morphogenetic protein (BMP) type I receptors (ALK 1-7) and five type II receptors (ActR-II, ActR-IIB, TGFβR-II, AMHR-II and BMPR-II). BMP type I and II receptors form hetero- and homo-oligomerization complexes at the cell membrane which occur either prior to ligand binding or upon ligang binding (Gilboa et al., 2000). BMPR-II initiates intracellular signaling in response to BMP-2, -4, -6, -7 and- 9, as well as in response to growth and different factors-5 and -6 (GDF-5 and -6) (Morrell, 2006; Upton et al., 2009). Within the TGF-β superfamily, BMPs are the largest group of cytokines regulating growth, differentiation and apoptosis, as well as contributing to the maintenance and repair of adult tissues (Miyazono et al., 2005). Upon BMP ligand binding on the type I or type II BMP receptor, the type II receptors phosphorylate the type I receptors at the Gly-Ser (GS)-box and activate them, propagating intracellular signals by phosphorylating the receptor SMADs 1, 5 and 8. These activated SMADs associate with SMAD4, a common partner, leading to nuclear translocation where they regulate transcription of target genes, such as the inhibitor of DNA binding protein (*Id*) genes (Nohe et al., 2004; Yang et al., 2010) (Illustration 1). The regulation of target genes arise

from different mechanisms: direct binding of the SMAD complex to DNA, interaction with other DNA proteins (e.g. activator protein-1) and recruitment of transcriptional coactivators (Massague et al., 2005). BMP signaling can be switched off by ubiquitinylation, endogenous inibitors (Noggin, Chordin, Follistatin, BAMBI and Smurfs) and phosphatases (Chen et al., 2006; Shi et al., 2004). The above-mentioned pathway is described as the canonic BMP signaling pathway, which is the most extensively studied. In addition, SMAD-independent pathways have been described and include the mitogen-activated protein kinase (MAPK) p38 and p42/44 (ERK1/2), as well as c-Jun-N-terminal kinase/stress-activated protein kinase (JNK/SAPK) (Adachi-Yamada et al., 1999; Massague, 2003).

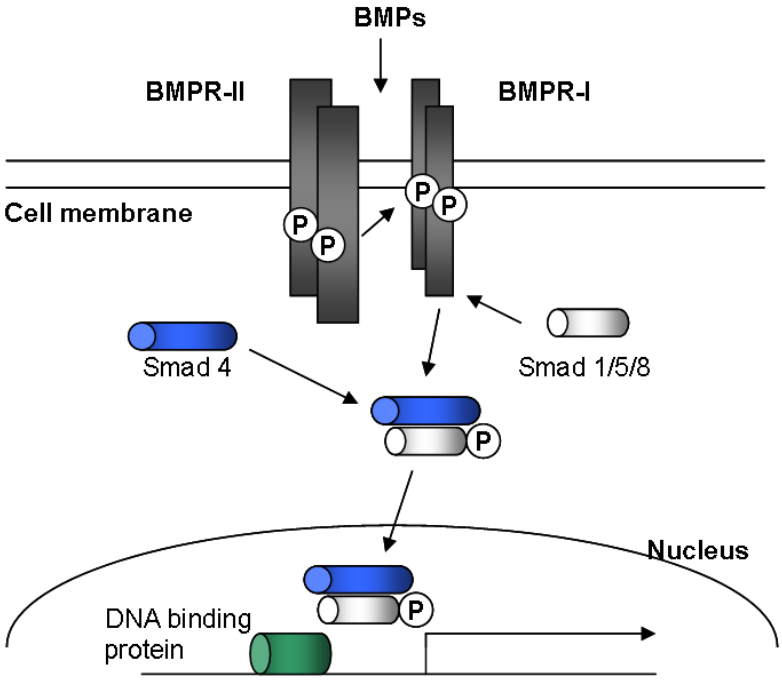

Illustration 1. BMPR-II canonical signal transduction. Adapted from (Yamaguchi et al., 2000).

1.1.8 BMPR-II Signaling in Vascular Cells

BMPR-II is widely expressed in normal tissues, highly expressed on the vascular endothelium of the pulmonary arteries and expressed at lower levels in pulmonary artery smooth muscle cells (PASMCs) and fibroblasts (Atkinson et al., 2002). Atkinson et al. have shown that expression of BMPR-II is markedly reduced in the pulmonary vasculature of patients with HPAH and IPAH, whether they have mutations in the *BMPR2* gene (Atkinson et al., 2002) or not. An opposite effect of BMPs on pulmonary artery endothelial cells (PAECs) and PASMCs has been documented, whereby BMPs promote anti-proliferative activities in PASMCs and pro-survival activities in PAECs along with promotion of migration and proliferation (Teichert-Kuliszewska et al., 2006; Valdimarsdottir et al., 2002; Yang et al., 2005). Indeed, Yang et al. have shown that PASMCs from patients with PAH harboring mutations in the gene *BMPR2* have a reduced capacity to activate Smad 1/5 and respond to BMP anti-proliferative signals (Yang et al., 2005). In addition, Teichert-Kuliszewska et al. have shown that human PAECs silenced with BMPR-II siRNA lead to an increase in apoptosis of almost 3-fold (Taraseviciene-Stewart et al., 2001). Therefore, mutations in the gene *BMPR2* are thought to affect the integrity of the endothelial cell barrier through the increase in endothelial cell apoptosis whereby PASMCs have increased accessibility to serum proteins promoting their growth and, consequently, vascular remodeling.

1.1.9 Pulmonary Vascular Homeostasis and Vascular Remodeling

The lung has the largest vascular bed of any organ in the body. It accommodates the entire cardiac output to oxygenate the blood and remove waste gases such as carbon dioxide. It has extensive microvascular networks, which can be fully recruited with exercise to adapt to increases in cardiac output while still maintaining a very low arterial resistance. The endothelium is central to the regulation of pulmonary flow, vascular

resistance, homeostasis, leukocyte trafficking and coagulation and barrier function (Budhiraja et al., 2004). It also produces various growth factors that can act via autocrine and/or paracrine effects. Under normal conditions, the endothelium is considered as being in a “quiescent state” (Budhiraja et al., 2004). However, under pathological conditions such as PAH, the endothelium state shifts towards an “activated state”, as it is subjected to a number of stimuli including shear stress from increased pulmonary blood flow, viral infection (HIV), inflammation, oxidative stress, toxins and alveolar hypoxia (Budhiraja et al., 2004; Farber and Loscalzo, 2004; Tuder et al., 2001). This activated state can lead to endothelial dysfunction, which is characterized by an imbalance in production of various endothelial vasoactive mediators, such as nitric oxide, prostacyclin, endothelin-1 and serotonin, as well as increased pro-inflammatory and pro-thrombotic factors, including tissue plasminogen activator inhibitor-1 (Altman et al., 1996; Tuder et al., 2001). Dysfunction of the endothelium is increasingly recognized to mediate the structural changes in the pulmonary vasculature by promoting vascular remodeling and proliferation of small pulmonary arteries (Budhiraja et al., 2004; Morrell et al., 2009; Tuder et al., 2001). The initiating steps which trigger endothelial dysfunction and the subsequent structural changes in the pulmonary vasculature in PAH are not completely understood, but multiple converging lines of evidence point towards endothelial cell injury as being an important triggering event.

1.1.10 Endothelial Cell Apoptosis

A concept has emerged in recent years that endothelia cell (EC) apoptosis resulting from environmental injury and/or genetic predisposition represents a critical triggering event possibly directly leading to the degeneration of pre-capillary arterioles and/or to the selection of hyperproliferative apoptosis-resistant vascular cells (ECs and SMCs) that may lead to "angioproliferative" plexiform lesion. Our group has previsouly shown that

silenced of BMPR-II with siRNA led to a more than 2-fold increase in apoptosis (Teichert-Kuliszewska et al., 2006). Furthermore, BMP-2 reduced apoptosis induced by serum withdrawal in early progenitor cells (EPCs) from normal subjects, but not from patients with IPAH (Teichert-Kuliszewska et al., 2006). Our group has also shown that overexpression of EC growth and survival factors such as VEGF, and angiopoietin-1, prevented the development of monocrotaline-induced PAH (Campbell et al., 2001; Zhao et al., 2003). These experimental findings from our group and others using the VEGF receptor antagonist SU5416 further implicate EC apoptosis as a central mechanism in the initiation of PAH. Using human pulmonary microvascular ECs seeded in an artificial capillary system, Sakao et al. demonstrated that SU5416 induces EC apoptosis under conditions of high fluid shear stress. In addition, they documented the generation of hyperproliferative and phenotypically altered ECs (Sakao et al., 2005). Seminal work by Taraseviciene-Stewart et al. showed that rats treated with a single dose of SU5416 (20 mg/kg) under chronic hypoxic conditions resulted in pulmonary arterial endothelial cell death, followed by obliteration of the artery lumen by proliferated endothelial cells, which is associated with severe PAH (Taraseviciene-Stewart et al., 2001). In addition, the effect of the VEGF receptor blockade could be abrogated by inhibitors of apoptosis, thus emphasizing the importance of EC apoptosis as a triggering mechanism in PAH. Based on this work, Abe et al. demonstrated the formation of plexiform-like lesions that are indistinguishable from the pulmonary arteriopathy of human PAH in the SU5416/hypoxia rat model, but only in the later stages (i.e. 13 to 14 weeks after the SU5416 injection) (Abe et al., 2010); whereas, increases in pulmonary arterial pressure was seen as early as 4 weeks. Therefore, the SU5416 model of severe PAH may recapitulate the etiological mechanisms involved in the pathogenesis of the human condition, involving abnormalities endothelial cell survival and growth that are believed to

be playing an important role in the plexogenic arteriopathy of human PAH and allows evaluation of preclinical drugs.

1.2 *In Vitro* System: Blood-Outgrowth Endothelial Cells (BOECs)

1.2.1 Relevance

Research aimed at addressing the underlying molecular etiology of PAH is complicated by the limited access to appropriate biological material from the early-stages of this disease. When using tissues or cells from PAH patients, one major limitation is that patients often have end-stage disease and there are nearly always the potential for confounding effects of drugs used for its treatment, as well as inflammation and other host responses can mask the underlying pathways in the pathogenesis of PAH (West et al., 2008). Culturing cells obtained from the patients can overcome this limitation by removing the effects of the host environment, unmasking the early molecular events to be studied (West et al., 2008). However, tissue from which to culture the cells is usually only available at post mortem or at the time of lung transplantation, and obtaining relevant control tissue and cells is problematic. Moreover, there is an inherent selection bias in the culture of cells from the diseased lung tissue favoring the more highly proliferative cells. Recently, there has been great interest in the use of inducible pluripotent cells to derive relevant cell lines to study the pathogenic mechanisms, particularly in monogenic disease (Chang et al., 2013; Riazi et al., 2009). However, this approach requires extensive manipulation and epigenetic modifications which may further confound the use of these cells in mechanistic studies. Thus, the ability to derive highly differentiated endothelial-like cells from peripheral blood samples provides a potentially powerful tool to study the direct effects of mutations linked to PAH on the biology of a cell type which is central to the pathogenesis of this disease. These so-called blood-outgrowth endothelial cells (BOECs) (Hur et al., 2004; Lavoie and Stewart,

2012), also termed endothelial colony forming cells (Ingram et al., 2004) or late-outgrowth endothelial progenitor cells (Richardson and Yoder, 2011), represent a very valuable source of cells used to investigate the molecular cues leading to endothelial cell dysfunction from PAH patients. Moreover, they are readily available from peripheral blood, relatively easy to harvest/expand and can be selectively differentiated in culture conditions to obtain a surrogate for mature endothelial cells. This method of derivation of patient-specific endothelial cells allows the study of proteins that could be at the origin of the disease. In addition, minimal manipulation is needed to derive the BOECs when compared to transformed lymphocytes from PAH patients (Meyrick et al., 2008; West et al., 2008) or transfected cells with plasmids for *BMPR2* mutants (Yang et al., 2011). Since the seminal discovery of mutations in *BMPR2* gene in patients with HPAH (Lane et al., 2000; Machado et al., 2001; Thomson et al., 2000), there have been only a few studies examining the effects of these mutations on the endothelial or progenitor cell function. For example, Dr. Morrell's group has used late-outgrowth EPCs (also known as blood-outgrowth endothelial cells) to investigate the impact of the *BMPR2* mutations on their functionality and has shown that the patient-derived cells have a hyperproliferative phenotype with impaired ability to form vascular structures, compared with control subjects (Toshner et al., 2009). They also have used PAECs transfected with mutant BMPR-II and shown that mutation in BMPR-II increases susceptibility to apoptosis of PAECs and leads to secretion of growth factors that stimulate the proliferation of PASMCs (Yang et al., 2011). This finding is in line with other reports describing phenotypic alterations in endothelial cells derived from patients with PAH (Teichert-Kuliszewska et al., 2006; Tuder et al., 1994).

1.2.2 Derivation

BOECs are highly differentiated endothelial-like cells that are derived after prolonged culture of mononuclear cells (MNCs) (Lavoie and Stewart, 2012; Richardson and Yoder, 2011). The MNCs are isolated from peripheral blood by Ficoll density centrifugation, and within a relatively brief culture period, they differentiate into so-called "early endothelial progenitor cells" (usually < 1 week) on collagen or fibronectin-coated plates supplemented with endothelial cell growth media (Illustration 1A) (Lavoie and Stewart, 2012). BOECs appear in cluster-like colonies after prolonged culture (usually > 2 weeks) of the early endothelial progenitor cells (Illustration 1B) and then rapidly overgrow the early endothelial progenitor cells (Illustration 1C) (Lavoie and Stewart, 2012). BOECs exhibit a high proliferative potential and are highly differentiated to an endothelial phenotype, as confirmed by their RNA, protein and ultrastructure analysis (Medina et al., 2010).

Illustration 2: Blood-outgrowth endothelial cell derivation from peripheral blood

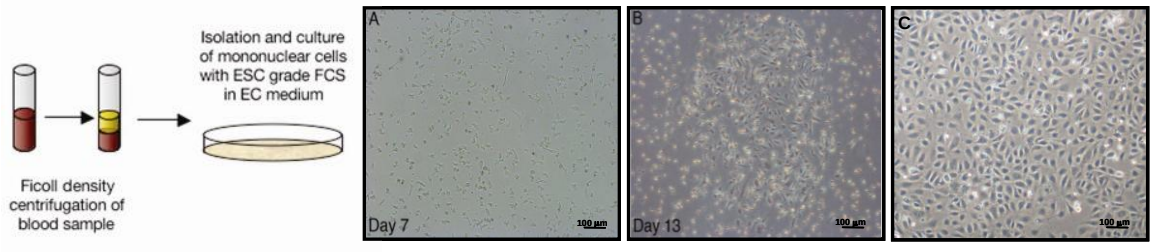

Courtesy of Mark Ormiston

1.3 Proteomics and Genomics Studies in PAH

Gene microarrays and proteomic analyses have been recently used as unbiased approaches to improve our understanding of the pathogenesis of PAH and to discover putative biomarkers characteristics of PAH. High-throughput protein expression studies have been conducted on plasma samples of IPAH patients (Abdul-Salam et al., 2006; Yu et al., 2007; Yuditskaya et al., 2009), on transformed blood lymphocytes of HPAH patients (Meyrick et al., 2008), on lung tissues from IPAH patients (Abdul-Salam et al., 2010) and from rodent models of PAH (e.g. rat monocrotaline and rat and mouse chronic hypoxia models of PAH) (Kwapiszewska et al., 2008; Laudi et al., 2007). These high-throughput proteomics studies were mostly performed with two-dimensional gel electrophoresis technology, which allows the quantification of protein abundance by gel staining and software analyses, as well as protein identification by liquid chromatography tandem mass spectrometry (LC-MS/MS) (Kwapiszewska et al., 2008; Laudi et al., 2007; Meyrick et al., 2008; Yu et al., 2007). Other proteomic studies have used surface-enhanced laser desorption/ionization time of flight mass spectrometry (SELDI-TOF MS) (Abdul-Salam et al., 2006; Yuditskaya et al., 2009), relying on the resulting spectra of the ion for internal quantitative calibration and on label-free LC-MS/MS, where

relative protein abundance is based on peptide ion intensity values (Abdul-Salam et al., 2010; Yuditskaya et al., 2009). These studies have yielded a number of protein candidates with differential expression in PAH relative to controls, including alpha-1-antitrypsin, vitronectin (Yu et al., 2007), apolipoproteins A-II and B, serum amyloid A (Yuditskaya et al., 2009) and complement component 4a (C4a) (Abdul-Salam et al., 2006) in plasma samples as well as chloride intracellular channel 4, periostin (Abdul-Salam et al., 2010) and four-and-a-half LIM domain-1 (Fhl-1) (Kwapiszewska et al., 2008) in the lungs of IPAH patients.

Gene microarray studies have also been conducted with lymphoblastoid lines derived from *BMPR2* mutation carriers with HPAH (West et al., 2008), blood cells (Bull et al., 2004) and lung tissue specimens from IPAH patients (Geraci et al., 2001; Rajkumar et al., 2010), as well as intrapulmonary arteries of hypoxia-induced PH in mice (Kwapiszewska et al., 2005). Gene expression signatures from these different studies have shown alterations in multiple pathways with known relationship to PAH, including regulation of actin-based motility, immune function, protein ubiquitination, calcium balance, growth and apoptosis (Rajkumar et al., 2010; West et al., 2008). Gene candidates with differential expression in PAH relative to controls found through this approach include the estrogen metabolizing gene CYP1B1 (West et al., 2008), coagulation factor II receptor-like 3, A--myb myeloblastosis viral oncogene homolog 1 and nuclear receptor coactivator 2 (Rajkumar et al., 2010) as well as S100 calcium binding protein A4, CD36 and FK506 binding protein 1A (Kwapiszewska et al., 2005). A microarray screen in total plasma RNA samples from patients with PAH was recently performed by the Wilkins group, in which they showed that microRNA-145 is associated with poor survival in PAH (Rhodes et al., 2013). Further validation studies will be needed

to describe the importance of the candidate genes and proteins in the development of PAH, which will allow a better understanding of the pathobiology of this disease.

1.4 Overview

There is compelling evidence supporting the concept of endothelial cell apoptosis, resulting from environmental injury and/or genetic predisposition, leading to the degeneration of pre-capillary arterioles and subsequently to the selection of hyperproliferative, apoptosis-resistant endothelial cells that may cause pathological vascular lesions in PAH. The identification of mutations in the gene *BMPR2* linked to PAH has provided some insight into the pathogenesis of the disease. The BMPR-II receptor has been described to be essential in maintaining cell survival and has recently been linked to cell death if down-regulated by RNAi. However, the underlying molecular pathways linking mutations in the *BMPR2* gene to PAH are not well understood.

Hypothesis

BMPR2 mutations produce an imbalance in endothelial cell protein expression and/or activity that is integrally related to the development of abnormalities in lung vascular function and structure in hereditary PAH (HPAH).

CHAPTER 2: PHENOTYPIC AND PROTEOMIC ANALYSES OF BOECs FROM HEALTHY CONTROLS AND PATIENTS WITH HPAH

2.1 Specific Aims

1. To characterize the functional activity of blood-outgrowth endothelial cells (BOECs) from patients with HPAH harboring *BMPR2* mutations compared with healthy controls.

2. To identify dysregulated proteins and phosphoproteins in BOECs of patients with HPAH harboring *BMPR2* mutations compared with healthy controls that may contribute to the pathogenesis of PAH under basal conditions and upon BMP9 treatment.

2.2 Material and Methods

2.2.1 Isolation and Culture of Blood-Outgrowth Endothelial Cells

Human peripheral blood mononuclear cells were isolated from 40-80 ml of venous blood by Ficoll density gradient centrifugation (GE Healthcare, Little Chalfont, U.K.) and plated onto collagen-coated flasks (BD Biosciences, Franklin Lakes, N.J.) in an endothelial selective medium (EGM2-MV; Lonza, Basel, Switzerland) supplemented with a 20% embryonic stem cell-grade fetal bovine serum (HyClone, Thermo Scientific, Basingstoke, U.K.) and additional growth factors (EGM2-MV bullet kit; Lonza, Basel, Switzerland). The medium was changed every 48 hours. Blood-outgrowth endothelial cells (BOECs) appeared after 2–3 weeks and were passaged when confluent onto tissue culture plastic dishes and maintained in EGM-2MV containing a 10% standard fetal bovine serum (FBS) (Gibco, Life Technologies, Burlington, ON). BOECs from healthy controls were studied at passage 4–8 and BOECs from HPAH patients at passage 4-12. BOECs were isolated from subjects with HPAH and from healthy control subjects (Table 2).

2.2.2 Two-Dimensional Polyacrylamide Gel Electrophoresis (2-D PAGE)

2.2.2.1 Protein Lysate Preparation

BOECs were incubated in a serum-deprived medium for 16 hours (EBM-2 + 0.1% FBS). After the 8th hour of treatment with or without BMP9 (1 ng/ml) (R&D Systems, Abingdon, U.K.), the medium was removed. A radioimmunoprecipitation assay (RIPA) lysis buffer (Tris-HCl 50 mM pH 7.4, NP-40 1%, NaCl 150 mM, EDTA 1 mM pH 7.0, glycerol 1%) completed with a 1X protease inhibitor cocktail (Roche Diagnostics, Laval, QC), as well as 1 mM of sodium fluoride and 1 mM of sodium orthovanadate, was added. After the addition of the lysis buffer, cells were scraped, and the lysates were collected, frozen at

-80°C and stored until use. Once needed, the lysates were thawed on ice and sonicated in a 4°C sonicating water bath (a 5-second pulse followed by 10 seconds off, and this for 10 cycles). Protein quantification of RIPA lysates was realized with bicinchoninic acid assay (BCA) (Sigma-Aldrich, Oakville, ON). An aliquot of each RIPA sample was added to four volumes of ice cold acetone and kept at -20°C for 75 minutes, while being inverted every 15 minutes. The samples were then centrifuged at 14,000 g and at 4°C for 10 minutes, before the supernatants were removed. The protein pellets were air-dried, suspended in a 2-D sample buffer (7M urea, 2M thiourea, 4% CHAPS, 1% dithiothreitol), incubated for 30 minutes at room temperature and vortexed before use. Protein quantification of the 2-D samples was realized with 2-D Quant kit (GE Healthcare, Mississauga, ON). Before being used for the 2-D gel experiment, a 1% 3-10 ampholyte solution was added to the sample.

2.2.2.2 Isoelectric Focusing and 2-D PAGE

The whole protein lysate (100 µg) was passively rehydrated overnight in a 0.22 ml 2-D rehydration/sample buffer and applied to immobilized pH gradient (IPG) strips (11 cm, pH 4-7) (Bio-Rad, Mississauga, ON). Isoelectric focusing (IEF) was carried out using an Agilent fractionator in the in-gel mode (Agilent Technologies, Mississauga, ON) programmed as follows: the voltage was initially held at 300 V for 1 minute, then linearly increased to 3500 V over 90 minutes, focused for 18,000 Vh and held at 500 V for 30 minutes. The current did not exceed 50 µA per strip. Each focused strip was subsequently equilibrated in 4.5 ml of equilibration buffer I (6M urea, 50 mM Tris-Cl pH 8.8, 2% SDS [w/v], 30% glycerol [v/v], bromophenol blue [trace], 1% dithiothreitol [w/v]) for 15 minutes with gentle agitation, followed by the equilibration buffer II (equilibration solution I with dithiothreitol replaced by 2.5% iodoacetamide [w/v]) for 15 minutes, with gentle agitation. The 2-D separation was performed on a 10% SDS-PAGE gel in the

DALT six electrophoresis system (GE Healthcare, Mississauga, ON), at 10 mA per gel and at 25°C, for approximately 18 hours, until the bromophenol blue reached the bottom of the gel. Two technical replicates were run for each biological sample for a total of 32 2-D gels.

2.2.2.3 ProQ Diamond and Sypro Ruby Gel Stains

The gels were first stained with a ProQ Diamond phosphoprotein gel stain (Invitrogen, Burlington, ON) for phosphoprotein staining and then subsequently stained with a Sypro Ruby protein gel stain, following manufacturer's instructions (Sigma-Aldrich, Oakville, ON), for total protein staining. Briefly, for the phosphoprotein staining procedure, all gels were fixed in 50% methanol and 10% acetic acid overnight, then stained for phosphoproteins with a ProQ Diamond gel stain for 2:30 hours and imaged on a Versa Doc 4000 imager (Bio-Rad, Mississauga, ON). After imaging, the gels were then stained with a Sypro Ruby gel stain overnight, washed in 10% methanol and 7% acetic acid for 30 minutes and imaged on a Versa Doc 4000 imager.

2.2.2.4 Image and Data Preprocessing

We processed the 2-D gel images with PDQuest (PDQuest version 8.0; BioRad, Mississauga, ON). After the images were cleaned and aligned and the spots matched, the values were normalized using a local regression method called LOESS. Technical duplicates were averaged, and the results were transformed to a $\log_2$ scale. For the total protein analysis, we identified a total of 423 different spots, including 410 complete cases of spots detected across all gels. Of these, 416 spots were detected in at least two of the four samples in both groups (healthy and HPAH). In these 416 cases, we imputed the few missing values with the minimum value of the corresponding gel. The spots that were significantly different between healthy- and HPAH-derived cells were considered for protein identification (Student's t-test, $P<0.05$). For the phosphoprotein analysis, there

were only 17 complete data spots. 287 spots were detected in at least two of the four samples in both groups (healthy and HPAH). In these 287, we imputed the missing values with the minimum value of the corresponding gel. The spots that were significantly different between healthy- and HPAH-derived cells were considered for protein identification (Student's t-test, $P<0.05$).

2.2.2.5 Mass Spectrometry and Protein Identification

Protein spots with differential expression patterns on 2-D maps were excised with the EXQuest spot cutter (Bio-Rad, Mississauga, ON). The 2-D gel spots or 1-D gel bands were analyzed for protein identification at the OHRI Proteomics Core Facility (Ottawa, ON). The samples were digested using trypsin (Promega, Madison, WI), in accordance with the method of Shevchenko (Shevchenko et al., 2006). The resulting peptide extracts were concentrated by vacufuge (Eppendorf, Mississauga, ON) and resuspended in 0.1% formic acid. Peptides were analyzed by liquid chromatography-tandem mass spectrometry (LC-MS/MS) on an LTQ Orbitrap XL hybrid mass spectrometer with a nanospray ionization source (Fisher Scientific, Nepean, ON) and an UltiMate 3000 RSLC Nano HPLC (Fisher Scientific, Nepean, ON). The system was controlled by the Xcalibur software, version 2.0.7 (Fisher Scientific, Nepean, ON). Peptides were loaded onto a trap column (Acclaim PepMap C18, Fisher Scientific, Nepean, ON) for 5 minutes, at a flow rate of 15 μl per minute, and then eluted over a 60 minute gradient of 3% - 45% acetonitrile with 0.1% formic acid, at a flow rate of 0.3 μl per minute, onto a 10-cm long column with integrated emitter tip [Picofrit PF360-75-15-N-5 (New Objective) packed with Zorbax SB-C18 5 micron (Agilent Technologies, Mississauga, ON)], and nanosprayed into the mass spectrometer. MS scans were acquired in FTMS mode using the Orbitrap, while the MS2 scans were acquired in the ion trap using data-dependent acquisition of the top 5 ions from each MS scan. The MASCOT 2.4 software (Matrix Science, Boston,

MA) was used to infer peptide and protein identities from the mass spectra. The observed MS/MS spectra were matched against a custom database of protein sequences (human sequences from the 2011_07 version of uniprot_sprot.fasta.gz downloaded from ftp.uniprot.org concatenated with a contaminants database downloaded from maxquant.org, June 9th 2011). Mass tolerance parameters were MS ± 7 ppm and MS/MS ± 0.6 Da. Enzyme specificity was set to 'Trypsin/P'. Oxidation of methionine, carbamidomethylation of cysteine, protein N-terminal acetylation, deamidation and/or conversion of Glu or Gln to Pyro-Glu were allowed as variable modifications.

2.2.3 Immunoblotting and Reagents

BOECs were washed twice with cold 1X PBS and then flash frozen on a bath of dry ice with methanol for 30 seconds. The flask containing the cells was removed from the bath, RIPA lysis buffer was added and cells were scraped for whole cell lysate collection. Protein lysates were sonicated for 30 seconds at 4°C and then centrifuged at 14,000 g for 15 minutes at 4°C. Supernatant was collected. Protein lysates were separated on 12% SDS-PAGE, transferred on PDVF membranes and probed with antibodies β-actin (mouse monoclonal; Sigma-Aldrich, Oakville, ON), BMPR-II (mouse monoclonal, BD Biosciences, Mississauga, ON), phospho-smad 1/5/8 (Cell Signaling, Whitby, ON), and inhibitor of DNA binding 1 (Id1; rabbit monoclonal, Biocheck, Lethbridge, AB). IRDye infrared secondary antibodies were used for the detection of the above-mentioned targets (Li-COR Odyssey Infrared Imaging System, Li-Cor Biosciences, Guelph, ON), except for the phospho-Smad 1/5/8 and Id1, in which case the horseradish peroxidase (HRP) conjugated system was used (GE Healthcare, Mississauga, ON). A total of 50 μg proteins was used for all the other molecular targets mentioned above.

2.2.4 AnnexinV/Propidium Iodide Staining and Flow Cytometry

Apoptosis was assessed by flow cytometric analysis using an AnnexinV staining kit (Roche Diagnostics, Laval, QC). Briefly, 48 hours after plating (2.0×10^5 cells per well of a 6-well plate for regular apoptosis or 3.0×10^4 per well of a 24-well plate for transfection studies), cells were washed and maintained in a normal medium (EGM-2MV with 10% FBS) or in a serum-deprived medium (EBM-2 with 2% FBS) for 16 hours. Thereafter, the cells were stimulated or not with tumor necrosis factor alpha (α-TNF) (R&D Systems, Minneapolis, MN, USA), at 10 ng/ml for 4 hours with cycloheximide (CHX) (Sigma-Alrich, Oakville, ON), at 20 μg/ml. The cells were harvested with TrypLE (Invitrogen, Burlington, ON), centrifuged and incubated at room temperature, in the dark, in a 0.1 ml staining buffer containing 2 μl of Annexin V-fluorescein isothiocyanate (FITC), for 10 minutes, followed by the addition of 2 μl of propidium iodide for 5 minutes. 0.4 ml of 1x binding buffer was added to each sample before analysis by flow cytometry (Beckman Coulter, SC Quanta, Mississauga, ON). A minimum of 2.5×10^5 events were analyzed per sample, within 30 minutes. Gates based on electronic volume and side scatter were set to eliminate cellular debris and cell clusters.

2.2.5 Human Cleaved Caspase-3 Infrared Immunoassay

BOECs were seeded into 96-well cell culture clear-bottom black plates (2.0×10^5 per well) with 0.1 ml of normal medium (EGM2-MV with 10% FBS) for 24 hours. BOECs were washed and maintained in a serum-deprived medium (EBM-2 with 2% FBS) medium for 16 hours. Thereafter, the cells were stimulated or not with tumor necrosis factor alpha (TNF-α) (R&D Systems, Minneapolis, MN, USA), at 10 ng/ml for 4 hours with cycloheximide (CHX) (Sigma-Alrich, Oakville, ON), at 20 μg/ml. The human cleaved caspase-3 (Asp 175) infrared immunoassay was conducted according to the manufacturer's instructions (R&D Systems, Minneapolis, MN, USA). Control wells with

no primary antibody (secondary antibody alone) were included as negative controls and the fluorescence from these wells was used as the background fluorescence and was substrated from all sample wells. Normalized results were determined by dividing the cleaved caspase-3 fluorescence at 800 nm in each well by the corresponding total GAPDH fluorescence at 700 nm in each well (Li-COR Odyssey Infrared Imaging System, Li-Cor Biosciences, Guelph, ON). The normalized triplicate readings for each sample were then averaged.

2.2.6 BrdU Assay

BOECs were seeded into 96-well plates (1,250 per well) with 0.2 ml of a normal medium (EGM2-MV with 10% FBS). Experiments were performed in triplicate for each biological sample. The medium was changed after 72 hours. Bromodeoxyuridine (BrdU) (100 µM, 6 hours) was added after 24 hours, 48 hours, 72 hours and 96 hours. The BrdU uptake was measured using a colorimetric cell proliferation ELISA (Roche Diagnostics, Laval, QC).

2.2.7 BOEC Proliferation

BOECs (3.0×10^4 per well) were seeded into 24-well plates with 1 ml of normal medium (EGM-2MV with 10% FBS). Experiments were performed in triplicate. Cells were trypsinized, stained with trypan blue and counted on days 1 and 2 with the Countess Automated Cell Counter (Invitrogen, Burlington, ON). Live cells corresponded to cells not stained with trypan blue.

2.2.8 Statistical Analysis

Results are presented as mean ± SEM. Statistical analysis was performed using the GraphPad Prism software, version 5.1. The means of two groups were compared using a Student t-test. The differences between multiple means were determined by one-way

analysis of variance (ANOVA), and when overall differences were detected, the Tukey's or Dunnett's post-hoc analysis was used to determine differences between individual means. A value of $P<0.05$ was considered statistically significant.

2.3 Results

2.3.1 Generation and Characterization of Blood-Outgrowth Endothelial Cells

Patient-specific blood-outgrowth endothelial cells (BOECs) was used as a surrogate for human mature endothelial cells in order to gain endothelial-cell specific insights into the molecular mechanisms underlying EC dysfunction in PAH. The baseline characteristics of the human subjects who have provided blood samples to derive the BOECs are presented in Table 2. BOECs from patients with HPAH harboring *BMPR2* mutations and healthy control subjects were observed to derive from colony-like clusters present in early-outgrowth endothelial progenitor cell culture and were grown to confluence before passaging. These cells exhibited a typical endothelial-like morphology through numerous passages (Figure 1A), with no apparent differences between the healthy controls and patients with HPAH. The identification of cell surface markers present on the BOECs have been previously published by the Stewart and Morrell groups (Geti et al., 2012; Ormiston et al., 2010). Flow cytometric analysis showed that they were positive for endothelial cell-specific markers, including VEGFR-2 and CD31, negative for monocyte markers, including CD14 and CD45, and positive for the hematopoietic stem cell marker CD34 (Geti et al., 2012; Ormiston et al., 2010). Immunofluorescence staining analysis further revealed expression of endothelial cell-specific markers, such as the von Willebrand Factor (vWF), CD146, CD31 and the hematopoietic stem cell marker CD34 (Geti et al., 2012; Ormiston et al., 2010).

Table 2. Patient characteristics

Diagnosis	Sex	Age, y	BMPR-II mutation	mPAP, mm Hg	CI (L/min/m^2)	PVR (Woods)	6MWD (m)	Treatment[a]
PAH patients *2D-PAGE, WB and functional assays*								
Heritable	F	35	W9X	65	1.90	N/A	459	ERA, PDEI
Heritable	F	51	G828R	48	2.40	8.50	420	ERA, PGI
Heritable	M	21	W9X	71	1.80	16.40	360	PGI, PDEI
Heritable *WB and functional assays*	M	32	c.*-944/5GC-AT	60	2.69	10.80	400	PGI, PDEI
Heritable	M	45	R320X	46	1.75	9.70	381	ERA, PDEI
Heritable	F	36	R213X	40	1.36	19.60	482	ERA, PGI
Heritable	F	79	R584X	52	2.25	10.96	124	PDEI
Healthy subjects *2D-PAGE, WB and functional assays*								
Healthy	F	37						
Healthy	F	45						
Healthy	M	28						
Healthy *WB and functional assays*	M	30						
Healthy	M	20						
Healthy	M	40						
Healthy	M	41						
Healthy	M	39						

[a]Treatment class abbreviations: ERA - Endothelin Receptor Antagonists, PGI - Prostacyclin Analogues, PDEI - Phosphodiesterase Inhibitors; mPAP indicates mean pulmonary artery pressure; CI, cardiac index; PVR, plumonary vascular resistance; WB, Western blot; M, male; F, female; 6MWD, 6 minute walk distance; y, years; N/A, not available

To study the effects of the mutations of the *BMPR2* gene on BMPR-II protein levels, immunoblotting analysis of BMPR-II levels of BOECs derived from patients with HPAH and healthy controls was performed (Figure 1). Noteworthly among the six HPAH samples used for this experiment, five had nonsense mutations in the *BMPR2* gene (i.e., R320X, R584X, R213X and W9X [2 patients]) and one had a GC > AT double-substitution mutation 944 bp upstream of the translation start site (i.e. c.*-944/5GC > AT). These disease-causing mutations are predicted to affect different domains of the BMPR-II protein (W9X, extracellular; R213X, R320X and R584X, kinase domain; the double substitution mutation creates a potential cryptic ATG site (Aldred et al., 2007)) and their impact may vary on the protein product. For example, mutations R213X, R320X and R584X are expected to yield a truncated version of the protein that is strongly susceptible to degradation and mutation W9X to no product at all for the mutated copy. Overall, BMPR-II levels from the HPAH group were found to be significanlty reduced by 2.8-fold when compared with healthy controls (0.50 ± 0.13 versus 1.39 ± 0.20; $P<0.01$) (Figure 1B). Interestingly, these results suggests that a mutation in a single allele of the *BMPR2* gene (i.e. haploinsufficiency) can lead to an overall low yield of the BMPR-II protein, even if a wild type copy of the gene is still present.

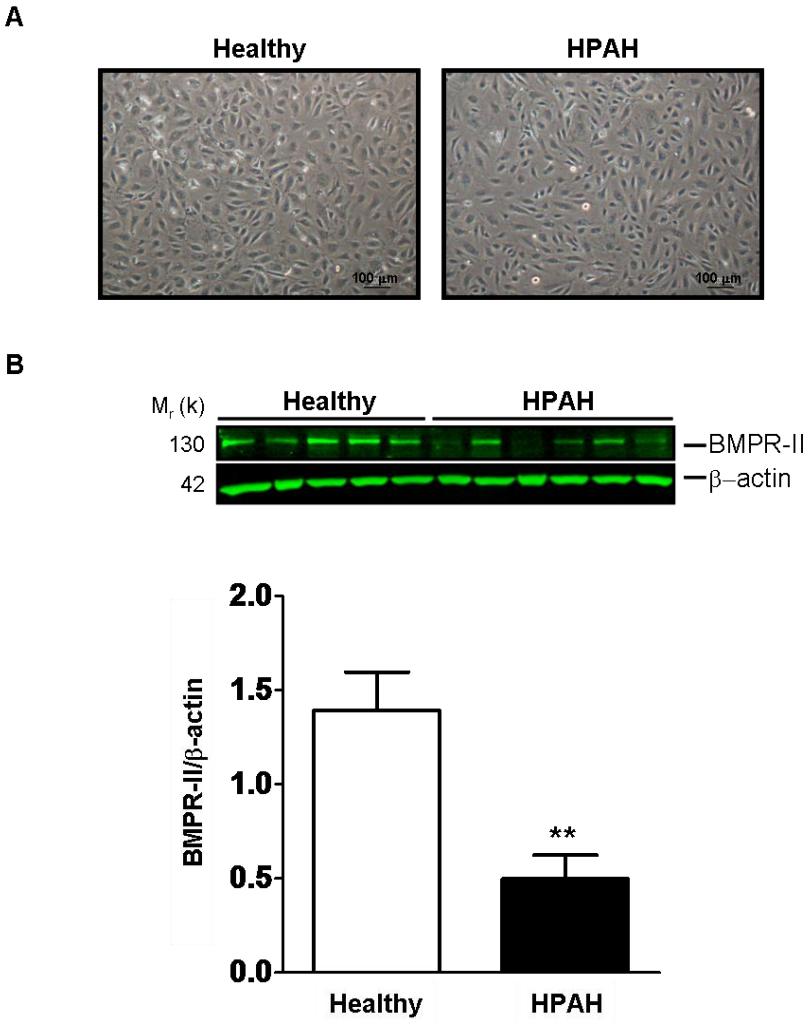

Figure 1. Reduced levels of BMPR-II in BOECs from patients with HPAH.
(A) Representative images of BOECs cultured on plastic flasks in EGM-2MV medium supplemented with 10% FBS. Original magnification x 10. Scale bar = 100 µm.
(B) BOECs from patients with HPAH (n=6) are showing significantly reduced BMPR-II levels compared to healthy controls (n=5). Results are expressed as mean ± SEM and as expression relative to β-actin. Statistical differences were assessed by Student t-test. **p<0.01

2.3.2 Greater Proliferative Capacity of BOECs from HPAH

In the next series of experiments, the functional differences between the BOECs derived from patients with HPAH and healthy controls were examined. The proliferative index of BOECs was studied by monitoring the incorporation capacity of bromodeoxyuridine (BrdU), which was quantitated by ELISA. BOECs from patients with HPAH showed a significantly greater BrdU incorporation capacity of 2.1-fold at day two when compared to BOECs from healthy controls (0.38 ± 0.06 versus 0.18 ± 0.04; $P<0.05$) (Figure 2A). In addition, there was also a significant increase by 2.0-fold in BrdU incorporation at day two for BOECs from patients with HPAH when compared to day one (0.38 ± 0.06 versus 0.19 ± 0.03; $P<0.05$) (Figure 2A). The greater proliferative capacity of BOECs derived from patients with HPAH was further confirmed with total live cell counts done by a trypan blue exclusion test of cell viability (Figure 2B). BOECs from patients with HPAH showed a significantly greater total live cell count of 1.5-fold at day two when compared to BOECs from healthy controls ($231,667 \pm 5,528$ versus $159,167 \pm 8,094$; $P<0.01$) (Figure 2B). In addition, there was also a significant increase by 1.4-fold in total live cells at day two for BOECs from patients with HPAH when compared to day one ($231,667 \pm 5,528$ versus $161,667 \pm 17,873$; $P<0.01$) (Figure 2B). These results suggest that under normal growth conditions, BOECs from HPAH patients have a greater proliferative potential when compared to healthy control cells.

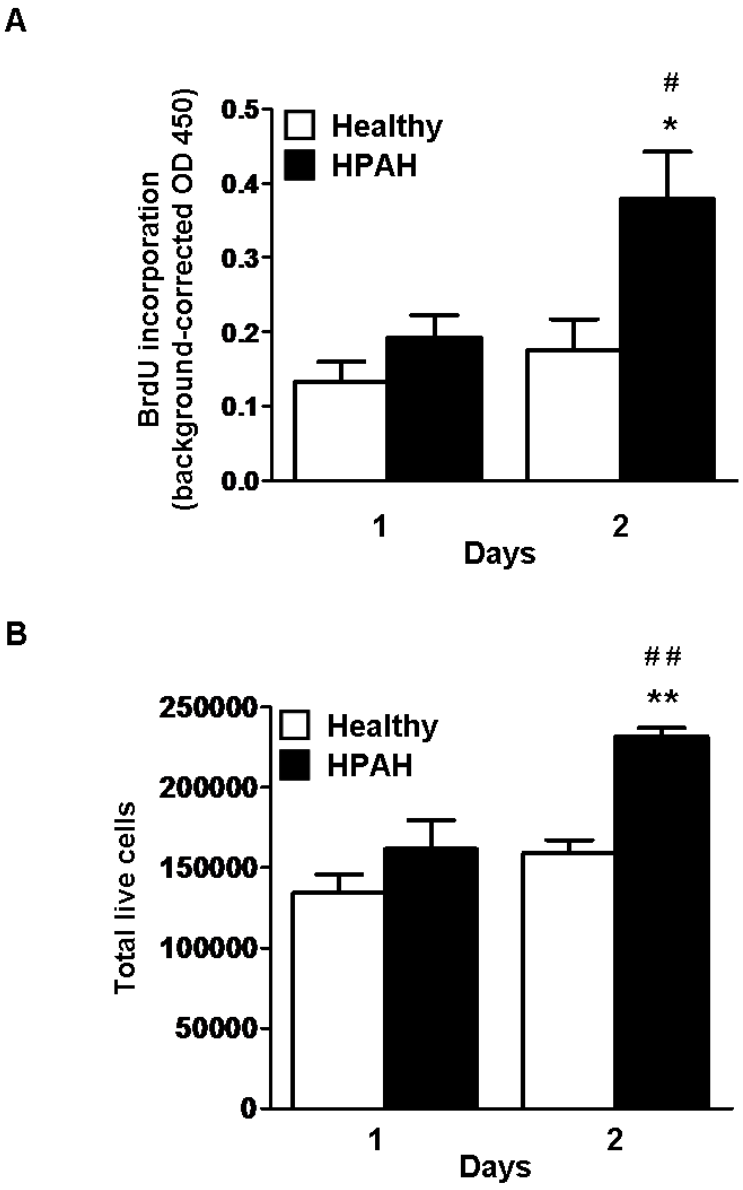

Figure 2. BOECs from HPAH patients have a greater proliferative capacity.
(A) BOECs were plated and at the indicated times, BrdU was added (6 hours, 100 μM) and its incorporation was quantitated by ELISA. Data represent mean ± SEM for control (n=5) and HPAH (n=4). **(B)** BOECs were plated and at the indicated times, total live cells were counted (trypan blue exclusion). Data represent mean ± SEM for control (n=4) and HPAH (n=4). Significant differences were assessed by one-way ANOVA followed by Tukey's Multiple Comparison Test. *$p<0.05$ or **$p<0.01$, HPAH vs. healthy cells at day 2. #$p<0.05$ or ##$p<0.01$, HPAH cells at day 2 vs. HPAH cells at day 1.

2.3.3 Greater Apoptosis Index of BOECs from HPAH

2.3.3.1 Apoptosis Levels by AnnexinV and PI Staining is increased in HPAH

Since endothelial cell apoptosis is a key event in the development of PAH (Jurasz et al., 2010) and that silenced BMPR-II with siRNA leads to apoptosis (Teichert-Kuliszewska et al., 2006), the apoptosis index of BOECs derived from patients with HPAH and compared with BOECs from healthy controls was investigated (Figure 3). A large body of evidence shows that inflammatory response of mammalian cells to tumor necrosis factor-alpha (TNF-α) can be switched to apoptosis by conjunction with cycloheximide, a protein synthesis inhibitor (Konishi et al., 2005; Wang et al., 2005). Flow cytometric analysis was used to study the effects of a 4-hour treatment of TNF-α (10 ng/ml), combined with cycloheximide (CHX, 20 μg/ml), following a 16-hour serum deprivation (EBM-2 with 2% FBS). The percentage of live cells (AnnexinV-negative and PI-negative) was significantly decreased in BOECs from patients with HPAH following the 4-hour incubation period with TNF-α and CHX, compared with a normal medium (EGM-2MV: EBM-2 with 10% FBS) (53.22 $\pm$ 6.28 versus 76.91 $\pm$ 6.69; $P<0.05$) (Figure 3C). The annexinV-positive cells were significantly increased in the HPAH group stimulated with TNF-α and CHX, when compared to normal medium (43.58 $\pm$ 6.49 versus 20.04 $\pm$ 6.76; $P<0.05$) (Figure 3F). The percentage of early-stage apoptotic cells (AnnexinV-positive and PI-negative) in BOECs from patients with HPAH following incubation with the apoptosis inducers was significantly greater than BOECs from healthy controls (37.97 $\pm$ 5.95 versus 23.00 $\pm$ 2.32; $P<0.05$) (Figure 3G). In addition, the percentage of early-stage apoptotic BOECs from patients with HPAH following incubation with TNF-α and CHX was significantly greater when compared with the serum-deprived condition alone (37.97 $\pm$ 5.95 versus 15.72 $\pm$ 2.86; $P<0.01$) (Figure 3G), but also when compared to normal medium (37.97 $\pm$

5.95 versus 11.58 $\pm$ 3.55; P<0.001) (Figure 3G). Moreover, the higher apoptosis index of BOECs derived from patients with HPAH following TNF-α and CHX treatment was also demonstrated by their change in morphology compared with BOECs from healthy controls (Figure 3A). These results suggest that under stress-induced conditions, BOECs from HPAH patients are more susceptible to apoptosis when compared to healthy control cells.

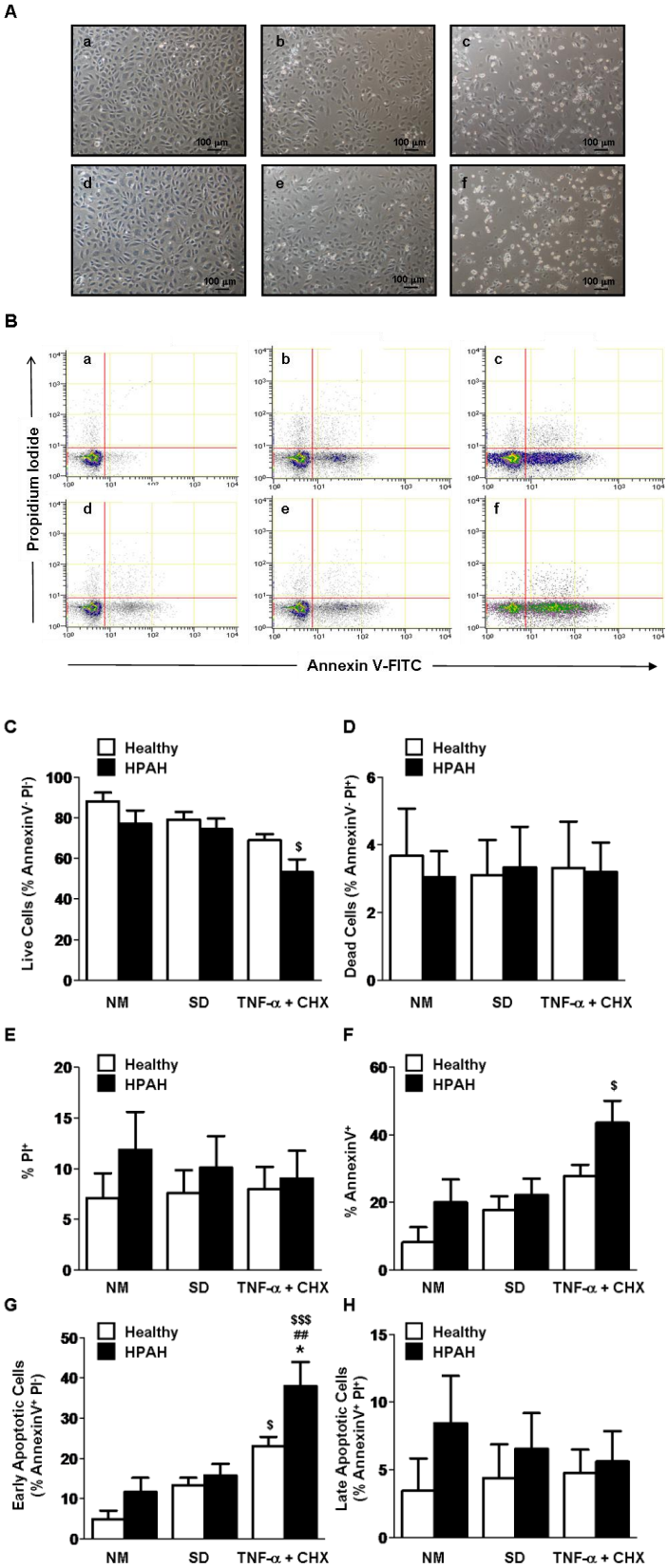
A
a
b
c
d
e
f
100 µm
B
Propidium Iodide
Annexin V-FITC
C
Healthy
HPAH
Live Cells (% AnnexinV- PI-)
NM
SD
TNF-α + CHX
$
D
Dead Cells (% AnnexinV- PI+)
E
% PI+
F
% AnnexinV+
G
Early Apoptotic Cells (% AnnexinV+ PI-)
$$$
##
*
H
Late Apoptotic Cells (% AnnexinV+ PI+)

Figure 3. BOECs from patients with HPAH are more susceptible to apoptosis. **(A)** Representative images of BOECs from healthy individuals (a-c) and from patients with HPAH (d-f) were either incubated in normal (NM) (a and d) or serum-deprived medium (SD) for 16 hours without (b and e) or with tumor necrosis tumor-alpha (TNF-α) and cycloheximide (CHX) (d and f). Scale bar = 100µm. **(B)** Representative scatter plots of propidium iodide (PI) (y-axis) vs. Annexin V-FITC (x-axis). BOECs from healthy individuals (a-c) and from patients with HPAH (d-f) were either incubated in NM (a and d) or SD for 16 hours without (b and e) or with TNF-α and CHX (d and f). Absence of both markers (lower left quadrants) indicates viable cells; PI positive alone (upper left quadrants) indicates cellular necrosis, whereas Annexin V staining alone or together with PI (lower right and upper right quadrants) is indicative of early and late-stage apoptosis, respectively. Color coding represents data distribution densities (high is red→low is blue). **C-G**, Summary data showing the effect of 4 hours of TNF-α (10 ng/ml) together with CHX (20 μg/ml) after a 16 hour incubation in SD medium on the percentage live cells **(B)**, dead cells **(C)**, PI-positive cells **(D)**, annexinV-positive cells **(E)**, or early **(F)** and late-stage apoptosis **(G).** Results are expressed as mean ± SEM (n=5 for healthy and HPAH-derived cells). Significant differences were assessed by one-way ANOVA followed by a post hoc Tukey's Multiple Comparison Test. *$p<0.05$, HPAH vs. healthy treated with TNF-α + CHX, $^{\#\#}p<0.01$, HPAH SD vs. HPAH treated with TNF-α + CHX; $^{\$}p<0.05$, $^{\$\$}p<0.01$, $^{\$\$\$}p<0.001$, HPAH or healthy treated with TNF-α + CHX vs. their respective NM.

2.3.3.2 Caspase-3 Activation is induced in HPAH

To validate the apoptotic effects of the cotreatment of TNF-α with CHX obtained by flow cytometric analysis in BOECs from patients with HPAH and to study its effects on the activation of caspase-3, an infrared immunoassay for human cleaved caspase-3 (Asp 175) was used (Figure 4). Caspase-3 is a cysteine protease that has been reported as an effector of apoptosis in many cell lines (Porter and Janicke, 1999). After the 4-hour incubation period with TNF-α and CHX, the amount of cleaved caspase-3 was significantly increased by 2.7-fold in BOECs from patients with HPAH when compared with BOECs from healthy controls (14.75 ± 3.74 versus 5.37 ± 1.68; $P<0.05$) (Figure 4B). In addition, the amount of cleaved caspase-3 of BOECs from patients with HPAH following incubation with apoptotic inducers was significantly greater by 2.6-fold when compared with the serum-deprived condition alone (14.75 ± 3.74 versus 5.58 ± 0.45; $P<0.01$) (Figure 4B). These results suggest that the activation of caspase-3 contributes, at least partially, to TNF-α/CHX-induced apoptosis in BOECs from patients with HPAH.

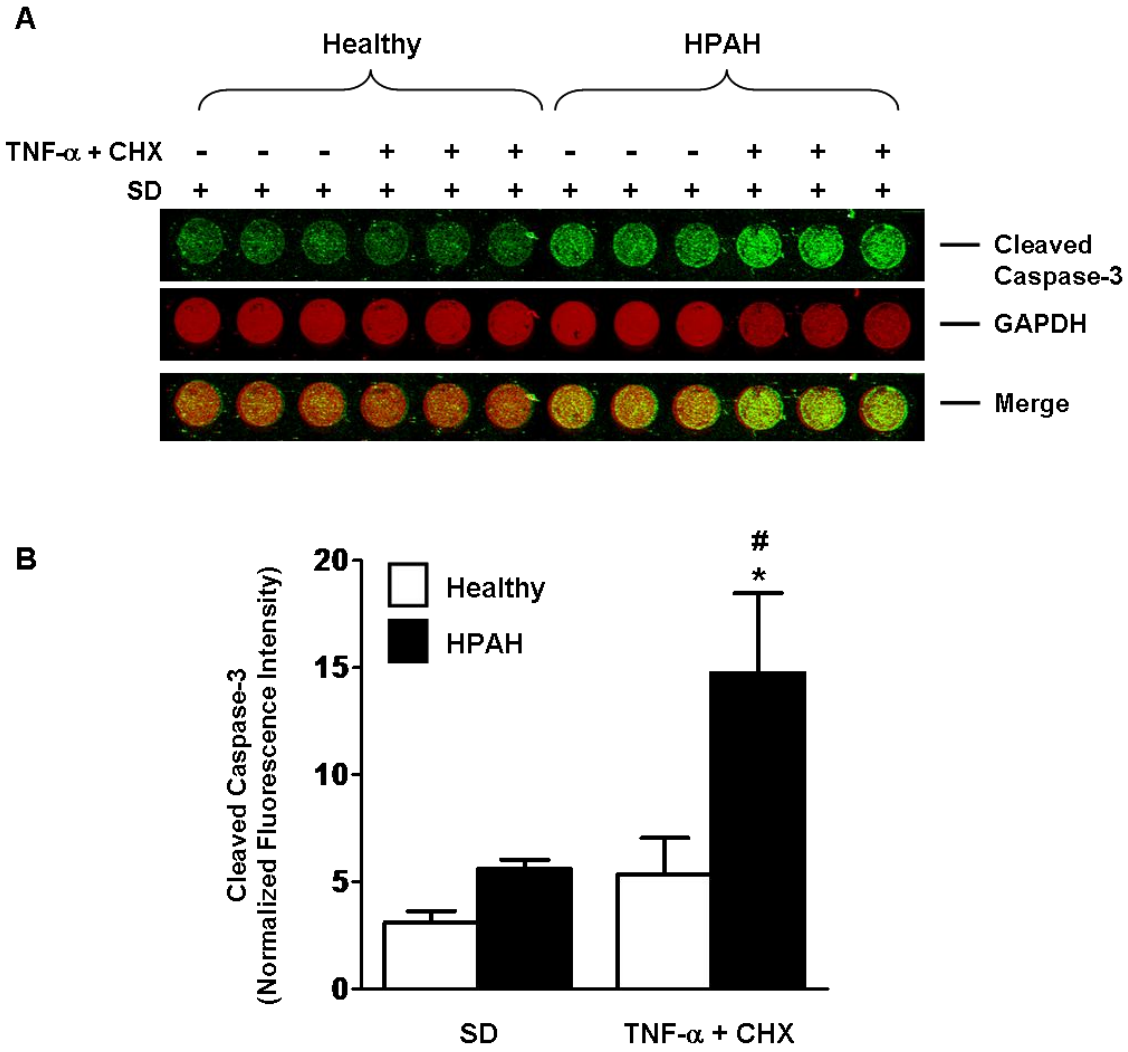

Figure 4. TNF-α and CHX-induced caspase-3 cleavage in BOECs from HPAH patients.

(A) Representative images of human cleaved caspase-3 (Asp175) infrared immunoassay. BOECs from healthy individuals and from patients with HPAH were cultured in 96-well plates and were incubated in serum deprived medium (SD) for 16 hours without or with tumor necrosis tumor-alpha (TNF-α, 10 ng/ml) combined with cycloheximide (CHX, 20 μg/ml) for 4 hours. **(B)** Summary data showing the effect of 4 hours of TNF-α together with CHX after a 16 hour incubation in SD medium on cleaved caspase-3 normalized to total GAPDH. Results are expressed as mean ± SEM (n=4 for healthy controls and HPAH patients). Significant differences were assessed by one-way ANOVA followed by a post hoc Tukey's Multiple Comparison Test *$p<0.05$, HPAH vs. healthy treated with TNF-α + CHX, $^{\#}p<0.05$, HPAH treated with TNF-α + CHX vs. HPAH in SD.

2.3.4 Quantitative Analysis of HPAH Patient-Derived BOEC Protein Profile using 2-D PAGE

2.3.4.1 Differential Protein Expression by 2-D PAGE

To uncover changes in a vast array of proteins that may be involved in the pathogenesis of PAH, the two-dimensional polyacrylamide gel electrophoresis (2-D PAGE) approach combined with Sypro Ruby protein gel stain and mass spectrometry analysis (LC-MS/MS) was used. Moreover, to specifically uncover changes in proteins involved in the BMPR-II activation pathway, a BMP9 treatment was used. BOECs from healthy controls and patients with HPAH were serum-deprived for 16 hours (EBM-2 with 0.1% FBS; SD) before being stimulated with BMP9 (1 ng/ml, 8 hours in SD medium) or not (SD medium only; basal condition). Protein lysates of BOECs from both groups obtained after the BMP9 treatment or under basal conditions were generated. With the 2-D PAGE in-gel protein separation and quantitation approach, proteins that were statistically differently regulated between the BOECs derived from patients with HPAH and healthy controls were quantified and identified (Figure 5).

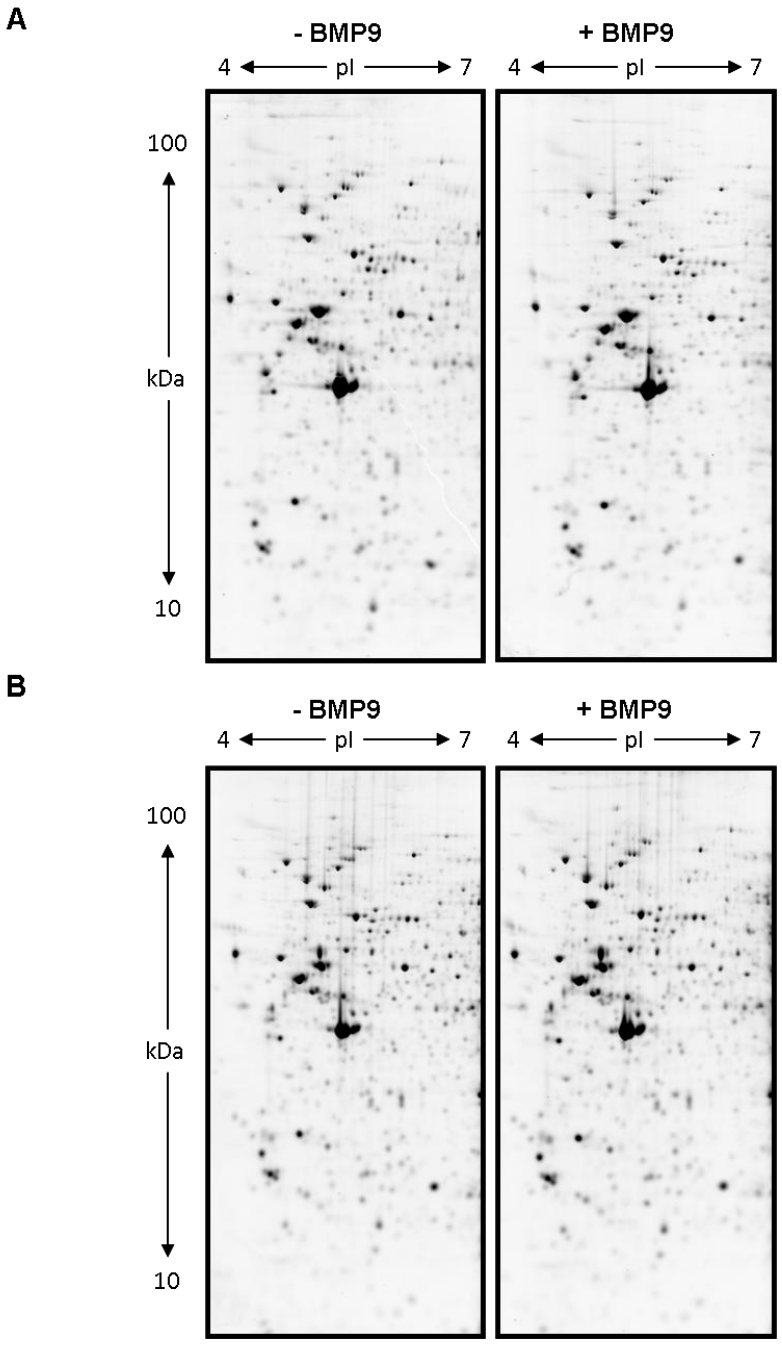

Figure 5. 2-D gel representation of the proteome from BOECs.
(A-B) Representative 2-D gels of protein lysates from BOECs of a healthy individual **(A)** or a patient with HPAH **(B)** treated (right panel) or not (left panel) with BMP9 (1 ng/ml for 8 hours). The gels were stained with Sypro Ruby protein gel stain to visualize the total proteins (proteome) before being scanned and analyzed . pI indicates isoelectric point. Representative gels of n=4 healthy controls and HPAH patients.

2.3.4.2 Differential Protein Expression by 2-D PAGE - Basal Condition

After 2-D PAGE analysis and under defined analysis criteria, a total of 416 proteins were found. Out of the 416 proteins, 22 were identified by Student t-test as differentially expressed ($P<0.05$) in BOECs from patients with HPAH, when compared with healthy control cells without BMP9 treatment (Figure 5). A total of 11 proteins were significantly downregulated in HPAH-derived cells ($<\log_2$ [HPAH/H] of 0.30), and 11 proteins were upregulated ($>\log_2$ [HPAH/H] of 0.30) (Figure 5 and Table 3). Namely, proteins that were found to be upregulated in HPAH were associated with vesicle-mediated transport (copine-1 and perilipin-3), cell proliferation (DNA replication licensing factor MCM7 and eukaryotic peptide chain release factor GTP-binding subunit ERF3A), regulation of apoptosis (26S protease regulatory subunit 7, proteasome activator complex subunit 1 and translationally controlled tumor protein), cell movement (alpha-actinin-1) and with metabolism (l-lactate dehydrogenase B chain, glutathione synthetase and uroporphyrinogen decarboxylase). Of the proteins with downregulated expression in HPAH, 5 were associated with cell movement (alpha-actinin-4, vinculin, pro-collagen-lysine,2-oxoglutarate 5-dioxygenase 3, lamin-B1 and B2), 2 with signal transduction (guanine nucleotide-binding protein G(I)/G(S)/G(T) subunit beta-2 and cAMP-dependent protein kinase type I-alpha regulatory subunit), 1 with regulation of apoptosis (26S protease regulatory subunit 6A), 1 with antigen processing (protein disulfide-isomerase A3) and 1 with ATP hydrolysis coupled protein transport (V-type proton ATPase subunit B, brain isoform). From the analysis under basal conditions (no BMP9 treatment) between HPAH and healthy controls, a volcano plot was generated by plotting the t-test p-value (y-axis; horizontal line represents $P=0.05$) against the relative abundance ratio between HPAH and healthy control samples on a logarithmic scale (x axis; $\log_2$ fold change) (Figure 6). From a total of 416 identified proteins for the proteome, 22 were

significant in differential expression (blue dots, P<0.05) (see Table 3 for a detailed list) (Figure 6).

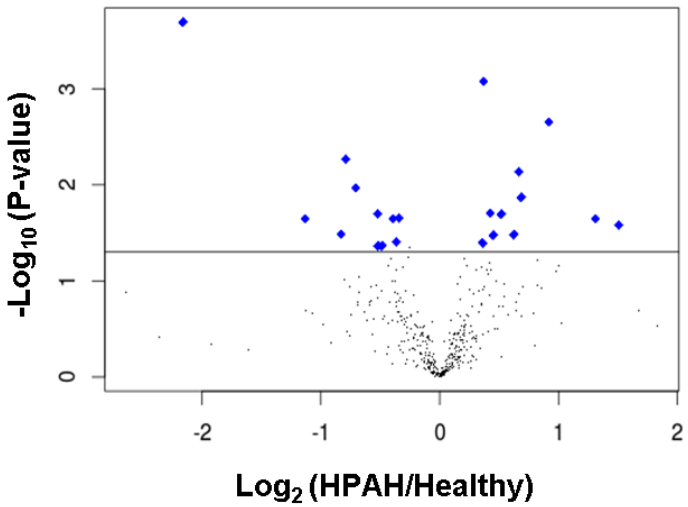

Figure 6. Proteome analysis of BOECs under basal conditions.
A volcano plot was generated by plotting the t-test p-value (y-axis; horizontal line represents p=0.05) against the relative abundance ratio between HPAH and healthy control samples on a logarithmic scale (x-axis; $\log_2$ fold change). From a total of 416 identified proteins for the proteome, 22 were significant in differential expression (blue dots, p<0.05) (see Table 3 for a detailed list). Statistical differences were assessed by Student t-test. p<0.05.

Table 3. LC-MS/MS data of proteins found to be statistically differentially expressed in BOECs from HPAH patients under basal conditions

No.	Protein identity	SWISS-PROT No.	Gene Symbol	MS Score	Nominal mass (Mr):	Calculated pI:	No. of significant peptide matches	Cov. (%)	Log_2 (HPAH/H)	*P*
1	Alpha-actinin-1	P12814	ACTN1	147	102993	5.25	6	22	1.50	0.0262
2	DNA replication licensing factor MCM7	P33993	MCM7	1284	81257	6.08	60	52	1.31	0.0223
3	26S protease regulatory subunit 7	P35998	PSMC2	2208	48603	5.71	99	73	0.92	0.0022
4	Copine-1	Q99829	CPNE1	1141	59022	5.52	43	42	0.69	0.0135
5	L-lactate dehydrogenase B chain	P07195	LDHB	2157	36615	5.71	112	61	0.66	0.0073
6	Perilipin-3	O60664	PLIN3	3009	47018	5.30	105	62	0.62	0.0329
7	Glutathione synthetase	P48637	GSS	705	52352	5.67	39	55	0.52	0.0201
8	Eukaryotic peptide chain release factor GTP-binding subunit ERF3A	P15170	GSPT1	205	55720	5.45	13	34	0.45	0.0333
9	Translationally controlled tumor protein	P13693	TPT1	189	19583	4.84	13	34	0.43	0.0195
10	Uroporphyrinogen decarboxylase	P06132	UROD	95	40761	5.77	7	15	0.37	0.0008
11	Proteasome activator complex subunit 1	Q06323	PSME1	655	28705	5.78	33	46	0.36	0.0403
12	WD repeat-containing protein 61	Q9GZS3	WDR61	456	33560	5.16	20	29	-0.34	0.0222
13	Vinculin	P18206	VCL	488	123722	5.50	26	26	-0.36	0.0395
14	Lamin-B1	P20700	LMNB1	796	66368	5.11	44	53	-0.39	0.0227
15	Procollagen-lysine,2-oxoglutarate 5-dioxygenase 3	O60568	PLOD3	322	84731	5.69	21	32	-0.48	0.0430
16	Lamin-B2	Q03252	LMNB2	1409	67647	5.29	71	57	-0.52	0.0428
17	Alpha-actinin-4	O43707	ACTN4	1458	104788	5.27	70	43	-0.52	0.0200
18	Protein disulfide-isomerase A3	P30101	PDIA3	1515	56747	5.98	64	61	-0.71	0.0106
19	cAMP-dependent protein kinase type I-alpha regulatory subunit	P10644	PRKAR1	720	42955	5.27	30	50	-0.79	0.0053
20	V-type proton ATPase subunit B, brain isoform	P21281	ATP6V1B	729	56465	5.57	37	42	-0.83	0.0328
21	26S protease regulatory subunit 6A	P17980	PSMC3	157	49172	5.13	14	41	-1.13	0.0224
22	Guanine nucleotide-binding protein G(I)/G(S)/G(T) subunit beta-2	P62879	GNB2	445	37307	5.60	23	25	-2.16	0.0002

The protein identities for each spot are listed. The other columns depict the SWISS-PROT No: SWISS-PROT accession number; MS Score: mass spectrometry score indicating the significance of protein identification from peptide mass finger print according to MASCOT software (score value > 50 for $p < 0.05$); Nominal mass (Mr): theoretical molecular weight of the matching protein; Calculated pI: theoretical isoelectric point of the matching protein; No. of significant peptide matches: number of statistically significant peptide matches matching to the protein; Cov (%): percent of identified sequence to the complete sequence of the known protein; Log2 (HPAH/H): relative abundance ratio of the spot between HPAH and healthy control samples (H) on a logarithmic scale; P: p-value calculated by Student's t-test (two-tail, 95% level of confidence).

2.3.4.3 Differential Protein Expression by 2-D PAGE - Post BMP9 Treatment

Following BMP9 treatment in the BOECs derived from healthy controls, 20 proteins were identified by Student t-test as differentially expressed ($P<0.05$) (Figure 5A and Table 4). A total of 9 proteins were significantly downregulated ($<\log_2$ [T/U] of 0.30), and 11 proteins were upregulated ($>\log_2$ [T/U] of 0.30) (Figure 5A and Table 4). Table 4 shows the identification of 18 out of the 20 differentially regulated proteins by BMP9 treatment in the BOECs derived from healthy controls. Of the proteins with increased expression following BMP9 treatment, 3 were associated with cell movement (tubulin beta-3 chain, moesin and dynactin subunit 2), 1 with vesicle-mediated transport (charged multivesicular body protein 4b), 2 with protein ubiquitination (ubiquilin-1 and proteasomal ubiquitin receptor ADRM1), 1 with signal transduction (guanine nucleotide-binding protein G(I)/G(S)/G(T) subunit beta-2), 1 with gene expression (polyadenylate-binding protein 2) and 1 with nuclear protein transport (importin subunit alpha-1). Proteins with decreased expression were associated with cell proliferation (eukaryotic initiation factor 4A-I and eukaryotic translation initiation factor 3 subunit H), cell movement (tubulin beta chain and vinculin), regulation of apoptosis (26S protease regulatory subunit 6A), protein ubiquitination (ubiquitin-like modifier-activating enzyme 1), gene expression (Lupus La protein) and protein repair (protein-L-isoaspartate(D-aspartate) O-methyltransferase).

Following BMP9 treatment in the BOECs derived from patients with HPAH, 10 proteins were identified by Student t-test as differentially expressed ($P<0.05$) (Figure 5B and Table 5). A total of 4 proteins were significantly downregulated in HPAH-derived cells ($<\log_2$ [T/U] of 0.30), and 6 proteins were upregulated ($>\log_2$ [T/U] of 0.30) (Figure 5B and Table 5). Of the proteins with increased expression, 2 were involved in gene expression (14-3-3 portein zeta/delta and heterogeneous nuclear ribonucleoprotein K), 1

in nuclear protein transport (importin subunit alpha-1), 1 in cell movement (tubulin beta chain) and 1 signal transduction (peptidyl-prolyl cis-trans isomerase FKBP4). Of the proteins with decreased expression, 2 were involved in cell movement (actin and vimentin), 1 in protein folding (heat shock protein HSP90-beta) and 1 in gene expression (heterogeneous nuclear ribonucleoprotein H).

When the analysis was conducted between BOECs derived from HPAH patients and healthy controls after BMP9 treatment, a total of 11 proteins were identified by Student t-test as differentially expressed between the two groups ($P<0.05$) (Figure 5 and Table 6). Of the proteins with altered expression between healthy and HPAH after BMP9 treatment, 4 were involved in cell movement (vimentin, plastin-3, actin and pro-collagen-lysine,2-oxoglutarate 5-dioxygenase 3), 1 in signal transduction (protein phosphatase 1 regulatory subunit 7), 1 in protein modification (neutral alpha-glucosidase), 1 in cell proliferation (eukaryotic initiation factor 4A-I) and 2 in regulation of apoptosis (cathepsin D and 26S protease regulatory subunit 6A). The statistically differentially regulated proteins from the different analyses mentioned above were selected to be identified by mass spectrometry using a thermo LTQ linear ion trap mass spectrometer with a nanospray ion source (Table 3-6). The resulting MS/MS spectra were matched to the Mascot database to properly identify the proteins.

Table 4. LC-MS/MS data of proteins found to be statistically differentially expressed in BMP9-treated BOECs derived from healthy subjects

No.	Protein identity	SWISS-PROT No.	Gene symbol	MS Score	Nominal mass (Mr):	Calculated pI:	No. of significant peptide matches	Cov. (%)	Log_2 (T/U) Healthy	*P*
1	WD repeat-containing protein 61	Q9GZS3	WDR61	456	33560	5.16	20	29	0.93	0.0005
2	Importin subunit alpha-1	P52294	KPNA1	308	60211	4.94	14	40	0.84	0.0309
3	Guanine nucleotide-binding protein G(I)/G(S)/G(T) subunit beta-2	P62879	GNB2	445	37307	5.60	23	25	0.73	0.0199
4	Proteasomal ubiquitin receptor ADRM1	Q16186	ADRM1	392	42127	4.96	26	20	0.70	0.0318
5	Polyadenylate-binding protein 2	Q86U42	PABPN1	360	32729	5.04	13	31	0.65	0.0430
6	Moesin	P26038	MSN	1356	67778	6.08	78	71	0.64	0.0205
7	Dynactin subunit 2	Q13561	DCTN2	558	44204	5.10	24	41	0.57	0.0279
8	Tubulin beta-3 chain	Q13509	TUBB3	891	50400	4.83	33	44	0.53	0.0042
9	Ubiquilin-1	Q9UMX0	UBQLN1	274	62479	5.02	14	19	0.44	0.0150
10	Charged multivesicular body protein 4b	Q9H444	CHMP4B	631	24935	4.76	20	42	0.39	0.0403
11	Protein-L-isoaspartate(D-aspartate) O-methyltransferase	P22061	PCMT1	266	24621	6.70	14	36	-0.33	0.0319
12	Eukaryotic initiation factor 4A-I	P60842	EIF4A1	567	46125	5.32	27	48	-0.37	0.0444
13	Vinculin	P18206	VCL	488	123722	5.50	26	26	-0.43	0.0272
14	Eukaryotic translation initiation factor 3 subunit H	O15372	EIF3H	469	39905	6.09	24	31	-0.47	0.0179
15	Ubiquitin-like modifier-activating enzyme 1	P22314	UBA1	493	117774	5.49	24	24	-0.59	0.0450
16	Tubulin beta chain	P07437	TUBB	10239	49639	4.78	426	65	-0.63	0.0254
17	26S protease regulatory subunit 6A	P17980	PSMC3	157	49172	5.13	14	41	-1.27	0.0195
18	Lupus La protein	P05455	SSB	200	46808	6.68	15	26	-1.41	0.0226

Table 5. LC-MS/MS data of proteins found to be statistically differentially expressed in BMP9-treated BOECs derived from HPAH patients

No.	Protein identity	SWISS-PROT No.	Gene symbol	MS Score	Nominal mass (Mr):	Calculated pI:	No. of significant peptide matches	Cov. (%)	Log_2 (T/U) HPAH	*P*
1	WD repeat-containing protein 61	Q9GZS3	WDR61	456	33560	5.16	20	29	0.69	0.0013
2	Heterogeneous nuclear ribonucleoprotein K	P61978	HNRNPK	405	50944	5.39	20	33	0.68	0.0027
3	Importin subunit alpha-1	P52294	KPNA1	308	60211	4.94	14	40	0.60	0.0362
4	Peptidyl-prolyl cis-trans isomerase FKBP4	Q02790	FKBP4	99	51772	5.35	6	17	0.58	0.0142
5	14-3-3 protein zeta/delta	P63104	YWHAZ	737	27728	4.73	26	33	0.47	0.0098
6	Tubulin beta chain	P07437	TUBB	10281	49639	4.78	425	50	0.39	0.0458
7	Heterogeneous nuclear ribonucleoprotein H	P31943	HNRNPH1	418	49198	5.89	22	28	-0.52	0.0299
8	Heat shock protein HSP 90-beta	P08238	HSP90AB1	510	83212	4.97	22	33	-1.48	0.0170
9	Actin, cytoplasmic 1	P60709	ACTB	309	41710	5.29	16	33	-3.00	0.0145
10	Vimentin	P08670	VIM	650	53619	5.06	34	52	-3.96	0.0002

Table 6. LC-MS/MS data of proteins found to be statistically differentially expressed in BMP9-treated BOECs between healthy subjects and HPAH patients

No.	Protein identity	SWISS-PROT No.	Gene symbol	MS Score	Nominal mass (Mr):	Calculated pI:	No. of significant peptide matches	Cov. (%)	Log_2 (T/U) Healthy	Log_2 (T/U) HPAH	*P*
1	Vimentin	P08670	VIM	650	53619	5.06	34	52	1.22	-3.96	0.0001
2	Vimentin	P08670	VIM	888	53619	5.06	52	45	0.76	-0.31	0.0005
3	Vimentin	P08670	VIM	1467	53619	5.06	76	53	0.59	-0.06	0.0084
4	Protein phosphatase 1 regulatory subunit 7	Q15435	PPP1R7	235	41539	4.84	12	31	0.53	0.04	0.0289
5	Plastin-3	P13797	PLS3	1231	70766	5.41	51	36	0.14	-0.11	0.0220
6	Procollagen-lysine,2-oxoglutarate 5-dioxygenase 3	O60568	PLOD3	322	84731	5.69	21	32	0.11	0.37	0.0127
7	Actin, cytoplasmic 1	P60709	ACTB	309	41710	5.29	16	33	-0.04	-3.00	0.0406
8	Eukaryotic initiation factor 4A-I	P60842	EIF4A1	3883	46125	5.32	157	50	-0.16	0.18	0.0270
9	Neutral alpha-glucosidase	Q14697	GANAB	711	106807	5.74	33	34	-0.19	0.11	0.0227
10	Cathepsin D	P07339	CTSD	236	44524	6.10	14	26	-0.30	0.10	0.0289
11	26S protease regulatory subunit 6A	P17980	PSMC3	157	49172	5.13	14	41	-1.27	0.15	0.0476

The protein identities for each spot are listed. The other columns depict the SWISS-PROT No: SWISS-PROT accession number; MS Score: mass spectrometry score indicating the significance of protein identification from peptide mass finger print according to MASCOT software (score value > 50 for $p < 0.05$); Nominal mass (Mr): theoretical molecular weight of the matching protein; Calculated pI: theoretical isoelectric point of the matching protein; No. of significant peptide matches: number of statistically significant peptide matches matching to the protein; Cov (%): percent of identified sequence to the complete sequence of the known protein; Log2 (HPAH/H): relative abundance ratio of the spot between HPAH and healthy control samples (H) on a logarithmic scale; T: treated with BMP9; U: untreated with BMP9; P: p-value calculated by Student's t-test (two-tail, 95% level of confidence).

2.3.4.4 Differential Protein Phosphorylation by 2-D PAGE

Protein lysates of BOECs from both groups obtained after the BMP9 treatment or under basal conditions were used in the 2-D PAGE approach for phosphoprotein profiling using ProQ Diamond phosphoprotein gel stain combined with LC-MS/MS analysis. With this in-gel protein separation and quantitation approach, phosphoproteins that were statistically and differently regulated between the BOECs derived from patients with HPAH and healthy controls, with or without BMP9 treatment (Figure 7), were quantified and identified.

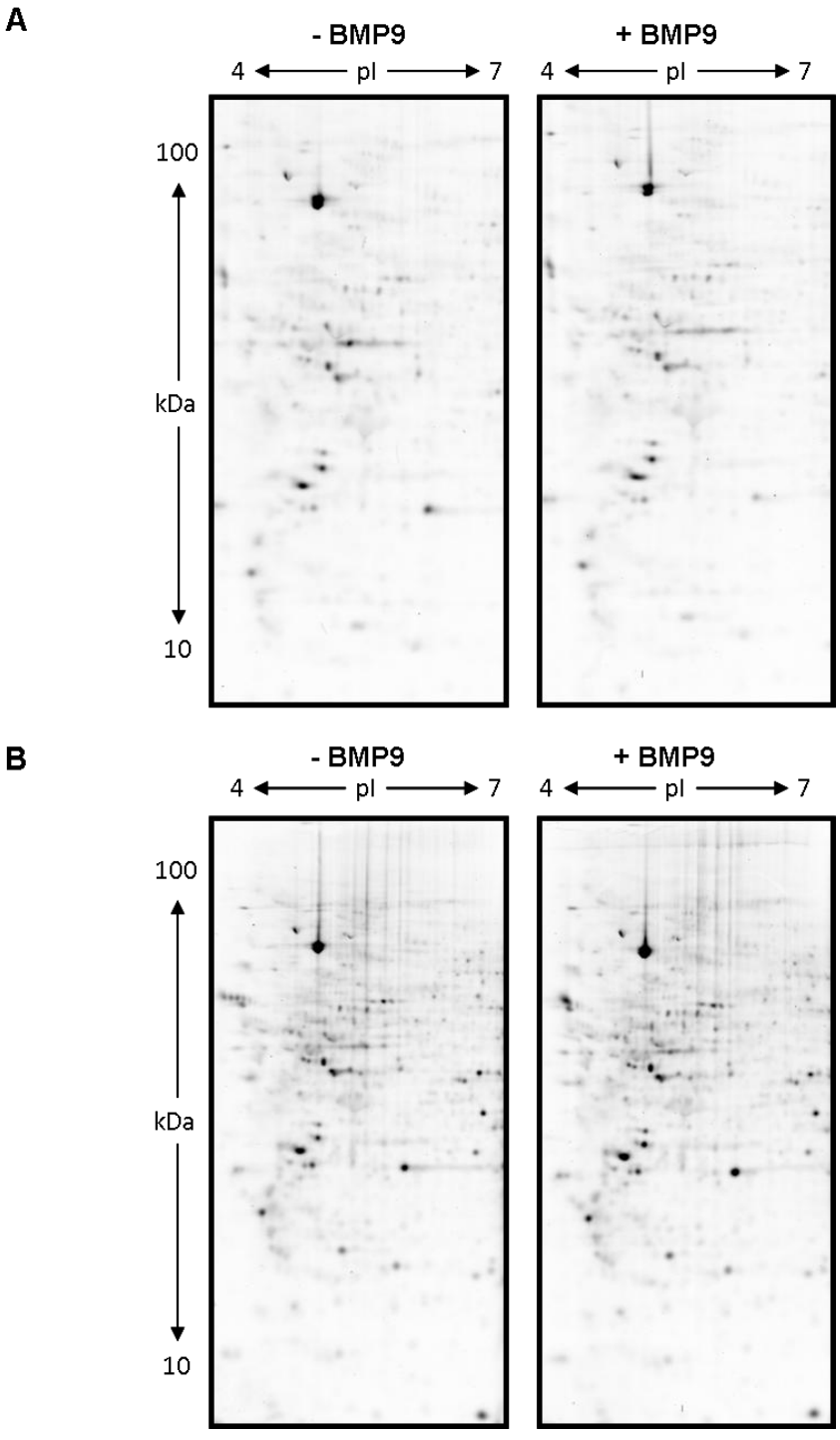

Figure 7. 2-D gel representation of the phosphoproteome from BOECs.
(A-B) Representative 2-D gels of protein lysates from BOECs of a healthy individual **(A)** or a patient with HPAH **(B)** treated (right panel) or not (left panel) with BMP9 (1 ng/ml for 8 hours). The gels were stained with ProQ Diamond phosphoprotein gel stain to visualize the phopshoproteins (phosphoproteome) before being scanned and analyzed. pI indicates isoelectric point. Representative gels of n=4 healthy controls and patients with HPAH.

2.3.4.5 Differential Protein Phosphorylation by 2-D PAGE - Basal Condition

After 2-D PAGE analysis under defined criteria, a total of 283 phosphoproteins were found. A total of 23 were identified by Student t-test as differentially expressed ($P<0.05$) in BOECs from patients with HPAH, when compared with healthy control cells without BMP9 treatment (Figure 7). One phosphoprotein was significantly downregulated in HPAH-derived cells ($<\log_2$ [HPAH/H] of 0.30) and 22 phosphoproteins were upregulated ($>\log_2$ [HPAH/H] of 0.30) (Figure 7 and Table 7). Due to the low abundance of these phosphoproteins, the identification of only 7 out of the 23 phosphoproteins was achieved (Table 7). The identified proteins with increased expression included proteins involved in cell movement (actin, vimentin and alpha-actinin-4), gene expression (ATP-dependent DNa helicase 2 subunit 2), signal transduction (chloride intracellular channel protein 1), regulation of apoptosis (26S protease regulatory subunit 7) and protein folding (T-complex protein 1 subunit gamma). From the analysis under basal conditions (no BMP9 treatment) between HPAH and healthy controls, a volcano plot was generated by plotting the t-test p-value (y-axis; horizontal line represents $P=0.05$) against the relative abundance ratio between HPAH and healthy control samples on a logarithmic scale (x axis; $\log_2$ fold change) (Figure 8). From a total of 283 identified phosphoproteins, 23 proteins were significant in differential expression (blue dots, $P<0.05$) (Figure 8 and Table 7).

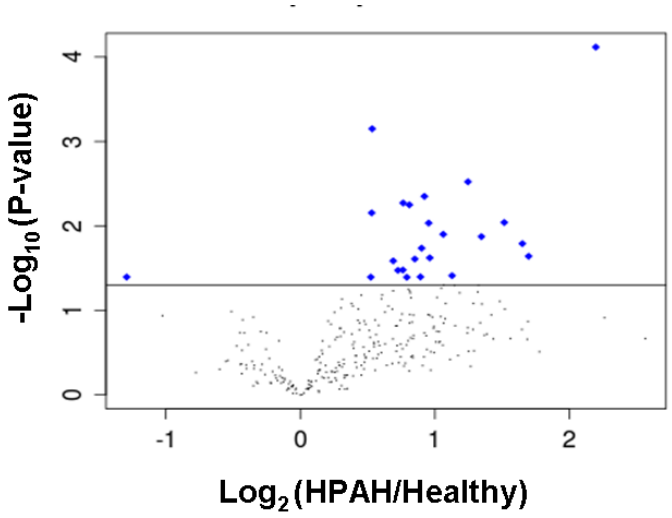

Figure 8. Phosphoproteome analysis of BOECs under basal conditions.
A volcano plot was generated by plotting the t-test p-value (y-axis; horizontal line represents p=0.05) against the relative abundance ratio between HPAH and healthy control samples on a logarithmic scale (x-axis; log_2 fold change). From a total of 283 identified phosphoproteins, 23 phosphoproteins were significant in differential expression (blue dots, $p<0.05$). Statistical differences were assessed by Student t-test. $p<0.05$.

2.3.4.6 Differential Protein Phosphorylation by 2-D PAGE - Post BMP9 Treatment

BMP9 treatment of BOECs from healthy controls led to the finding of 17 differentially regulated phosphoproteins, 2 of which were found to be downregulated ($<\log_2$ [T/U] of 0.30) and 15 to be upregulated ($>\log_2$ [T/U] of 0.30) (Figure 7A and Table 8). Again, due to the low abundance of these phosphoproteins, the identification of only 3 out of 17 phosphoproteins was achieved (Table 8). One protein with increased expression was identified and is involved in gene expression (nucleosome assembly protein 1-like 4). Of the 2 proteins identified with decreased expression, 1 was found to be involved in cell movement (alpha-actinin-4) and 1 in regulation of apoptosis (26S protease regulatory subunit 7). Following BMP9 treatment in BOECs derived from patients with HPAH, 8 phosphoproteins were identified by Student t-test as differentially expressed ($P<0.05$) (Figure 7B). A total of 1 phosphoprotein was significantly downregulated in HPAH-derived cells ($<\log_2$ [T/U] of 0.30) and 7 phosphoproteins were upregulated ($>\log_2$ [T/U] of 0.30) after BMP9 treatment (Figure 7B). Unfortunately, none of these could be identified by mass spectrometry analysis due to their low abundance. When the analysis was conducted between BOECs derived from patients with HPAH and healthy controls treated with BMP9, a total of 12 phosphoproteins were identified by Student t-test as differentially regulated between the two groups after the treatment ($P<0.05$) (Figure 7 and Table 9). The identity of 2 out of 12 phosphoproteins was found by mass spectrometry (Table 9). One protein was found to be involved in signal transduction (chloride intracellular channel protein 1) and 1 in the regulation of apoptosis (proteasome activator complex subunit 2). All 9 unique phosphoproteins found through the different analyses have been previously described as phosphoproteins (PhosphoSite databases) and 2 out of 9 have been identified based on peptides containing phosphorylated residues, giving a good indication of the reliability of the ProQ Diamond

phosphoprotein gel staining method used. The statistically differentially regulated phosphoproteins from the different analyses mentioned above were selected to be identified by mass spectrometry, as explained in section 2.4.4.1 (Table 7-9**)**.

Table 7. LC-MS/MS data of phosphoproteins found to be statistically differentially expressed in BOECs from HPAH patients

No.	Protein identity	SWISS-PROT No.	Gene Symbol	MS Score	Nominal mass (Mr):	Calculated pI:	No. of significant peptide matches	Cov. (%)	Log_2 (HPAH/H)	*P*
1	Vimentin	P08670	VIM	393	53619	5.06	18	54	0.89	0.8927
2	Actin	P60709	ACTB	861	41710	5.29	47	51	1.52	0.0405
3	Chloride intracellular channel protein 1	O00299	CLIC1	5352	26906	5.09	192	83	1.35	0.0336
4	Alpha-actinin-4	O43707	ACTN4	10349	104788	5.27	389	83	0.95	0.0162
5	26S protease regulatory subunit 7	P35998	PSMC2	1384	48603	5.71	70	76	1.25	0.0126
6	ATP-dependent DNA helicase 2 subunit 2	Q04437	YKU80	3862	82652	5.55	151	79	0.85	0.0070
7	T-complex protein 1 subunit gamma	P49368	CCT3	3951	60495	6.10	150	75	0.90	0.0056

Table 8. LC-MS/MS data of phosphoproteins found to be statistically differentially expressed in BMP9-treated BOECs derived from healthy subjects

No.	Protein identity	SWISS-PROT No.	Gene Symbol	MS Score	Nominal mass (Mr):	Calculated pI:	No. of significant peptide matches	Cov. (%)	Log_2 (T/U) Healthy	*P*
1	Nucleosome assembly protein 1-like 4	Q99733	NAP1L4	332	42797	4.60	16	29	1.14	0.0019
2	Alpha-actinin-4	O43707	ACTN4	10349	104788	5.27	389	83	-0.80	0.0474
3	26S protease regulatory subunit 7	P35998	PSMC2	1384	48603	5.71	70	76	-0.73	0.0295

Table 9. LC-MS/MS data of phosphoproteins found to be statistically differentially expressed in BMP9-treated BOECs between healthy subjects and HPAH patients

No.	Protein identity	SWISS-PROT No.	Gene Symbol	MS Score	Nominal mass (Mr):	Calculated pI:	No. of significant peptide matches	Cov. (%)	Log_2 (T/U) Healthy	Log_2 (T/U) HPAH	*P*
1	Chloride intracellular channel protein 1	O00299	CLIC1	5352	26906	5.09	192	83	-1.06	-0.10	0.0362
2	Proteasome activator complex subunit 2	Q9UL46	PSME2	514	27344	5.44	20	74	-0.56	-0.12	0.0139

The protein identities for each spot are listed. The other columns depict the SWISS-PROT No: SWISS-PROT accession number; MS Score: mass spectrometry score indicating the significance of protein identification from peptide mass finger print according to MASCOT software (score value > 50 for $p < 0.05$); Nominal mass (Mr): theoretical molecular weight of the matching protein; Calculated pI: theoretical isoelectric point of the matching protein; No. of significant peptide matches: number of statistically significant peptide matches matching to the protein; Cov (%): percent of identified sequence to the complete sequence of the known protein; Log2 (HPAH/H): relative abundance ratio of the spot between HPAH and healthy control samples (H) on a logarithmic scale; T: treated with BMP9; U: untreated with BMP9; P: p-value calculated by Student's t-test (two-tail, 95% level of confidence).

2.3.5 BMP9 Treatment Global Effect on the Phosphoproteome

Interestingly, when computing the number of undetected phospho spots before and after BMP9 treatment in BOECs from healthy controls and patients with HPAH, a striking difference was seen between the two groups (Figure 9). After BMP9 treatment, healthy cells had less undetected phospho spots, as they responded to the BMP9 treatment, which led to phosphorylation of proteins (179 ± 32 versus 84 ± 20; $P<0.05$) (Figure 9). In contrast, undetected phospho spots in BOECs derived from patients with HPAH were already found in lower numbers, under basal conditions, and BMP9 treatment did not affect it (30 ± 7 versus 20 ± 5) (Figure 9), indicating that phosphorylation events had already taken place before BMP9 treatment for the proteins visualised by the ProQ Diamond phosphoprotein stain. Moreover, under basal conditions, there was a significant difference between the number of undetected phospho spots in the BOECs derived from healthy controls and patients with HPAH (179 ± 32 versus 30 ± 7; $P<0.001$) (Figure 9), suggesting that cells from the patients have a hyperactivation state regarding their pattern of phosphorylation for the proteins represented in the 2-D PAGE experiment. Of note, further studies will have to be done to validate this observation.

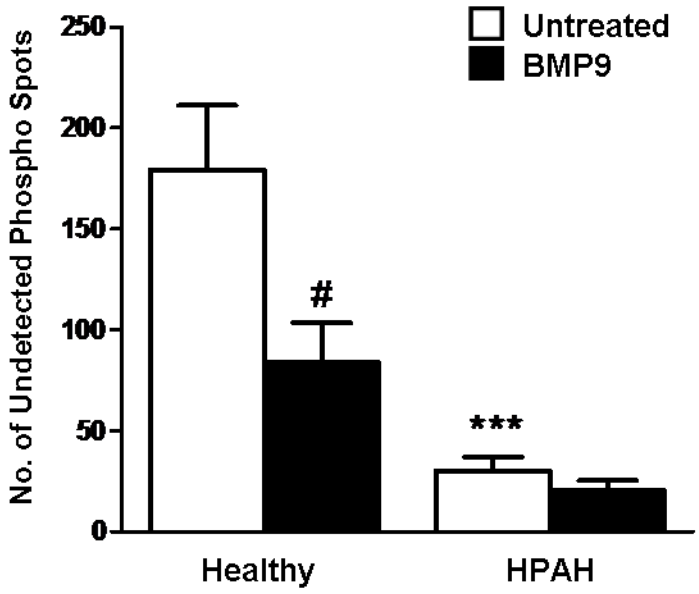

Figure 9. Number of undetected phospho spots in BOECs.
Number of undetected spots from the phosphoproteome analysis of BOECs for healthy controls and patients with HPAH treated or not with BMP9 (1 ng/ml for 8 hours). Data represent mean ± SEM for healthy controls (n=4) and HPAH (n=4). Significant differences were assessed by one-way ANOVA followed by Tukey's Multiple Comparison Test. ***$p<0.001$, HPAH vs. healthy cells untreated. $^{\#}p<0.05$, Healthy cells treated with BMP9 vs. untreated.

2.3.6 Validation of BMP9 Treatment by BMPR-II Canonical Targets

To validate the efficacy of the BMP9 treatment that was used with the BOECs for the 2-D PAGE experiments, the activation status of two targets of the BMPR-II canonical signaling pathway (phospho-Smad 1/5/8 and Id1) was evaluated by immunoblotting (Figure 10). After treatment of BOECs by BMP9 (1 ng/ml, 8 hours), phospho-Smad 1/5/8 (P-Smad 1/5/8) levels were significantly greater in both groups when compared with basal conditions (Healthy: 0.67 ± 0.08 versus 0.19 ± 0.02; $P<0.05$ and HPAH: 0.56 ± 0.11 versus 0.22 ± 0.03; $P<0.05$) (Figure 10B). Id1 levels were also significantly elevated in BOECs from both groups once treated by BMP9 (Healthy: 0.62 ± 0.07 versus 0.19 ± 0.03; $P<0.05$ and HPAH: 1.24 ± 0.30 versus 0.33 ± 0.12; $P<0.05$) (Figure 10C). These results indicate that the BMP9 treatment used in this study was effective, at least in regards to activating these two classic targets. Since the activation of the canonical targets in HPAH-derived BOECs was unexpected based on the fact that a mutated copy of the *BMPR2* gene has been described in some studies using PASMCs (Yang et al., 2008; Yang et al., 2005) to lead to loss-of-function of BMPR-II signaling, the BMP9-mediated Id1 induction was further confirmed in human pulmonary artery endothelial cells (HPAECs) after siRNA knockdown of BMPR-II (Appendix A). Indeed, Id1 levels in HPAECs treated with BMP9 (1 ng/ml) 1, 4 and 8 hours after BMPR-II silencing were not decreased and were sustained throughout the 8-hour induction (Appendix A), suggesting that reduced levels of BMPR-II in BOECs do not lead to loss-of-function of the BMPR-II canonical signaling pathway.

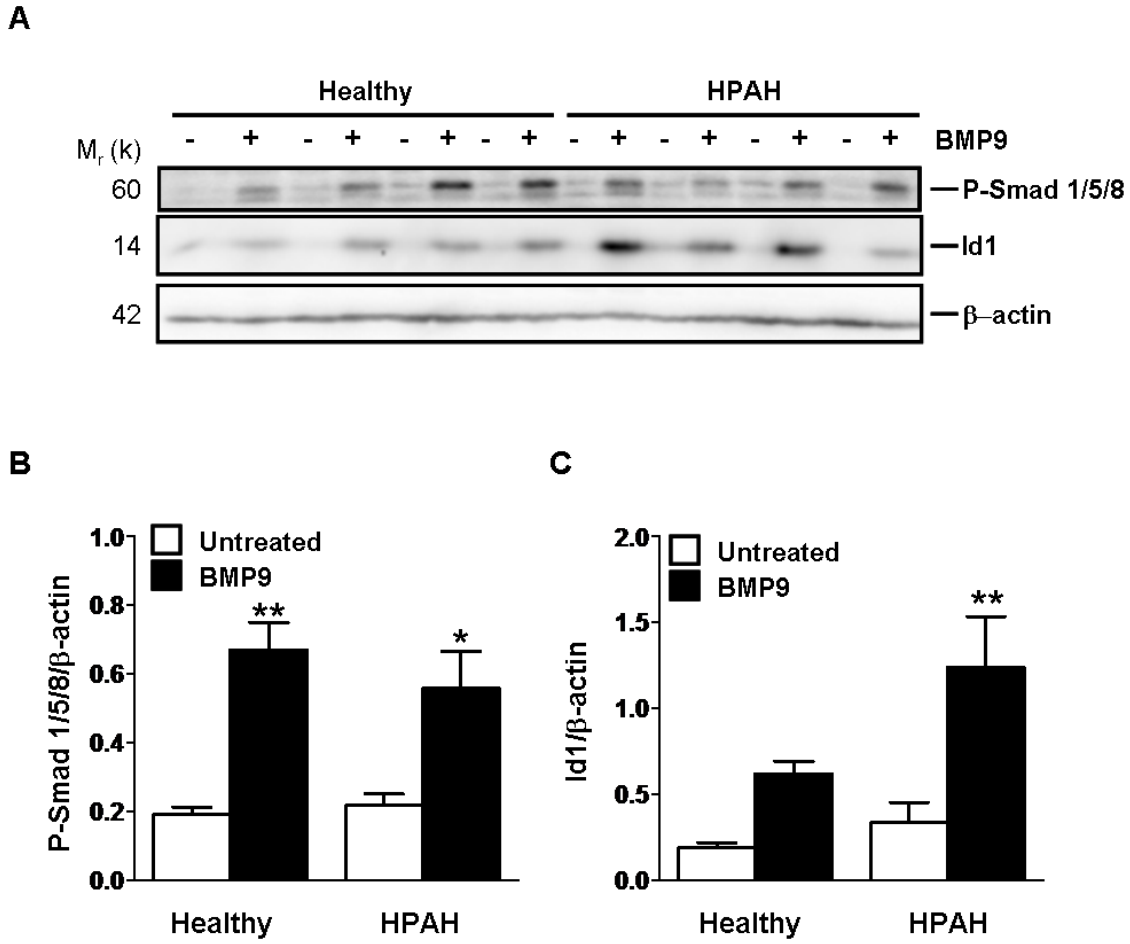

Figure 10. Activation status of P-Smads 1/5/8 and Id1 in BOECs.
(A) Representative images of activation of the canonical Phospho-Smad 1/5/8 signaling pathway in response to BMP9 in healthy- (n=4) or HPAH- (n=4) derived BOECs. Serum-deprived cells (16 hours, EBM-2 with 0.1% FBS) were treated with BMP9 (1 ng/ml) or serum-deprived medium (EBM-2 with 0.1% FBS) alone for 8 hours. Protein lysates were immunoblotted for phosphorylated Smad1/5/8 (P-Smad 1/5/8) **(B)** and the Smad-dependent canonical BMP transcriptional target Id1 **(C)**. Results are expressed as mean ± SEM and as an expression relative to β-actin. Significant differences were assessed by one-way ANOVA followed by Tukey's Multiple Comparison Test. **p<0.01, *p<0.05; untreated vs. treated with BMP9 either for healthy cells or for HPAH-derived cells.

2.4 Discussion

2.4.1 Endothelial Cell Dysfunction in PAH

PAH is a progressive vascular disorder characterized by dysregulated smooth muscle and endothelial cell survival/growth leading to vascular obliteration and remodeling of the pre-capillary pulmonary arteries (Humbert et al., 2004a). Although the precise sequence of events that initiates this disease and leads to vascular remodeling still remains unclear, EC apoptosis has been increasingly recognised as a trigger mechanism (Gaine and Rubin, 1998; Jurasz et al., 2010; Stenmark and Mecham, 1997). The most significant contribution to the PAH field is undoubtedly the identification, in 2000, of heterozygous germline mutations in the *BMPR2* gene of patients with PAH (Atkinson et al., 2002; Lane et al., 2000; Tuder et al., 2001). However, since that seminal discovery, there have been only a few studies examining the functional impact of these mutations on relevant vascular cells. For example, the Stewart lab was the first to describe phenotypic alterations, such as increased apoptosis in endothelial progenitor cells from patients with PAH (Teichert-Kuliszewska et al., 2006; Tuder et al., 1994). The Morrell group has used blood-outgrowth endothelial cells (BOECs) to investigate the impact of the *BMPR2* mutations on their functionality and has shown that patient-derived cells have a hyperproliferative phenotype with impaired ability to form vascular structures, compared to control subjects (Toshner et al., 2009). Altogether, these reports highlight that the presence of mutations in the *BMPR2* gene prediposes to EC apoptosis, which may contribute to disease progression, including endothelial dysfunction, the direct loss of precapillary arteriolar continuity and the remodeling of the pre-capillary pulmonary arteries.

In this thesis, patient-specific BOECs were used to better understand the molecular etiology of PAH in relation to EC dysfunction. Since these BOECs were derived from circulating mononuclear cells, which have not been directly exposed to the disease environment in the lungs, they offered the possibility of studying the molecular cues in endothelial cells that could potentially be the initiating events in PAH. The functional differences in BOECs from patients with HPAH was studied first, in regards to their survival and growth potential, and then used in an unbiased proteomic approach to unravel new molecular targets that could be involved in the EC dysfunction described in PAH. Previous studies have shown that BMPR-II expression is reduced in the pulmonary vasculature of PAH patients, whether they harbor mutations in the *BMPR2* gene or not (Atkinson et al., 2002). This finding was confirmed in this work by immunoblotting analysis of the protein lysates from BOECs derived from five patients with heterozygous mutations to the coding region of *BMPR2,* and from one patient with HPAH with a GC > AT double-substitution mutation 944 bp upstream of the translation start site (i.e. c.*-944/5GC > AT); altogether BMPR-II levels were reduced by 64% in the HPAH group compared with healthy control group. Additional evidence was provided in this thesis in relation to BOECs derived from patients with HPAH harboring *BMPR2* mutations, being more susceptible to apoptosis than healthy control cells. A 1.7-fold increase in the percentage of early-stage apoptotic cells in HPAH-derived BOECs compared with healthy controls, under stress-induced apoptosis (TNF-α in combination with cycloheximide), was found. As well, an increased of 2.7-fold in cleaved caspase-3 from HPAH-derived BOECs was found under these same conditions. These findings are in line with a previous study from our group, in which we showed that *BMPR2* gene silencing with siRNA in PAECs led to a more than 2-fold increase in apoptosis (Teichert-Kuliszewska et al., 2006). In addition to an increase susceptibility of HPAH-derived cells to stress-induced apoptosis, I also found that under normal conditions, HPAH-derived

cells harboring *BMPR2* mutations exhibited a 2.1-fold increase in BrdU incorporation compared with healthy control cells, as well as a 1.5-fold change increase in total live cells. These results indicate that BOECs derived from patients with HPAH harboring mutations in the *BMPR2* gene, have phenotypic alterations relating to their survival and growth. These observations are in line with the concept of endothelial cell apoptosis being a trigger in PAH that may lead to the selection of apoptotic-resistant and hyperproliferative cells causing the complex vascular lesions seen in the lung pathology (Jurasz et al., 2010; Taraseviciene-Stewart et al., 2001; Tuder et al., 1994).

2.4.2 2-D Gel-based Proteomic Approach to Unravel New Molecular Targets in PAH

In this thesis, multiplex-staining of high-resolution 2-D gels for proteins (Sypro Ruby) and phosphoproteins (Pro-Q Diamond) was used as a strategy for quantifying protein/phosphoprotein changes in BOECs of HPAH patients. This approach combined with imaging software analysis (PDQuest), spot picking (spot cutter), mass spectrometry analysis (LC-MS/MS) and statistical analysis (Student t-test) allowed protein and phosphoprotein high resolution profiling and quantitation. To ensure a good reproductility of the 2-D gel staining approach, technical duplicates were done independently for each of the BOEC sample for a total of thirty-two 2-D gels. The Sypro Ruby protein gel stain is a total protein stain that is quantitative over three orders of magnitude with a lower detection limit of 0.25 to 1 ng. ProQ Diamond phosphoprotein gel stain allows in-gel detection of phosphate groups attached to tyrosine, serine or threonine residues and depending on the phosphorylation state of the protein, it allows detection of as little as 1 to 16 ng of phosphoprotein per band. It also has a linear dynamic range over three orders of magnitude. It should be noted that a quantitative change in the intensity of a phosphoprotein spot can result either from a difference in the amount of its abundance or its phosphorylation status. In theory, this multiplex staining approach allows the

determination of the ratio of ProQ Diamond dye to Sypro Ruby dye signal intensities for each spot, providing a measure of the phosphorylation level normalised to the total amount of protein. Hence, this multiplex staining approach would allow the detection of a highly phosphorylated protein of low total abundance and vice versa. However, matching the phosphorylated spots with their corresponding total spots with the PDQuest software was not as straightforward as expected. Most of the phosphorylated spots were barely detectable by Sypro Ruby gel stain, as well as by mass spectrometry analysis, suggesting a high degree of phosphorylation level with a low total abundance level. Therefore, matching all the phosphorylated spots with their corresponding total spots was not accurate enough to be executed with the PDQuest software. As a result, relative quantitation was not executed in this work. It is therefore not possible to know if the increase in intensity of a particular phosphoprotein was due to a higher phosphorylation state or a higher abundance. Further studies examining the phosphorylation status over the total abundance of each selected candidates would have to be pursued by other approaches, such as immunoblotting.

Two major limitations were encountered in this study: limited access to cell material and limited use of protein sample to load for an analytical approach with the 2-D gel method (ranging from 100 to 200 micrograms of proteins), which led to the use of whole protein lysate. Indeed, no enrichment method could be used in this work since these techniques require a great amount of protein (i.e. milligrams) and hence, a great number of cells. BOECs had to be expanded up passage 3 in order to secure a few vials for the entire study and since the cells have limited proliferative potential, they were used between passage 4 to 8 and, in rare instances, up to passage 12 for some of the HPAH-derived samples with higher proliferative potential. The use of 100 micrograms of whole protein lysate therefore limited the dynamic range of proteins that could be studied and led to the

overrepresentation of high abundant proteins. The results obtained from the analyses conducted for the proteome and phosphoproteome of the BOECs were therefore mainly based on the dysregulation of the most abundant proteins.

2.4.3 Functional Annotation of Proteins Found to be Differentially Regulated between Healthy and HPAH

Highthroughput technologies, such as microarray-based gene expression profiling and mass spectrometry have been recently employed to study the molecular basis of PAH. These studies using lung tissues (Abdul-Salam et al., 2010), plasma samples (Abdul-Salam et al., 2006; Yu et al., 2007; Yuditskaya et al., 2009) and transformed lympocytes (Meyrick et al., 2008) revealed that the expression level of genes and proteins involved in key pathways, such as proliferation, apoptosis, metabolism and protein ubiquitination, differ significantly between healthy and patients with PAH. Protein expression profiling using relevant patient-derived endothelial cells (BOECs) thus appeared as an effective approach to define the molecular cues that underlie the endothelial cell dysfunction in PAH. This study indeed allowed to gain additional insights into the molecular basis of PAH with the identification of interesting candidates involved in important functions which are relevant to the disease.

The proteomics findings resulting from the published studies and ours support the concept that patients with PAH demonstrate abnormalities in pathways of cell proliferation, apoptosis, signal transduction, protein ubiquitination and signal transduction. Of interest, proteins involved in signal transduction found through this 2-D gel approach (chloride intracellular channel 1, guanine nucleotide-binding protein G(I)/G(S)/G(T) subunit beta-2 and cAMP-dependent protein kinase type-I alpha regulatory subunit) are known to be altered in PAH. Chloride intracellular channel 1

(CLIC1), found to have increased levels of phosphorylation in HPAH in this study, was previously shown to be have increased abundance levels in lungs of MCT- and chronic hypoxia-induced PAH (Laudi et al., 2007) and of PAH patients (Abdul-Salam et al., 2010). CLIC1, a member of the highly evolutionarily conserved CLIC family of chloride ion channel proteins, exhibits both nuclear and plasma membrane chloride ion channel activity (Warton et al., 2002). Two other interesting proteins involved in signal transduction were found to have decreased abundance levels in HPAH: guanine nucleotide-binding protein G(I)/G(S)/G(T) subunit beta-2 and cAMP-dependent protein kinase type-I alpha regulatory subunit, both proteins involved in the cAMP signal transduction pathway (Barradeau et al., 2002) known to be important in PAH. Guanine nucleotide-binding proteins (G proteins) superfamily consist of heterodimeric complexes of distinct alpha, beta and gamma subunits and are involved as transducers in various transmembrane signaling systems (Eglen et al., 2007). Specifically, the beta chain is required for the GTPase activity, for replacement of GDP by GTP, and for G protein-effector interaction (Eglen et al., 2007). Of note, guanine nucleotide-binding protein G(I)/G(S)/G(T) subunit beta-2 was also found to be significantly increased in BOECs from healthy controls after BMP9 treatment, suggesting that this molecular transducer is involved in the BMPR-II pathway. cAMP-dependent protein kinase type-I alpha regulatory subunit is one of the two regulatory chains of protein kinase A (PKA) (Barradeau et al., 2002). Decreased cAMP levels has been documented in pulmonary arteries from chronic hypoxia-induced PAH in rats and PASMCs isolated from PAH patients (Maclean et al., 1997; MacLean et al., 1996; Murray et al., 2007). Current therapies in PAH include drugs that increase cellular content of cAMP (e.g isoproterenol, prostaglandins and prostacyclins) aiming at regulating vascular tone, cellular proliferation, and hypertrophy, which are known mechanisms that remodel the pulmonary artery (Galie et al., 2005; Rubin et al., 2011).

Proteins involved in cell proliferation, such as DNA replication licensing factor MCM7 and eukaryotic peptide chain release factor GTP-binding subunit ERF3A, were found to have increased abundance levels in HPAH-derived BOECs compared with healthy controls. These findings are in line with the experimental findings shown in this thesis and by others by which vascular cells in PAH have a higher proliferative potential (Taraseviciene-Stewart et al., 2001; Tuder et al., 2001). DNA replication licensing factor MCM7 is a component of the pre-replicative complex required for unwinding of origin DNA before DNA replication occurs (Stoeber et al., 2001). Interestingly, MCM (miniature chromosome maintenance) proteins are highly expressed in malignant human cancers cells, including endometrial carcinoma (Li et al., 2005), melanoma (Gambichler et al., 2009) and colorectal adenocarcinoma (Nishihara et al., 2008). Liu et al. have recently reported that MCM7 in tumor tissues may be potential markers of a poor prognosis for non-small-cell lung cancer (NSCLC) patients (Liu et al., 2012). In addition, Fujioka et al. have shown that MCM7 is an independent prognostic marker in lung adenocarcinomas with a diameter less than 3 cm as well as in human stage I adenocarcinomas (Fujioka et al., 2009). Therefore, MCM7 is a protein of interest in the context of PAH and further studies will help understanding its role in the disease. Interestingly, after BMP9 treatment in healthy control BOECs, eukaryotic initiation factor 4A-I and eukaryotic translation initiation factor 3 subunit H have been found to be decreased upon BMP9, which fits with BMP9 being a vascular quiescence factor (David et al., 2008; Scharpfenecker et al., 2007). Indeed, Scharpfenecker et al. have shown that BMP9 inhibits basic fibroblast growth factor (bFGF)-stimulated proliferation and migration of bovine aortic ECs (Scharpfenecker et al., 2007). Furthermore, eukaryotic initiation factor 4A-I was found to be differentially epxressed between BMP9 treated HPAH and healthy control cells, in which healthy cells demonstrated a decrease of the protein following the treatment;

whereas, HPAH-derived cells showed an increase. This finding brings additional support to the hypothesis that BMPR-II signaling is dysregulated in PAH.

2.4.4 BMP Signaling in BOECs from HPAH

BMPR-II signaling was studied in the BOECs from healthy controls and patients with HPAH. BMP9 ligand was chosen because it is the only ligand that strongly induces BMP signaling in human ECs (David et al., 2008; Scharpfenecker et al., 2007; Upton et al., 2009). A specific dose and time of treatment of 1 ng/ml for 8 hours were chosen based on the study realised by Upton et al., in which they showed that BMP9 stimulated the induction of Id1, Id2, E-selectin and IL-8 transcription, with a maximal response at 1 ng/ml, and this for 8 hours (Upton et al., 2009). The effect of BMP9 was studied by the 2-D PAGE experiment and the BOECs from healthy controls were found to respond better to the treatment than the cells derived from patients with HPAH. Indeed, at the proteome and phosphoproteome level, more proteins and phosphoproteins were found to be activated in the healthy cells after the BMP9 treatment (9 down- and 11 up-regulated proteins; 2 down- and 15 up-regulated phosphoproteins) when compated with cells from patients with HPAH (4 down- and 6 up-regulated proteins; 1 down- and 7 up-regulated phosphoproteins). The striking difference between the healthy and HPAH groups lies in the phosphoproteome profile compared to the number of undetected phospho spots. Under basal conditions, BOECs from healthy controls had a significantly greater number of undetectable phosphorylated proteins when compared with HPAH (179 ± 32 versus 30 ± 7; $P<0.001$). However, upon BMP9 stimulation, only the healthy cells exhibited a significant decreased in the number of undetected phosphorylated spots (84 ± 20 versus 179 ± 32; $P<0.05$), indicating an activation of BMP signaling and phosphorylation cascade, whereas stimulation of the HPAH-derived cells with BMP9 did not lead to a significant decrease in the number of undetected phospho

spots (20 ± 5 versus 30 ± 7), indicating a lower response to BMP9 in regards to the phosphorylation of proteins of high abundance in the sample. To confirm the BMP9 treatment effect, Smad 1/5/8 and Id1 were used as validation targets in an immunoblotting analysis, since they are involved in the BMPR-II canonical pathway. Signaling molecules such as Smad 1/5/8 and Id1 were unlikely to be identified with the 2-D gel approach for the reasons mentioned in section 2.5.2. Contrary to expectations, BOECs-derived from HPAH patients responded to the BMP9 treatment by activating phospho-Smad 1/5/8 and inducing expression of Id1 to the same extent as the BOECs derived from healthy controls. This somewhat counterintuitive result suggests that the reduced expression of BMPR-II in HPAH does not necessarily decrease BMP9-mediated Smad1/5/8 and Id1 induction in BOECs. The discrepancy between the results obtained by the 2-D gel approach in relation to the phosphoproteome can be explained by the fact that the 2-D gel method mainly allows the study of highly abundant proteins and rarely that of less abundant proteins, such as signaling molecules, leading towards the overrepresentation of highly abundant proteins. Therefore, the global increase in phosphorylation of proteins from HPAH-derived cells might be related to a small subset of highly abundant proteins and this effect cannot be translated to all proteins, including these two small signaling molecules. Further studies will have to be conducted to confirm this observation.

Studies conducted in PASMCs (all from the same group) have reported that loss-of-function mutations in the *BMPR2* gene reduce BMP canonical signaling. Namely, human PASMCs harbouring mutations in *BMPR2* were shown to be deficient in Smad1/5 signaling in response to BMP4 and in BMP4-stimulated Id1 and Id2 gene and protein expressions (Yang et al., 2008; Yang et al., 2010; Yang et al., 2005). Nevertheless, another group reported that ablation of *BMPR2* in PASMCs, using an *ex vivo* conditional

knockout approach, as well as siRNA knockdown technology, reduced BMP signaling (pSmad1/5/8 and Id1) in response to BMP2 and BMP4, but increased signaling by BMP6 and BMP7 (Yu et al., 2005). Thus, alterations in BMPR-II signaling may depend of the specific ligand and, in Yu et al. study, the gain of signaling for BMP6 and BMP7 resulted from signal transduction by receptor complexes consisting of the activin receptor type IIa (ActRIIa) receptor and a set of type I co-receptors distinct from those utilized by BMPR-II (Yu et al., 2005). Consistent with this finding, studies in PAECs showed that only abolition of both TGF-β type II receptors (ActR-II and BMPR-II) significantly reduced the Smad1/5 and Id1 responses to BMP9 (Upton et al., 2009). Indeed, BMPR-II knockdown alone only diminished BMP9-mediated Smad1/5 phosphorylation by 20-25% when compared with siRNA control (Upton et al., 2009). Additional support of *BMPR2* mutations in endothelial cells leading to a loss of responsiveness to the BMP9 ligand from patients with HPAH comes from a RNA array study that was conducted with RNA samples from BOECs used in this thesis by the Stewart and Morrell groups. mRNA levels of Smad 6, an inhibitor of the BMP/Smad 1 signaling pathway by specifically competing with Smad 4 (Hata et al., 1998), were found to be significantly decreased under basal conditions in HPAH-derived BOECs compared with healthy controls (personnal communication). This data suggests that *BMPR2* mutations or reduction in BMPR-II protein levels resulted in the loss of responsiveness to the BMP9 ligand, thereby causing a profound constitutive increase in phosphorylation of BMP signaling proteins which was independent of ligand availability. This could explain how a single copy of a mutant *BMPR2* gene can have such an important effect on EC biology. Further mechanistic studies will be needed to support the observation that BOECs derived from patients with HPAH might have a hyperphosphorylation state. As explained below in the section entitled future studies, other approaches will be needed to confirm the

upregulation of the phosphoproteome of BOECs derived from HPAH patients obtained by the 2-D gel experiment.

CHAPTER 3: POTENTIAL ROLE OF TCTP IN PAH

3.1 Introduction

3.1.1 Translationally Controlled Tumor Protein (TCTP)

Translationally controlled tumor protein (TCTP) was initially identified by Thomas et al. in 1981, in Swiss mouse 3T3 fibroblasts, and named Q23 based on its position on a gel and was found to be up-regulated 5-fold following serum stimulation of quiescent Swiss 3T3 cells (Thomas and Luther, 1981). A year after its initial discovery, TCTP was identified in mammalian tumor cells and mouse sarcoma 180 ascites cells, and named p21 (Yenofsky et al., 1982). The designation TCTP came a few years later and was based on the fact that the first cDNA sequence of the human homolog was derived from a mammary carcinoma (Gross et al., 1989) and the observation that its rate of synthesis is translationally controlled (Bohm et al., 1989; Thomas and Luther, 1981). Hence, TCTP is known under different names (i.e., Q23, p21), has been identified in many normal tissues/cells (e.g. human mammary gland (Bini et al., 1997) and testes (Gross et al., 1989; Guillaume et al., 2001), and has been described to be both transcriptionally (Andree et al., 2006; Thiele et al., 2000) and post-transcriptionally regulated (Bohm et al., 1989; Chitpatima et al., 1988). Since these initial reports, TCTP has been given other names reflecting other major activities of this protein, including histamine releasing factor (HRF) (MacDonald et al., 1995) and fortilin (Li et al., 2001). TCTP was originally described as a growth-related protein (Thomas and Luther, 1981), but since then a wide range of intracellular functions have been attributed to this protein, including apoptosis inhibition (Li et al., 2001), malignant transformation (Tuynder et al., 2002) and various other growth-related functions (Gachet et al., 1999; Yarm, 2002). In addition to this broad spectrum of intracellular activities, it has been reported to exert important extracellular functions, for example in human allergic responses in the context of asthma (MacDonald et al., 1995). In addition, TCTP has been implicated in various other pathophysiological

processes, such as, hypertension (Kim et al., 2008b), atherosclerosis (Cho et al., 2012) and systemic arterial remodelling (Sirois et al., 2011). These functions, described in more detail below, made TCTP an interesting target to study in the context of pulmonary arterial hypertension.

Illustration 3: TCTP is a multifunctional protein with intra- and extra-cellular activities
(Adapted from (Telerman and Amson, 2009))

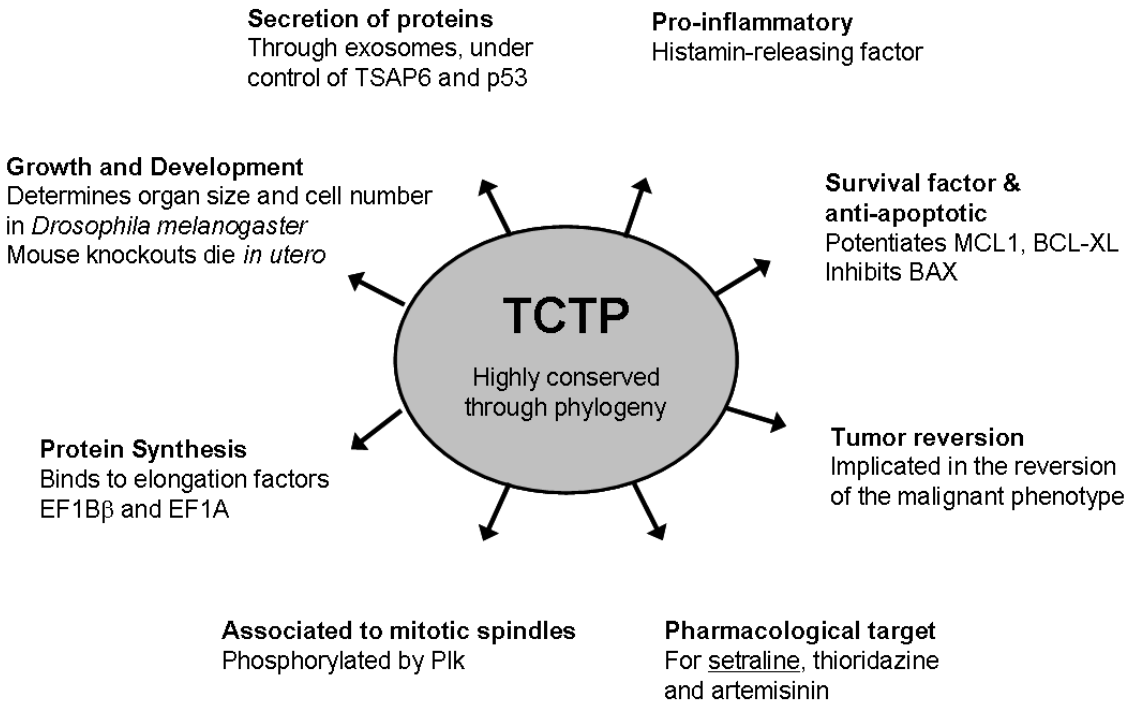

3.1.2 Highly Conserved and Essential

Sequence analysis of human TCTP cDNA revealed it to be a 172-amino acid polypeptide highly conserved through phylogeny (Nagano-Ito and Ichikawa, 2012). The calculated size of human TCTP is about 19 kDa (Nagano-Ito and Ichikawa, 2012). TCTP has been identified in many eukaryotes, including yeast, fungus, insects, plants and mammals (Thaw et al., 2001; Yenofsky et al., 1982). The high degree of conservation during evolution suggests that it plays crucial functions; TCTP-knockout mice die around embryonic stage day E9.5-E10.5 with a severe growth-retarded and disorganized structure (Chen et al., 2007). The developmental defects of the $TCTP^{-/-}$ mutants reside in mesoderm and endoderm patternings (Chen et al., 2007).

3.1.3 Translational and Transcriptional Regulation

TCTP was initially termed translationally controlled tumor protein because its rate of protein synthesis was found to be controlled at the translational level by sequestration of the mRNA in translationally repressed postpolysomal mRNP-complexes (Bohm et al., 1989; Chitpatima et al., 1988). It has been suggested that this accumulation of untranslated mRNA could enable a rapid elevation of protein synthesis in response to a wide range of extracellular signals and cellular conditions (Bommer and Thiele, 2004; Thomas and Luther, 1981). Bommer et al. have found that the mRNA of TCTP is a highly structured RNA which may both activate the double-stranded RNA-dependent protein kinase PKR and be subjected to mRNA translational regulation by this kinase, resulting in changes in TCTP protein synthesis, but not in differential transcription or mRNA stability (Bommer et al., 2002). Although TCTP was first described to be regulated at its translational level, transcriptional regulation was also reported (Andree et al., 2006; Baudet et al., 1998; Sage-Ono et al., 1998; Thiele et al., 2000). In humans, the *TPT1* gene (locus ID 7178) encoding TCTP protein consists of six exons and five introns

(Andree et al., 2006). It generates two mRNAs of about 0.8 and 1.2 kb which contain the same coding region and 5′-UTR, but differ in the length of their 3′ untranslated regions by the use of alternative polyadenylation signals (Andree et al., 2006). Thiele et al. investigated the distribution of these two transcripts in 50 human tissues and found that both mRNAs were transcribed in all tissues examined, but differed considerably in their quantity and ratio of expression (Thiele et al., 2000). This is indicative of an extensive transcriptional control and involvement of tissue-specific factors (Thiele et al., 2000). In agreement, Andree et al. demonstrated that the transcription of TCTP is controlled by cAMP signaling via phosphorylation-dependent activation of CRE/CREB interaction in human bladder carcinoma (T24) cells (Andree et al., 2006).

3.1.4 Functional Properties

3.1.4.1 Growth-related Functions and Development

Several studies have demonstrated that TCTP has properties of a tubulin-binding protein (Gachet et al., 1999; Yarm, 2002). Gachet et al. have shown that TCTP associates with microtubules in a cell cycle-dependent manner (Gachet et al., 1999). At metaphase, TCTP is bound to the mitotic spindle and is detached from the spindle during the metaphase-anaphase transition (Gachet et al., 1999). Yarm et al. described TCTP to be phosphorylated by polo-like kinase (Plk), which leads to a decrease in its microtubule-stabilizing activity, promoting an increase in microtubule assembly and disassembly dynamics after metaphase (Yarm, 2002). Consistent with these two studies, many cellular proteins involved in cell growth have been reported to interact with TCTP, including elongation factor eEF1A and its guanine nucleotide exchange factor eEF1B beta (Cans et al., 2003; Langdon et al., 2004), Mcl-1 (Li et al., 2001; Liu et al., 2005), TSAP6 (Amzallag et al., 2004) and Na,K-ATPase (Jung et al., 2004) (Illustration 3). In agreement with these studies, TCTP expression has been reported to be elevated in

many cancer cell lines (e.g. H1299, MCF-7, A549 and U937) (Li et al., 2001; Liu et al., 2005; Tuynder et al., 2002) and human tumor tissues (e.g. liver, lung and prostate) (Arcuri et al., 2004; Chan et al., 2012; Kim et al., 2008a). In addition, Chen et al. generated a gene-disrupted mouse model to address TCTP physiological roles and provided genetic evidence that it plays a critical role in the normal proliferation and survival of mouse embryonic fibroblasts (Chen et al., 2007). The authors suggested that the reduced cell number in the epiblast of the E5.5 TCTP-null embryos compared with wild type is mainly due to reduced cellular proliferation in the epiblast beginning at E5.5 or earlier stages and increased cell death starting around E6.5 (Chen et al., 2007).

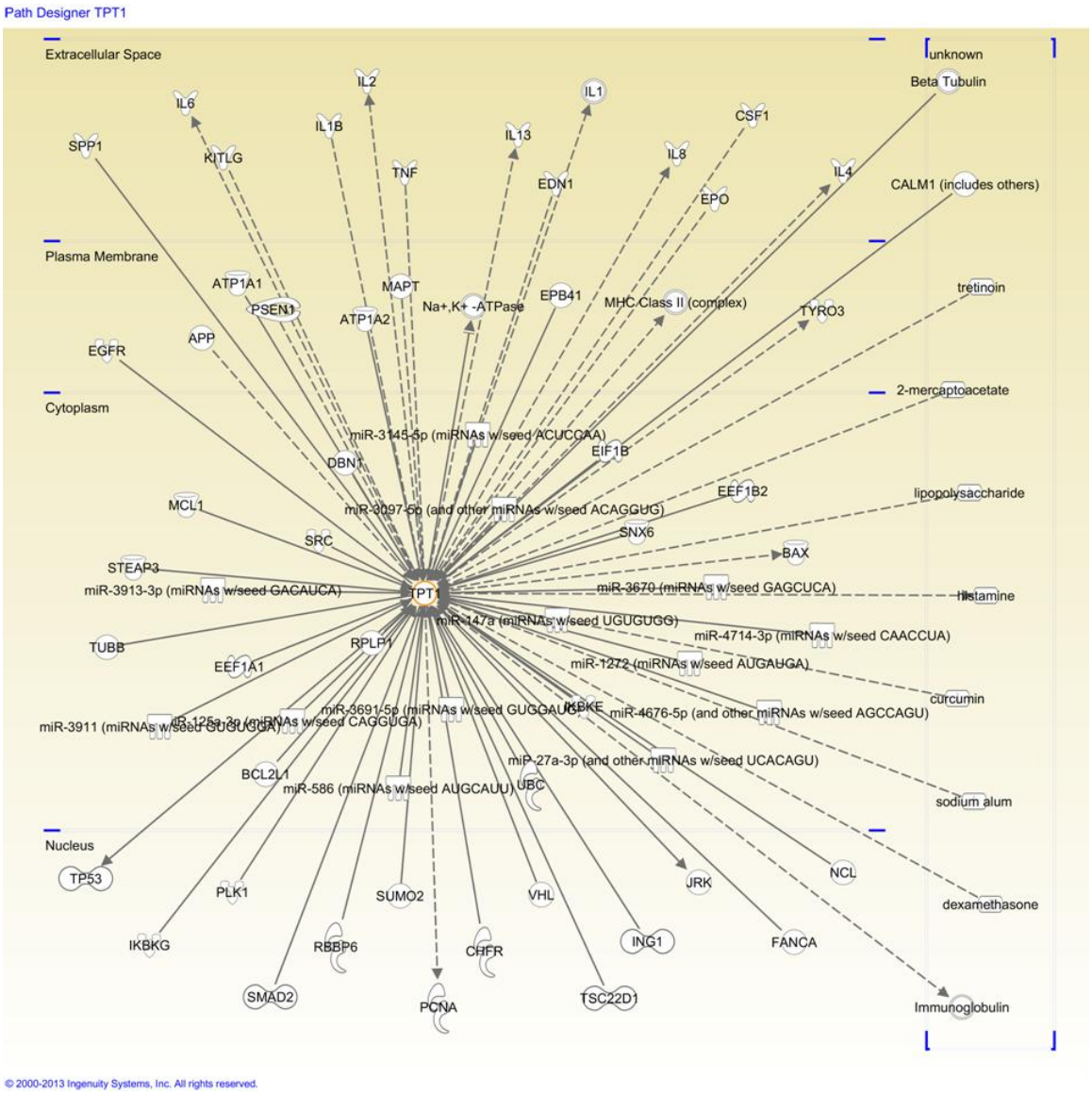

Illustration 4. Proteins that interact with TCTP.
Molecular interactions associated with *TPT1* (gene name for TCTP) were analyzed using Ingenuity Pathway Analysis. Solid lines represent direct interactions, whereas dotted lines represent indirect interactions.

3.1.4.2 Pro-inflammatory Actions

In 1995, seminal work by MacDonald et al. revealed an extracellular cytokine-like function for TCTP (MacDonald et al., 1995). The authors reported the subcloning, sequencing and expression of a unique IgE-dependent histamine releasing factor (HRF) named HRF (herein termed TCTP) (MacDonald et al., 1995). The authors found TCTP to be the component present in allergic patients' biological fluids that stimulated histamine release from basophils (MacDonald et al., 1995). A year later, Schröder et al. demonstrated that stimulation of human basophils by TCTP triggered the secretion of interleukin-4, a pro-inflammatory cytokine (Schroeder et al., 1996). These initial reports suggested that secreted TCTP has a prominent role in allergic diseases. As demonstrated by Kim et al., dimerization of TCTP seems to be essential for its cytokine-like activity, as the cytokine-releasing activity of extracellular TCTP is generated only when TCTP dimerizes via the intermolecular disulfide bond (Kim et al., 2009). The authors showed that the dimerized form of the protein was found in sera in allergic patients and bronchoalveolar lavage fluids from airway inflamed mice (Kim et al., 2009). Although TCTP function has been well-described in late-phase allergic reactions and chronic allergic inflammation, its function in asthma has only recently been addressed. Kashiwakura et al. reported that TCTP promotes allergic inflammation in the skin and lung from mouse models of asthma and allergy (Kashiwakura et al., 2012). The authors reported that bioactive TCTP (i.e., dimers and oligomers) interacted with IgE molecules and could crosslinked IgE-bound FcεRI, in which aggregation led to activated mast cells *in vitro* (Kashiwakura et al., 2012). Furthermore, this group has shown that Ig-interacting HRF/TCTP peptides, shown to block TCTP/Ig interactions *in vitro*, inhibited IgE/HRF-induced mast cell-dependent inflammation *in vivo* (i.e. acute passive cutaneous anaphylaxis and airway inflammation) (Kashiwakura et al., 2012). Collectively, these

studies indicate that HRF/TCTP has a pro-inflammatory role in asthma and allergic reactions.

3.1.4.3 Secretion Mode of TCTP

Although explicit secretion of TCTP has been demonstrated in the above-mentioned studies, its mechanisms of release have only been recently addressed. TCTP has no classical signal sequences comprising hydrophobic amino acids at its N-terminal, which places it among the non-typically secreted proteins that exit from a cell without passing through the classical secretion pathway (Muesch et al., 1990). Amzallag et al. have shown that TCTP secretion proceeded via an endoplasmic reticulum/golgi-independent or nonclassical pathway, since it was insensitive to either brefeldin A or monensin (Amzallag et al., 2004). More importantly, Amzallag et al. were the first to identify a novel role for TSAP6 (Tumor Suppressor Activated Pathway 6) in the export of TCTP in exosomes (Amzallag et al., 2004). Exosomes are small vesicles (50–100 nm in diameter) of cup shape appearance (when examined under an electron microscope) originating from large multivesicular endosomes containing nucleic acids, proteins, lipid rafts and exposed phosphatidylserine (Thery et al., 2009). They are enriched in cholesterol, spingomyclin and ceramide (Thery et al., 2009) and are responsible for the secretion of proteins, such as major histocompatibility class I and II, integrins and tetraspanins, through the non-classical pathway (Nickel, 2003). In 2011, Sirois et al. identified TCTP in nanovesicle fractions (corresponding to exosomes) purified from medium conditioned by apoptotic endothelial cells (Sirois et al., 2011). Interestingly, they showed that these exosomes induced an anti-apoptotic phenotype in vascular smooth muscle cells, where TCTP played a major role (Sirois et al., 2011). These results highlight a function for TCTP as a component of the paracrine apoptotic program of potential importance in vascular repair and remodeling.

3.1.4.4 TCTP in Cancer

Increased expression of TCTP was found in various tumors (e.g. tumours of liver, lung, breast and rectum) (Arcuri et al., 2004; Chan et al., 2012; Kim et al., 2008a; Tuynder et al., 2002; Wu et al., 2012), and its implication in tumor reversion, a process by which some cancer cells lose their malignant phenotype, was highlighted more than a decade ago (Tuynder et al., 2002). While searching for differentially expressed genes between tumor cells and their revertant counterparts, Tuynder et al. identified TCTP as being the most down-regulated protein in tumor revertant cells (Tuynder et al., 2002). As a proof-of-concept, the inhibition of TCTP expression by anti-sense cDNA or small interfering RNA molecules resulted in suppression of the malignant phenotype and in cellular reorganization (Tuynder et al., 2002). Subsequent studies confirmed TCTP as a target of tumor reversion (Tuynder et al., 2004), and pharmacological approaches to diminish the level of TCTP in tumor cells have been undertaken. A Phase I/II clinical trial with sertraline, a widely used anti-depressive drug, was initiated for patients with end-stage acute myeloid leukaemia (Telerman and Amson, 2009).

3.1.4.5 TCTP in Apoptosis

A series of publications have highlighted the importance of TCTP in cancer and its link to its anti-apoptotic activities (Amson et al., 2012; Li et al., 2001; Liu et al., 2005; Rho et al., 2011). An anti-apoptotic activity for TCTP has been first reported by Li et al. in 2001, who showed that TCTP inhibited etoposide-induced apoptosis in both HeLa cells (cervical tumor cell line) and U2OS cells (human osteosarcoma cell line) (Li et al., 2001). More importantly, the authors reported that antisense depletion of TCTP from MCF-7, a breast cancer cell line, caused massive cell death (Li et al., 2001). TCTP stabilization of the anti-apoptotic protein myeloid cell leukemia sequence-1 (Mcl-1), leading to the inhibition of Bax dimerization, has been suggested by Liu et al. as a molecular mechanisms

underlying TCTP antiapoptotic activities (Liu et al., 2005; Susini et al., 2008). Very recently, TCTP has been shown to be an important regulator in the P53 pathway, acting in a negative feedback loop such that overexpression of TCTP blocks P53-mediated apoptotic activity by inducing the degradation of p53 (Amson et al., 2012; Rho et al., 2011), and in turn P53 directly represses TCTP transcription (Amson et al., 2012). Interestingly, Mizuno et al. reported recently that P53 deficiency promotes hypoxia-induced PAH and vascular remodeling in mice (Mizuno et al., 2011).

3.2 Specific Aims

1. To elucidate the role of TCTP in the molecular and functional abnormalities of ECs from patients with HPAH harboring *BMPR2* mutations by manipulating its expression *in vitro* in BOECs using siRNA knockdown technology.

2. To begin to explore the mechanisms by which dysreguated expression of TCTP may contribute to abnormalities in vascular function and structure (arteriolar remodeling) in PAH.

3.3 Material and Methods

3.3.1 Protein Lysate Preparation and Immunoblotting

BOECs were washed with cold 2X PBS and then flash frozen on a bath of dry ice with methanol for 30 seconds. The flasks containing the cells were removed from the bath, RIPA lysis buffer was added and cells were scraped for whole cell lysate collection. Lysates were sonicated for 30 seconds at 4°C and then centrifuged at 14,000 g for 15 minutes at 4°C. Supernatant was collected. Protein lysates were separated on 12% SDS-PAGE or NuPAGE 4-12% bis-tris mini gels (Life technologies, Burlington, ON), transferred on PDVF membranes and probed with antibodies against TCTP (rabbit polyclonal, Abcam, Toronto, ON), β-actin (mouse monoclonal; Sigma-Aldrich, Oakville, ON) and CD81 (Santa Cruz, Heidelberg, Germany). IRDye infrared secondary antibodies were used for the detection of the above-mentioned targets (Li-COR Odyssey Infrared Imaging System, Li-Cor Biosciences, Guelph, ON). A total of 10 μg of whole cell lysate was used for TCTP blots and 15-25 μg were used for CD81 blots.

3.3.2 TCTP Silencing with siRNA in BOECs

BOECs grown in 6-well plates (2.0×10^5 cells per well) or in 24-well plates (3.0×10^4 cells per well) were transfected 2 days later with Dharmafect agent 1 (Fisher Scientific, Nepean, ON) using ON-TARGET plus SMART pool for TCTP and AllStars negative control siRNA (Qiagen, Toronto, ON). Four different siRNAs were tested for their efficiency of knocking down TCTP protein levels following WB analysis, and one was chosen for the subsequent studies (Hs_TPT1_8 FlexiTube siRNA [SI02664186, Qiagen, Toronto, ON] 5'-CCGCGCTCGCTCCGAGTTTCA-3'). Simply put, BOECs were incubated in an Opti-MEM medium for 3 hours (Life technologies, Burlington, ON) before being incubated with a final concentration of 10 nM of annealed oligo, mixed in

Dharmafect agent 1 and diluted in an Opti-mem medium for 4 hours. After this 4-hour incubation period, a normal medium (EGM-2MV with 10% FBS) was added for the next 48 hours, after which cells were either collected for Western blot analysis, as described in section 3.3.1, or used for apoptosis and Brdu incorporation studies, as described in sections 2.3.4 and 2.3.6.

3.3.3 Human Lung Tissue Immunostaining

Human lung tissues were fixed in 10% phosphate-buffered formalin by airway perfusion immediately after resection, then processed for sectioning (6 μm). Sections of formalin-fixed and paraffin-embedded lung tissue from patients and controls were deparaffinized and rehydrated with an ethanol series followed by 5 minutes in water. Slides were treated with 0.3% H_2O_2 in water for 20 minutes to remove endogenous peroxidase activity and washed in PBS for 5 minutes. Incubate for 20 minutes in normal blocking serum (specific for rabbit primary, Vectastain Elite ABC kit). Blot excess blocking serum and incubate sections in a 1:200 dilution of rabbit α-TCTP (Abcam, Cambridge, U.K.) for 1 hour at room temperature. Wash sections for 5 minutes in PBS. Incubate sections for 30 minutes in biotinylated anti-rabbit secondary antibody solution (Vectastain Elite ABC kit). Wash sections for 5 minutes in PBS. Incubate sections for 30 minutes with Vectastain Elite ABC reagent. Wash slides 3 x 5 minutes in PBS. Incubate sections in peroxidase solution for only 1 minute then rinse in tap water and mount. As for the immunofluoresence staining on human lung tissues was performed on frozen sections. Slides were blocked in 10% FBA in PBS and incubated with these antibodies at 4ºC overnight: 1:50 poly rabbit-α-TCTP (Abcam, Cambridge, U.K.), 1:150 mouse-α-human CD31 (Dako, Cambridge, U.K.). These antibodies were used at room temperature for 1 hour: 1:200 goat-α-rabbit-NL637 (R&D systems, Abingdon, U.K.), goat-α-mouse-AF488 (Sigma-Aldrich, Gillingham Dorset,

U.K.),1:200 Cy3-conjugated mouse-α-SMA (Sigma-Aldrich, Gillingham Dorset, U.K.). Washing were performed as such: 5x 2 minutes after primary antibody incubation except for SMA, which required 3 x 5 minutes and secondaries were washed for 3 x 5 minutes. Slides were counterstained with DAPI for nuclear staining. An additional wash was performed before mounting: 2 x 5 minutes in water.

3.3.4 Purification of Exosomes and Microparticles from BOECs

For exosome and microparticle preparations, BOECs were cultured in an exosome-free medium which was generated by ultracentrifugating the complete medium for 4 hours, at 100,000 g. Exosome and microparticle samples were prepared from a BOEC-derived conditioned medium by differential centrifugation. For exosome isolation, the conditioned medium was centrifuged sequentially at 1,200 g for 20 minutes to remove cell debris, at 50,000 g for 15 minutes to eliminate apoptotic blebs and at 100,000 g for 18 hours (Beckman SW-41 Ti rotor) to purify the exosomal fraction (50-100 nm in size). An additional 100,000 g ultracentrifugation was performed for 1 hour with 1X PBS to wash the exosomes before use. For the microparticle isolation, the conditioned medium was centrifuged sequentially at 300 g for 10 minutes, at 2,000 g for 10 minutes and at 10,000 g for 30 minutes (Beckman SW-41 Ti rotor) to purify the microparticle fraction (100-1000 nm in size). For protein profiling and western blotting, 15-25 μg of exosomes were solubilized in a 4X LDS loading buffer (Life technologies, Burlington, ON) with a NuPAGE reducing agent (10X) (Life technologies, Burlington, ON) containing 500 mM dithiothreitol (DTT), and heated at 70ºC for 10 minutes. Then, the exosome samples were loaded on NuPAGE 4-12% bis-tris mini gels (Life technologies, Burlington, ON), which were stained with Sypro Ruby gel stain (Sigma-Alrich, Oakville, ON), in accordance with the manufacturer's protocol. For mass spectrometry analysis (2D LC-MS/MS) of exosome preparation, 20 μg of exosomes were processed by the

NuPAGE system described above, in which case the gel bands were extracted for protein identification (refer to section 2.2.5 for details).

3.3.5 *In Vitro* Testing of Small Hairpin RNA (shRNA) Plasmid Strategy

3.3.5.1 Cell Culture of Rat Mammary Gland Carcinoma Epithelial Cells

Rat mammary gland carcinoma epithelial cells (cat. no. CCL-38, ATCC, Burlington, ON) were cultured on plastic flasks in a M199 medium supplemented with 5% horse serum (ATCC, Burlington, ON) and 1% penicilline/streptomycin (Gibco/Life Technologies, Burlington, ON).

3.3.5.2 Transfection of Rat Mammary Gland Carcinoma Epithelial Cells with shRNA Plasmids

An evaluation of the knockdown efficiency of the four shRNA plasmids containing different sequences for TPT1 shRNA (pRS-shTPT1) was conducted in rat mammary gland walker carcinoma epithelial cells using an *in vitro* jetPRIME technique (Polyplus, New York, USA). Rat epithelial cells were seeded (40,000 cells per well of a 24-well plate) for 48 hours before being transfected with shRNA plasmids mixed with a jetPRIME reagent, at a ratio of 1:2 plasmid, to jetPRIME for 4 hours. The transfection medium was replaced after the 4-hour incubation by a complete growth medium (M199 with 5% horse serum). After 48 hours of transfection, cells were imaged and then lysed for protein extraction and for analysis of TCTP knockdown efficiency by Western blotting, as described in section 3.3.1. One of the pRS-shTPT1 plasmid was then selected to be used in the *in vivo* pilot trial.

3.3.5.3 shRNA Plasmids

The DNA sequence 5' CATGACGAGCTGTTCTCCGACATCTACAA 3', which encodes a short hairpin RNA structure, was used to generate the plasmid pRS-shTPT1 that was selected for the *in vivo* pilot trial (cat. no. TR712215, Origene Technologies/Cederlane, Burlington, ON). The expression vector pRS-shRNA (Origene echnologies/Cederlane, Burlington, ON) without a nucleotide insert was the plasmid vector pRS-null (Origene Technologies, Rockville, MD), and the scrambled pRS-shRNA with a scrambled nucleotide insert sequence (5' GCACTACCAGAGCTAACTCAGATAGTACT 3') was the plasmid vector pRS-scrambled (Illustration 2-3). E. coli cells were transformed with the different plasmids and induced into high copy numbers. Transformed E. coli cells were preserved at -80°C, in cryogenic tubes containing 20% sterile glycerol, until use. pRS-shRNA plasmids were mass produced and purified with endotoxin-free plasmid giga prep kit (Qiagen, Toronto, ON) using the E. coli glycerol stock.

3.3.6 *In Vivo* Pilot Study of TCTP Silencing in Experimental Model of PAH

3.3.6.1 Animals

All animal procedures were approved by the University of Ottawa Animal Care and Use Committee (Ottawa, ON). Adult male Sprague-Dawley rats (CD IGS rats, strain code 001, Charles River, Canada) weighing 160-200 g were injected subcutaneously with SU5416 (20 mg/kg) (Tocris Bioscience, Bristol, UK), which was suspended in CMC solution (0.5% [w/v] carboxymethylcellulose [CMC] sodium, 0.9% [w/v] sodium chloride, 0.4% [v/v] polysorbate 80, 0.9% [v/v] benzyl alcohol in deionized water) (Sigma-Alrich, Oakville, ON). Control rats received only CMC, as a vehicle. The treatment protocol consisted of 1 subcutaneous injection of SU5416 at 20 mg/kg.

Illustration 5: Timelines for the *in vivo* experiments

1. Timeline of established model of severe PAH (SU5416 model)

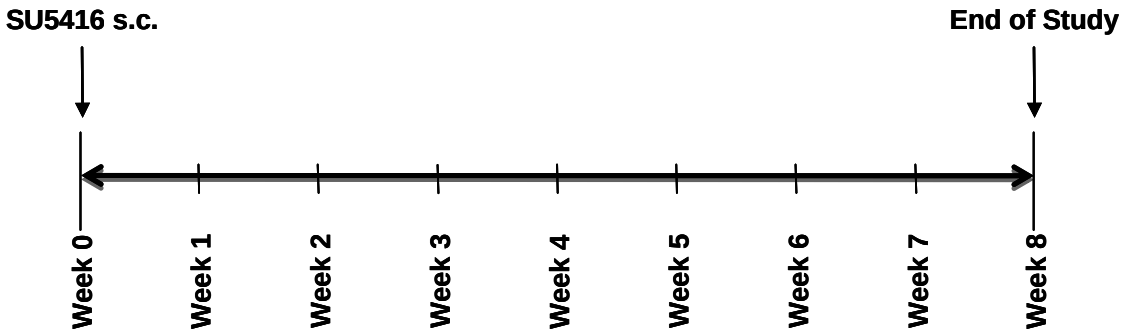

2. Timeline of pilot study for TCTP inhibition

Question: Can TCTP inhibition in the SU5416 model prevent PAH?

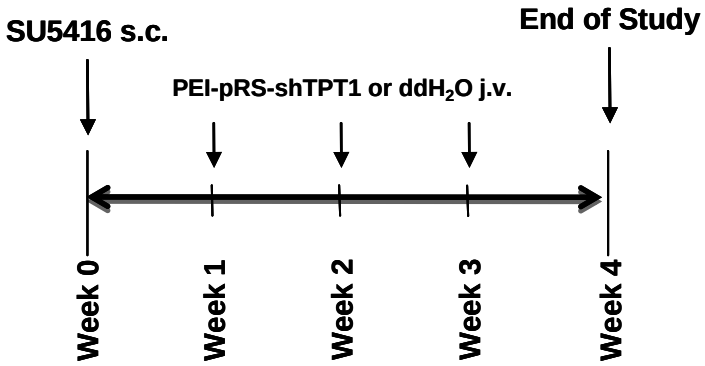

3.3.6.2 *In Vivo* Gene Transfer to the Lung Vasculature

At week 0, adult male Sprague-Dawley rats received a subcutaneous injection of SU5416, as described in section 3.3.6.1. *In vivo* transfections were carried out using the *in vivo*-jetPEI cationic polymer transfection reagent (Polyplus-transfection SA, Illkirch, France) delivered by jugular vein injection, to target the intravascular lung endothelial cells. Rats were either given an injection of pRS-shTPT1/jetPEI complex or sterile ddH_2O one week after SU5416 injection and once a week for 3 weeks. Transfection was achieved by delivering 100 µg of shRNA plasmid (DNA) complexed with *in vivo* jetPEI to obtain a PEI nitrogen/DNA phosphate (N/P) ratio of 6 in a total volume of 1 ml of 5% glucose (Illustration 4).

3.3.6.3 Hemodynamic Evaluation

Following the experimental endpoint (4 weeks), rats were anaesthetized by an intraperitoneal injection of ketamine (35 mg/kg) and xylazine (7 mg/kg). Right ventricular systolic pressure (RVSP) was determined using a 1.4 French Millar catheter (Millar Instruments, Inc., Houstan, TX) connected to the PowerLab computer system (AdInstruments, Colorado Springs, CO). This catheter was inserted into a small incision in the medial aspect of the jugular vein and advanced through the superior vena cava and right atrium into the right ventricle. The correct placement of the catheter was confirmed by observing the pattern of the pressure tracing, and the average RVSP measurement was recorded from 1 minute of pressure reading, once the pressure was deemed to have stabilized. Data was analyzed with the LabScribe2 software (IWorx, Dover, NH).

3.3.6.4 Lung Isolation

The right lung lobes were clamped off at the level of the right bronchus, dissected and snaped frozen in liquid nitrogen for protein and RNA extraction. The left lobe was then insufflated with a 50% OCT-saline solution (Tissue-Tek OCT; Qiagen, Mississauga, ON) via the trachea, and the lung was then removed. The left lobe was sectioned in pieces which were preserved in 4% paraformaldehyde for 16 hours, rinsed in 1X PBS and stored in 70% ethanol until the day of paraffin embedding.

3.3.6.5 Assessment of Right Ventricular Hypertrophy

The heart was first dissected free from the atria, the aorta and the pulmonary trunk. The right ventricle was then dissected from the left ventricle and the ventricular septum. Right ventricular hypertrophy was assessed by evaluating the mass ratio of the right ventricle (RV) to the left ventricle plus septum (LV+S).

3.3.6.6 Paraffin-embedded Tissue Immunostaining

Lung tissues were fixed in 4% paraformaldehyde, dehydrated in alcohol and embedded in paraffin. Tissue blocks were sectioned with a microtome (Leica Microsystems, Concord, ON), placed onto poly-L-lysine-coated slides, dried at 37°C for 16 hours and then dewaxed and dehydrated through graded alcohols. Paraffin-embedded samples were either stained with H&E (haematoxylin and eosin) (7 µm) or processed for immunofluorescence studies (5 µm). For immunofluorescence staining, slides were microwaved for 30 minutes, in a sodium citrate buffer (0.4 mol/L), at pH 6.0 (Dako, Markham, ON), and incubated in 0.25% triton-X100 (Fisher Scientific, Nepean, ON) for 10 minutes. Tissue slides were blocked with 3% bovine serum albumin (BSA) and 5% goat serum for 90 minutes, at room temperature, before being incubated with primary antibodies. These primary antibodies were incubated overnight at 4°C: polyclonal rabbit

anti-TCTP (Abcam, ab37506, Toronto, ON), proliferating cell nuclear antigen (PCNA; Cell Signaling, Whitby, ON). Monoclonal mouse anti-α-smooth muscle actin (α-SMA)-Cy3 and von Willebrand factor (vWF) (Dako, Markham, ON) antibodies were incubated 1 hour at room temperature. The specificity of immunostaining for the primaries (TCTP, PCNA, vWF) was demonstrated by the use of an isotype control used at the same concentration as the corresponding primary: Mouse (G3A1) mAb IgG1 Isotype Control (Cell Signaling Technology, #5415, Whitby, ON) (for PCNA) and Rabbit IgG Isotype Control (Novus Biologicals, NB810-56910, Oakville, ON) (for vWF and TCTP). These secondary antibodies were incubated for 1 hour at room temperature: Alexa Fluor® 555 Goat Anti-Mouse IgG (H+L) (Invitrogen, A21422, Burlington, ON), Alexa Fluor® 488 Goat Anti-Rabbit IgG (H+L) (Invitrogen, A11008, Burlington, ON). Images were acquired using a confocal microscope (Olympus, Richmond Hill, ON).

3.3.6.7 Assessment of Luminal Occlusion of Pulmonary Vessels

Hematoxylin and eosin (H&E)-stained lung sections were scanned and 10 random fields were chosen for counting the total identifiable and occluded blood vessels (25-100 μm) as well as plexiform lesions. For the percentage of occluded vessels, a total of 342 and 466 blood vessels were counted for the vehicle-treated and the PEI-pRS-shTPT1 group, respectively. The counts were confirmed by a blinded investigator.

3.3.7 Statistical Analysis

Results are presented as mean ± SEM or mean ± SD as indicated in the figure legends. Statistical analysis was performed using the GraphPad Prism software, version 5.1. The means of two groups were compared using either an unpaired Student t-test. The differences between multiple means were determined by one-way analysis of variance (ANOVA), and when overall differences were detected, the Tukey's or Dunnett's post-

hoc analysis was used to determine differences between individual means. A value of $P<0.05$ was considered statistically significant.

3.4 Results

3.4.1 TCTP: An Upregulated Protein in HPAH found by the 2-D PAGE Approach

The translationally controlled tumor protein (TCTP) was one of the upregulated proteins (log_2 [HPAH/H] of 0.43) found in the analysis of statistically and differentially regulated proteins of BOECs derived from patients with HPAH, compared with healthy controls under basal conditions in the 2-PAGE experiment (i.e. cells incubated in EBM-2 with 0.1% FBS for 24 hours with no BMP9 treatment). The 2-D spot corresponding to TCTP on representative 2-D gels is presented in Figure 11A and its corresponding intensity in Figure 11B.

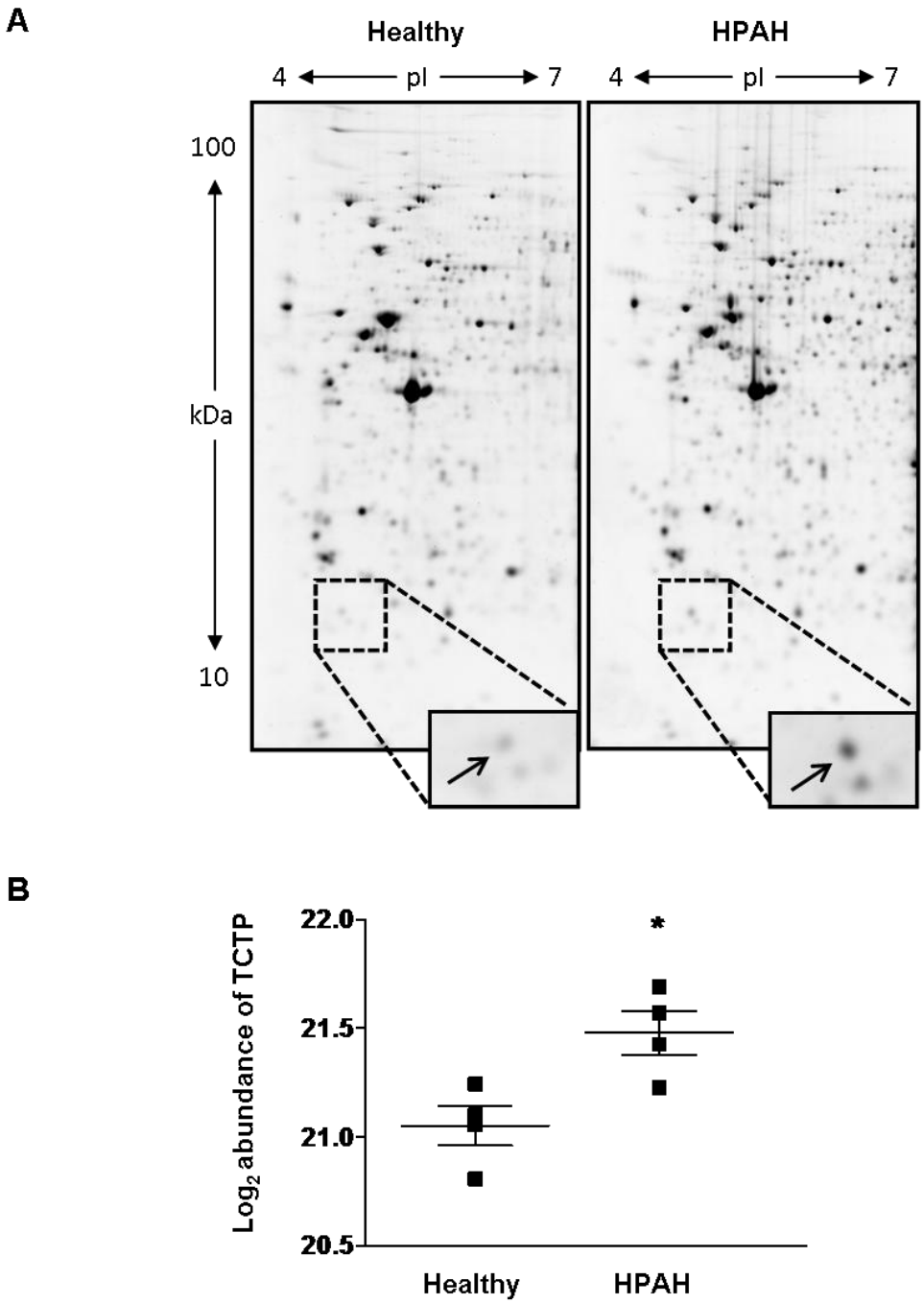

Figure 11. Identification of TCTP as an upregulated protein in BOECs from patients with HPAH.
(A) Representative 2-D gels from a healthy individual and a patient with HPAH. Arrows indicate the differentially regulated spot corresponding to TCTP. (**B)** Quantification of spot intensity corresponding to TCTP. Each spot indicates the quantification of a sample (n=4 in each group). Mean ± SEM. Statistical differences were assessed by Student t-test. *p<0.05.

3.4.2 TCTP: An Upregulated Protein in HPAH confirmed by Immunoblotting

To validate the 2-D gel results and to study TCTP expression under normal growth conditions, TCTP abundance levels in BOECs from healthy controls and patients with HPAH were monitored by immunoblotting under normal medium conditions (EGM-2MV 10% FBS) (Figure 12). TCTP abundance levels were found to be upregulated by 1.7-fold in HPAH-derived BOECs when compared with healthy controls (0.46 ± 0.07 versus 0.26 ± 0.04; $P<0.05$) (Figure 12B). Based on the mounting evidence that TCTP is implicated in growth, malignant transformation (Telerman and Amson, 2009; Tuynder et al., 2002), inflammation (MacDonald et al., 1995) and systemic arteriolar remodeling (Sirois et al., 2011), the potential importance of TCTP in PAH was further pursued.

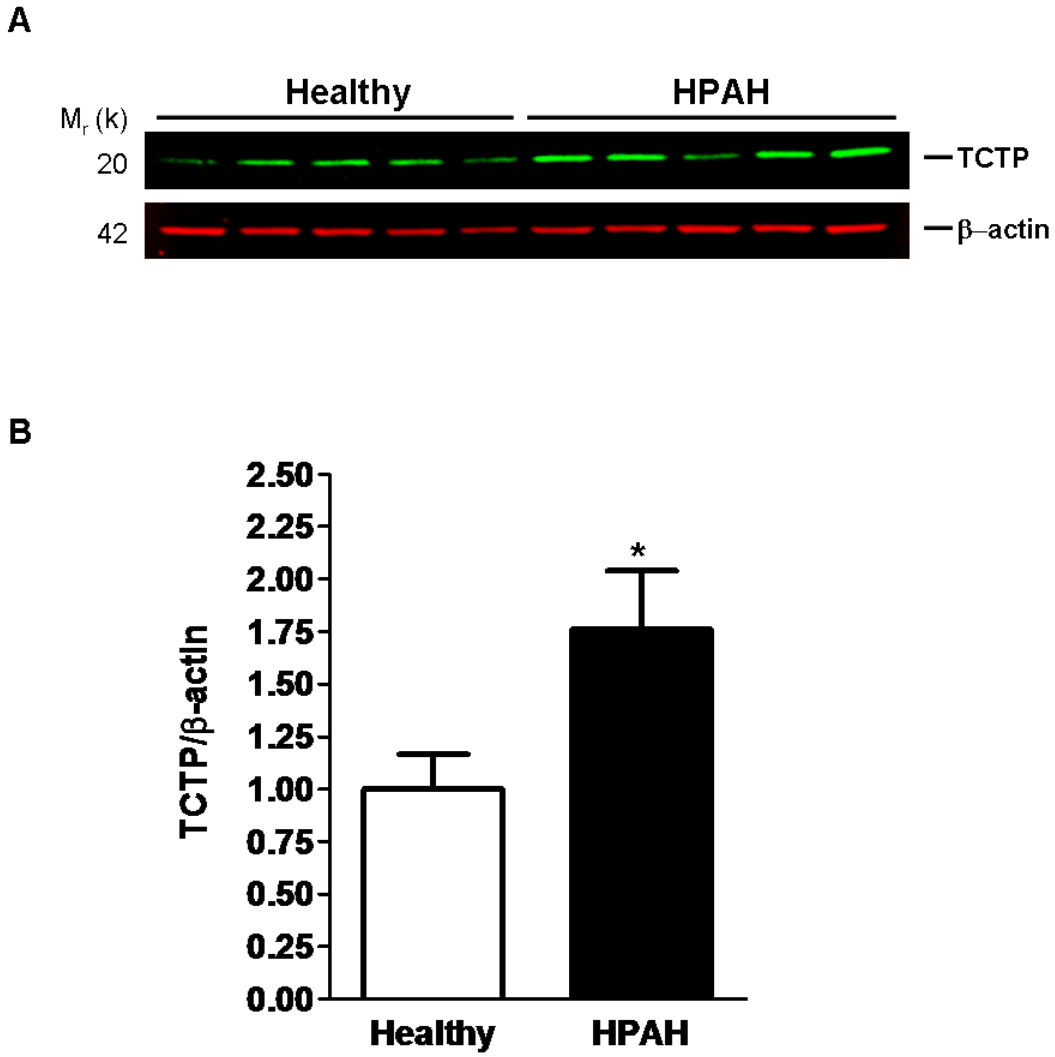

Figure 12. TCTP abundance levels are upregulated in BOECs from patients with HPAH under normal growth conditions.
(A) Representative immunoblotting image of TCTP abundance levels in BOECs from healthy or HPAH under normal growth conditions (EGM-2MV with 10 %FBS).
(B) Results are expressed as mean ± SEM of four experiments and as expression relative to β-actin and normalized to the healthy group. n=5 in healthy and HPAH groups. Significant differences were assessed by unpaired Student t-test. *p<0.05.

3.4.3 TCTP: siRNA Technology to knockdown TCTP Protein Levels

Since TCTP has been described as a protein with growth-promoting and anti-apoptotic properties, we evaluated the effects of TCTP knockdown with siRNA technology on endothelial cell growth and apoptosis using BOECs. TCTP-specific knockdown experiments were performed with siRNA directed against TCTP and with a negative control siRNA. To confirm the silencing efficacy of the TCTP siRNA used for these experiments, immunoblotting analysis was performed in BOECs following a 48-hour transfection experiment with a TCTP siRNA (siTCTP) and a control siRNA (siCTRL) at 10 nM. Of note, the specific siRNA used to silence TCTP was chosen among 4 different siRNAs tested for their efficiency at knocking down TCTP protein level (Appendix C). Treatment with TCTP siRNA decreased TCTP protein levels by over 90% compared with the cells transfected with control siRNA (Figure 13B).

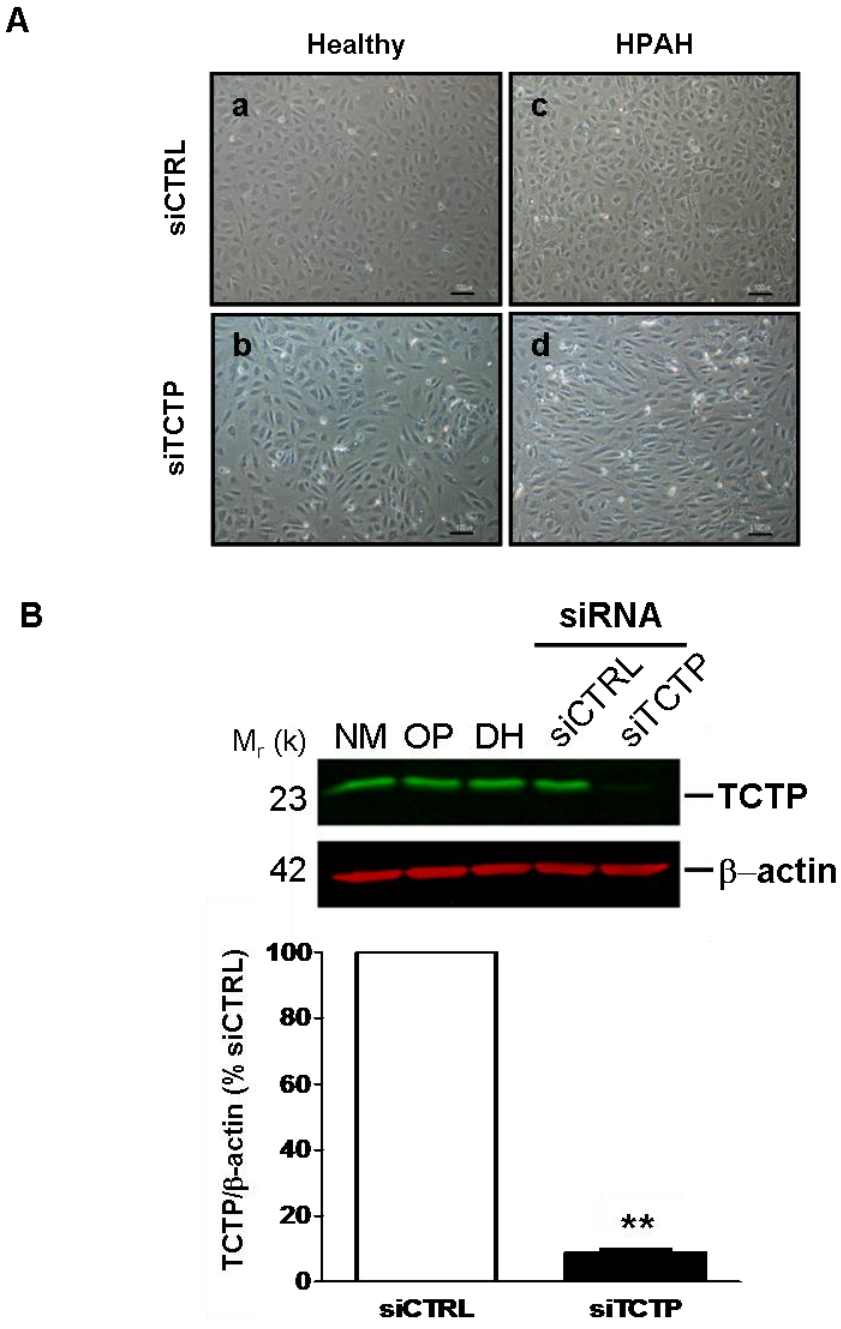

Figure 13. TCTP inhibition in BOECs.
(A) Representative images of BOECs following transfection with a control siRNA (siCTRL, a and c) as a negative control or TCTP siRNA (siTCTP, b and d) at 10 nM for 48 hours. Scale bar = 100µm. **(B)** Representative Western blot analysis showing TCTP protein inhibition following transfection with specific silencing siRNA (siTCTP) and control siRNA (siCTRL) at 10 nM for 48 hours (upper panel). Summary data showing the protein levels of TCTP normalized to the level of β-actin after transfection with silencing siRNA for TCTP (lower panel). NM indicates normal media; OP, Opti-mem; and DH, Dharmafect. n = 5. Data are mean ± SEM. Statistical differences were assessed by Student t-test. **p<0.01.

3.4.3.1 TCTP: Growth-promoting Properties

When TCTP-knockdowned BOECs from patients with HPAH were used in a BrdU incorporation assay, a significant marked reduction in BrdU incorporation capacity was observed when compared to its control siRNA over the 4 days (Figure 14). This result indicates that TCTP is an important mediator in cell growth in BOECs from patients with HPAH suggesting that it plays an essential role in the hyperproliferative state observed in Figure 2.

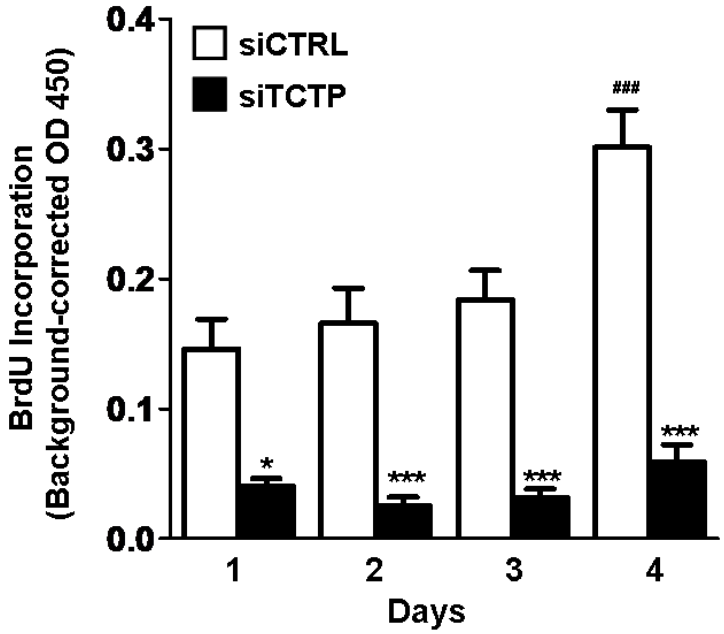

Figure 14. TCTP inhibition in BOECs decreases cell proliferation.
BOECs from patients with HPAH (n=4) were transfected with control siRNA (siCTRL) as a negative control or TCTP siRNA (siTCTP) at 10 nM for 48 hours. Cells were plated and, at the indicated times (day 1-4), BrdU was added (100 μM, 6 hours) and its incorporation quantitated by ELISA on day 1-4. Data represent mean ± SEM. Significant differences were assessed by one-way ANOVA followed by Tukey's Multiple Comparison Test. *p<0.05, ***p<0.001. vs. respective siCTRL; $^{###}$p<0.001. vs. siCTRL at day 1.

3.4.3.2 TCTP: Anti-apoptotic Properties

The effect of TCTP inhibition on BOEC apoptosis was assessed using annexinV and PI staining with flow cytometric analysis, following TCTP siRNA knockdown. Inhibition of TCTP levels significantly increased the percentage of early-stage apoptosis of BOECs from both healthy controls (42.50% $\pm$ 4.78 versus 29.81% $\pm$ 6.11; $P<0.05$) and HPAH patients (40.14% $\pm$ 2.86 versus 25.76% $\pm$ 2.76; $P<0.01$) when compared to their respective control siRNA conditions (Figure 15E). Annexin V-positive cells were also significantly increased from both healthy controls (55.09% $\pm$ 5.20 versus 33.62% $\pm$ 6.00; $P<0.05$) and HPAH patients (59.45% $\pm$ 3.40 versus 37.35% $\pm$ 2.88; $P<0.05$) when compared to their respective control siRNA conditions (Figure 15D). These results suggest that TCTP plays a role in the regulation of apoptosis in BOECs.

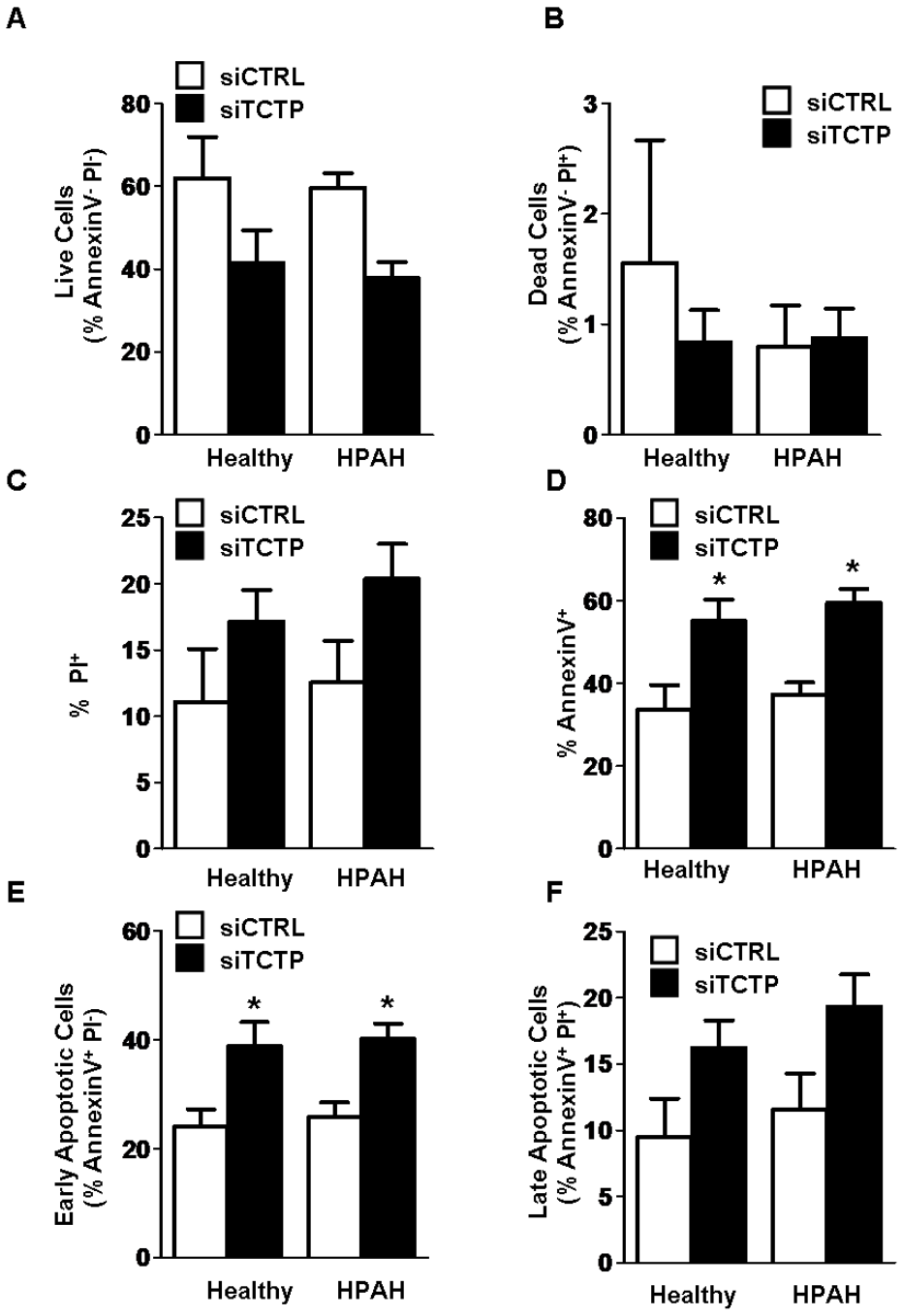

Figure 15. TCTP inhibition in BOECs decreases cell survival.
BOECs from healthy controls and patients with HPAH were transfected either with control siRNA (siCTRL) or TCTP specific siRNA (siTCTP) at 10 nM for 48 hours. Levels of apoptosis were detected by annexin-V and propidium iodide (PI) staining and flow cytometry. Summary data showing the effect of TCTP silencing on percentage live cells **(A)**, dead cells **(B)**, PI-positive cells **(C)**, annexinV-positive cells **(D)** or early- **(E)** and late-stage apoptosis **(F)**. Results are expressed as mean ± SEM (n = 4 for both groups). Significant differences were assessed by one-way ANOVA followed by Tukey's Multiple Comparison Test. *p<0.05, **p<0.01 versus respective control siRNA.

3.4.4 Increased TCTP Expression in Human PAH Lungs

To further investigate the expression and function of TCTP in PAH, we analyzed its protein levels in the lung of donor subjects and patients with HPAH. As depicted in Figure 16, immunohistochemical staining of human lung sections from patients with HPAH revealed a high expression of TCTP compared with lungs from control individuals (Figure 16 and Appendix D). A further examination of TCTP expression was done by confocal immunofluorescence study, to better visualize its spatial and cellular distribution. Consistent with the immunohistochemical results, immunofluorescence microscopic results confirmed the increased in TCTP staining in lungs from patients with HPAH and further revealed a pattern of expression which localises with endothelial cells and with smooth muscle cells within complex vascular lesions found in lungs of patients with HPAH (Figure 17 and Appendix E).

A

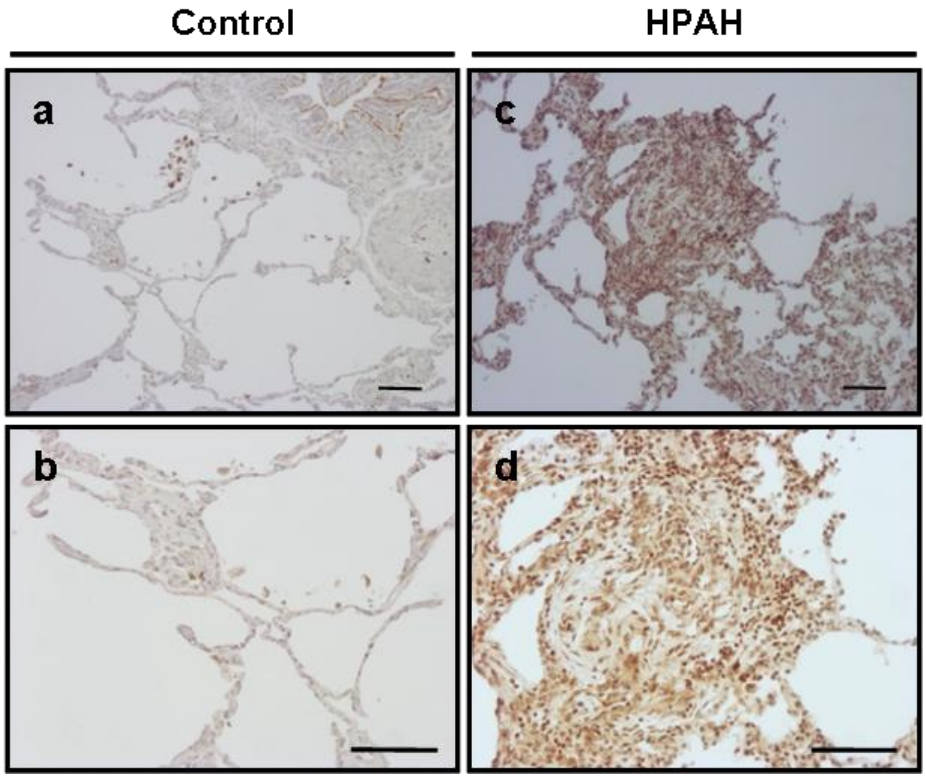

Figure 16. TCTP expression is elevated in lung vascular lesions of patients with HPAH.
(A) Representative lung sections from control subjects showing weak immunoreactivity for TCTP (a-b, brown) and from patients with HPAH (c-d) showing intense immunoreactivity for TCTP in lumen-occluding lesions and vascular wall. Original magnification x 10 (a and c) x 20 (b and d). Representative images of n=6 in each group. Scale bar = 100 µm.

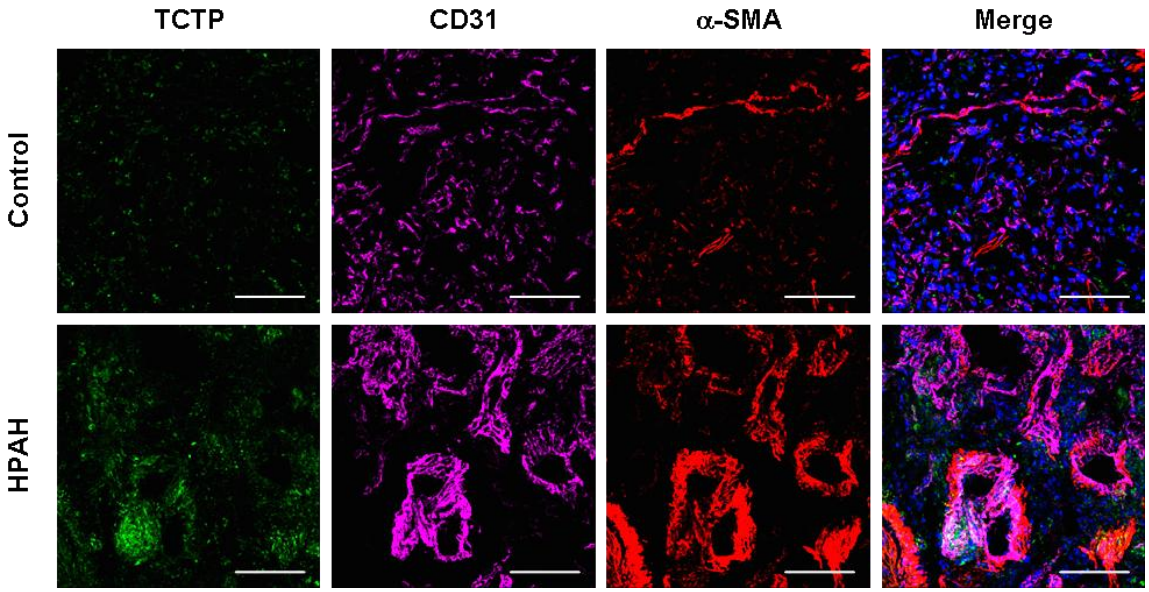

Figure 17. TCTP expression is elevated in lung vascular lesions of patients with HPAH and localizes with endothelial and smooth muscle cells.
Representative lung sections from control subjects showing weak immunoreactivity for TCTP (green), CD31 (purple) and α-SMA (red). Representative lung sections from patients with HPAH showing intense immunoreactivity for TCTP, CD31 and α-SMA in remodeled blood vessels. Merge images include TCTP, CD31, α-SMA and DAPI (blue) staining. Representative images of n=3 in each group. Original magnification x 20. Scale bar = 100μm.

3.4.5 SU5416 Rat Model of Severe PAH

The potential role of TCTP in PAH was further studied *in vivo* in the SU5416 rat model of severe angioproliferative PAH. In this model, SU5416 (a VEGFR-2 antagonist) induces lung endothelial cell apoptosis, which then results in reactive vascular cell proliferation and the formation of complex lung vascular lesions (Taraseviciene-Stewart et al., 2001). Our group has identified a strain of Sprague-Dawley rats that have high susceptibity to SU5416, and develops severe and progressive PAH even with a single injection of the SU5416 compound and without the need for concomitant hypoxia (Jiang, 2012). Thus, molecular changes in this model system can be directly attributed to the effects of VEGFR2 inhibition and apoptosis without the potential confounding influences of chronic hypoxia. Rats received a single injection of SU5416 (20 mg/kg) and marked increases of right ventricular systolic pressures (RVSP) developed over the following 8 weeks when compared with the vehicle-treated controls (carboxymethylcellulose solution, CMC) (98.33 ± 3.38 versus 28.60 ± 0.50; $P<0.01$) (Figure 18A). In addition, SU5416-treated rats had a significantly higher right ventricular mass than control rats (0.71 ± 0.05 versus 0.28 ± 0.02; $P<0.01$) (Figure 18B). Besides the increase in RVSP and right ventricular mass, SU5416-treated rats exhibited complex pulmonary arterial remodeling, even without exposure to hypoxia (Figure 18C). Therefore, this model allowed us to study the changes in TCTP expression induced by endothelial cell apoptosis without the confounding effects of hypoxia.

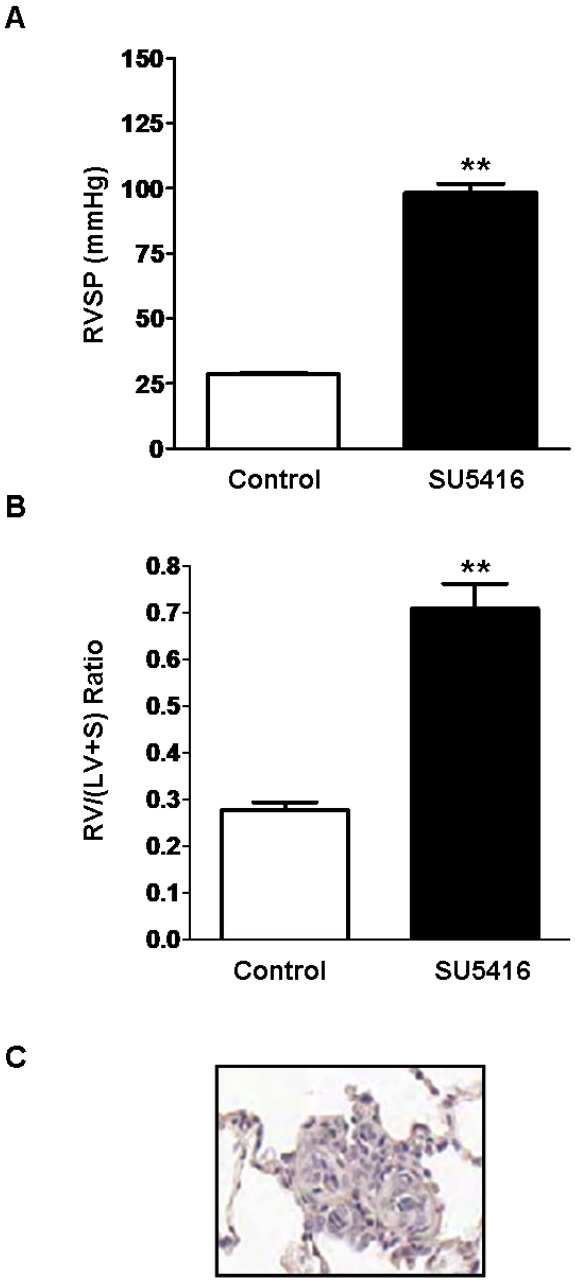

Figure 18. Right ventricular systolic pressures and right ventricular hypertrophy of the SU5416 rat model of severe PAH.

Animals were either injected with vehicle (carboxymethylcellulose solution, CMC) (Control, n=3) or with SU5416 (SU5416; n=3). **(A)** Histograms showing values of right ventricular systolic pressures (RVSP) as a surrogate of mean pulmonary arterial pressures at 8 weeks after SU5416 injection. **(B)** Histograms showing values of ratio of right ventricle weight to left ventricle plus septum weight (RV/[LV+S]), as a measurement of right ventricular hypertrophy at 8 weeks after SU5416 injection. Data are mean ± SD. Significant differences were assessed by Student t-test. **p<0.01. **(C)** H&E-stained lung section of SU5416-treated rats showing complex pulmonary arterial remodeling.

3.4.6 Increased TCTP Expression in the Remodeled Arterioles of the SU5416 Severe Rat Model of PAH

To investigate whether TCTP protein expression levels were induced in the lungs of the SU5416-treated animals, immunofluorescence staining was performed. No immunoreactivity was observed with the presence of an isotype control (Appendix F). In the normal lungs, immunofluorescence staining revealed very little staining for TCTP, which was localised almost exclusively to the endothelium of small arterioles (Figure 19). As expected, there was only minimal staining for alpha-smooth muscle actin (α-SMA) for these normal vessels (Figure 19). In contrast, SU5416-treated rats showed a marked increase in expression of TCTP tightly associated with remodeled arterioles, as shown by the increase in α-SMA staining (Figure 19). In many cases, TCTP-positive cells were observed to be occluding the lumen of these small arterioles (Figure 19).

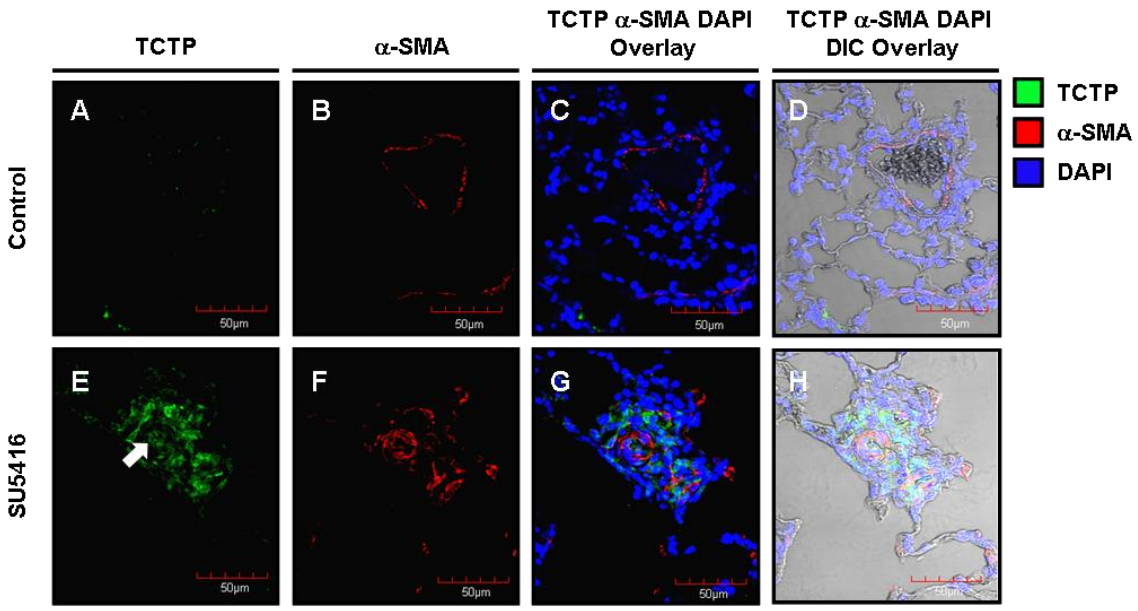

Figure 19. TCTP-positive cells are found in vascular plexiform lesions of the SU5416 rat model of severe PAH.
Representative TCTP (green) and α-SMA (red) immunofluorescence stainings in small pulmonary arteries from control **(A-D)** and SU5416-treated rats **(E-H)**. Nuclei are counterstained with DAPI (blue). Differential interference contrast (DIC) images merged with TCTP, α-SMA and DAPI are shown in panels **D** and **H**. Arrow is highlighting TCTP-positive cells occluding the lumen of the small arterioles. Results are representative sections from 3 animals per group. Scale bar = 50 μm.

3.4.7 TCTP-positive cells are of Endothelial Cell Phenotype

To investigate whether these TCTP-positive cells are of endothelial cell phenotype, immunostaining of adjacent lung sections in the SU5416-treated rats with the endothelial-cell specific marker von Willebrand factor (vWF) was performed (Figure 20, E-H). As presented in Figure 20, TCTP staining was highly localised to remodeled arterioles and exhited a distribution similar to that of the endothelial marker vWF (Figure 20).

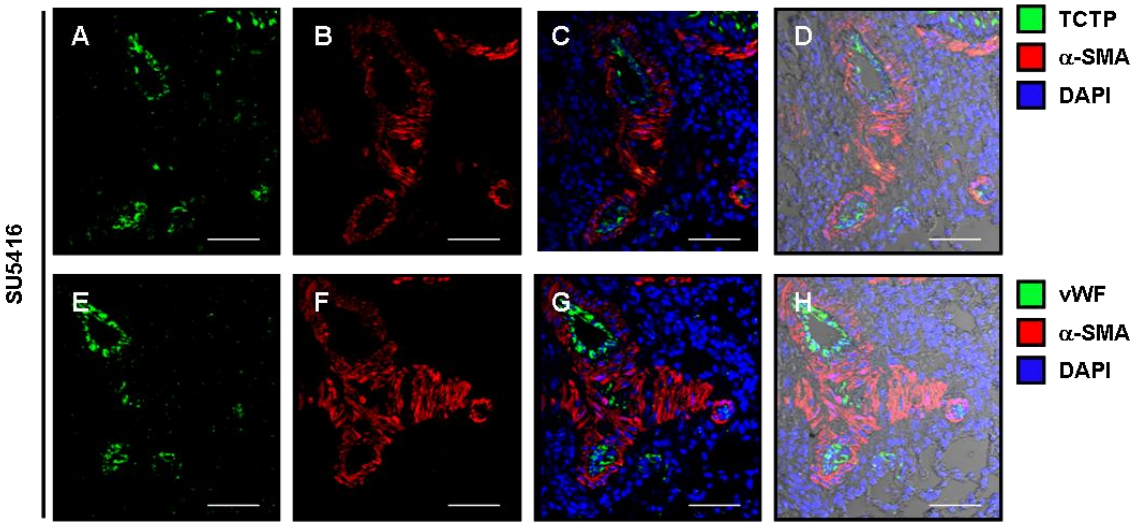

Figure 20. TCTP-positive cells are highly localised in the endothelium of the SU5416 rat model of severe PAH.
(A-D) Representative TCTP (green) and α-SMA (red) immunofluorescence stainings in small pulmonary arteries from a SU5416-treated rat. **(E-H)** Representative vWF (green) and α-SMA (red) immunofluorescence stainings in small pulmonary arteries from a SU5416-treated rat. Nuclei are counterstained with DAPI (blue). Differential interference contrast (DIC) images merged with TCTP or vWF, α-SMA and DAPI are shown in panel D and H. Results are representative sections from 3 animals per group.
Scale bar = 50 µm.

3.4.8 TCTP-positive Cells are Tighly Localised to Proliferating Cells

To know whether TCTP-positive cells are localised to proliferating cells in the vascular plexiform lesions in the SU5416 rat model of severe PAH, immunostaining of lung sections with proliferating cell nuclear antigen (PCNA) was performed. No immunoreactivity was observed with the presence of isotype controls (Appendix G). Immunofluorescence staining revealed high expression of TCTP in arteriolar vascular cells of PAH lungs tightly localized to proliferating cells (proliferating cell nuclear antigen [PCNA]-positive cells) within vascular plexiform lesions (Figure 21).

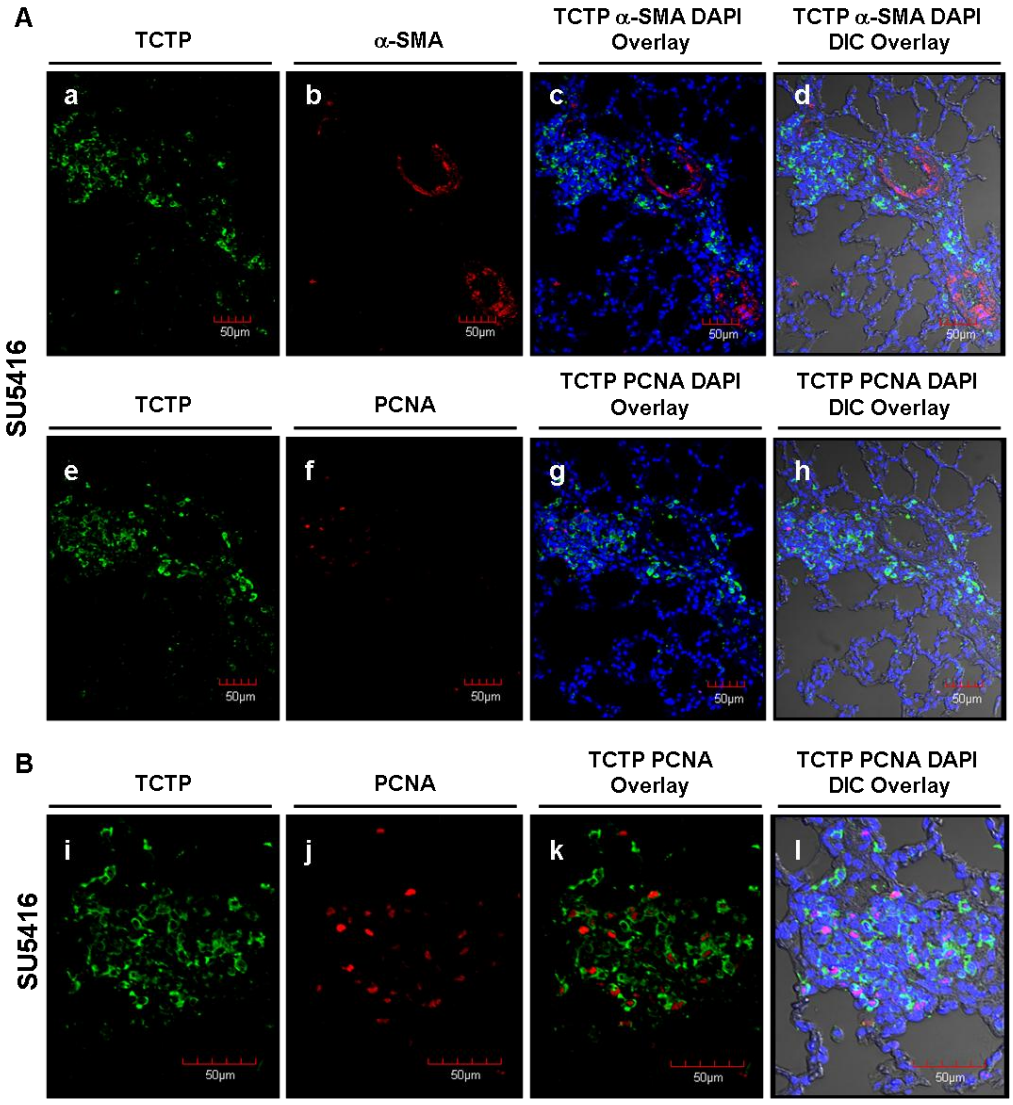

Figure 21. TCTP-positive cells are co-localizing with proliferating cells in vascular plexiform lesions of the SU5416 rat model of severe PAH.
(A) Representative immunofluorescence stainings in lung tissue sections from a SU5416-treated rat (8 weeks) for TCTP (a, e and i, in green) alpha-smooth muscle actin (b, α-SMA in red) and proliferating cell nuclear antigen (f and j, PCNA in red) in small pulmonary arteries. Nuclei are counterstained with DAPI (blue) and merged images with TCTP, α-SMA or PCNA are shown in panels c and g. Differential interference contrast (DIC) images merged with TCTP, α-SMA or PCNA and DAPI are shown in panel d, h and i. **(B)** Higher magnification of TCTP and PCNA stained lung section is showing that TCTP-positive cells (i) are co-localizing with PCNA-positive cells (k). Results are representative sections from 3 animals. Scale bar = 50 μm.

3.4.9 TCTP-positive Cells Are Present As Early As 1 Week After SU5416 Injection

To investigate how early TCTP-positive cells are present after SU5416 exposure, a time point experiment was conducted. Rats received a single injection of the SU5416 compound and at different time points (1, 2, 4 and 8 weeks) right ventricular systolic pressures (RVSP) and right ventricular hypertrophy were measured (Figure 22). A time-dependent significant increase in RVSP and in RVH was observed (Figure 22). To investigate whether TCTP protein expression also occurred in the early time point after SU5416 injection, immunofluorescent staining of lung sections from SU5416-treated rats at these different times was executed (24 hours as well as 1, 2, 4 and 8 weeks). As expected, staining for alpha-smooth muscle actin (α-SMA) was progressively increased over time. Interestingly, strong TCTP-positive cells were present as early as 1 week after SU5416 injection (Figure 23). Similar to previous results with the 8 week time point showing TCTP primarily localized with remodeled arterioles, TCTP was localised almost exclusively to remodeled vessels as early as 2 weeks. Of particular interest, strong isolated TCTP-positive cells were found as early as 2 weeks suggesting that these single TCTP-positive cells might be involved in mediating the formation of the angioproliferative vascular plexiform lesions (Figure 23). Further studies will be needed to confirm the potential role of TCTP in mediating the formation of angioproliferative vascular lesions.

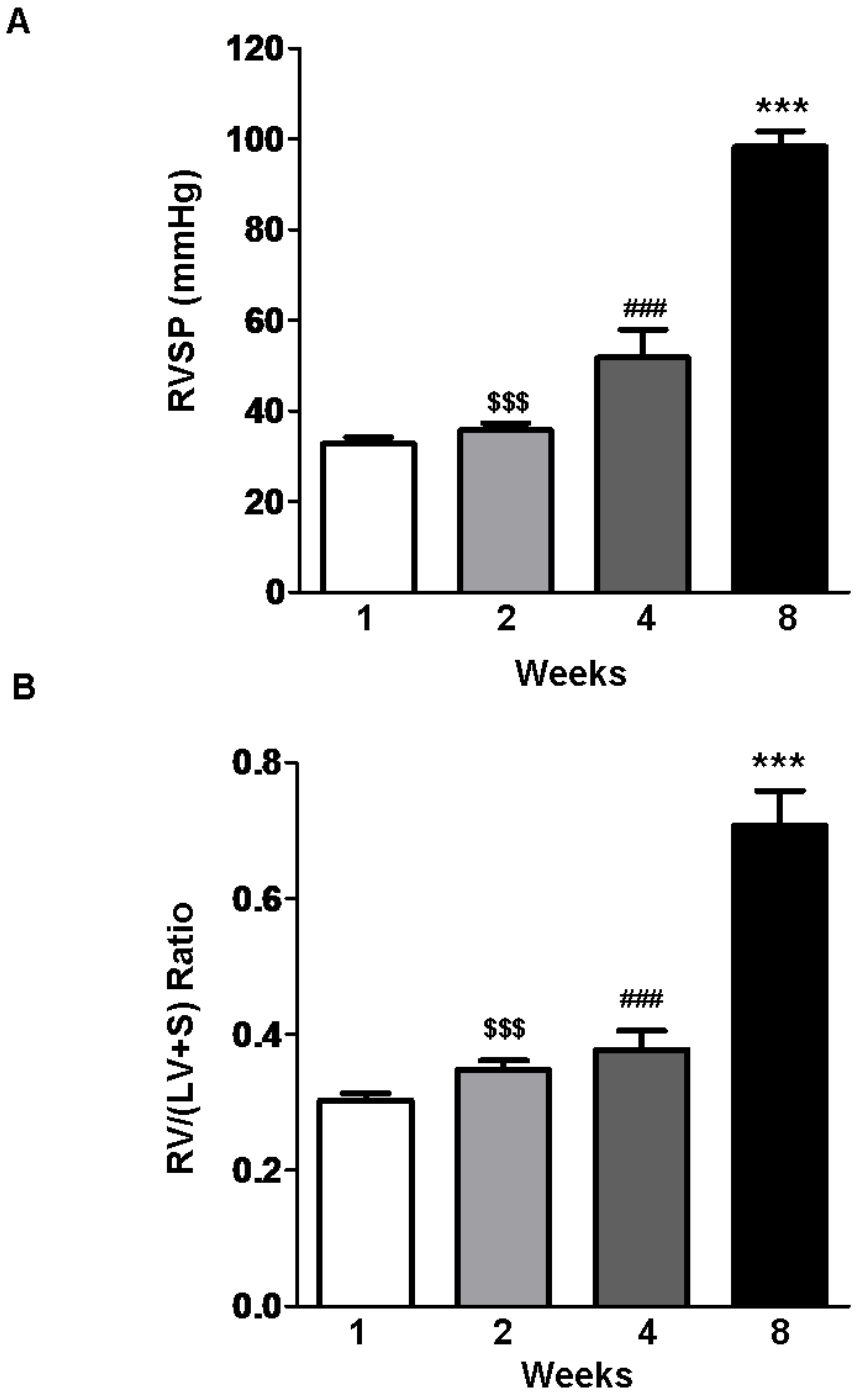

Figure 22. Right ventricular systolic pressures and right ventricular hypertrophy in SU5416-treated rats over time.
Sprague-Dawley rats were injected with SU5416 (20 mg/kg) and right ventricular systolic pressures (RVSP) and right ventricule hypertrophy (right ventricle weight to left ventricle plus septum weight RV/[LV+S]), were measured before the rats were sacrificed at 1, 2, 4 and 8 weeks (n=3-9 per group). Data are mean ± SEM. Significant differences were assessed by one-way ANOVA followed by a post hoc Tukey's. ***p<0.001 (1w vs. 8w), $^{###}$p<0.001 (2w vs. 8w), $^{\$\$\$}$p<0.001 (4w vs. 8w).

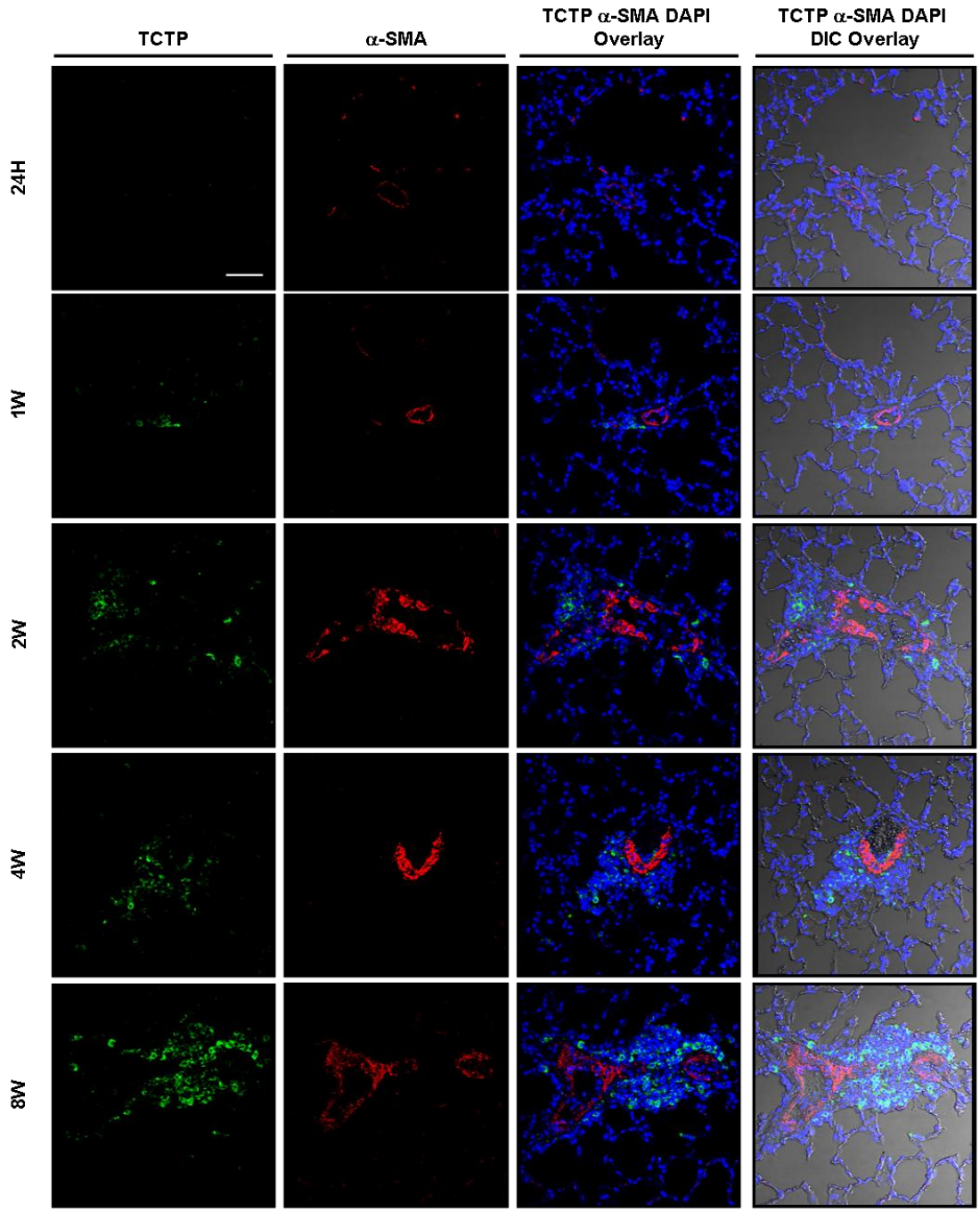

Figure 23. TCTP-positive cells are present as early as 1 week following SU5416 injection.
TCTP (green) and α-smooth muscle-actin (α-SMA) (red) immunofluorescence staining of lung sections from rats injected with SU5416 and sacrified at different time points (24 hours as well as 1, 2, 4 and 8 weeks). Nuclei are counterstained with DAPI (blue). Differential interference contrast (DIC) image merged with TCTP, α-SMA and DAPI are shown in right panels. Results are representative sections from 3-9 animals.
Scale bar = 50 μm.

3.5 Discussion

3.5.1 TCTP in PAH: Role in Lung Vascular Remodeling

A 2-D gel-based proteomic approach identified TCTP as an upregulated protein in BOECs from patients with HPAH harboring *BMPR2* mutations. TCTP was chosen as a candidate protein to further study in PAH, as its biological functions (anti-apoptotic, involved in malignant transformation, growth and inflammation) made it a promising potential molecular candidate to contribute to the pathological features described in PAH. In particular, its previously described role in mediating cell-cell signaling between apoptosing ECs and surrounding SMCs raises the possibility that TCTP may represent the link between pulmonary EC apoptosis, which is a trigger for PAH, and the subsequent reactive vascular cell proliferation and inflammation that characterize the established disease. This hypothesis is supported by the observation that TCTP expression was markedly increased in the lung tissue sections of patients with PAH, which may better reflect the disease milieu of the lungs of a PAH patient with late-stage disease, mainly within complex occlusive intimal and plexiform lesions. Transcriptomic analyses of lymphoblastoid lines derived from *BMPR2* mutation carriers with HPAH (West et al., 2008), blood cells (Bull et al., 2004), and lung tissue specimens from IPAH (Geraci et al., 2001; Rajkumar et al., 2010), as well as intrapulmonary arteries of hypoxia-induced PH in mice have been previously conducted. Interestingly, the TCTP gene (i.e. *TPT1*) was not found to be among the genes statistically differentially regulated in individuals with PAH versus normal individuals in all these above-mentioned studies, which suggests that the TCTP protein over-expression is due primarly to post-transcriptional regulation and/or that its dysregulation is specific to endothelial cells of patients with PAH. As such, the study of the mRNA expression of TCTP in the BOECs would be more relevant to further understand the changes in TCTP protein expression,

although the correlation between mRNA and protein levels is often moderate and insufficient to predict protein expression levels (Guo et al., 2008; Gygi et al., 1999).

The relevance of TCTP in lung vascular remodeling was further studied *in vivo* in the SU5416 rat model of severe angioproliferative PAH. The rats received a single injection of the SU5416 compound and even without the exposure to chronic hypoxia, the rats progressively developed increases in right ventricular systolic pressures and right ventricular hypertrophy as well as complex pulmonary arterial plexiform-like lesions. In addition, this is the first description of angioproliferative lesions following SU5416 injection without exposure to chronic hypoxia. In the original report of the SU5416 rat model from the Tuder group, the authors reported that neither SU5416 nor hypoxia alone developed severe progressive PAH associated with the formation of occlusive neointimal lesions in small pulmonary arteries and arterioles (Taraseviciene-Stewart et al., 2001). The Oka group have used the SU5416/hypoxia/normoxia-exposed rat and examined the rats hemodynamically and histologically a very late stage (i.e. 13 to 14 weeks after the SU5416 injection) (Abe et al., 2010). The authors reported that the SU5416/hypoxia/normoxia-exposed rats developed severe PAH accompanied by pulmonary arteriopathy strikingly similar to that observed in human severe PAH (i.e., concentric laminar neointimal and two different patterns of complex plexiform lesions), but have not studied the response to SU5416 alone.

When studying the importance of TCTP expression in our SU5416 rat model, TCTP-positive cells appeared to be occluding the lumen of the small arterioles of the SU5416-treated rats, and many of these TCTP-positive proliferating cells were seen within the lumen of occluded vessels of PAH rats, further supporting TCTP importance in cell proliferation. The time point experiment executed in the SU5416 rat model of PAH

indicated that TCTP expression is present as early as 1 week after the EC injury (i.e. apoptosis) in vascular cells, but becomes more evident at 2 weeks and is markedly expressed during prolonged injury (8 weeks), when PAH is fully established. TCTP-positive cells were observed to be localised to arteriolar lesions, suggesting a role in mediating the angioproliferative vascular observed as early as 2 weeks. Interestingly, TCTP staining was also executed in the MCT rat model of PAH, and its expression was minimal, providing further evidence that TCTP might be involved in the formation of angioproliferative lesions observed in the SU5416 model, which are not present in the MCT model, mainly characterized by SMC hypertrophy (Appendix H). Further studies will be needed to prove that TCTP increased in expression is directly leading to the development of lesions. Future experiments to be done are discussed in Chapter 4.

Under conditions of chronic pro-apoptotic stress *in vivo*, such as in the SU5416 model, there may be selection pressures that favour the appearance of ECs expressing higher levels of survival factors, such as survivin (McMurtry et al., 2005) and TCTP, which are thought to contribute to a neoplastic-like transformation of the vascular cells within the developing intimal lesions. Indeed, TCTP has been strongly implicated in malignant transformation in cancer cells (Chan et al., 2012; Jung et al., 2011; Ma et al., 2010). TCTP's role in neoplasia has been described in different studies, such as the one conducted by Chang et al., where they showed that TCTP is implicated in the malignant transformation of hepatocytes with the phenotypes of accelerated mitotic progression and the production of aneuploidy (Chan et al., 2012). TCTP has also been shown to induce human breast epithelial cell transformation through the activation of Src (Jung et al., 2011). The hypothesis in which cells found in the pulmonary vascular lesions might be abnormal in PAH was first suggested in 1998, by Voelkel et al., and has led to a cancer paradigm of severe PAH (Rai et al., 2008; Voelkel et al., 1998). The complex

vascular lesions are described as neoplasms, because abnormal and uncontrolled cell growth is present, and possess certain of the cancer-defining mechanisms (Hanahan and Weinberg, 2000), such as angiogenesis (Tuder et al., 2001), evasion of apoptosis (Ameshima et al., 2003; Levy et al., 2007; McMurtry et al., 2005) and presence of anti-apoptotic factors (McMurtry et al., 2005 (Yeager et al., 2001). Hence, the concept of endothelial cell as a “quasi-malignant” cell led to the development of therapies aiming to reverse the proliferative remodeling in severe PAH. For instance, McMurtry et al. showed that inhibition of survivin — a member of the mammalian “inhibitor of apoptosis” family shown to be highly expressed in complex vascular lesions in PAH lungs — reversed established monocrotaline-induced PAH (McMurtry et al., 2005). Survivin is essentially expressed in all cancers, but not in most normal adult cell types, and is known to promote cell proliferation (Altieri, 2003). Interestingly, TCTP characteristics fit some aspects of the profile of survivin, which makes it an interesting target to pursue for antiproliferative and proangiogenic therapies in PAH. Certainly, increased levels of TCTP in the SU5416 model of severe PAH were highly localized to proliferating vascular cells within the occlusive arteriolar lesions. TCTP expression was found to be markedly increased in complex vascular lesions found in the pulmonary microvasculature of patients with HPAH, as well as in the SU5416-treated rats.

3.5.2 TCTP in PAH: A Survival Factor

Studies using small interfering RNA to knockdown TCTP showed that TCTP was involved in BOEC proliferation and apoptosis. TCTP silencing markely reduced cell proliferation in BOECs from patients with HPAH harboring *BMPR2* mutations, suggesting that the higher proliferative index of HPAH-derived BOECs is mainly mediated by TCTP. In addition, TCTP silencing caused apoptosis in BOECs from both patients with HPAH and healthy controls to the same extent. These findings are in agreement with earlier

gene silencing studies of TCTP by siRNA, where a role of TCTP in cell growth/proliferation and apoptosis has been reported in different cancer cells: human prostate cancer cells (Gnanasekar et al., 2009), human metastatic carcinoma cell lines MCF7 and human skin squamous cell carcinoma. One caveat of the RNA interference (i.e. siRNA and shRNA) experiments conducted in this thesis is the use of only one sequence for TCTP. Although the chosen siRNA and shRNA were shown to downregulate TCTP protein expression levels by immunoblotting analyses, off-target effects cannot be ruled out for the observed siRNA phenotype. Indeed, off-target effects have been documented with the use of siRNA and shRNA (Jackson and Linsley, 2010). Therefore, to increase confidence in the data from the siRNA/shRNA experiments conducted in this thesis, two or more siRNA/shRNA should be used to target TCTP. If the phenotypes described in this study (i.e. decrease cell growth and survival) are validated with different siRNAs exhibiting comparable gene silencing efficacy, then it can be concluded that the observed phenotype is specifically due to gene silencing of TCTP. On the contrary, if the observed phenotype is not reproducible with a different siRNA, then the changes induced by the single siRNA might be attributed to off-target effects rather than the gene-specific effect. Other strategies to corroborate a single siRNA or shRNA include overexpression experiments of TCTP, the use of small molecules (i.e. pharmalogical compounds such as sertraline and thioridazine) or microRNAs that target TCTP. Indeed, the use of these methods could provide complementary data to support the *in vitro* RNA interference data. Unfortunately, these experiments could not be conducted in this study due to the lack of availability of BOECs. The use of microRNAs to induce gene silencing of TCTP could be used in future studies. MicroRNAs (miRNAs) are small non-coding single stranded RNAs (21-23 nucleotides long) that play a role in the post-transcriptional regulation of mRNA through base pairing with target mRNAs to induce RNA degradation or translation suppression of the targeted transcripts (Farh et

al., 2005). Lo et al. reported candidate microRNAs for the regulation of TCTP using the mirSVR predicted target site scoring method (Betel et al., 2010) and the online tools at MicroRNA.org (http://www.mirbase.org), and they came up with these overlapping miRNAs (miR): miR-19a, miR-27a, miR-27b,miR-19b, miR-186, miR-203 and miR-377 (Lo et al., 2012). Interestingly, Lo et al. reported that human miR-27b regulates the expression of the TCTP protein in oral cancer cells (Lo et al., 2012), where overepression of miR-27b leads to a significant decrease in TCTP mRNA and protein expressions.

In addition to its effects on cell growth and survival, recent studies have indicated that TCTP exhibits potent cytokine-like functions, including inducing the release of histamine and immunoglobulin production during late phase allergic inflammation (MacDonald et al., 1995), an aspect of TCTP that is worth pursuing since inflammation is an important component of PAH (Jurasz et al., 2010). As described in the introduction of Chapter 3, TCTP has been implicated as a key mediator leading to persistence of chronic allergic inflammation in the context of asthma (Choi et al., 2009; Kashiwakura et al., 2012; Macdonald, 2012). Interestingly, Choi et al. have shown in a murine model of ovalbumin-induced allergy that pretreatment with pantoprazole (i.e. a proton pump inhibitor) reduced infiltration of inflammatory cells and inhibited TCTP secretion induced by ovalbumin challenge, indicating that pantoprazole might exert its anti-allergic effect by blocking TCTP secretion (Choi et al., 2009). PAH is known to be associated with diseases in which inflammation has a central role (e.g. autoimmune diseases such as scleroderma and systemic lupus erythematosus, as well as HIV infection) (El Chami and Hassoun, 2012), leading to the suggestion that inflammation may be a major pathogenic component of pulmonary vascular remodeling and PAH (Hassoun et al., 2009). Data from patients with PAH are in line with this hypothesis: increased levels of inflammatory

infiltrates (macrophages and lymphocytes) (Tuder and Voelkel, 1998), increased expression of chemokines RANTES and fractalkine (Balabanian et al., 2002; Dorfmuller et al., 2002) have been found in the remodeled vessels as well as increased levels of pro-inflammatory cytokines such as IL-1b and IL-6 have been found in the serum of PAH patients (Humbert et al., 1995). Interestingly, the Voelkel group showed that the combination of ovabulmin immunization and SU5416 treatment resulted in severe angio-obliterative PAH, accompanied by increased IL-6 expression in the lungs (Mizuno et al., 2012).

3.5.3 TCTP in PAH: Schematic Model

As shown by our group and others, apoptosis represents a critical link between vascular injury and vascular remodeling in the development of PAH (Jeffery and Wanstall, 2001; Jurasz et al., 2010; Tuder et al., 2001; Zhao et al., 2003). In addition, reduced levels of BMPR-II have been shown to increase apoptosis (Teichert-Kuliszewska et al., 2006). Therefore, sustained increased in TCTP expression during chronic endothelial cell injury due to mutations in *BMPR2* or the use of an apoptotic inducer such as SU5416 could promote endothelial cell survival in a cell-autonomous manner leading to the survival and hyperproliferation of cells with higher TCTP abundance levels. Ultimately, the survival of these apoptotic-resistant endothelial cells could contribute to the obliterative and degenerative changes to the pulmonary microvasculature that characterize the advanced stages of PAH (Figure 24).

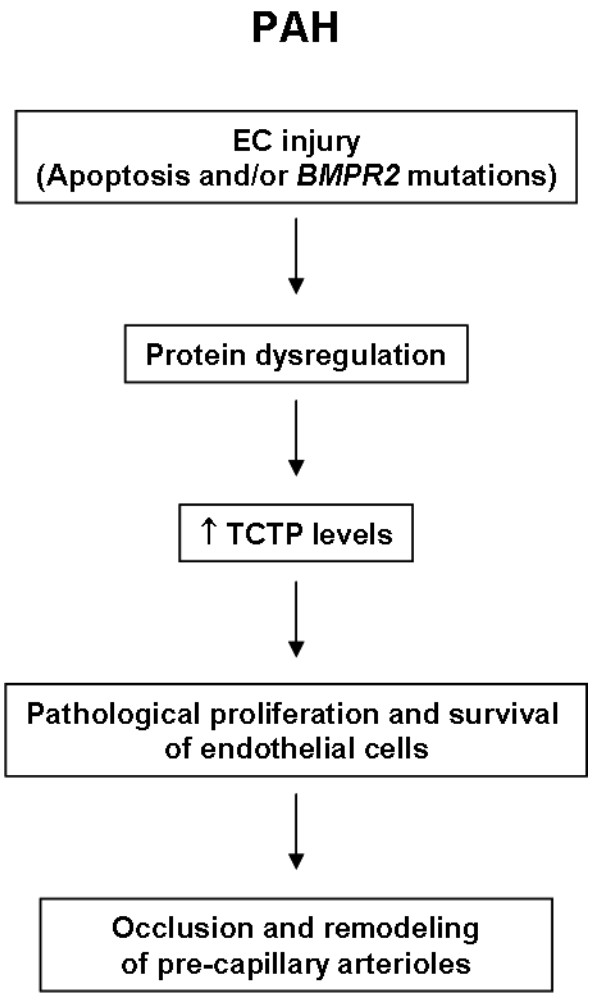

Figure 24. Schematic model of the potential role of TCTP in PAH.
Endothelial cell injury caused by SU5416 compound or *BMPR2* mutations lead to an altered protein profile in endothelial cells such as increased TCTP levels. TCTP promotes cell survival in an cell-autonomous manner and may participate in the selection of apoptotic-resistant cells that will result in the pathological proliferation and survival of endothelial cells leading to the occlusion and remodeling of pre-capillary arterioles.

CHAPTER 4: PERSPECTIVES

4.1 Future Studies

4.1.1 Studying Other Candidates Identified through the 2-D PAGE Approach

Many other protein hits found through the 2-D gel approach are interesting candidates and will require further examination to determine whether they play a role in PAH. For example, candidates involved in the regulation of apoptosis, such as proteasome activator complex subunit 1, as well as in cell proliferation such as DNA replication licensing factor MCM7, and signal transduction, such as cAMP-dependent protein kinase type I-alpha regulatory subunit and guanine nucleotide-binding protein, should be examined because their associated functions are important in PAH, as supported by the findings in this thesis and the litterature.

4.1.2 A Global Proteomic Approach: ITRAQ-Based Quantitative Proteomic Analysis

During the writing of this thesis, I was involved in the implementation of another high-throughput proteomic approach named isobaric tag for relative and absolute quantitation (iTRAQ)-based quantitative proteomic analysis in order to identify/generate more protein candidates that could be involved in the pathogenesis of PAH. iTRAQ is a very powerful proteomic technique because it simultaneously quantitates up to eight samples (i.e. 8-plex) under the same experimental conditions (i.e. in this case, 4 HPAH with *BMPR2* mutations and 4 healthy controls). We only recently have undertaken this other quantitative proteomic approach because we were not equipped to use this technology at the start of the study. In addition, 2-D gel electrophoresis approach was chosen over other available proteomic approaches at the time of designing this study as it allows the quantitation and comparison of protein changes in many samples (i.e. 8 in this case) with minimal protein quantity (i.e. 100 μg). The goal was to use iTRAQ with the

same BOEC samples that were used in this thesis to try to confirm the observation obtained by the 2-D gel experiment and to obtain more protein hits to better understand the changes occuring in HPAH at the protein level. We used whole protein lysate again (i.e. 100 μg) with the iTRAQ approach as we were limited in BOEC material. We combined iTRAQ labeling with an off-gel fractionation method, which fractionates the iTRAQ-labeled peptide sample into 24 fractions based upon the peptide isolectric points, to target a good dynamic range of concentration of proteins. In addition, each of the 24 peptide fractions was analysed by 2-D LC-MS/MS to further increase the sensitivity in protein detection and identification. iTRAQ is thought to preserve post-translational modification information and to allow the global study of protein signaling in a specific system. The advanced combination of proteomics and bioinformatics will provide the opportunity to study quantitative changes and allow a better representation of the global protein changes occuring. Mass spectrometry results of the first run were recently obtained and 1600 identifiable and quantifiable proteins from different families were found. Further examination of this new protein data set will help better understanding the molecular events underlying the pathogenesis of PAH.

4.1.3 Potential Role of TCTP in Mediating Angioproliferative Lesions in PAH

TCTP was found through the 2-D gel electrophoresis approach in BOECs and was studied *in vivo* in the human and rat lung tissues to better comprehend its importance in PAH and was found to be highly localised to occlusive arteriolar lesions. The roles of TCTP in the formation of occlusive arteriolar lesions and in PAH will have to be further pursued to know if this protein could be used as a therapeutic target. Preliminary results from a pilot study in the SU5416-treated rats have been obtained and are presented in the appendices. The strategy that I have used in this pilot trial was the use of a shRNA plasmid for TCTP mixed with *in vivo*-jetPEI, a nucleic acid delivery reagent for functional

studies and RNAi experiments, using weekly jugular vein injections. Unfortunately, the preliminary results did not lead to significant reduction in hemodynamic measurement of PAH (RSVP and RVH) in the animals receiving the shRNA plasmid for TCTP. For the next phase, optimal time of administration (later time point for shRNA plasmid administration) and shRNA plasmid transfection conditions (increase dose of shRNA plasmid and *in vivo*-jetPEI) will have to be tested to ensure a good transfection efficacy. In addition, to monitor the efficiency of the knockdown of TCTP with the shRNA strategy, TCTP protein and mRNA expression analyses will have to be conducted in future studies with whole lung tissues of the animals receiving the shRNA plasmid for TCTP compare with the scrambled negative control. In this thesis, immunofluorescence analysis was conducted to monitor TCTP protein expression levels at the 4 week time point after the weekly injections of the shRNA plasmid. The immunoflorescence analysis results presented in the appendix R shows that strong TCTP-positive cells were found in the vascular lesions of animals receiving the shRNA plasmid for TCTP as well as the vehicle. This result indicates that TCTP expression levels were not decreased at the 4 week time point and that vascular lesions were present, suggesting that TCTP inhibition was not achieved. Further studies will have to be conducted to achieve an optimal inhibition of TCTP using this strategy. For instance, a more effective way to test the efficacy of the inhibition of TCTP will be to study TCTP protein and mRNA expression levels in the lung tissues shortly after injection of the plasmid, and this, at multiple time points after injection (i.e., 2, 4 and 7 days) to monitor the length of time of the inhibition of TCTP by the shRNA plasmid. This experiment will indicate the timeframe at which the shRNA plasmid can suppress TCTP gene expression, which will indicate the proper timing of the injections of the shRNA plasmid. In addition, to ensure that the phenotype observed in the animals is specific to TCTP gene silencing by the shRNA plasmid and not by off-target effects, the results will have to be confirmed with another shRNA

expression vector with a different sequence for TCTP. As explained in Chapter 3 in section 3.5.2, off-target effects can compromise the specificity of the shRNA used if sequence identity between siRNA or shRNA and random mRNA transcripts leads to knockdown expression of non-targeted genes. The time point experiment where TCTP expression was examined after SU5416 injection is indicative of TCTP being present as early as 1 week, which might rather be protective than pathological at this time point. Therefore, TCTP manipulation will have to be targeted to a time point where overexpression is present and where it might participate in the formation of the angioproliferative lesions. TCTP manipulation and silencing with pharmacological compounds, such as sertraline and thioradizine, which have been shown to decrease TCTP protein levels in cancer cells (Tuynder et al., 2004), could also be tested in order to be clinically relevant.

4.1.4 TCTP Presence in Exosomes: Mechanism for Vascular Remodeling?

The study of exosomes is another avenue that will need to be further explored as it is increasingly recognised that these microvesicles might play important roles in pathological disorders such as cancer (Park et al., 2010) and neurodegenerative diseases such as Alzheimer's disease (Mattson, 1997) .These microvesicles contain RNA, microRNA and proteins that might considerably influence intercellular communication with neighborouring cells. In PAH, it might have a tremendous importance, as the formation of complex vascular lesions involves the interactions of multiple cell types (e.g., ECs, SMCs, myofibroblasts, stem cell-like and immune cells). Quantitative measurement of the number of released exosomes from BOEC-derived from patients with HPAH compared with healthy controls should be studied to determine if the release in PAH is dysregulated. In a preliminay experiment, TCTP was found to be present in the exosomes derived from BOECs of a healthy control and two patients with

HPAH (Appendix I). The importance of the presence of TCTP in the exosomes should also be determined under normal and apoptotic conditions and its effects on SMC proliferation and survival should be accessed to further decipher its role in vascular remodeling. These experiments will bring further insights into the mechanisms of pathological intercellular communication in PAH by the means of exosomes and TCTP.

4.2 Conclusions

In conclusion, in this thesis I provided additional evidence supporting the concept of endothelial cell dysfunction (e.g. endothelial cell apoptosis and proliferation) in PAH and reported TCTP as a potential novel mediator of occlusive vascular remodeling in PAH. I also demonstrated that TCTP protein expression is upregulated in BOECs from patients with HPAH harboring *BMPR2* mutations, in lungs of patients with PAH and in lungs of the SU5416 rat model of PAH. Using an *in vitro* system, I showed that TCTP plays a prominent role in endothelial cell growth and survival. Additionally, TCTP-positive cells were observed in PAH lungs of remodeled blood vessels, suggesting it contributes to angioproliferative vascular lesions. TCTP is a mulfunctional protein having intra- and extra-cellular roles, essential for endothelial cell survival and proliferation, which may under pathological conditions, such as PAH, be implicated in the functional loss of the lung microvasculature. TCTP may therefore play an important role in PAH by mediating the transformation of vascular cells to a pro-survival and hyperproliferative phenotype triggered by EC apoptosis, thus contributing to occlusive pulmonary vascular remodeling. The work presented in this thesis clearly shows that TCTP could be a potential therapeutic target that may have direct clinical implications in PAH.

CHAPTER 5: APPENDICES

Appendix A - BMP9-mediated Id1 Induction in HPAECs

A

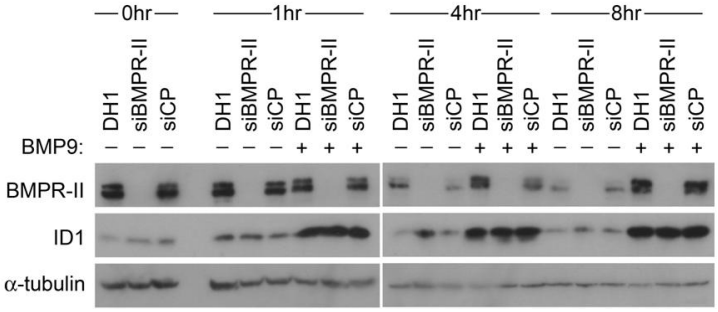

B

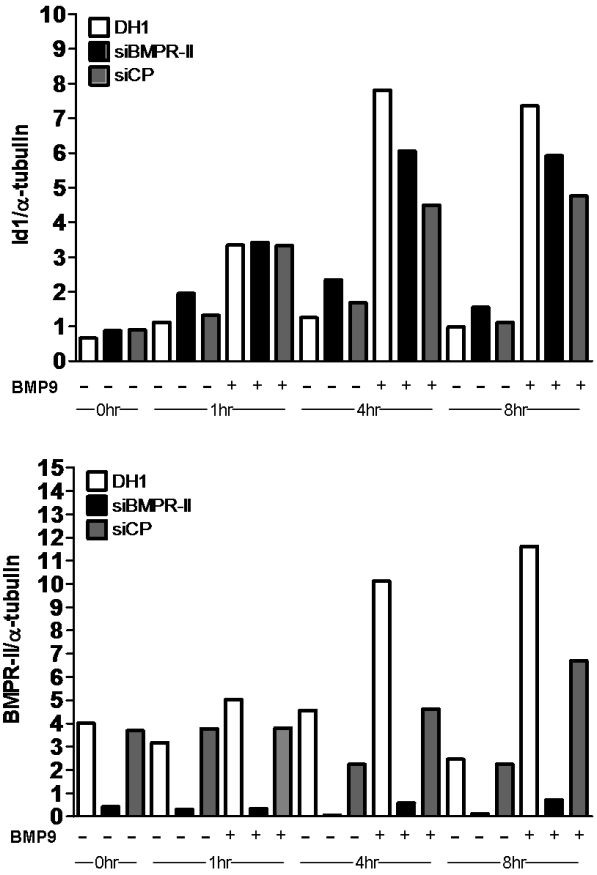

Appendix A. BMP9-mediated Id1 induction after siRNA knockdown of BMPR-II in human pulmonary artery endothelial cells.
(A) Western blots showing BMPR-II and Id1 levels in human pulmonary artery endothelial cells (HPAECs) treated with BMP9 (1 ng/ml) for 1, 4 and 8 hours after treatment with Dharmafect 1 siRNA transfection agent (DH1) alone or with siRNA for BMPR-II (siBMPR-II) or siRNA control (siCP). α-tubulin served as a loading control. **(B)** Quantification results expressed as expression relative to α-tubulin.

Appendix B - TCTP Inhibition in BOECs from Healthy Controls: BrdU Incorporation

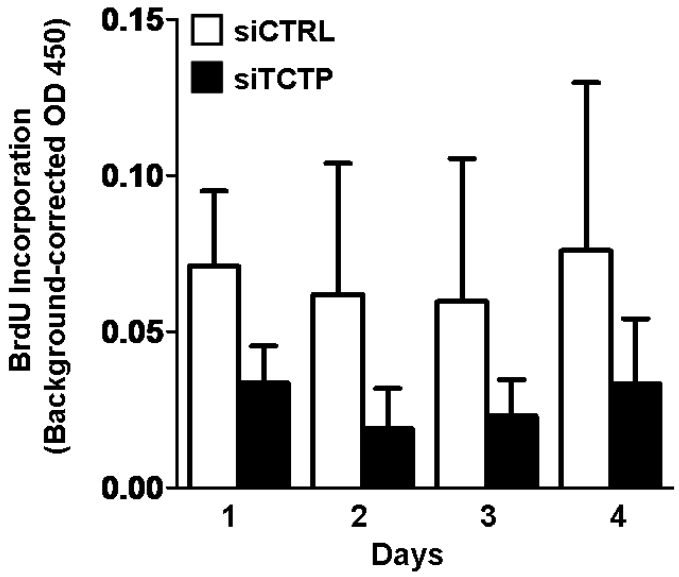

Appendix B. TCTP inhibition in BOECs from healthy controls on BrdU incorporation.
BOECs from healthy controls (n=3) were transfected with control siRNA (siCTRL) as a negative control or TCTP siRNA (siTCTP) at 10 nM for 48 hours. Cells were plated and at the indicated times (day 1-4), BrdU was added (6 hours, 100 μM), and its incorporation was quantitated by ELISA on day 1, 2, 3 and 4. Data represent mean ± SEM. No significant differences were detected by 1-way ANOVA.

Appendix C - TCTP Knockdown with Specific siRNAs

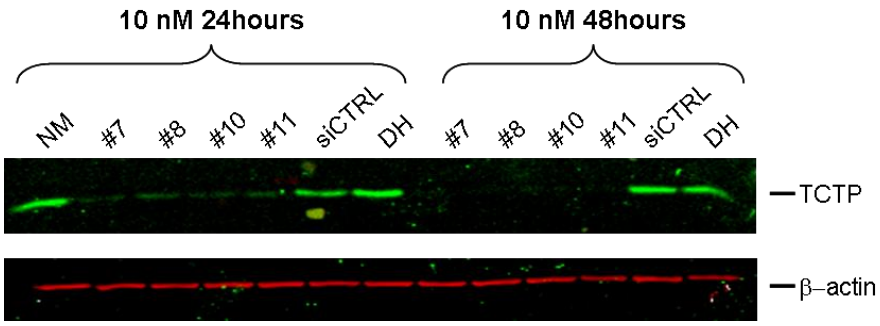

Appendix C. TCTP inhibition in BOECs with 4 different siRNAs targeting TCTP. Representative immunoblotting images showing TCTP protein inhibition following transfection with 4 different specific silencing siRNAs (#7, 8, 10 and 11) and one negative control siRNA (siCTRL) at 10 nM for 24 and 48 hours. NM indicates normal media (no treatment) and DH, Dharmafect (transfecting agent).

Appendix D - TCTP Staining in Human Lung Tissues

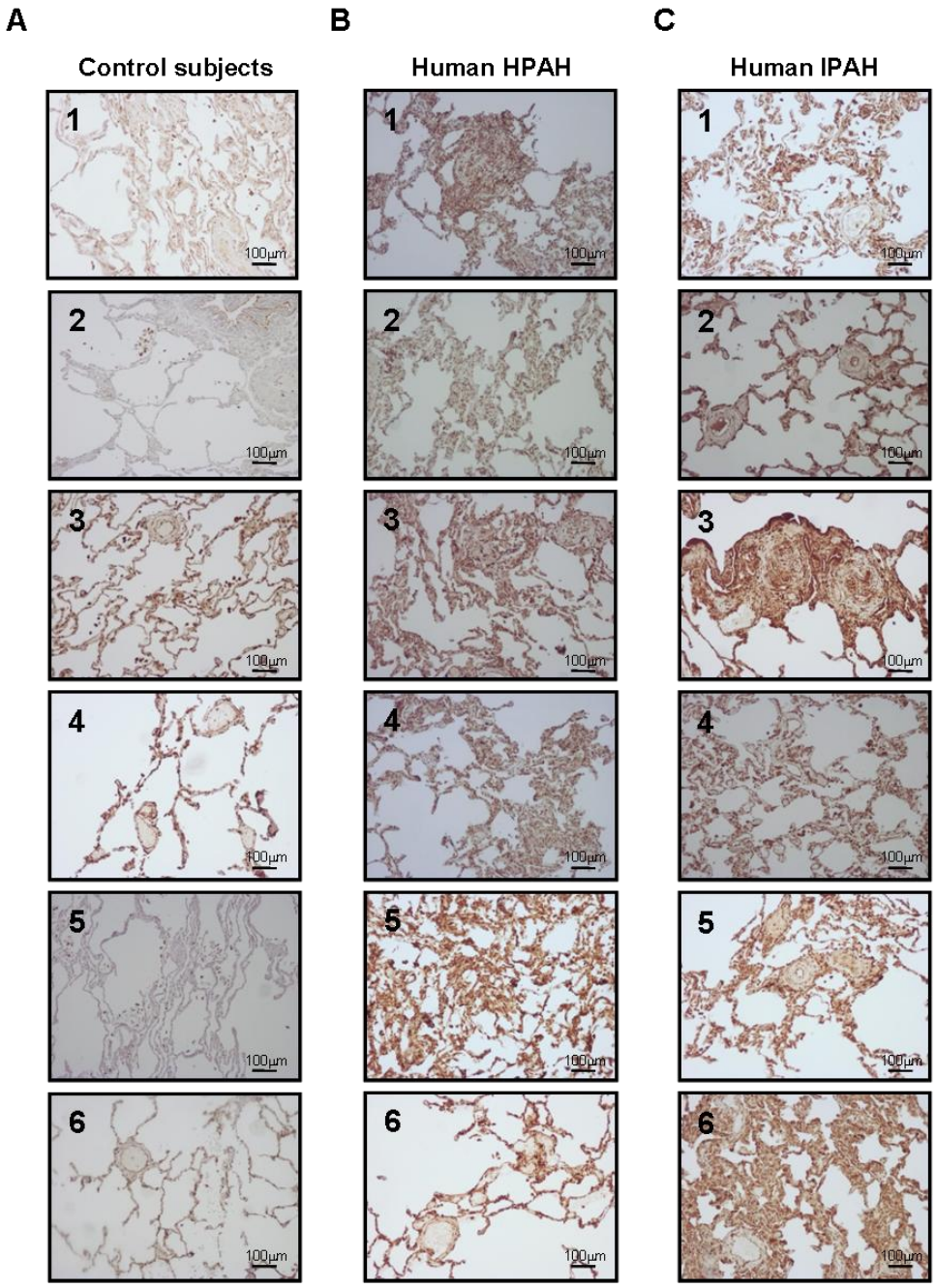

Appendix D. TCTP expression is elevated in vascular lesions of patients with PAH. **(A)** Lung sections from control subjects (n=6) showing weak to medium immunoreactivity for TCTP (brown). **(B-C)** Lung sections from patients with HPAH (n=6) **(B)** and IPAH (n=6) **(C)** showing intense immunoreactivity for TCTP in lumen-occluding lesions and vascular wall. Original magnification x 10. Scale bar = 100 μm**.**

Appendix E - TCTP Expression is elevated in Lung Vascular Lesions of Patients with HPAH

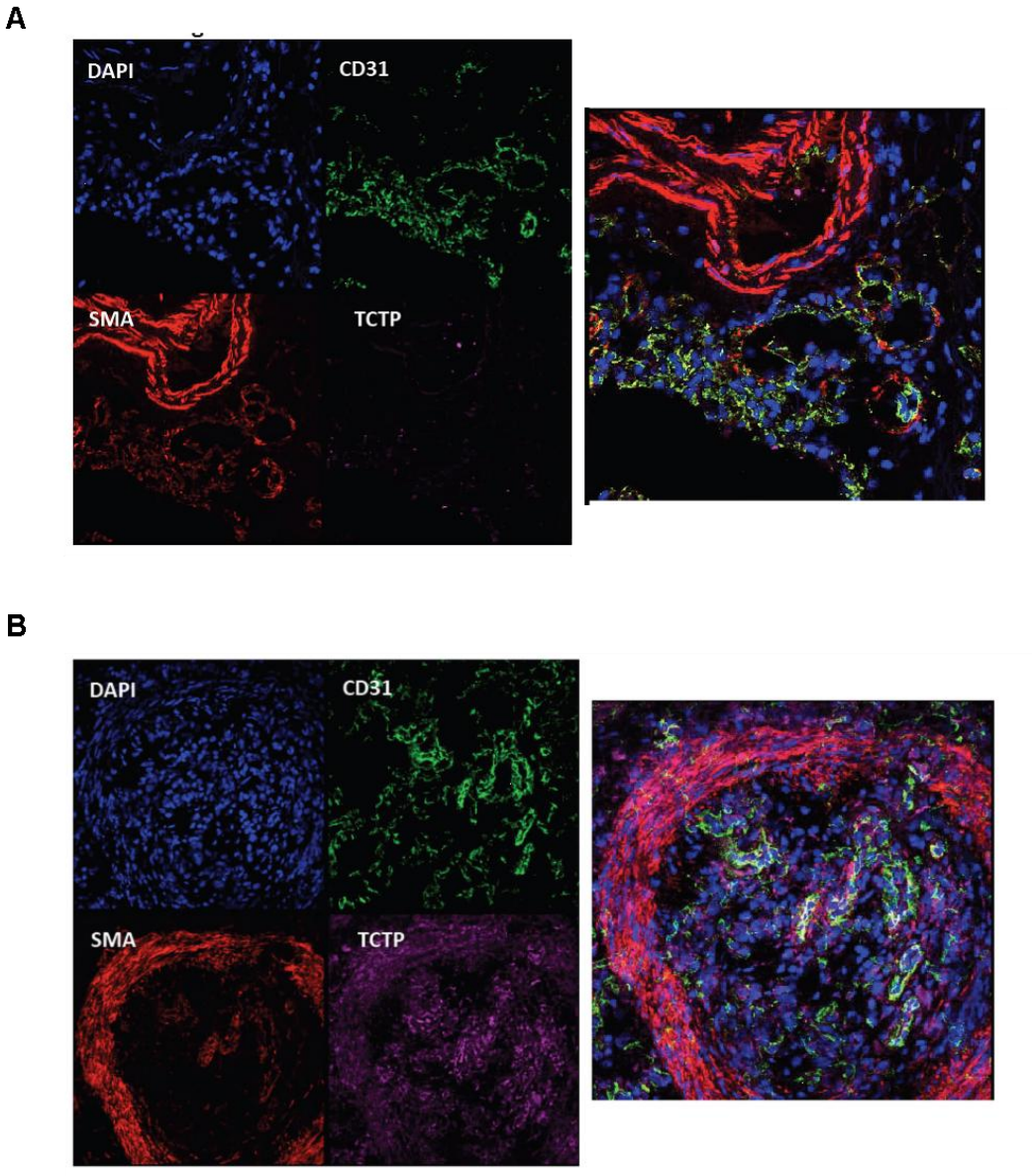

Appendix E. TCTP expression is elevated in lung vascular lesions of patients with HPAH.
(A) Representative lung sections from control subjects (n=3) showing weak immunoreactivity for TCTP (purple), CD31 (green) and α-SMA (red). **(B)** Representative lung sections from patients with HPAH (n=3) showing intense immunoreactivity for TCTP, CD31 and α-SMA in remodeled blood vessels. Original magnification x 20.

Appendix F - Isotype Control for Immunofluorescence Staining for TCTP

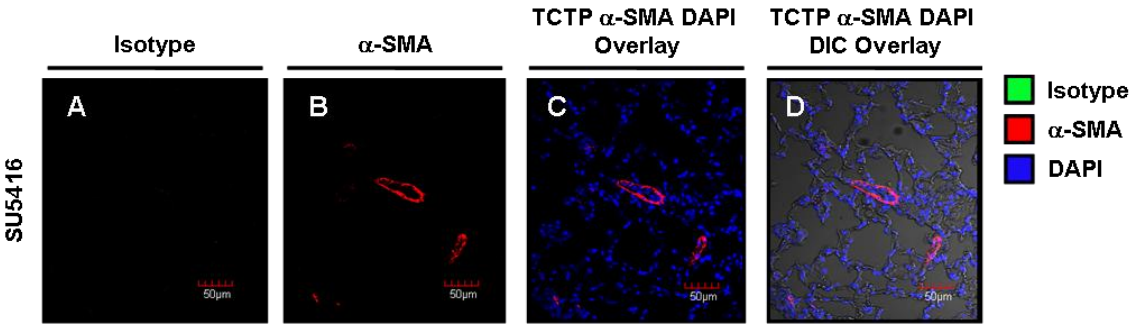

Appendix F. No immunoreactivity was observed in the presence of an isotype control for TCTP.
A rabbit IgG isotype control (A, green) was used under the same staining and imaging conditions and is showing no immunoreactivity in a lung section from a SU5416-treated rat. Alpha-smooth muscle-actin (B, α-SMA) is shown in red and nuclei are counterstained with DAPI (C, blue). Differential interference contrast (DIC) image merged with TCTP, α-SMA and DAPI are shown in panels D. Results are representative sections from 3 animals. Scale bar = 50 μm.

Appendix G - Isotype Controls for Immunofluorescence Staining for PCNA and TCTP

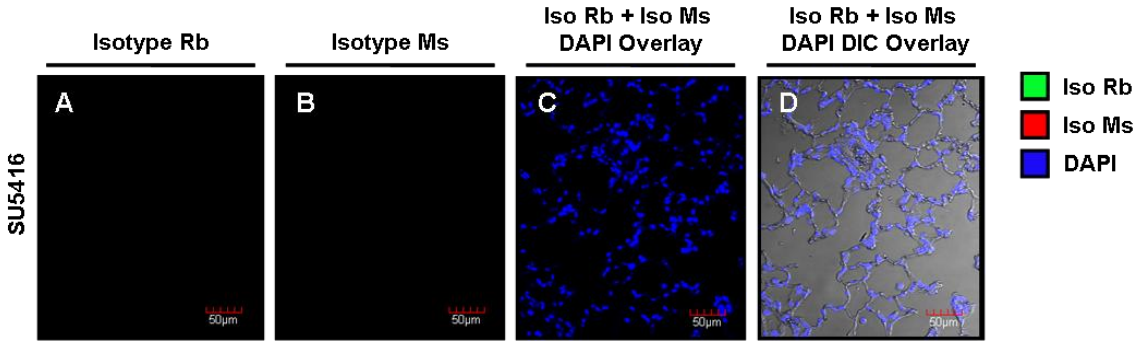

Appendix G. No immunoreactivity was observed in the presence of both isotype controls for TCTP and PCNA.
A rabbit IgG (A, green) and a mouse IgG (B, red) isotype controls were used in combination under the same staining and imaging conditions as the positive staining and is showing no immunoreactivity in a lung section from a SU5416-treated rat. An overlay of both isotypes with DAPI nuclear staining is shown in panel C. Differential interference contrast (DIC) image merged with rabbit isotype, mouse isotype and DAPI is shown in panels D. Results are representative sections from 3 animals. Scale bar = 50 μm.

Appendix H - TCTP Expression is Minimal in the MCT Model of PAH

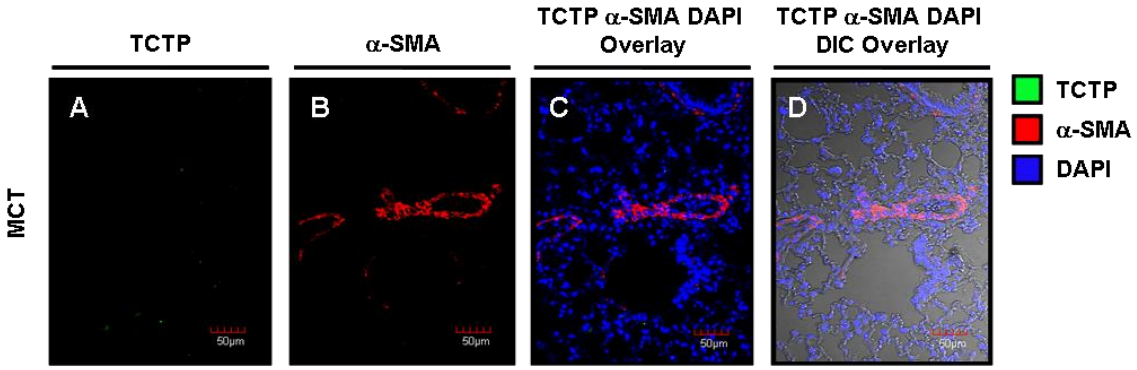

Appendix H. TCTP expression is minimal in the MCT model of PAH.
TCTP (A, green) and α-smooth muscle-actin (B, α-SMA) (red) immunofluorescence staining of lung sections from monocrotaline-treated rats (MCT, 70 mg/kg, 22 days). Nuclei are counterstained with DAPI (blue). Differential interference contrast (DIC) image merged with TCTP, α-SMA and DAPI are shown in panels D. Results are representative sections from 3 animals. Scale bar = 50 μm.

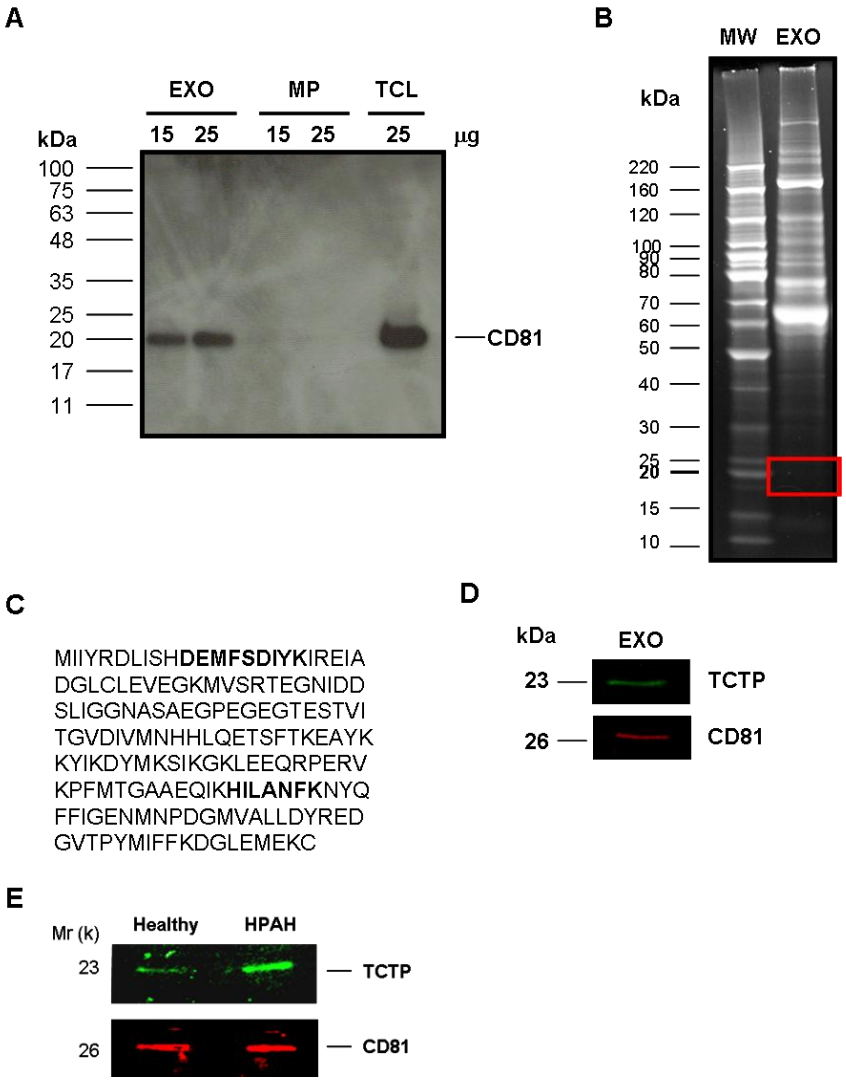

Appendix I. TCTP in exosomal fraction of BOECs.
(A) Western blot indicates that CD81 antigen is specifically found in BOEC-derived exosomes (EXO) and total cell lysate (TCL), but not in BOEC-derived microparticles (MP) obtained from a healthy control. **(B)** Sypro Ruby gel image of an exosome sample obtained from the medium supernatant of BOECs derived from a healthy control cultured in a complete exosome-free medium. The red square indicates the location of the gel band that was cut for TCTP protein identification in mass spectrometry. **(C)** Data base searching identified TCTP in the gel band with 2 matching peptides that represent 12% sequence coverage and a total mass score of 65. The identified peptides within TCTP sequence are presented in boldface black letters. **(D)** Western blot analysis of TCTP in BOEC-derived exosomes to confirm TCTP presence. **(E)** Western blot indicates that TCTP is present in both BOEC-derived exosomes from a healthy control and from a HPAH patient under normal conditions, but at a greater levels in HPAH.

Appendix J - Testing shRNA Plasmid Efficacy: Cell Morphology After Transfection

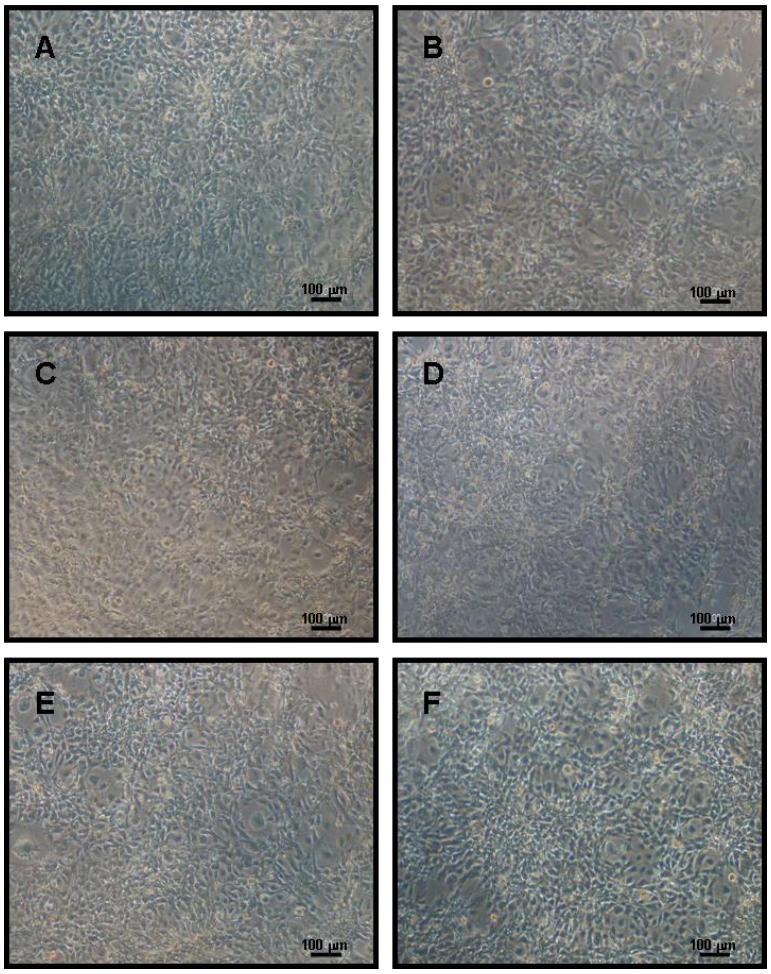

Appendix J. Rat mammary gland Walker carcinoma epithelial cells transfected with pRS-shRNA plasmids.
Representative images of rat mammary gland Walker carcinoma epithelial cells non-transfected **(A)** or 48 hours after transfection with 0.5 μg of an empty pRS-shRNA vector **(B)** or with 0.5 μg of 4 different pRS-shTPT1 vectors **(C-F)**. Scale bar = 100 μm.

Appendix K - Testing shRNA Plasmid Efficacy: TCTP Levels After Transfection

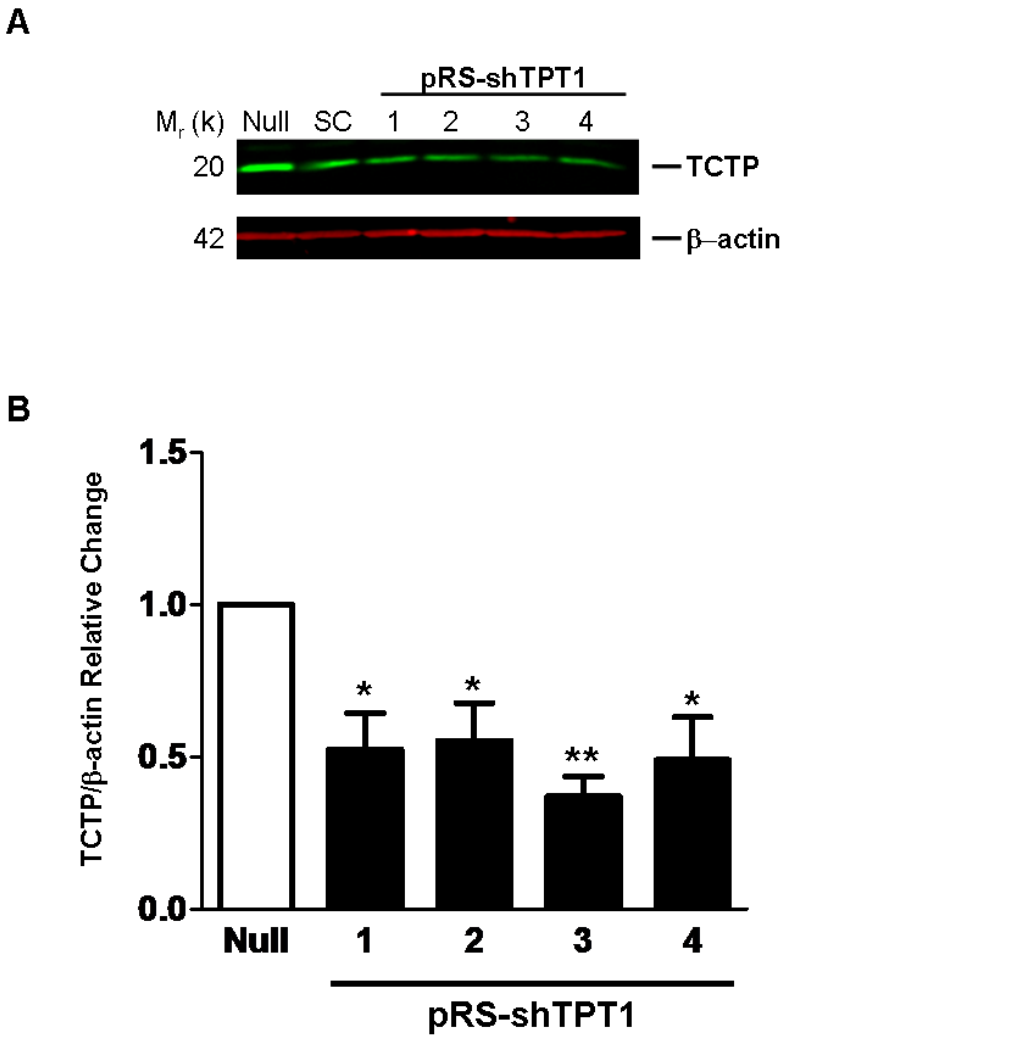

Appendix K. TCTP silencing in rat mammary gland Walker carcinoma epithelial cells following transfection with pRS-shRNA plasmids.
(A) Representative Western blot image of rat mammary gland Walker carcinoma epithelial cells 48 hours after transfection with 0.5 μg of an empty pRS-shRNA vector (null), a scrambled vector (SC) or 4 different pRS-shTPT1 vectors (1-4). **(B)** Summary data showing the protein level of TCTP normalized to the level of β-actin and its relative change to the null pRS-shRNA vector. Data represent mean ± SEM (n = 3 independent experiments). pRS-shTPT1 plasmid #3 was selected for the *in vivo* pilot trial. Significant differences were assessed by one-way ANOVA followed by Dunnett's Multiple Comparison Test. *p<0.05, **p<0.01.

Appendix L - In Vivo Pilot Study: Timeline

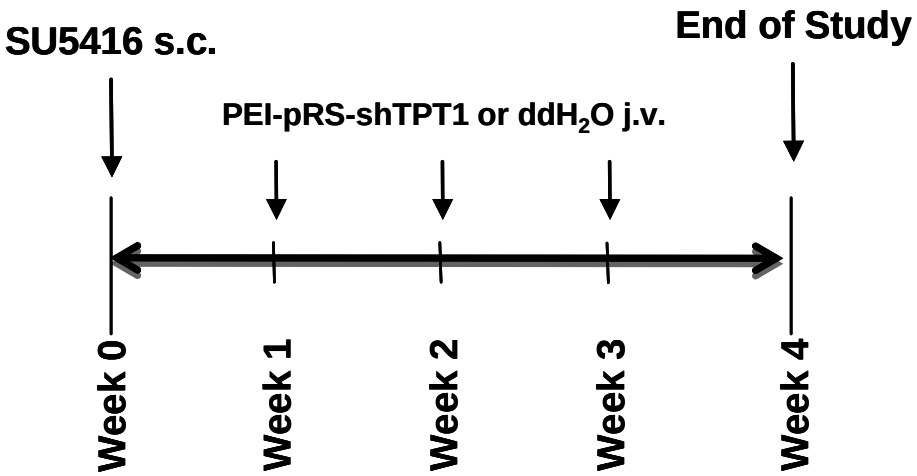

Appendix L. Timeline for pilot study of TCTP silencing *in vivo* with shRNA plasmid technology.
Male Sprague-Dawley rats all received a subcutaneous injection of the SU5416 compound at week 0 (20 mg/kg) (n=20). Rats were either injected with a vehicle (ddH_2O) (n=9) or with a shRNA plasmid containing shRNA sequence of TPT1 mixed with *in vivo*-jetPEI (PEI-pRS-shTPT1; n=11) for 3 consecutive weeks. Hemodynamic measurements were taken at week 4.

Appendix M - In Vivo Pilot Study: Body Weight Changes in Animals

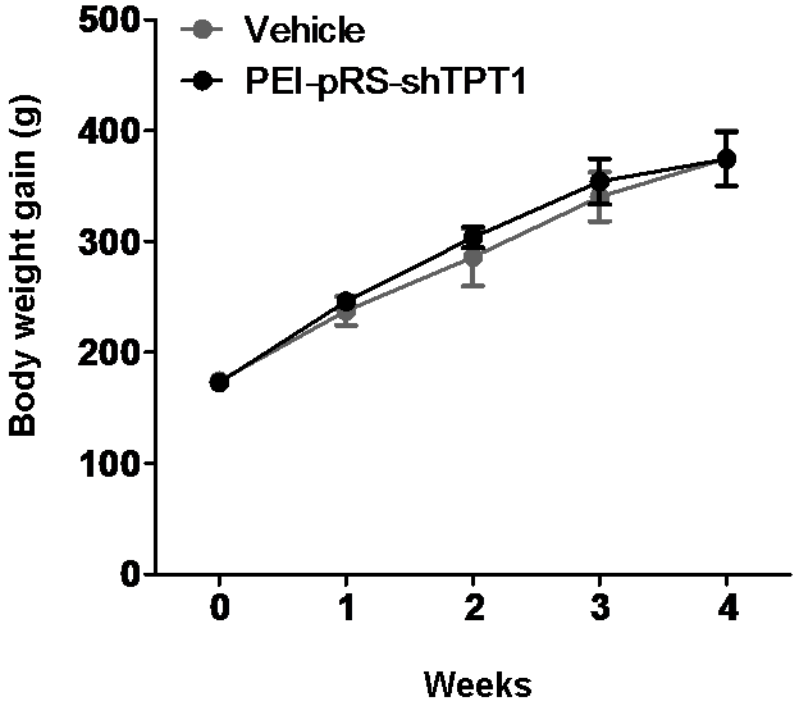

Appendix M. Time course of body weight changes of male rats.
At week 0, male rats were administered subcutaneously 20 mg/kg of the SU5416 compound or a vehicle (ddH_2O). At week 1, 2, and 3, animals were either injected with a vehicle (ddH2O) (vehicle, n=9) or with the shRNA plasmid containing shRNA sequence of TPT1 mixed with *in vivo*-jetPEI (PEI-pRS-shTPT1; n=11). Body weights were recorded once weekly. Data is presented as mean ± SD.

Appendix N - In Vivo Pilot Study: Hemodynamic Measurements

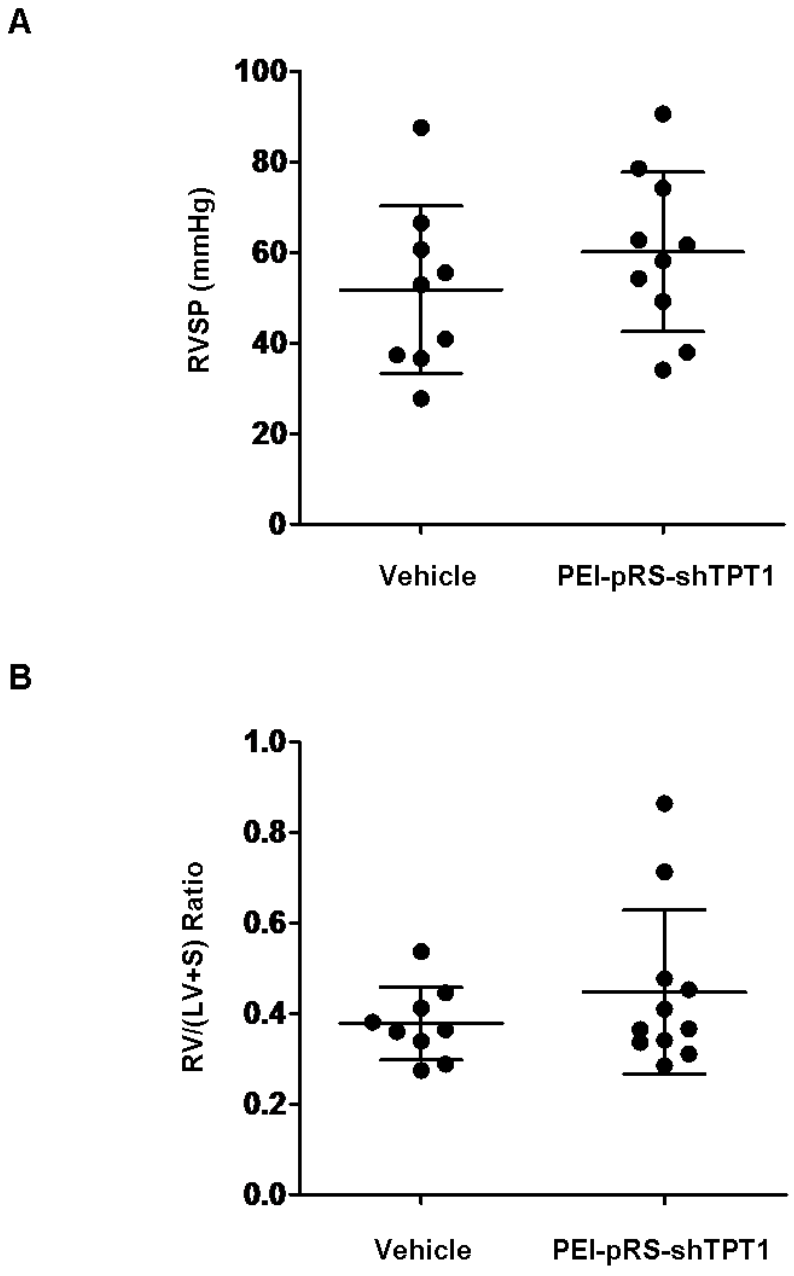

Appendix N. Right ventricular hypertrophy and right ventricular systolic pressures.
(A) Scatter plots showing values of right ventricular systolic pressures (RVSP) as a surrogate of mean pulmonary arterial pressures. **(B)** Scatter plots showing values of ratio of right ventricle weight to left ventricle plus septum weight RV/(LV+S), as a measurement of right ventricular hypertrophy. **(A-B)** Animals were either injected with a vehicle (ddH_2O) (vehicle, n=9) or with the shRNA plasmid containing shRNA sequence of TPT1 mixed with *in vivo*-jetPEI (PEI-pRS-shTPT1; n=11). RV hypertrophy and RVSP values were not different between the two groups. Data are mean ± SD.

Appendix O - In Vivo Pilot Study: Lung Architecture

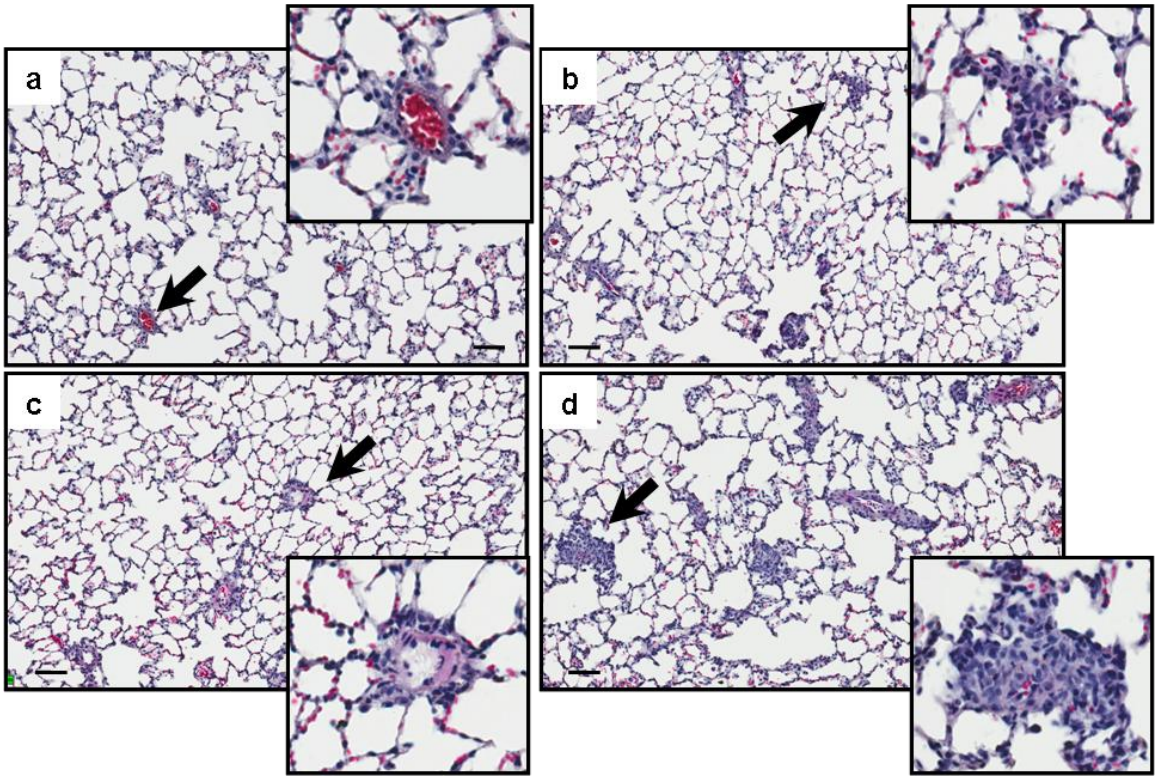

Appendix O. Hematoxylin and eosin stained pulmonary cross-sections at 4 weeks following either vehicle or shRNA plasmid containing shRNA sequence of TPT1. Representative hematoxylin and eosin (H&E) images of lungs from animals injected with either vehicle (ddH_2O) (a-b, n=9) or with the shRNA plasmid containing shRNA sequence of TPT1 mixed with *in vivo*-jetPEI (c-d, n=11). H&E images from a and c represent animals with lower RVSP measurements (27.7 and 37.9 mmHg, respectively) and b and d with higher RVSP measurements (60.7 and 90.7 mmHg, respectively). Arrows are pointing at blood vessels which are enlarged in the boxes. Original magnification x 10. Scale bar = 100μm.

Appendix P - In Vivo Study: Percentage of Occluded Vessels and Total Plexiform Lesions

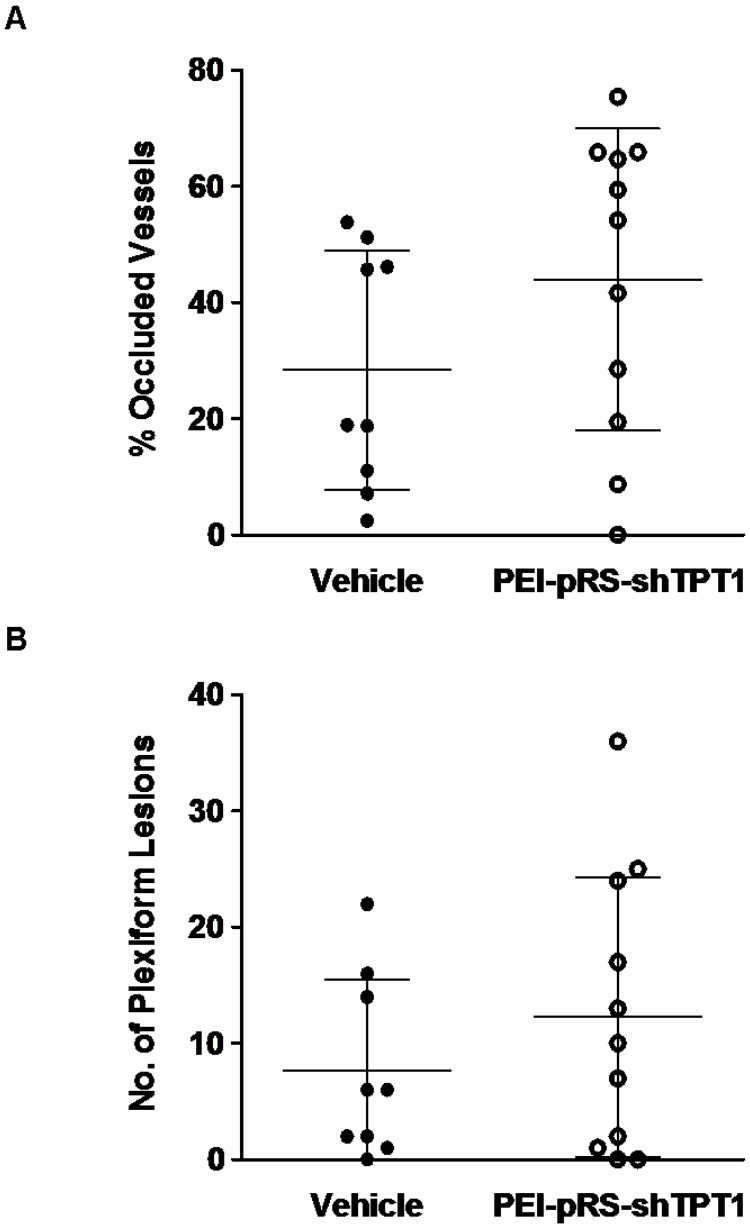

Appendix P. Percentage of occluded pulmonary vessels and total number of plexiform lesions.
(A) Scatter plots showing values of the percentage of occluded vessels of pulmonary blood vessels from animals injected either with vehicle (ddH_2O) (vehicle, n=9) or with the shRNA plasmid containing shRNA sequence of TPT1 mixed with *in vivo*-jetPEI (PEI-pRS-shTPT1; n=11). Data are mean ± SD. **(B)** Scatter plots showing values of the number of pulmonary plexiform lesions from animals injected either with vehicle (ddH_2O) (vehicle, n=9) or with the shRNA plasmid containing shRNA sequence of TPT1 mixed with *in vivo*-jetPEI (PEI-pRS-shTPT1; n=11). Data are mean ± SD.

Appendix Q - In Vivo Study: Correlation Between RVSP Mesurements and the Percentage of Occluded Vessels or the Total Plexiform Lesions

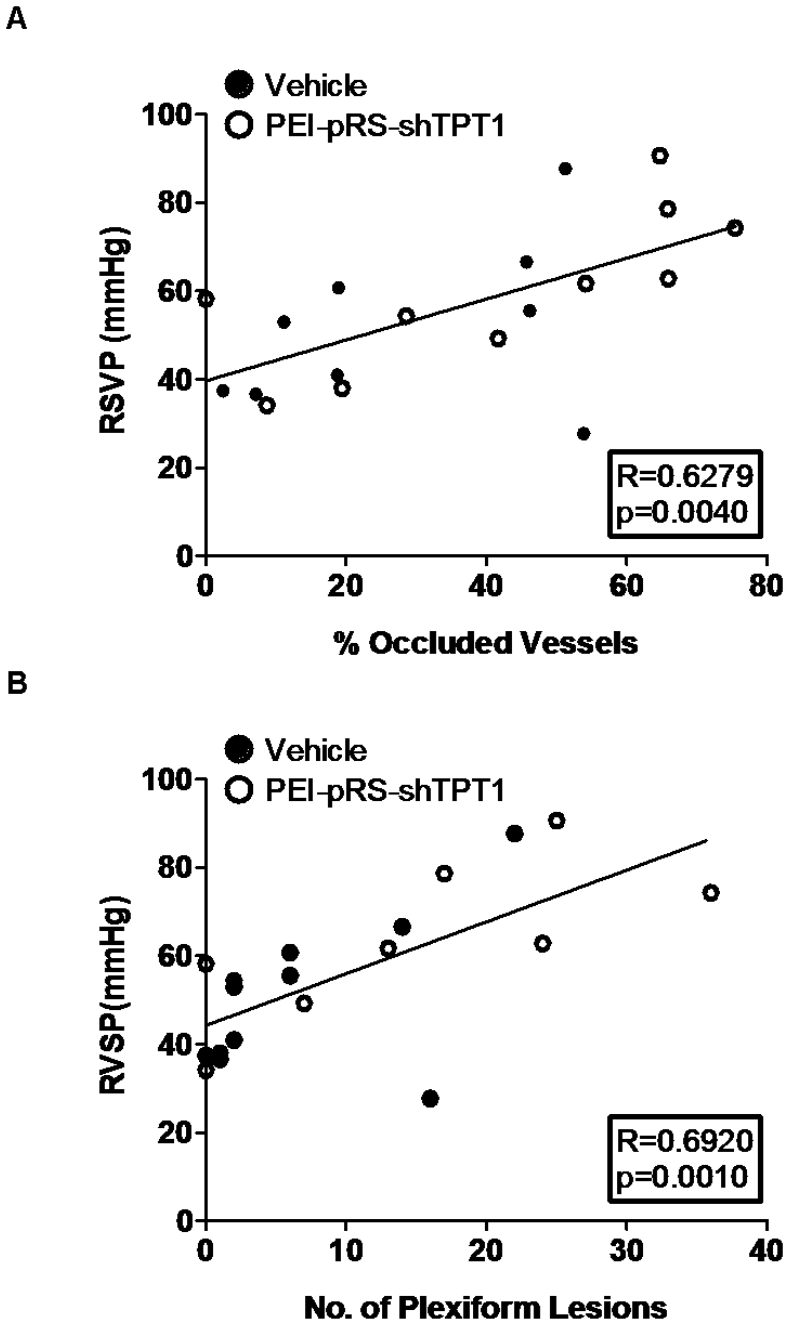

Appendix Q. Correlation between RVSP measurements and the percentage of occluded vessels or plexiform lesions in the lungs.
(A-B) The correlation analysis was performed by the Pearson's correlation test (n=19: Vehicle [n=9], PEI-pRS-shTPT1 [n=10]). ***p<0.001. R, Pearson's correlation coefficient.

Appendix R - In Vivo Study: TCTP Staining in the Lungs

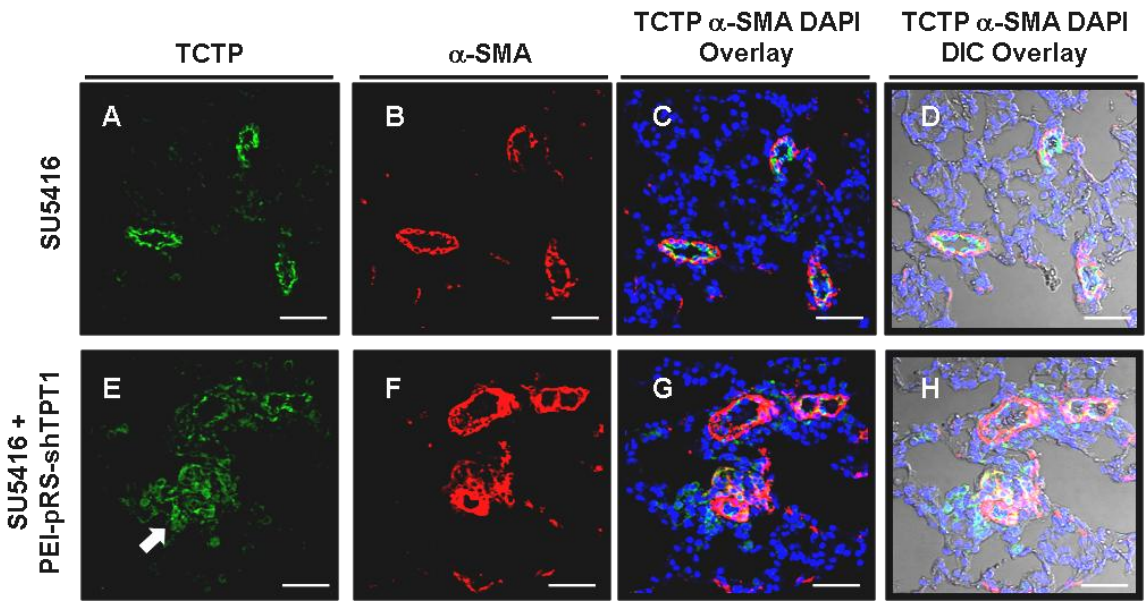

Appendix R. TCTP-positive cells are found in the remodeled vessels of animals receiving shRNA plasmid containing shRNA sequence of *TPT1*.
SU5416-treated animals were injected either with the vehicle (ddH_2O) (vehicle, n=9) or with the shRNA plasmid containing shRNA sequence of *TPT1* mixed with *in vivo*-jetPEI (PEI-pRS-shTPT1; n=11). TCTP (green) and α-smooth muscle-actin (α-SMA) (red) immunofluorescence staining in small pulmonary arteries from vehicle-treated animals (A-D) and PEI-pRS-shTPT1-treated rats (E-H). Nuclei are counterstained with DAPI (blue). Differential interference contrast (DIC) image merged with TCTP, α-SMA and DAPI are shown in panels D and H. Arrow is highlighting TCTP-positive cells occluding the lumen of the small arterioles. Scale bar = 50 μm.

Appendix S - pRS-shRNA vector details

Nucleotide sequence for OriGene's pRS-shRNA-29 expression vector

GAATTCCCCAGTGGAAAGACGCGCAGGCAAAACGCACCACGTGACGGAGCGTGACCGCGCGCCGAGC
GCGCGCCAAGGTCGGGCAGGAAGAGGGCCTATTTCCCATGATTCCTTCATATTTGCATATACGATACAA
GGCTGTTAGAGAGATAATTAGAATTAATTTGACTGTAAACACAAAGATATTAGTACAAAATACGTGACGT
AGAAAGTAATAATTTCTTGGGTAGTTTGCAGTTTTAAAATTATGTTTTAAAATGGACTATCATATGCTTACC
GTAACTTGAAAGTATTTCGATTTCTTGGGTTTATATATCTTGTGGAAAGGACGCGGGATCCACTGGACCA
GGCAGCAGCGTCAGAAGACTTTTTTGGAAAAGCTTGTCGACCCTGTGGAATGTGTGTCAGTTAGGGTGT
GGAAAGTCCCCAGGCTCCCCAGCAGGCAGAAGTATGCAAAGCATGCATCTCAATTAGTCAGCAACCAT
AGTCCCGCCCCTAACTCCGCCCATCCCGCCCCTAACTCCGCCCAGTTCCGCCCATTCTCCGCCCCATG
GCTGACTAATTTTTTTTATTTATGCAGAGGCCGAGGCCGCCTCGGCCTCTGAGCTATTCCAGAAGTAGT
GAGGAGGCTTTTTTGGAGGCCTAGGCTTTTGCAAAAAGCTAGCTTACCATGACCGAGTACAAGCCCACG
GTGCGCCTCGCCACCCGCGACGACGTCCCCAGGGCCGTACGCACCCTCGCCGCCGCGTTCGCCGAC
TACCCCGCCACGCGCCACACCGTCGATCCGGACCGCCACATCGAGCGGGTCACCGAGCTGCAAGAAC
TCTTCCTCACGCGCGTCGGGCTCGACATCGGCAAGGTGTGGGTCGCGGACGACGGCGCCGCGGTGG
CGGTCTGGACCACGCCGGAGAGCGTCGAAGCGGGGGCGGTGTTCGCCGAGATCGGCCCGCGCATGG
CCGAGTTGAGCGGTTCCCGGCTGGCCGCGCAGCAACAGATGGAAGGCCTCCTGGCGCCGCACCGGC
CCAAGGAGCCCGCGTGGTTCCTGGCCACCGTCGGCGTCTCGCCCGACCACCAGGGCAAGGGTCTGG
GCAGCGCCGTCGTGCTCCCCGGAGTGGAGGCGGCCGAGCGCGCCGGGGTGCCCGCCTTCCTGGAGA
CCTCCGCGCCCCGCAACCTCCCCTTCTACGAGCGGCTCGGCTTCACCGTCACCGCCGACGTCGAGTG
CCCGAAGGACCGCGCGACCTGGTGCATGACCCGCAAGCCCGGTGCCTGAGTTTGTTTGAATGAGGCTT
CAGTACTTTACAGAATCGATAAAATAAAAGATTTTATTTAGTCTCCAGAAAAAGGGGGGAATGAAAGACC
CCACCTGTAGGTTTGGCAAGCTAGCTTAAGTAACGCCATTTTGCAAGGCATGGAAAAATACATAACTGA
GAATAGAGAAGTTCAGATCAAGGTCAGGAACAGATGGAACAGCTGAATATGGGCCAAACAGGATATCTG
TGGTAAGCAGTTCCTGCCCCGGCTCAGGGCCAAGAACAGATGGAACAGCTGAATATGGGCCAAACAGG
ATATCTGTGGTAAGCAGTTCCTGCCCCGGCTCAGGGCCAAGAACAGATGGTCCCCAGATGCGGTCCAG
CCCTCAGCAGTTTCTAGAGAACCATCAGATGTTTCCAGGGTGCCCCAAGGACCTGAAATGACCCTGTGC
CTTATTTGAACTAACCAATCAGTTCGCTTCTCGCTTCTGTTCGCGCGCTTCTGCTCCCCGAGCTCAATAA
AAGAGCCCACAACCCCTCACTCGGGGCGCCAGTCCTCCGATTGACTGAGTCGCCCGGGTACCCGTGT
ATCCAATAAACCCTCTTGCAGTTGCATCCGACTTGTGGTCTCGCTGTTCCTTGGGAGGGTCTCCTCTGA
GTGATTGACTACCCGTCAGCGGGGGTCTTTCATTTCCGACTTGTGGTCTCGCTGCCTTGGGAGGGTCT
CCTCTGAGTGATTGACTACCCGTCAGCGGGGGTCTTCACATGCAGCATGTATCAAAATTAATTTGGTTTT
TTTTCTTAAGTATTTACATTAAATGGCCATAGTTGCATTAATGAATCGGCCAACGCGCGGGGAGAGGCG
GTTTGCGTATTGGCGCTCTTCCGCTTCCTCGCTCACTGACTCGCTGCGCTCGGTCGTTCGGCTGCGGC
GAGCGGTATCAGCTCACTCAAAGGCGGTAATACGGTTATCCACAGAATCAGGGGATAACGCAGGAAAG
AACATGTGAGCAAAAGGCCAGCAAAAGGCCAGGAACCGTAAAAAGGCCGCGTTGCTGGCGTTTTTCCA
TAGGCTCCGCCCCCCTGACGAGCATCACAAAAATCGACGCTCAAGTCAGAGGTGGCGAAACCCGACAG
GACTATAAAGATACCAGGCGTTTCCCCCTGGAAGCTCCCTCGTGCGCTCTCCTGTTCCGACCCTGCCG
CTTACCGGATACCTGTCCGCCTTTCTCCCTTCGGGAAGCGTGGCGCTTTCTCATAGCTCACGCTGTAGG
TATCTCAGTTCGGTGTAGGTCGTTCGCTCCAAGCTGGGCTGTGTGCACGAACCCCCCGTTCAGCCCGA
CCGCTGCGCCTTATCCGGTAACTATCGTCTTGAGTCCAACCCGGTAAGACACGACTTATCGCCACTGGC
AGCAGCCACTGGTAACAGGATTAGCAGAGCGAGGTATGTAGGCGGTGCTACAGAGTTCTTGAAGTGGT
GGCCTAACTACGGCTACACTAGAAGGACAGTATTTGGTATCTGCGCTCTGCTGAAGCCAGTTACCTTCG
GAAAAAGAGTTGGTAGCTCTTGATCCGGCAAACAAACCACCGCTGGTAGCGGTGGTTTTTTTGTTTGCA
AGCAGCAGATTACGCGCAGAAAAAAAGGATCTCAAGAAGATCCTTTGATCTTTTCTACGGGGTCTGACG
CTCAGTGGAACGAAAACTCACGTTAAGGGATTTTGGTCATGAGATTATCAAAAAGGATCTTCACCTAGAT
CCTTTTAAATTAAAAATGAAGTTTGCGGCCGCAAATCAATCTAAAGTATATATGAGTAAACTTGGTCTGAC
AGTTACCAATGCTTAATCAGTGAGGCACCTATCTCAGCGATCTGTCTATTTCGTTCATCCATAGTTGCCT
GACTCCCCGTCGTGTAGATAACTACGATACGGGAGGGCTTACCATCTGGCCCCAGTGCTGCAATGATA
CCGCGAGACCCACGCTCACCGGCTCCAGATTTATCAGCAATAAACCAGCCAGCCGGAAGGGCCGAGC
GCAGAAGTGGTCCTGCAACTTTATCCGCCTCCATCCAGTCTATTAATTGTTGCCGGGAAGCTAGAGTAA
GTAGTTCGCCAGTTAATAGTTTGCGCAACGTTGTTGCCATTGCTACAGGCATCGTGGTGTCACGCTCGT
CGTTTGGTATGGCTTCATTCAGCTCCGGTTCCCAACGATCAAGGCGAGTTACATGATCCCCCATGTTGT
GCAAAAAAGCGGTTAGCTCCTTCGGTCCTCCGATCGTTGTCAGAAGTAAGTTGGCCGCAGTGTTATCAC
TCATGGTTATGGCAGCACTGCATAATTCTCTTACTGTCATGCCATCCGTAAGATGCTTTTCTGTGACTGG
TGAGTACTCAACCAAGTCATTCTGAGAATAGTGTATGCGGCGACCGAGTTGCTCTTGCCCGGCGTCAAC
ACGGGATAATACCGCGCCACATAGCAGAACTTTAAAAGTGCTCATCATTGGAAAACGTTCTTCGGGGCG
AAAACTCTCAAGGATCTTACCGCTGTTGAGATCCAGTTCGATGTAACCCACTCGTGCACCCAACTGATC
TTCAGCATCTTTTACTTTCACCAGCGTTTCTGGGTGAGCAAAAACAGGAAGGCAAAATGCCGCAAAAAA

GGGAATAAGGGCGACACGGAAATGTTGAATACTCATACTCTTCCTTTTTCAATATTATTGAAGCATTTATC
AGGGTTATTGTCTCATGAGCGGATACATATTTGAATGTATTTAGAAAAATAAACAAATAGGGGTTCCGCG
CACATTTCCCCGAAAAGTGCCACCTGCAGCCTGAATATGGGCCAAACAGGATATCTGTGGTAAGCAGTT
CCTGCCCCGGCTCAGGGCCAAGAACAGATGGAACAGCTGAATATGGGCCAAACAGGATATCTGTGGTA
AGCAGTTCCTGCCCCGGCTCAGGGCCAAGAACAGATGGTCCCCAGATGCGGTCCAGCCCTCAGCAGT
TTCTAGAGAACCATCAGATGTTTCCAGGGTGCCCCAAGGACCTGAAATGACCCTGTGCCTTATTTGAAC
TAACCAATCAGTTCGCTTCTCGCTTCTGTTCGCGCGCTTCTGCTCCCCGAGCTCAATAAAAGAGCCCAC
AACCCCTCACTCGGGGCGCCAGTCCTCCGATTGACTGAGTCGCCCGGGTACCCGTGTATCCAATAAAC
CCTCTTGCAGTTGCATCCGACTTGTGGTCTCGCTGTTCCTTGGGAGGGTCTCCTCTGAGTGATTGACTA
CCCGTCAGCGGGGGTCTTTCATTTGGGGGCTCGTCCGGGATCGGGAGACCCCTGCCCAGGGACCACCC
GACCCACCACCGGGAGGTAAGCTGGCCAGCAACTTATCTGTGTCTGTCCGATTGTCTAGTGTCTATGAC
TGATTTTATGCGCCTGCGTCGGTACTAGTTAGCTAACTAGCTCTGTATCTGGCGGACCCGTGGTGGAAC
TGACGAGTTCTGAACACCCGGCCGCAACCCTGGGAGACGTCCCAGGGACTTTGGGGGCCGTTTTTGTG
GCCCGACCTGAGGAAGGGAGTCGATGTGGAATCCGACCCCGTCAGGATATGTGGTTCTGGTAGGAGA
CGAGAACCTAAAACAGTTCCCGCCTCCGTCTGAATTTTTGCTTTCGGTTTGGAACCGAAGCCGCGCGTC
TTGTCTGCTGCAGCATCGTTCTGTGTTGTCTCTGTCTGACTGTGTTTCTGTATTTGTCTGAAAATTAGGG
CCAGACTGTTACCACTCCCTTAAGTTTGACCTTAGATCACTGGAAAGATGTCGAGCGGCTCGCTCACAA
CCAGTCGGTAGATGTCAAGAAGAGACGTTGGGTTACCTTCTGCTCTGCAGAATGGCCAACCTTTAACGT
CGGATGGCCGCGAGACGGCACCTTTAACCGAGACCTCATCACCCAGGTTAAGATCAAGGTCTTTTCAC
CTGGCCCGCATGGACACCCAGACCAGGTCCCCTACATCGTGACCTGGGAAGCCTTGGCTTTTGACCCC
CCTCCCTGGGTCAAGCCCTTTGTACACCCTAAGCCTCCGCCTCCTCTTCTTCCATCCGCGCCGTCTCTC
CCCCTTGAACCTCCTCTTTCGACCCCGCCTCAATCCTCCCTTTATCCAGCCCTCACTCCTTCTCTAGGC
GCCGGCCGGATCGGT

Appendix S. pRS-shRNA vector details

Appendix T - Features for pRS-shRNA vector

Start	End	Description
1	6	EcoRI
75	331	U6 promoter
335	340	BamHI
379	385	HindIII
386	391	SalI
413	604	SV40 promoter
671	1270	Puromycin-N-acetyl transferase sequence
1349	1942	3' LTR
2299	2918	pBS ORI
3080	3940	Beta-lactamase for ampicillin resistance
4076	4547	5' LTR

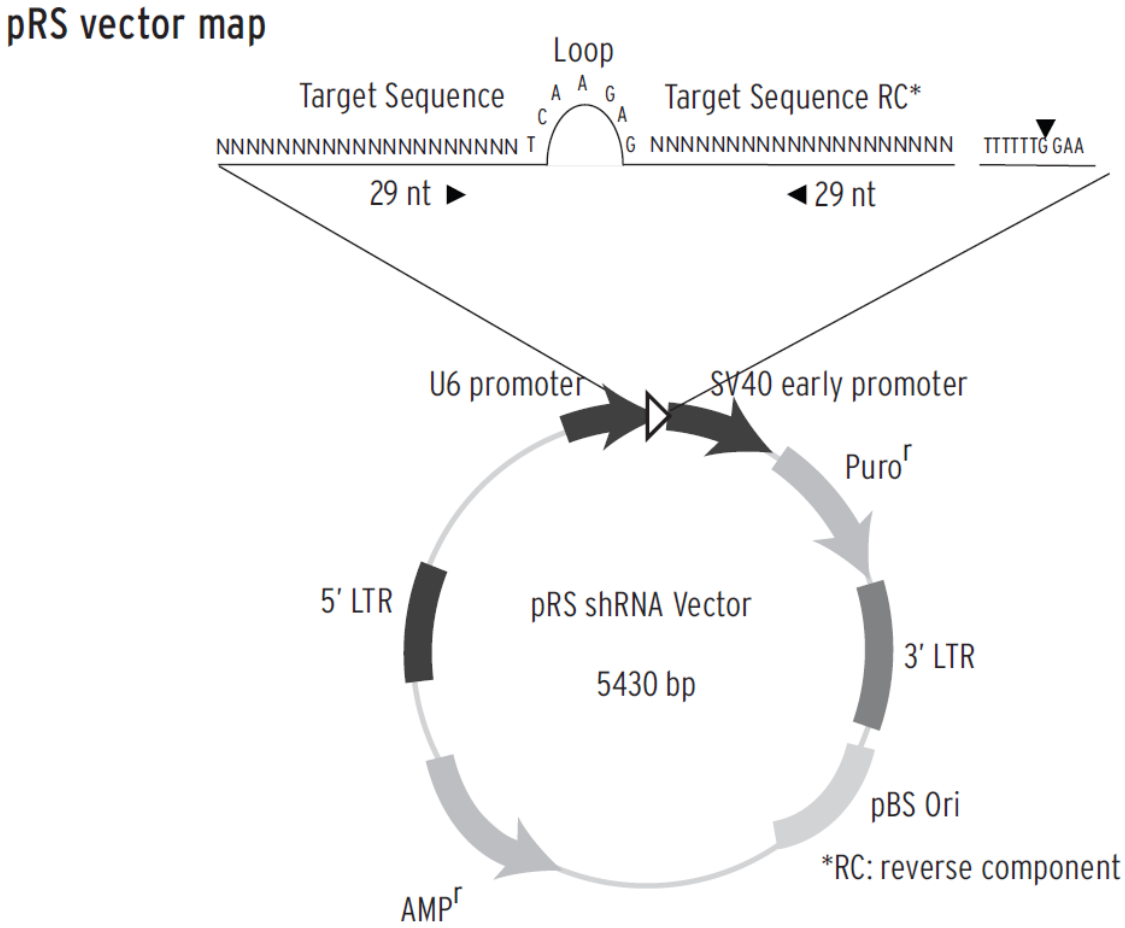

Appendix T. Features for pRS-shRNA vector

CHAPTER 6: PUBLICATIONS

6.1 Publication #1

Glycogen Synthase Kinase-3β Inhibition Augments Diabetic Endothelial Progenitor Cell Abundance and Functionality via Cathepsin B: Novel Therapeutic Opportunity for Arterial Repair

Benjamin Hibbert MD[a,b], **Jessie R. Lavoie MSc[c,e]**, Xiaoli Ma MD PhD[a], Tara Seibert MSc[b], Joshua Raizman PhD[a], Trevor Simard MD[a], Yong-Xiang Chen MD PhD[a], Lionel Filion PhD[b], Duncan Stewart MD[c,e], Edward R. O'Brien MD[a,d]

a- Division of Cardiology, University of Ottawa Heart Institute, Ottawa, ON, Canada
b- Department of Biochemistry, Microbiology and Immunology, University of Ottawa, Ottawa, ON, Canada
c- Ottawa Hospital Research Institute, The Ottawa Hospital, Ottawa, ON, Canada
d- Division of Cardiology, Libin Cardiovascular Institute of Alberta, Calgary, AB, Canada
e- Department of Cellular and Molecular Medicine, University of Ottawa, Ottawa, ON, Canada

As submitted for publication to Circulation Research Journal

(CIRCRES/2013/301388)

Contributions of the Candidate

The work described in the manuscript is the result of a collaboration established between my PhD supervisor's, Dr. Duncan J. Stewart, and a senior scientist at the Ottawa Heart Institute, Dr. Edward R. O'Brien. I was principally involved in the design and execution of the experiments related to the proteomics (2-D gel electrophoresis), as well as the acquisition and analysis of the data in relation with the 2-D experiment. I was also involved in drafting and editing the manuscript.

Abstract

Rationale: Progenitor cell therapy is hindered in patients with diabetes mellitus (DM) because of cell senescence. Glycogen synthase kinase 3β (GSK3β) activity is increased in DM and previously we demonstrated that GSK3β antagonism enhances progenitor cell therapy in the absence of DM , we proposed that may improve cell based therapy in patients with DM.

Objectives: This study aimed to determine if and how a small molecule GSK3β inhibitor (GSKi) can improve therapeutic efficacy of endothelial progenitor cells (EPC) from patients with DM.

Methods and Results: Patients with DM had 50% fewer EPCs and increased rates of apoptosis. DM-EPCs also exhibited higher levels of GSK3β activity resulting in increased levels of phosphorylated β-catenin. Proteomic profiling of DM EPCs treated with GSKi identified 37 non-redundant, differentially regulated proteins compared to untreated or non-DM EPCs. Target proteins were validated by Q-PCR and Western blot. Cathepsin B (CatB) was differentially regulated by GSKi and showed 40% less baseline activity in DM-EPCs but responded by 400% with GSKi treatment resulting in attenuation of apoptosis. Finally, *in vivo* efficacy of cell based therapy was assessed in a xenotransplant mouse model 14 days post-wire injury. DM EPCs produced a 41% reduction in the intima:media – an effect that was further augmented by a 40% when DM EPCs were pre-treated with GSKi, yet absent when CatB was antagonized by CA074.

Conclusions: Increased basal GSK3β activity contributes to accelerated EPC apoptosis and cellular senescence in patients with DM. Up regulation of CatB by small molecule antagonism of GSK3β reduces apoptosis and enhances cell based therapy following vascular injury.

Introduction

Use of endothelial progenitor cell (EPC) populations for cell based therapies is beneficial in a host of cardiovascular conditions including peripheral vascular disease, pulmonary arterial hypertension, and myocardial infarction.(1) However, the administration of autologous EPCs in patients with established disease is often hindered due to attenuated cellular yield and biologic activity. Accordingly, a myriad of strategies have been employed with the goal of improving EPC cellular yield, survival, and function, including our own efforts to over-expressing endothelial nitric oxide synthase(2) or administer small molecule inhibitors of glycogen synthase kinase 3-Beta (GSK3β).(3)

GSK3β is a ubiquitously expressed serine/threonine protein kinase which is negatively regulated by Wnt signaling. Under basal conditions GKS3 β phosphorylates β-catenin (βcat) resulting in proteasomal degradation of this important nuclear transcription factor. Pharmacologic GSK3β inhibition or Wnt3a stimulation promotes hematopoietic stem cell self-renewal and repopulation of cell lineages *in vitro* and *in vivo*.(4;5) In EPCs, GSK3β inhibition by either transfection of a dominant negative mutant or small molecule inhibition improves the therapeutic capacity of cells, thereby augmenting angiogenesis in ischemia models and improving arterial repair following vascular injury.(6;7) This is of particular interest given that GSK3β expression and activity are dysregulated in patients with diabetes mellitus (DM)(8) a population in whom EPC function is severely attenuated.(9;10)

Hence, we sought to explore the potential for pharmacologic inhibition of GSK3β to improve vascular homeostasis and repair in patients with DM. Herein we demonstrate that inhibition of GSK3β in DM EPCs abrogates apoptosis and improves EPC yields *in*

vitro. Moreover, using a proteomic approach we identify and confirm the differential regulation of candidate proteins for the observed benefits of GSK3β inhibition. Among the identified proteins, increased cathepsin-B (catB) activity is demonstrated to be essential for reductions in EPC apoptosis and necessary for increased efficacy with cell based therapeutic arterial homeostasis. These findings suggest that inhibition of GSK3β is an important strategy for improving autologous cell based therapy in patients with DM and acts via a novel mechanism involving increased activity of catB.

Materials and Methods

Cell Isolation

Endothelial progenitor cells were isolated as previously described.(3;11;12) Briefly, blood was collected by venipuncture and anti-coagulated with EDTA. Subsequently, density gradient centrifugation was performed with Ficoll Histopaque 1077 (Sigma) to isolated PBMCs. Cells were washed with PBS and plated on human fibronectin (Sigma) coated 6-well plates at a density of 5.0×10^6 PBMCs/well in endothelial growth media -2 (EGM2, Lonza). Following 4 days in culture, non-adherent cells were removed and plates washed with PBS. All experiments performed with day 4-7 cells with samples from individual donors representing a single replicate. For enumeration, EPCs were incubated with 1,1'-dioctadecyl-3,3,3',3'-tetramethlyiodocarbocyanine-acetylated LDL (acLDL, 2.5 μg/mL; Invitrogen) followed by FITC-conjugated *Ulex europaeus* agglutinin I (5 μg/mL, Sigma) then counterstained with DAPI. Six optical fields were blindly evaluated per patient with the mean results reported.

GSK3β Inhibitors

GSK-3β small molecule and peptide inhibitors (GSKi) were purchased and assayed for efficacy in increasing cell yield and blocking phosphorylation of β-catenin (βcat). All inhibitors were diluted in DMSO to a final concentration of 0.1% *or* sterile PBS if water soluble. Vehicle controls were utilized in all experiments. Specifically, AR-A014418 (Sigma), CHIR98014 (Cedarlane), (22,3E)-6-Bromoindirubin-3-oxime (Calbiochem), GSK peptide inhibitor (Calbiochem), and LiCl (20nmol/L, Sigma) were tested for *in vitro* efficacy.

Apoptosis Assay

EPCs were maintained under basal culture conditions *or* serum starved for 24 hours as indicated. Non-adherent cells were removed by washing with PBS. Subsequently, adherent cells were lifted by gentle agitation with 1 mmol/L of EDTA. Cells were enumerated and $1x10^5$ EPCs were stained with Annexin V-FITC and propidium iodide (PI) as per manufacturers instructions (BD). All flow studies were performed on a Beckman Coulter Cytomics FC 500 cytometer. Early apoptotic cells were defined as AnnexinV+/PI-.

Protein lysate preparation

Media was aspirated and cells were washed twice with PBS. After all PBS was removed, TrypLE was added for 5 minutes at 37°C to lift off the cells. The reaction was neutralized by adding complete growth culture media (EGM-2MV 5% FBS) and cells were collected. The cells were then centrifuged at 220 g for 5 minutes at RT. After the centrifuge, supernatant was discarded and cells were resuspended in DPBS (Lonza) to wash them. An aliquot of cells was then taken before the next centrifugation at 220 g for 5 minutes at RT in order to count the cells. After the centrifugation, the supernatant was removed and cell pellets in the 50-ml tubes were frozen down in liquid nitrogen before being put at -80°C. Once needed, cell pellets were put on ice and cell lysis buffer (7M Urea (w/v), 2M Thiourea (w/v), 4% CHAPS (w/v), 1% DTT (w/v)) was added immediately according to the recorded cell number. Cell lysates were vortexed and kept at RT for 30 minutes to enable protein solubilisation. Cell lysates were then sonicated in a 4°C ultrasonic bath sonicator with the following program: 5 second pulse followed by 10 seconds off and for 10 cycles. Cell lysates were vortexed and then centrifuged at 14,000 g for 15 minutes at RT. The supernatant was transferred and protein quantification was realized with 2D Quant kit (GE Healthcare). Before being used for the 2D gel experiments, 1% 3–10 ampholytes (Bio-Rad) was added to the sample.

Two-dimensional polyacrylamide gel electrophoresis – 2D PAGE

The total proteins (30 µg) were passively rehydrated overnight in 220 µL rehydration/sample buffer (same buffer as described in 2-D sample preparation) and applied to immobilized pH gradient (IPG) strips (11 cm, pH 4–7; Bio-Rad). Isoelectric focusing (IEF) was carried out using the Agilent fractionator (Agilent) in the in-gel mode and programmed as follows: the voltage was initially held at 300 V for 1 min, then linearly increased to 3500 V over 90 min, and focused at 3500 V for 5 hours until it reached 18,000 Vh. The current did not exceed 50 µA per strip. Each focused strip was subsequently equilibrated in 4.0 ml of equilibration buffer I [(6 M urea (w/v); 50 mM Tris-Cl, pH 8.8; 2% SDS (w/v); 30% glycerol (v/v); bromophenol blue (trace); 1% DTT (w/v)] for 15 min with gentle agitation followed by the equilibration buffer II [equilibration solution I with DTT replaced by 2.5% iodoacetamide (w/v)] for 15 min with gentle agitation. The second-dimensional separation was performed on a 10% SDS-PAGE gel in Ettan DALT six electrophoresis system (GE Healthcare) at 10 mA per gel at 25°C for approximately 18h until the bromophenol blue reached the bottom of the gel. Two technical replicates were done independently for each biological sample, for a total of 18 gels.

Sypro Ruby gel stain

The gels were stained with Sypro Ruby gel stain (Sigma) for total protein staining. Briefly, the gels were fixed in 10% methanol and 7% acetic acid for 30 minutes before being stained with Sypro Ruby gel stain overnight. The next day, gels were washed in 10% methanol and 7% acetic acid for 30 minutes before being imaged on a Gel Doc imaging system (Bio-Rad).

Image acquisition and 2-D gel analyses

The same scanning conditions were ussed for each Sypro Ruby-stained gel. The scanned gels were analyzed using PDQuest 2-D analysis software (advanced version 8.0; BioRad) according to the protocol provided by the developer. The 2-D gel analysis software PDQuest was used for gel-to-gel matching and identifying differences between the different groups. Each spot was visually inspected for proper matching and localization on the other gels of the same group using the group consensus tool. The gel images were normalized in the PDQuest software with the local regression model to even out differences in staining intensities between gels. Each matched protein spot was assigned a unique SSP (sample spot protein) number. For gel comparison, a statistical approach was applied for determining statistically differentially regulated proteins using the PDQuest software. Student's t-test was performed with 95% significance level to determine which proteins were statistically differentially regulated between the healthy cells and the patient cells non-treated and the patient cells non-treated and treated with GSKi. A minimum of 1.5-fold change was considered for the upregulated proteins and 0.67-fold for downregulated proteins. Each analysis set was visually inspected to match PDQuest software spot detection and 5 spots were removed from the final analysis due to poor quality. Protein spots with differential expression patterns on 2-DE maps were excised with the automated spot excision robot, the EXQuest spot cutter (Bio-Rad).

Protein identification

LC-MS analysis was performed at the OHRI Proteomics Core Facility (Ottawa, Ontario, Canada). Gel bands were in-gel digested according to the method of Shevchenko (Nat Protocols 2006;1(6):2856-60). Peptide extracts were concentrated by vacufuge (Eppendorf) and diluted in 0.1% trifluoroacetic acid. Peptides were loaded onto a peptide trap (Agilent) for 5 minutes at 15 microlitres per minute using a Dionex UltiMate 3000 RSLC nano HPLC. Peptides were eluted over a 20 minute gradient of 3% - 45%

acetonitrile with 0.1% formic acid at 0.3 microlitres per minute onto a 10-cm analytical column (New Objective Picofrit self-packed with Zorbax C18) and sprayed directly into a LTQ Orbitrap XL hybrid mass spectrometer using a nanospray source (Thermo Scientific, USA). Mass spectra were acquired in a data-dependent fashion, with MS scans acquired in the FT cell while MS^2 scans were acquired in the ion trap module.

MS/MS spectra were matched against a custom database (2011_07_human_con) comprised of human sequences from SwissProt (2011_07 version of uniprot_sprot.fasta.gz from ftp.uniprot.org) concatenated with a database of common contaminants (Contaminant db downloaded from maxquant.org, downloaded june 9th 2011) using MASCOT 2.3.01 software (Matrix Science, UK) with MS tolerance of ±5 ppm and MS/MS tolerance of 0.6 Da. Oxidation of methionine, carbamidomethylation of cysteine, deamidation, protein N-terminal acetylation, conversion of peptide N-terminal Glu or Gln to Pyro-Glu and phosphorylation of serine or threonine were allowed as potential modifications.

Quantitative PCR

Total RNA was isolated using Trizol (Invitrogen) and purified utilizing RNeasy mini kits. Subsequently, RNA was quantified utilizing a NanoDrop 1000 (Thermo Scientific) and reverse transcription performed using Omniscript kit as directed (Qiagen). All real-time PCR experiments were performed using the SYBR Green Jumpstart Taq Ready Mix (Sigma) on a Lightcycler 480 (Roche) and analyzed with accompanying software as per the Pfaffl method.(13;14)

Western Blots

Western blots were performed using standard techniques. Briefly, protein was isolated in RIPA buffer using a ratio of 50 µL per 1 million cells. The sample was then allowed to incubate on ice for 30 minutes followed by centrifugation. The supernatant was assayed using a standard BCA assay (Thermoscientific). Protein was then separated on 10% acyladmide gels and transferred to PVDF membranes using iBlot as directed (Invitrogen). After transfer, the membrane was blocked for one hour with 5% skim milk in TBS-T at room temperature. Primary antibodies were incubated overnight at 4 degrees. Primary antibodies included: PAI-2 (Abgent, AP6562c, 8:1000), β-actin (Sigma, 1:100000), Gelsolin (Abcam, ab11081, 1:1000), GDI2 (Abcam, ab49193, 1:2000), SCaMC-1 (Santa Cruz, sc-133987, 1:500), CatB (Abcam, ab58802, 1:10000). Membranes were then washed and incubated with biotinylated secondary antibodies (Santacruz) for a period of 1 hour then visualized using ECL Plus (Amersham Biosciences).

Cathepsin B activity assay

Cathepsin B activity was assayed in day 5 EPCs using a standardized CatB fluorometric assay kit as directed (Abcam). Briefly, EPCs were washed with PBS, lifted with EDTA and 5 $x10^6$ cells collected by centrifugation. Cells were lysed by incubation with cell lysis buffer, pelleted, and 50 µL transferred to a 96 well plate. Subsequently, 2 µL 10 mmol/L AC-RR-AFC was added and samples incubated for 2 hours. Plates were read on the SynergyMx microplate reader (Bio Tek).

VEGF Secretion Assay

EPCs were cultured using standard techniques to day 4. Cells were subsequently lifted, counted, and replated in 96 well plates at equivalent densities in VEGF free media with treatment as indicated. Following 24 hours, media was removed and assayed for VEGF

levels using a standard VEGF ELISA kit (R&D Systems) using the manufacturers protocol.

HUVEC Adhesion Assay

HUVEC were cultured to confluence in 96 well plates then treated with 10ng/mL of TNF-α for 6 hours to activate cells. 10^6 EPCs were cultured in with 5 μmol/L calcein for 30 minutes, lifted with EDTA, pelleted and resuspended in EGM-2. Subsequently, $4x10^4$ cells were plated on the activated HUVECs and allowed to adhere for 1 hour. Plates were read on the SynergyMx microplate reader, washed 3 times with PBS, and re-read. Adherence is expressed as % fluorescence retained after washing.

Cell Invasion Assay

Day 5 EPCs were treated as indicated. Using a modified Boyden chamber and a nucleopore filter (12 μm BD) with a matrigel matrix (BD), EPC invasiveness was assayed. Briefly, $5x10^6$ EPCs were placed in the upper chamber with EBM with EGM-2 in the lower chamber. Cells were permitted to migrate for 24 hours at 37 degrees. Cells were counterstained with DAPI and enumerated in 6 random high power fields.

CD-1 Nude Femoral Artery Wire Injury Model

Thirty-two CD-1 nude athymic male mice were purchased from Charles River Laboratories and permitted to acclimatize for 2-6 weeks prior to surgery. Under isoflurane anesthesia, mice underwent blunt dissection of the femoral neurovascular bundle with isolation of the femoral artery.(15) A branch of the femoral artery was isolated, incised and a 0.014-inch intravascular guidewire was introduced and passed in the main lumen denuding the artery and initiating neointima formation as previously described. Flow was restored to the main femoral artery and the incised branch was

ligated. Subsequently, $2x10^5$ EPCs from patients with DM were infused into the adjacent vein utilizing a blunt needle. None of the animals exhibited ischemia in the hind limb. Mice were recovered and were sacrificed at 14 days for tissue analysis.

Tissue Processing

Mice underwent perfusion fixation with buffered formalin at time of sacrifice. Arteries were then fixed for 24 hours in formalin and dehydrated in ethanol. Arteries were mounted in paraffin blocks and sectioned in 5 μm sections till 100 μm from the branch vessel site. These sections were then haematoxylin and eosin stained and analysis performed using a computer-assisted digital imaging system (Image-Pro Plus, Media Cybernetics).

Ethics and Statistics

All protocols involving human donors were approved by the Ottawa Heart Insitute Research Ethics Committee with participants providing written informed consent. These studies conform with the Declaration of Helsinki for the use of human tissue. Animal experimental protocols were approved by the University of Ottawa Animal Care committee and adhere to the Canadian Council on animal Care guidelines.

Data are expressed as mean plus or minus standard error of the mean. Statistical significance was determined for $p<0.05$. Pairwise comparisons was performed using a paired student t-test with multiple comparisons performed with a one-way ANOVA with Holm-Sidak *post hoc* testing.

Results

Diabetes Accelerates Apoptosis in EPCs Through Increased GSK3β Activity

EPCs isolated from human subjects were cultured for seven days and then characterized using immunolabeling for *ulex europeus agglutinin*-1 and acetylated-LDL uptake (**Figure 1A**). The baseline characteristics of the human subjects are presented in **Table 1**. Samples derived from patients with DM yielded fewer EPCs than those derived from healthy controls (n=12, 14.9 ± 4.6 vs 38.5 ± 6.7 cells per high power field, p<0.01, **Figure 1B**). Several GSK3β inhibitors were supplemented in increasing concentrations to identify the optimal inhibitor and concentration. CHIR98014 at a concentration of 1 μM yielded optimal EPC yields and significantly greater inhibition of GSK3β (**Figure 2B & C**). Subsequently, CHIR98014 was used as the preferential GSK3β inhibitor (GSKi) in all experiments.

Notably, supplementation of the culture media with GSKi resulted in an approximately 300% increases in the yields of EPCs in both DM and healthy controls (p<0.01, **Figure 1C**). Under basal conditions, the apoptosis index at 96 hours was higher in patients with diabetes as measured by Annexin V and propidium iodide double labelling (9.2 ± 0.9 vs 7.3 ± 0.9, p=0.02, **Figure 1D**) an effect attenuated through GSK3β inhibition. As expected, serum starvation, used to reproduce cell stress following therapeutic transplantation, resulted in marked increases in apoptosis index in both DM and healthy cells – an effect abrogated with GSKi treatment to near basal levels (**Figure 1D**). Importantly, higher levels of phosphorylated β-catenin (pβcat), the product of active GSK3β activity, in EPCs derived from diabetic patients (0.55 ± 0.08 vs 0.42 ± 0.04, p=0.04) were markedly reduced in both cohorts of cells following GSKi treatment (**Figure 1E**, p<0.01). These findings demonstrate that increased basal activity of GSK3β in EPCs

from patients with DM results in accelerated apoptosis *in vitro* – an effect abrogated by use of isoform specific small molecule inhibitors.

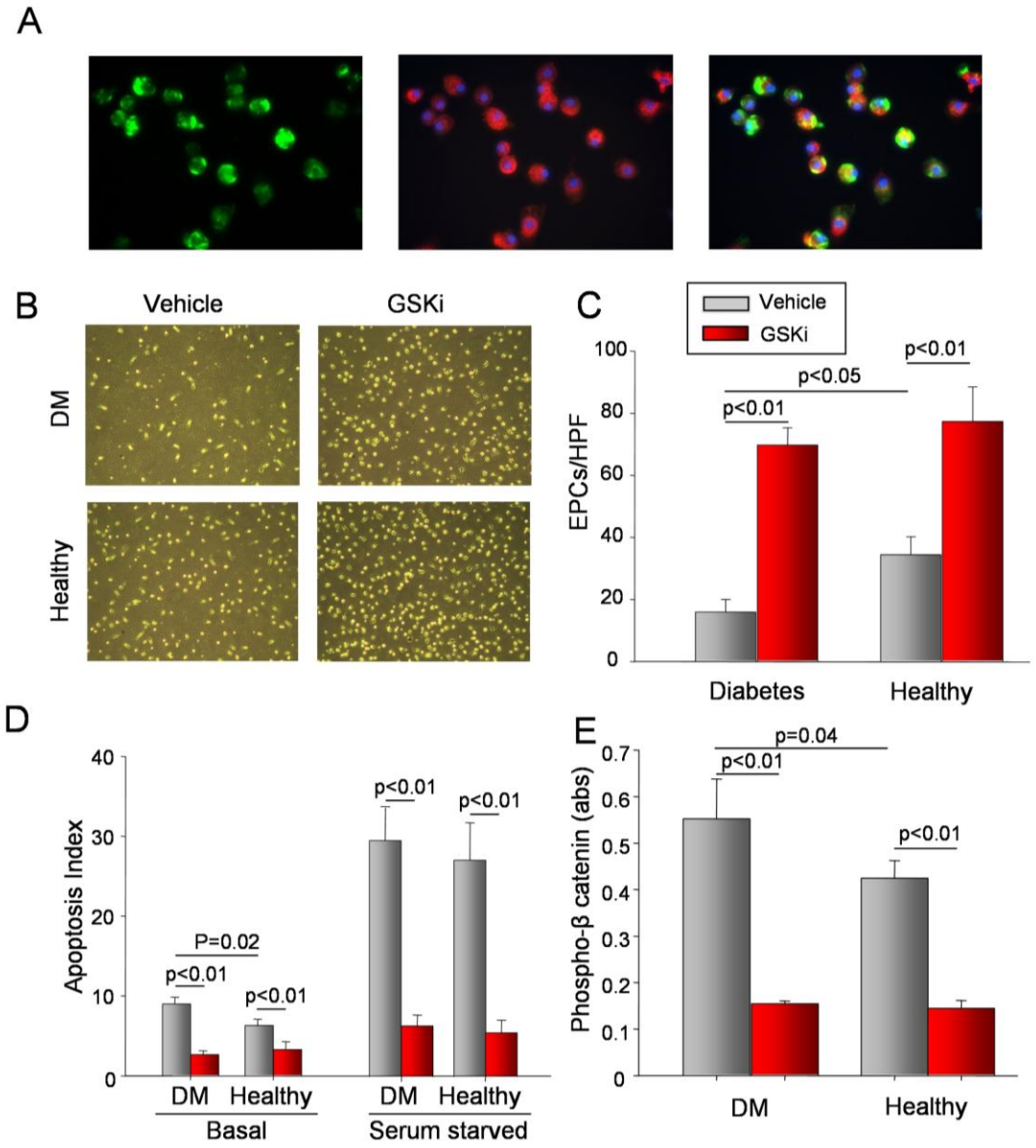

Figure 1. Increased GSK3β Signaling in Diabetic EPC Reduces *in vitro* Cell Yield. **A** - EPCs at 7 days labeled with DAPI (blue), AcLDL-DiI (Red),UEA-1-FITC (green), and merged image. **B** - Light microscopy images of cells from patients with DM and healthy controls under basal conditions or treated with GSKi. **C** - GSKi treatment increases EPC yield in both healthy controls and patients with DM. **D** - GSKi treatment attenuates apoptosis under both basal and serum starved conditions. **E** - EPCs from patients with DM have higher levels of phospho-β catenin. GSKi treatment in both groups markedly reduced these levels.

Table 1 – Baseline Characteristics

	Diabetes (n=12)	**Healthy (n=12)**	**p-value**
Age – years (SD)	45.5 (13.8)	52.3 (17.4)	0.30
Males – no. (%)	6 (50.0)	8 (66.7)	0.68
Hypertension – no. (%)	1 (8.3)	0 (0.0)	1.00
Diabetes – no. (%)	12 (100.0)	0 (0.0)	<0.001
Dyslipidemia – no. (%)	3 (25.0)	1 (8.3)	0.59
Smoking – no. (%)	1 (8.3)	2 (16.6)	1.00
Family History – no (%)	2 (16.6)	2 (16.6)	1.00
CAD – no. (%)	0 (0.0)	0 (0.0)	1.00
Fasting Glucose – mmol/L (IQR)	8.4 (7.3-9.0)	5.3 (5.0-5.8)	<0.001
HbA1C – mean (SD)	8.5 (1.3)	5.3 (0.5)	<0.001
LDL cholesterol – mmol/L (SD)	2.5 (1.1)	3.0 (0.8)	0.18

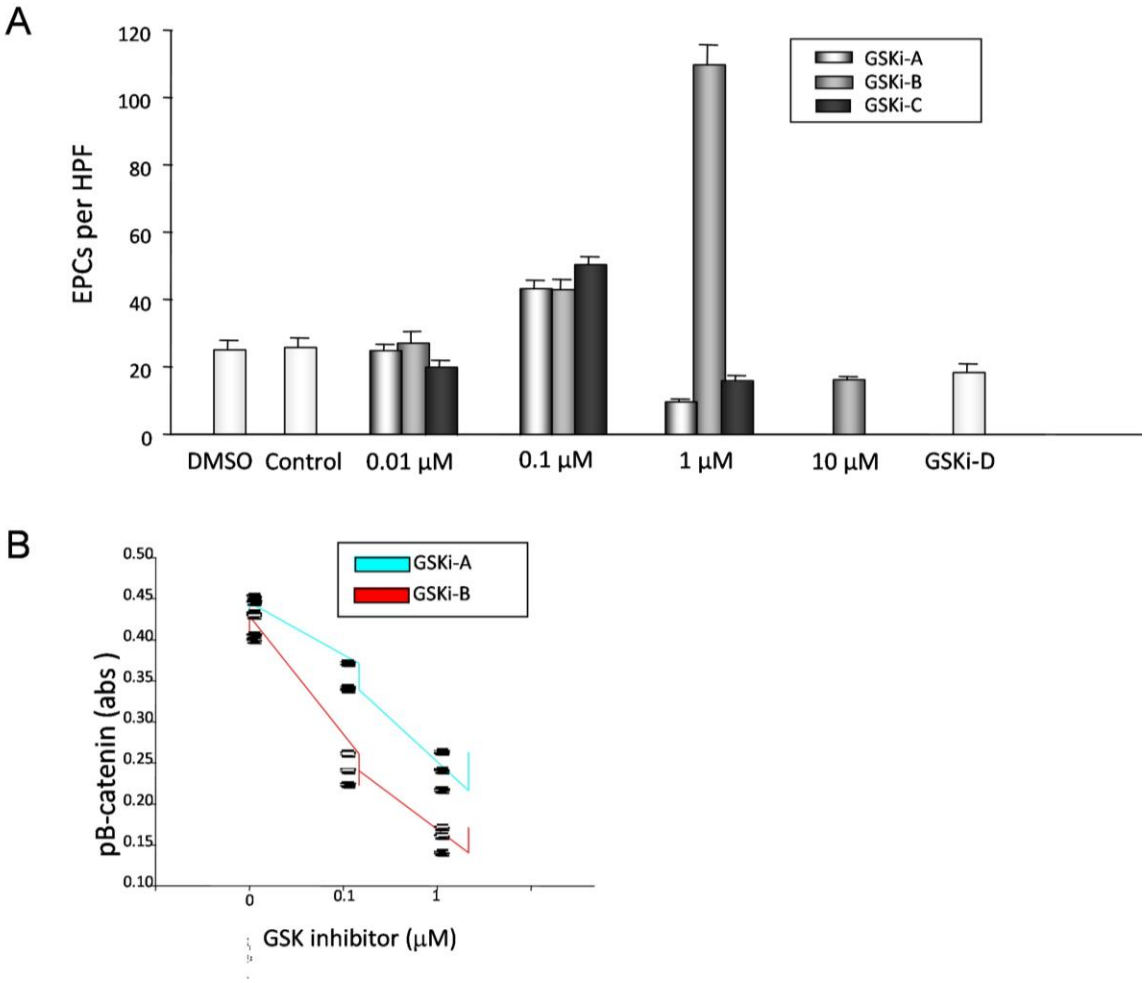

Figure 2. Identification of Optimal GSK Inhibitor. A - Effect of increasing doses of GSKi-A (AR-A014418), GSKi-B (CHIR98014), and GSKi-C (Indirubin-3'-monoxime) on EPC yield. GSKi-B at 1µM doses yielded optimal EPC yields with no toxicity.
B - Comparison of efficacy of GSK3-β inhibition between GSKi-A and GSKi-B. At equimolar dosing GSKi-B demonstratedmore efficient inhibition.

Proteomic Profiling of EPCs in DM

To ascertain mechanistic insight into the beneficial effects of GSKi on EPCs, analyses of the proteome of EPCs from patients with DM, DM treated with GSKi, and healthy controls was performed (n=3 for each). Isolation protocols were scaled up to yield sufficient cellular yields for the analyses. Differential yields between healthy controls and diabetic patients were maintained in scaled up protocols as were the effects of GSKi (**Table 2**). Following 2D gel electrophoresis and digital image analysis, 242 unique protein spots were identified. Differentially regulated candidate targets were identified if there was either a 2.0 fold up regulation or 0.5 down regulation of spot intensity identified between the groups (**Figure 3**). In total, 37 non-redundant proteins met these criteria for significant differential expression ($p<0.05$). These spots were excised from the Sypro-Ruby stained gels and submitted to in-gel trypsinization and the peptide mixtures were analyzed by LC-MS/MS analysis and the results of mass spectroscopy identification are presented in (**Table 3**).

Western blot analysis of three target proteins of interest was performed. Specifically catB up regulation (1.9 ± 0.06 vs. 5.8 ± 2.0), Gelsolin down regulation (5.6 ± 1.5 vs. 1.9 ± 0.9), and Plasminogen activator inhibitor-2 (PAI-2) up regulation (2.1 ± 0.7 vs. 5.1 ± 0.5) was confirmed in EPCs from patients with DM ($p<0.05$ for all comparisons, **Figure 4B&C**). As βcat acts as a transcription factor with Transcription factor 7 and Lymphoid enhancer-binding factor 1, we hypothesized that regulation of protein levels seen by GSKi were most likely transcriptional in nature. Indeed, quantitative PCR of mRNA isolated from DM EPCs under basal and GSKi treated conditions revealed a 4.6 fold increase in catB ($\pm$ 1.2, $p<0.01$, **Figure 4D**), 0.5 fold reduction in Gelsolin (0.4, $p<0.05$), and 10.4 fold increase in PAI-2 (± 5.0, $p<0.01$). Neither Calcium-binding mitochondrial carrier protein

SCaMC-1 nor GDP dissociation inhibitor-2 (GDI-2) appeared differentially regulated at the mRNA or protein level. These findings confirmed the validity of the proteomics results and identified several targets known to regulate apoptosis *and* to be expressed in EPCs. In this manuscript, we summarize the relevant findings and experiments that evolved from our study of catB.

Table 2 – Proteomics baseline characteristics and cellular yields

	Diagnoses	Cell number	Total μg protein
Healthy 1	none	5.0×10^6	217
Healthy 2	none	7.5×10^6	252
Healthy 3	none	5.0×10^6	275
DM 1	DMII, CAD	3.5×10^6	178
DM 1 + GSKi	DM II, CAD	4.5×10^6	374
DM 2	DMI, PVD	2.5×10^6	90
DM2 + GSKi	DMI, PVD	6.0×10^6	429
DM 3	DMII	3.0×10^6	192
DM 3 + GSKi	DMII	8.0×10^6	726

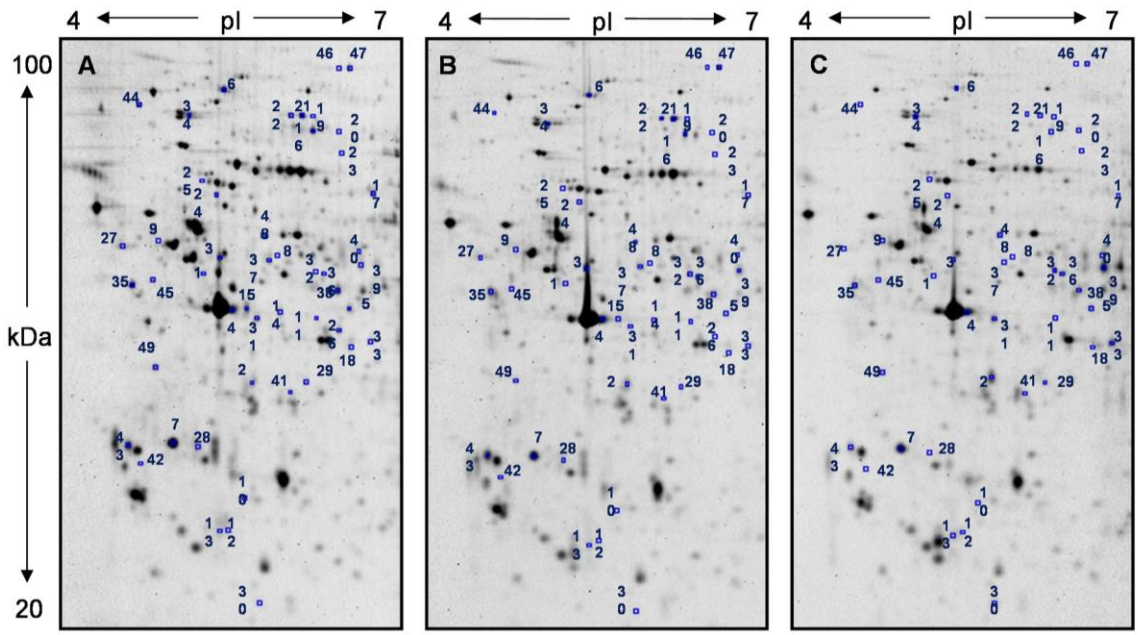

Figure 3. Sample 2D Gel Electrophoresis. Sample protein gels from EPCs derived from a patient with DM, DM EPCs treated with GSKi, and a healthy control. Numerical designation of spots correspond to proteins in Table 4.3.

Table 3 – Proteomics Analysis

Dot No.	Protein Identity	Swissprot No.	MS Score	Theoretical MW	# of statistically significant matches	Coverage (%)	Ratio (DM/Healthy)	Ratio (DM+GSKI vs. DM)
1	26S protease regulatory subunit 6A	P17980	401	49172	26	46	0.94	**1.73**
2	Actin, cytoplasmic 1	P60709	1796	41710	82	55	1.53	**2.99**
3	Actin, cytoplasmic 1	P60709	2638	41710	115	50	**2.9**	**0.42**
4	Actin, cytoplasmic 1	P60709	635	41710	27	33	**2.09**	1.79
5	Adenosylhomocysteinase	P23526	1246	47685	71	31	**0.64**	1.84
6	Alpha-actinin-4	O43707	364	104788	18	35	1.46	**0.51**
7	Annexin A5	P08758	2639	35914	159	52	**0.65**	1.42
8	ATP-dependent RNA helicase DDX39A	O00148	292	49098	13	33	0.86	**1.54**
9	Beta-hexosaminidase subunit alpha	P06865	786	60664	38	29	0.98	**2.12**
10	Beta-hexosaminidase subunit beta	P07686	83	63071	8	14	**0.55**	0.97
11	Calcium-binding mitochondrial carrier protein SCaMC-1	Q6NUK1	325	53320	16	34	1.12	**1.76**
12	Cathepsin B	P07858	559	37797	21	33	**0.45**	**4.06**
13	Cathepsin B	P07858	522	37797	15	30	0.56	**3.08**
14	Cathepsin D	P07339	788	44524	33	32	**0.42**	nd
15	Cathepsin D	P07339	1212	44524	55	31	0.49	nd
16	Coagulation factor XIII A chain	P00488	594	83215	28	25	**1.62**	0.51
17	Dihydropyrimidinase-related protein 2	Q16555	1478	62255	59	62	0.6	**0.47**
18	Galactokinase	P51570	269	42246	13	26	**0.57**	1.77
19	Gelsolin	P06396	447	85644	20	30	**1.57**	0.8
20	Gelsolin	P06396	144	85644	8	10	1.41	**1.82**
21	Gelsolin	P06396	3025	85644	108	38	1.3	**0.38**
22	Gelsolin	P06396	2006	85644	72	45	1.97	**0.34**
23	Glycyl-tRNA synthetase	P41250	560	83113	40	32	0.79	**1.51**
24	Heterogeneous nuclear ribonucleoprotein K	P61978	603	50944	44	53	0.77	**0.62**
25	Lamin-B1	P20700	1251	66368	51	49	0.91	**2.45**
26	Leukocyte elastase inhibitor	P30740	1214	42715	48	49	**0.47**	nd
27	Lymphocyte-specific protein 1	P33241	600	37169	35	44	0.94	**0.34**
28	Microtubule-associated protein RP/EB family member 1	Q15691	602	29980	33	59	0.56	**0.33**
29	N-acetyl-D-glucosamine kinase	Q9UJ70	313	37352	12	24	0.95	**1.56**
30	Peroxiredoxin-2	P32119	578	21878	32	38	**1.65**	0.88
31	Plasminogen activator inhibitor 2	P05120	2097	46566	80	56	**0.47**	**4.43**
32	Pyruvate kinase isozymes M1/M2	P14618	3019	57900	96	59	**2.89**	1.9
33	Pyruvate kinase isozymes M1/M2	P14618	1053	57900	34	35	0.94	**2.62**
34	Ras GTPase-activating-like protein IQGAP1	P46940	1155	189134	58	13	**1.5**	0.86
35	Ribonuclease inhibitor	P13489	769	49941	28	37	**1.65**	0.94
36	Sorting nexin-6	Q9UNH7	259	46620	16	27	**1.76**	1.44
37	Spliceosome RNA helicase DDX39B	Q13838	887	48960	42	37	1.8	**0.38**
38	Synaptic vesicle membrane protein VAT-1 homolog	Q99536	1046	41893	55	50	0.68	**1.73**
39	Tissue alpha-L-fucosidase	P04066	2138	53655	71	43	0.96	**5.41**
40	Tissue alpha-L-fucosidase	P04066	995	53655	35	21	**0.18**	2.59
41	Transaldolase	P37837	142	37516	9	19	1.08	**1.63**
42	Tropomyosin alpha-1 chain	P09493	271	32689	12	20	**2.56**	**0.47**
43	Tropomyosin alpha-4 chain	P67936	2259	28504	107	39	1.82	**0.43**
44	Vimentin	P08670	51	53619	1	6	0.68	**1.51**
45	Vimentin	P08670	735	53619	34	35	**2.03**	1.26
46	Vinculin	P18206	4302	123722	142	58	**2.1**	0.77
47	Vinculin	P18206	2976	123722	119	41	**2.05**	**0.4**
48	V-type proton ATPase subunit B, brain isoform	P21281	1523	56465	64	48	0.99	**1.95**

49	V-type proton ATPase subunit d 1	P61421	271	40303	12	25	0.63	**1.55**

The protein identities for each spot are listed. The other columns depict the SWISS-PROT No: SWISS-PROT accession number; MS Score: Mass spectrometry score indicating the significance of protein identification from peptide mass finger print according to MASCOT software application 2.3.01 (Matrix Sciences, London, UK) (score value > 50 for $p < 0.05$); Theor. Mr: Theoretical molecular weight of the matching protein; No of significant peptide matches: Number of spectrum-to-peptide matches that were evaluated to be statistically significant (Expect <0.05); Density values were normalized by the local regression model. Student's t-test (two-tail, 95% level of confidence) was calculated for pair-wise comparisons to identify proteins that were expressed at significantly different levels Mean fold change values are indicated in the final two columns and significant changes are indicated in bold. By computational 2D gel image comparison, a total of 49 protein spots were found to be differentially expressed, each exhibiting ≥1.5 fold-change (either increase or decrease) of mean value spot intensity among the three different samples. ND: non-detectable.

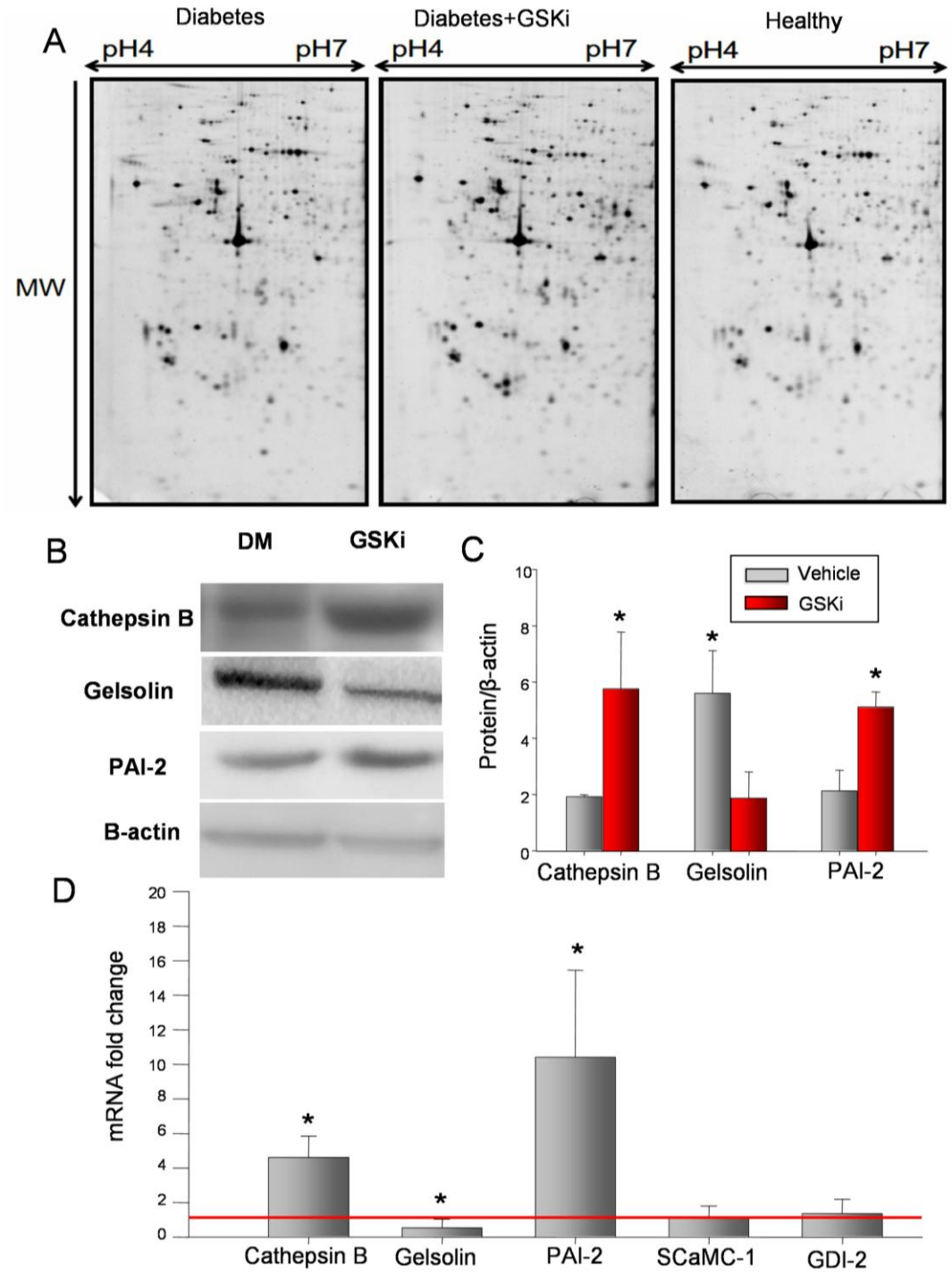

Figure 4. Proteomic Analyses of EPCs from Patients with DM with and without GSK3β Inhibition. **A** - Sample 2D gels utilized in proteomics analysis. **B,C** - Western blot analysis of catB, Gelsolin, and PAI-2 (n=6). **D** - Quantitative PCR analysis of candidate genes identified byproteomics analysis. Fold change represents GSKi sample compared to control sample in EPCs derived from patients with DM (n=6). * represents $p<0.05$.

Cathepsin-B is required for GSKi mediated reductions in apoptosis

To ascertain the role of catB activity in EPC dysfunction in patients with DM, we assayed enzyme activity levels. As predicted by mRNA and protein levels, EPCs from patients with diabetes had 40% less measurable activity compared to healthy control cells (5587.3 ± 1455.1 vs. 8251.2 ± 771.9 RFU, p=0.03, **Figure 5A**). Treatment with GSKi raised measurable activity 4-fold in both groups ($p<0.01$). To ascertain if catB activity was required for changes in phenotype associated with GSKi, we used a specific inhibitor of catB, CA074.(16) Supplementation of the culture media with CA074 abrogated a GSKi induced dose dependent increase in catB activity at all levels assayed (**Figure 5B**). In turn, functional assays were performed to ascertain the necessity of intact catB activity for phenotypic changes in apoptosis rates, VEGF secretion, and endothelial adhesion by EPCs cultured from patients with DM. Notably, the effect of GSKi on apoptosis could be attenuated when cells were cultured in the presence of the catB inhibitor CA074 (**Figure 5C**). Blockade of catB activity demonstrated no effect on VEGF secretion *or* binding of EPCs to activated HUVECs (**Figure 5D,E**). Instead, only EPC invasive capacity as assessed by matrigel invasion was also catB dependent, as this parameter increased 3-fold with GSKi treatment (**Figure 5F,** $p<0.01$). These findings demonstrate that EPCs derived from patients with DM have intrinsically lower catB activity and that induction of expression by GSKi attenuates higher levels of apoptosis and improves invasiveness *in vitro*.

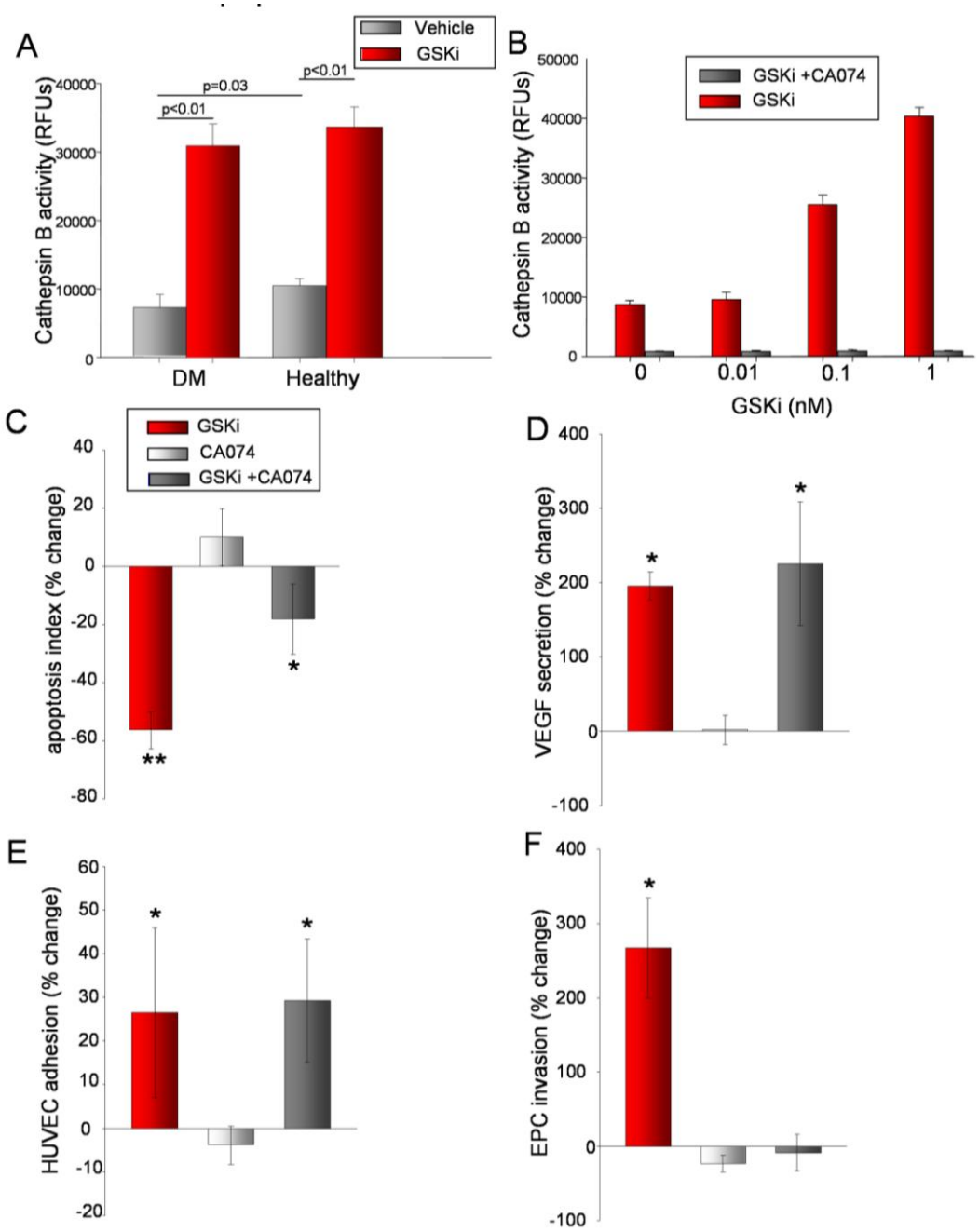

Figure 5. Cathepsin B is Required for GSKi-Mediated Reduction in the Rate of Apoptosis in Diabetic EPCs. **A** - Cathepsin B activity is reduced at baseline in DM-EPCs and increased by treatment with GSKi (n=6). **B** - Dose dependent increase in cathepsin B activity is achieved with GSKi and effect abrogated by treatment with the cathepsin B inhibitor, CA074(n=12). **C** - The basal rate of apoptosis reduced by 60% in EPCs treated with GSKi. This effect is lost with cathepsinB inhibition (n=12). **D** - Improvements in VEGF secretion achieved with GSKi occur independently of cathepsin B activity(n=12). **E** - Increased EPC adhesionachieved with GSKi occur independently of cathepsin B activity (n=12). **F** - Improvement in EPC invasion achieved with GSKi is dependent of cathepsin B activity (n=6).

GSK3β inhibition mediated improvements in EPC based cell therapy require Cathepsin B activity

Efficacy of cell based therapies depends on the dose, functional capacity, and survival of cells following administration. To investigate the therapeutic necessity of catB up regulation to EPC mediated arterial healing, we administered cells from 6 diabetic patients in a xenotransplant femoral artery wire injury model in CD-1 nude mice (**Figure 6A**). Following wire injury, 2.5×10^5 cells were administered intravenously. Administration of cells alone reduced the intima:media (IM) ratio 41% (e.g., 1.37 ± 0.15 vs. 0.81 ± 0.12, $p<0.01$, **Figure 6B**) at 14 days. Pre-treatment of cells with GSKi resulted in a further 40% reduction in IM ratio compared to untreated EPCs (0.50 ± 0.07, $p=0.02$) – an effect lost when cells were co-cultured with GSKi and CA074 (0.77 ± 0.11, $p=0.03$ vs. EPC+GSKi). Of note, effects were observed in each individual subject (**Figure 6C**). These findings confirm that reductions in apoptosis achieved through up regulation of catB by GSK3β inhibition in part explain the therapeutic enhancement of EPC based therapy in patients with DM.

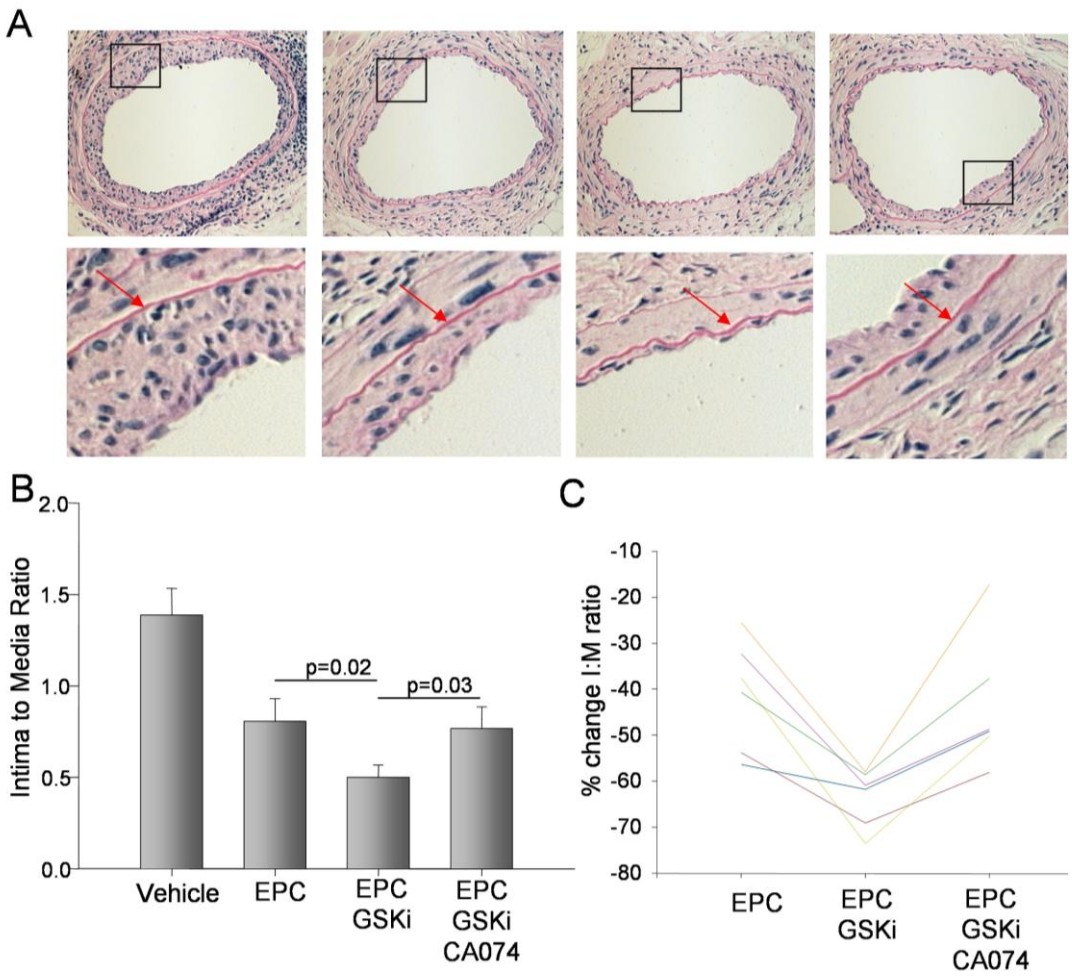

Figure 6 Cathepsin B is Required for EPC mediated Arterial Repair with Diabetic EPCs. A - Representative 14 day cross-sections at low magnification with magnified regions of NI highlighted. Arrows indicate the internal elasticlamina. **B** - GSKi treatment of DM-EPCs results in important reductions in NI formation, an effect lost with cathepsin B inhibition (n=6). **C** - Changes in NI formation of individual patients as per treatment group. All patients demonstrated improvement in arterial homeostasis with GSKi treatment (n=6).

Discussion

Identifying cell enhancement strategies, be it genetic modification,(2) small molecule antagonism of signaling cascades,(3) or use of adjuvant biomaterials is essential to improve the therapeutic efficacy of cell based therapies. Indeed, transplanted cells in a wide variety of models demonstrate poor engraftment with high rates of cell attrition limiting therapeutic benefit. Herein, we highlight important differences in GSK3β signalling as a factor for enhanced EPC senescence in DM resulting in accelerated rates of apoptosis, decreased VEGF secretion and attenuated adhesion. Moreover, using a proteomics approach we identified up regulation of catB as essential for GSKi induced reductions in basal and stress induced apoptosis. Finally, in a xenotransplant model, we confirm that catB activity is required for GSKi-induced improvements in EPC mediated arterial repair.

Patients with DM have increased rates of cardiovascular disease and markedly higher rates of in-stent restenosis following revascularization due to impaired arterial healing.(17) This, in part, is owing to attenuated EPC function in patients with DM who have not only fewer circulating cells(18) but higher rates of EPC apoptosis and increased senescence.(19;20) Multiple mechanisms of EPC dysfunction have been identified including eNOS uncoupling,(21) increased reactive oxygen species and the effects of advanced glycation end products.(10) GSK3β is known to be highly upregulated in a number of tissues in DM,(8) with our data now confirming increased pβ-cat, the end product of GSK3β, in EPCs derived from diabetics. Thus, dysregulation of β-cat signalling represents a new target for cell enhancement of EPCs in patients with DM - the current study noting improvements in both yield of available cells as well as EPC function.

To date, three studies suggest a beneficial effect of GSK3β antagonism in EPC-based therapy.(3;6;7) The current report is the first to use an unbiased proteomic approach to identifying differentially regulated proteins in EPCs derived from patients with DM and with GSKi treatment. Using this technique, we identified catB, a protein with known roles as both a pro- and anti-apoptotic roles. Similar to observations in several cell lines,(22-24) we noted catB downregulation in DM derived EPCs resulted in enhanced apoptosis – an effect rescued with GSKi therapy. Interestingly, catB has been linked to cell invasiveness in several cancer cell lines which in turn reduces apoptosis and increases metastatic potential. Our data replicates these findings from the cancer literature, with striking parallels in which transplanted cells with more “malignant” phenotypes are able degrade extra-cellular matrix and integrate into surrounding tissues more efficiently – in the case of cell based therapy improving therapeutic effect.

This study is not without limitations. Indeed, the definition of EPCs continues to be in flux(25) and we cannot be certain that the mechanisms described in the current study apply to circulating EPC populations. However, the current experiments were performed in primary cells commonly used for therapeutic administration from patients with DM. Second, while there are clear improvements in apoptosis and invasiveness, we do not demonstrate increased cell retention in our *in vivo* model. However, it is well documented that in numerous animal models of cell based therapy that cellular retention is a rare event that is noted at later time points, while the paracrine effect of cell therapy may be an important early beneficial mechanisms.(26) Despite these limitations, our study is the first to highlight catB regulation by GSK3β as a potential cell enhancement strategy for patients with DM and our unbiased proteomic approach highlights potential future targets, such as PAI-2, for future investigation.

Conclusions

Inhibition of GSK3β activity in EPCs from patients with DM results in up regulation of catB expression and activity. Increased catB activity improves EPC invasiveness, reduces apoptosis, and ameliorates therapeutic effect of cell based therapy. Small molecule antagonism of GSK3β is a cell enhancement strategy for patients with DM.

Sources of Funding

The Canadian Institute for Health Research and Medtronic collectively provide EOB with a peer-reviewed Research Chair (URC #57093; IGO 94418) and operating grant.

Disclosures

None

Reference List

(1) Hibbert B, Olsen S, O'Brien E. Involvement of progenitor cells in vascular repair. Trends Cardiovasc Med 2003 Nov;13(8):322-6.

(2) Lavoie JR, Stewart DJ. Genetically modified endothelial progenitor cells in the therapy of cardiovascular disease and pulmonary hypertension. Curr Vasc Pharmacol 2012 May;10(3):289-99.

(3) Hibbert B, Ma X, Pourdjabbar A, Holm E, Rayner K, Chen YX, Sun J, Filion L, O'Brien ER. Inhibition of endothelial progenitor cell glycogen synthase kinase-3beta results in attenuated neointima formation and enhanced re-endothelialization after arterial injury. Cardiovasc Res 2009 Jul 1;83(1):16-23.

(4) Trowbridge JJ, Xenocostas A, Moon RT, Bhatia M. Glycogen synthase kinase-3 is an in vivo regulator of hematopoietic stem cell repopulation. Nat Med 2006 Jan;12(1):89-98.

(5) Trowbridge JJ, Moon RT, Bhatia M. Hematopoietic stem cell biology: too much of a Wnt thing. Nat Immunol 2006 Oct;7(10):1021-3.

(6) Choi JH, Hur J, Yoon CH, Kim JH, Lee CS, Youn SW, Oh IY, Skurk C, Murohara T, Park YB, Walsh K, Kim HS. Augmentation of therapeutic angiogenesis using genetically modified human endothelial progenitor cells with altered glycogen synthase kinase-3beta activity. J Biol Chem 2004 Nov 19;279(47):49430-8.

(7) Ma X, Hibbert B, Dhaliwal B, Seibert T, Chen YX, Zhao X, O'Brien ER. Delayed re-endothelialization with rapamycin-coated stents is rescued by the addition of a glycogen synthase kinase-3beta inhibitor. Cardiovasc Res 2010 May 1;86(2):338-45.

(8) Eldar-Finkelman H, Schreyer SA, Shinohara MM, LeBoeuf RC, Krebs EG. Increased glycogen synthase kinase-3 activity in diabetes- and obesity-prone C57BL/6J mice. Diabetes 1999 Aug;48(8):1662-6.

(9) Desouza CV, Hamel FG, Bidasee K, O'Connell K. Role of inflammation and insulin resistance in endothelial progenitor cell dysfunction. Diabetes 2011 Apr;60(4):1286-94.

(10) Jarajapu YP, Grant MB. The promise of cell-based therapies for diabetic complications: challenges and solutions. Circ Res 2010 Mar 19;106(5):854-69.

(11) Hibbert B, Ma X, Pourdjabbar A, Simard T, Rayner K, Sun J, Chen YX, Filion L, O'Brien ER. Pre-procedural atorvastatin mobilizes endothelial progenitor cells: clues to the salutary effects of statins on healing of stented human arteries. PLoS One 2011;6(1):e16413.

(12) Ma X, Hibbert B, White D, Seymour R, Whitman SC, O'Brien ER. Contribution of recipient-derived cells in allograft neointima formation and the response to stent implantation. PLoS One 2008;3(3):e1894.

(13) Pfaffl MW. A new mathematical model for relative quantification in real-time RT-PCR. Nucleic Acids Res 2001 May 1;29(9):e45.

(14) Pfaffl MW. A new mathematical model for relative quantification in real-time RT-PCR. Nucleic Acids Res 2001 May 1;29(9):e45.

(15) Sata M, Maejima Y, Adachi F, Fukino K, Saiura A, Sugiura S, Aoyagi T, Imai Y, Kurihara H, Kimura K, Omata M, Makuuchi M, et al. A mouse model of vascular injury that induces rapid onset of medial cell apoptosis followed by reproducible neointimal hyperplasia. Journal of Molecular and Cellular Cardiology 2000;32(11):2097-104.

(16) Szpaderska AM, Frankfater A. An intracellular form of cathepsin B contributes to invasiveness in cancer. Cancer Res 2001 Apr 15;61(8):3493-500.

(17) Haffner SM, Lehto S, Ronnemaa T, Pyorala K, Laakso M. Mortality from coronary heart disease in subjects with type 2 diabetes and in nondiabetic subjects with and without prior myocardial infarction. N Engl J Med 1998 Jul 23;339(4):229-34.

(18) Fadini GP, Boscaro E, de KS, Agostini C, Seeger F, Dimmeler S, Zeiher A, Tiengo A, Avogaro A. Time course and mechanisms of circulating progenitor cell reduction in the natural history of type 2 diabetes. Diabetes Care 2010 May;33(5):1097-102.

(19) Fadini GP, Sartore S, Albiero M, Baesso I, Murphy E, Menegolo M, Grego F, Vigili de KS, Tiengo A, Agostini C, Avogaro A. Number and function of endothelial progenitor cells as a marker of severity for diabetic vasculopathy. Arterioscler Thromb Vasc Biol 2006 Sep;26(9):2140-6.

(20) Zerbini G, Maestroni A, Palini A, Tremolada G, Lattanzio R, Maestroni S, Pastore MR, Secchi A, Bonfanti R, Gerhardinger C, Lorenzi M. Endothelial progenitor cells carrying monocyte markers are selectively abnormal in type 1 diabetic patients with early retinopathy. Diabetes 2012 Apr;61(4):908-14.

(21) Thum T, Fraccarollo D, Schultheiss M, Froese S, Galuppo P, Widder JD, Tsikas D, Ertl G, Bauersachs J. Endothelial nitric oxide synthase uncoupling impairs endothelial progenitor cell mobilization and function in diabetes. Diabetes 2007 Mar;56(3):666-74.

(22) Szpaderska AM, Frankfater A. An intracellular form of cathepsin B contributes to invasiveness in cancer. Cancer Res 2001 Apr 15;61(8):3493-500.

(23) Malla R, Gopinath S, Alapati K, Gondi CS, Gujrati M, Dinh DH, Mohanam S, Rao JS. Downregulation of uPAR and cathepsin B induces apoptosis via regulation of Bcl-2 and Bax and inhibition of the PI3K/Akt pathway in gliomas. PLoS One 2010;5(10):e13731.

(24) Nalla AK, Gorantla B, Gondi CS, Lakka SS, Rao JS. Targeting MMP-9, uPAR, and cathepsin B inhibits invasion, migration and activates apoptosis in prostate cancer cells. Cancer Gene Ther 2010 Sep;17(9):599-613.

(25) Fadini GP, Losordo D, Dimmeler S. Critical reevaluation of endothelial progenitor cell phenotypes for therapeutic and diagnostic use. Circ Res 2012 Feb 17;110(4):624-37.

(26) Gnecchi M, Zhang Z, Ni A, Dzau VJ. Paracrine mechanisms in adult stem cell signaling and therapy. Circ Res 2008 Nov 21;103(11):1204-19.

6.2 Publication #2

Stem Cell Res. 2012 Dec 3;10(2):195-202

Feeder-independent derivation of induced-pluripotent stem cells from peripheral blood endothelial progenitor cells

Wing Y. Chang [a, b, 1], **Jessie R. Lavoie** [a, b], Sarah Y. Kwon [a, c], Zhaoyi Chen [a, b,] Janet L. Manias [a, b], John Behbahani [a, b], Vicki Ling [a], Rita A. Kandel [d], Duncan J. Stewart [a, b], William L. Stanford [a, b, c]

[a] Sprott Centre for Stem Cell Research, Regenerative Medicine Program, Ottawa Hospital Research Institute, Ottawa, Canada

[b] Department of Cellular and Molecular Medicine, Faculty of Medicine, University of Ottawa, Ottawa, Canada

[c] Department of Chemical Engineering and Applied Chemistry, University of Toronto, Toronto, Ontario, Canada

[d] Department of Pathology and Laboratory Medicine, Mount Sinai Hospital and Department of Laboratory Medicine and Pathobiology, University of Toronto, Toronto, Ontario, Canada

Copyrights

Contributions of the Candidate

The work described in the manuscript is the result of a collaboration established between my PhD supervisor's, Dr. Duncan J. Stewart, and a senior scientist at my Institute, Dr. William L. Stanford. I was principally involved in the design and execution of the experiments related to the generation of the late outgrowth endothelial progenitor cells (L-EPCs) from peripheral blood and leukapheresis products. I also executed the characterization of the L-EPC surface markers by flow cytometry and tested their functionality through Matrigel assay, as well as acquired and analyzed the data related to those experiments. I was also involved in drafting and editing the manuscript.

Abstract

Induced-pluripotent stem cells (iPSCs) are a potential alternative cell source in regenerative medicine, which includes the use of differentiated iPSCs for cell therapies to treat coronary artery and/or peripheral arterial diseases. Late-outgrowth endothelial progenitor cells (late-EPCs) are a unique primary cell present in peripheral blood that exhibit high proliferative capacity, are being used in a wide variety of clinical trials, and have the ability to differentiate into mature endothelial cells. The objective of this study was to reprogram peripheral blood-derived late-EPCs to a pluripotent state under feeder-free and defined culture conditions. Late-EPCs that were retrovirally transduced with OCT4, SOX2, KLF4, c-MYC, and iPSC colonies were derived in feeder-free and defined media conditions. EPC-iPSCs expressed pluripotent markers, were capable of differentiating to cells from all three germ-layers, and retained a normal karyotype. Transcriptome analyses demonstrated that EPC-iPSCs exhibit a global gene expression profile similar to human embryonic stem cells (hESCs). We have generated iPSCs from late-EPCs under feeder-free conditions. Thus, peripheral blood-derived late-outgrowth EPCs represent an alternative cell source for generating iPSCs.

Highlights

Reprogramming of peripheral blood derived late-EPCs to iPSCs was performed. EPC-iPSCs were derived in a feeder-free, defined media conditions. Late-EPC reprogramming has a similar efficiency to dermal fibroblast reprogramming.

Introduction

Cell therapies hold great promise for the treatment of numerous human diseases and disorders. For example, atherosclerotic vascular disease is a major cause of heart failure and contributes importantly to the growing burden of chronic disease. The use of stem cells to promote cardiac repair or restore perfusion to tissues represents an important strategy to avoid the deleterious consequences of occlusive vascular disease. In preclinical studies, the administration of adult stem and progenitor cells has been shown to improve cardiac function post acute myocardial infarction and restore perfusion to the ischemic hindlimb; however, their efficacy in clinical trials has been at best modest (Lasala and Minguell, 2011). These include endothelial progenitor cells (EPCs) that can be isolated from bone marrow or circulating mononuclear cells by surface marker selection of culture specification. The latter can be classified into early outgrowth EPCs (or circulating angiogenic cells) that appear within 3 days of culture, and late outgrowth EPCs (or blood outgrowth endothelial cells) that only appear after 2 weeks and then rapidly overgrow the early growth cells. Unlike the early cells, late-outgrowth EPCs are highly differentiated to an endothelial phenotype and exhibit high growth and colony forming potential (Lavoie and Stewart, 2012).

The recent discovery of iPSCs provides a potential alternative cell source for cell therapies and regenerative medicine (Takahashi and Yamanaka, 2006; Takahashi et al., 2007). However, a more immediate impact of iPSCs is its application to modeling human diseases and disorders (Chang et al., 2012 and Grskovic et al., 2011); for example, iPSCs derived from patients harboring genetic perturbations that result in premature atherosclerosis can be used to screen for novel anti-atherosclerosis therapies. Since the initial demonstration of somatic reprogramming to a pluripotent state by the exogenous expression of Oct4, Sox2, Klf4, and c-Myc in dermal fibroblasts (Takahashi et al., 2007),

numerous additional somatic cell types have been reprogrammed into iPSCs including neural progenitors (Eminli et al., 2008), B-cells (Choi et al., 2011), T-cells (Brown et al., 2010, Loh et al., 2010 and Seki et al., 2010), adipocytes (Sun et al., 2009), and endothelial cells (Ho et al., 2010). Although some of these cell types can be reprogrammed with high efficiency, many are not readily accessible. Blood cells are perhaps the most easily accessible but lymphocytes, the targets of most established blood-derived iPSCs, have limited proliferative capacity preventing banking of sufficient primary cells for future reprogramming with improved technologies and use in genomic and proteomic assays. Alternatively, late-outgrowth EPCs (late-EPCs) can also be isolated from peripheral blood, in fact, from as little as 3–5 ml of blood (Martin-Ramirez et al., 2012). These cells exhibit high proliferative capacity; for example, 1019 cells can be generated from a starting 100 ml culture within 2 months (Lin et al., 2000). Interestingly, peripheral blood late-EPC progenitor frequencies are often altered in disease states. However, in general, pathogenic states increase the frequency of circulating late-EPC progenitors (Jodon de Villeroche et al., 2010 and Thill et al., 2008) making them generally accessible from controls and patient's blood samples of 20–30 ml. In this report, we isolate late-EPCs from peripheral blood and reprogram these cells into iPSCs under feeder-free and defined media conditions.

Materials and methods

Derivation and cell culture of late-outgrowth EPCs

Three healthy donors were used to derive late-EPCs with informed consent. Leukapheresis product (lines 106 and 124) was isolated from patients using a Cobe Spectra 7.0 Apheresis System. Approximately 200 ml of mononuclear cell volume was collected from each patient. To derive late-EPCs from leukapheresis product, 40 ml from each sample was diluted with 3 volumes of Dulbecco's phosphate-buffered saline (DPBS) and centrifuged in a Ficoll-Paque PLUS (GE Healthcare) density gradient according to the manufacturer's instructions, whereas the PB1 late-EPC line was derived from 30 ml of whole peripheral blood. Mononuclear cells (MNCs) were fractionated from other components of peripheral blood by centrifugation on Ficoll-Paque PLUS. MNCs can be used immediately for late-EPC isolation or frozen in 10% DMSO without affecting isolation of late-EPCs or affecting the capacity of the late-EPCs to be reprogrammed. MNCs were then cultured on fibronectin-coated plates (Roche Applied Science) in Endothelial Growth Medium-2MV (CC-3202, Lonza) (basal endothelial media-2 (EBM), 20% human serum, VEGF, bFGF, IGF, EGF, gentamicin, ascorbic acid, and hydrocortisone). Late-outgrowth EPCs (late-EPCs) formed approximately 18 days after culturing in EGM-2MV. Late-EPCs exhibited a high proliferative capacity and had a cobblestone appearance. All experiments were performed with passage 7 or earlier late-EPCs. To passage late-EPC, cells were washed with PBS and trypsinized with 0.05% Trypsin-EDTA (25300120, Life Technologies).

In vitro endothelial cell tube formation assay

Endothelial tube formation assays were performed in 96-well plates coated with Matrigel (354230, Becton Dickinson), a reconstituted basement membrane matrix. Approximately,

2 × 104 late-EPCs were seeded into each well with 200 µL EGM-2MV + 20% human serum media. Capillary-like networks were then monitored and imaged 16 h later.

Reagents and cell culture of EPC-iPSCs

EPC-iPSCs were maintained on matrigel (BD Biosciences) in E8 media (DMEM/F12, L-ascorbic acid-2-phosphate magnesium) (Sigma), sodium selenium (14 µg/l, Sigma), FGF2 (100 µg/l, Life Technologies), insulin (19.4 mg/l, Roche), NaHCO3 (543 mg/l, Sigma), transferrin (10.7 mg/l, Sigma), and TGFβ1 (2 µg/l, Life Technologies) (Chen et al., 2011) under hypoxic conditions (10% CO2, 5% O2). EPC-iPS colonies were initially passaged mechanically and then enzymatically with collagenase (#07923 or #07909, Stem Cell Technologies). Enzymatic passaging was performed by first washing the cells with 2 ml of PBS and then 1 ml of collagenase was added and the iPSCs were incubated at 37 °C for 10 min. The collagenase solution was removed and cells were rinsed once with DMEM/F12. Colonies were scraped with a cell scraper, dissociated to smaller clumps by resuspending E8 medium.

Retrovirus generation and transduction of late-outgrowth EPCs

Retrovirus was generated using constructs pMXs-hOCT4, pMXs-hSOX2, pMXs-hKLF4, and pMXs-hc-MYC (Addgene) as described previously (Hotta et al., 2009a and Hotta et al., 2009b). To generate VSV-G pseudotyped retrovirus, Plat-GP cells were transfected overnight with 15 µg of each Yamanaka expression vector and 5 µg of pVSV-G using Lipofectamine 2000 according to the manufacturer. The next day, the medium was replaced with 10 ml of Endothelial Growth Medium-2MV to collect viral particles. Two days post-transfection, retrovirus was collected and filtered through a 0.45 µm filter. Transduction of 5 × 104 late-EPCs was performed by the addition of protamine sulfate to a final concentration of 4 µg/ml to a retroviral cocktail containing 500 µl of each

transcription factor. Late-EPCs were transduced overnight with the retroviral cocktail. After transduction, late-EPCs were maintained in complete EGM-2MV medium for 7–14 days, then trypsinized and replated onto matrigel coated plates. Unlike fibroblast reprogramming, in which we transfer on day 7 to hESC conditions (E8 media), we found that reprogramming efficiencies were enhanced for EPC reprogramming by growing in EGM-2MV until colonies resembling hESCs in morphology emerged. These were then mechanically picked and replated onto matrigel. These iPSCs were mechanically dissociated for a few passages and then adapted to collagenase IV passaging. To determine reprogramming efficiency, the number of ES-like colonies was counted based on morphology and divided by the number of starting cells that were transduced with the retroviral cocktail of Oct4, Sox2, Klf4, and c-Myc.

Microarray analyses

Total RNA was isolated with the Nucleospin RNA II kit (Macherey-Nagel) according to the manufacturer and microarray analyses were performed at the Stem Core Facility (Ottawa Hospital Research Institute) on the Affymetrix Human Gene 1.0 ST arrays. Data analyses were performed as previously described (Walker et al., 2010). The microarray data has been deposited into the GEO database with the accession number GSE42947.

Embryoid body and teratoma assays

Embryoid bodies (EBs) were formed by treating EPC-iPSCs with collagenase IV (STEMCELL Technologies) for 30–40 min, scraped and transferred to ultra-low attachment dishes (#3471, Costar). EBs were cultured for 7 days in suspension in E8 medium (without bFGF, and supplemented with 10% FBS) and outgrowths were formed by plating the EBs onto gelatin-coated plates. Teratomas were generated by injecting 1.5

million cells intramuscularly; tumors were removed approximately 8 weeks later, sectioned and stained with H&E.

Flow cytometry analysis

Flow cytometry analysis was performed as previously described (Ormiston et al., 2010); briefly, late-EPCs were trypsinized with TrypLE (Invitrogen), washed, and then incubated with 10% mouse serum for 30 min on ice and stained with the following: α-CD14–PE (#555398), α-CD45–PE (#555483), α-CD31–PE (#555446) and α-KDR–PE (#560494) (all flow cytometry antibodies were purchased from BD Biosciences). Isotype-matched antibodies were used as negative controls. Cells were analyzed on a Quanta SC flow cytometer (Beckman Coulter).

Immunofluorescence analysis

Immunofluorescence analyses were performed a previously described (Chang et al., 2004). Briefly, cells were fixed in 3.7% formaldehyde for 20 min at room temperature and washed with PBS. Samples were then permeabilized with 0.1 Triton X-100 for 20 min and blocked for 1 h with 3% skim milk in PBS, and primary antibodies were incubated for 2 h at room temperature or overnight at 4 °C. Primary antibodies for pluripotency markers were purchased from Millipore, Tra-1-60 (MAB4360), Tra-1-81 (MAB4381), and SSEA4 (MAB4304) and were used at 1:200, 1:200, and 1:500 dilutions, respectively. Differentiation markers used were βIII-tubulin (MAB1637, Millipore), smooth muscle actin (CBL171, Millipore), and Gata4 (G1610, Santa Cruz) at a dilution of 1:500.

Results

Reprogrammed late-outgrowth EPCs under feeder-free conditions are pluripotent

Late-EPCs were isolated from peripheral blood by apheresis or from 30 ml whole blood, characterized and exhibited their typical cobblestone morphology (Fig. 1B and Supplemental Fig. 1A) similar to endothelial cells and readily formed a capillary-like network when cultured on Matrigel (Supplemental Fig. 1B). Cell surface marker examination demonstrated that these cells were CD31+/VEGFR2+/CD14−/CD45−, characteristic of late-EPCs (Supplemental Fig. 1C) (Ormiston et al., 2010). To reprogram late-EPCs, cells were retrovirally transduced with OCT4, SOX2, KLF4, and c-MYC. After 7–14 days, cells were replated on matrigel in hESC E8 defined media (Chen et al., 2011) (schematic of reprogramming, Fig. 1A). Colonies exhibiting morphology similar to hESCs arose between 21 and 30 days (Fig. 1C), consistent with the time course for reprogramming of fibroblasts. Three late-EPC lines (106, 124, and PB1) were reprogrammed exhibiting a reprogramming efficiency varying between 0.006% and 0.7% depending on the line (Table 1), which is consistent with the range of reprogramming efficiency observed using a variety of dermal fibroblasts in our laboratory as well as other published cell types (Ho et al., 2010, Hotta et al., 2009a, Sun et al., 2009 and Takahashi et al., 2007). ESC-like colonies were then picked and expanded under feeder-free conditions. To assay their pluripotency potential, we examined several iPSC clones generated from each late-EPC line for the expression of alkaline phosphatase (ALP), SSEA4, TRA-1-81, and TRA-1-60 (see Fig. 1D–K and Supplemental Fig. 2 for examples of 106 and PB1 lines). Further, karyotype analyses demonstrated no gross chromosomal anomalies in our EPC-iPSC lines (Fig. 1L).

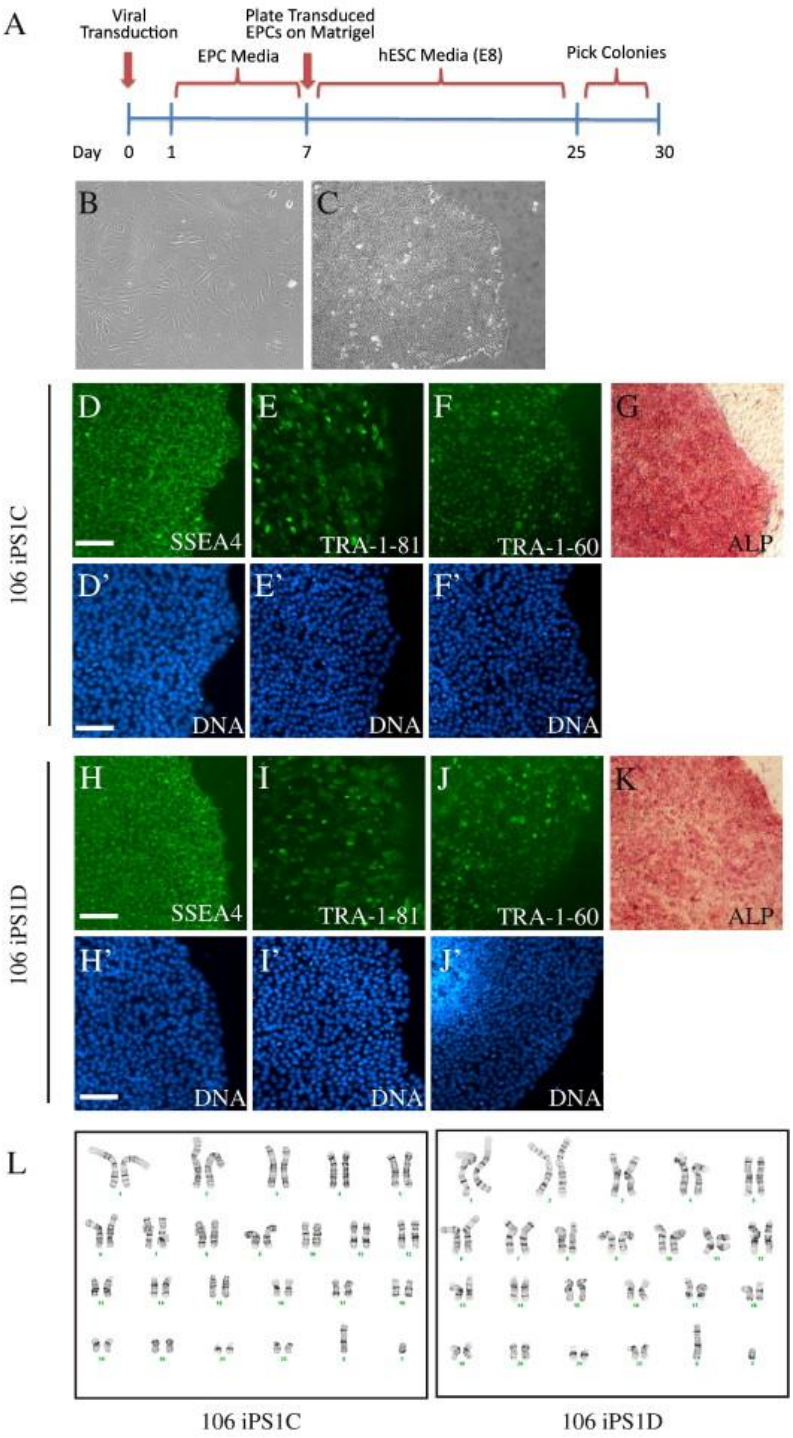

Figure 1. EPC-derived iPSCs express pluripotent markers, and retain normal karyotype. (A) Schematic of the feeder-independent method for reprogramming late-EPCs to iPSCs. Approximately 4 weeks after retroviral transduction of (B) late-EPCs, colonies resembling (C) ES-like morphology appeared. These colonies expressed pluripotent markers SSEA4, TRA1-81, TRA1-60, and ALP. Two clones are shown from the 106 donor, 106-iPS1C (D–G) and 106-iPS1D (H–K), scale bar = 200 μm. (L) EPC-iPSC exhibit normal karyotype.

Table 1. Reprogramming efficiency of late-outgrowth endothelial progenitor cells transduced with retrovirus expressing Oct4, Sox2, Klf4, and c-Myc.

L-EPC line	Number of cells transduced	Number of ES-like colonies based on morphology	Reprogramming efficiency (%)
106	50000	389	0.7
124	50000	3	0.006
PB1	50000	10	0.02

To assess whether the global gene expression patterns were reverted to an ESC-like state, we performed global transcriptome microarray analyses of four 106-iPSC clones and compared their signature to the parental late-EPC and H9 hESC lines. Shown in Fig. 2A are the global gene expression scatter plot analyses of clones 106-iPS1C and 106-iPSC1D compared to H9 hESCs and the parental late-EPC line. Pearson coefficient of all the 106-iPSC clones shows high correlation greater than 0.97 with the H9 hESC line, whereas the correlation with parental EPCs was less than 0.90. While we found that SOX2 and OCT4 (POU5F1) expression in EPC-iPSC lines essentially equivalent to H9 hESCs, c-MYC and KLF4 expression were slightly increased, although their expression was much decreased compared to the 106 parental EPC line (Fig. 2). This may be due to incomplete reprogramming, as RNA was isolated from very early passage cells for microarray analysis. Analysis of specific probes in our microarray data showed that genes involved in pluripotency are upregulated in EPC-iPSCs such as NANOG, hTERT, and SALL4, whereas genes involved in endothelial function including GATA2, NOS3, TEK, and EBPH4 are down-regulated compared to the parental late-EPCs (heatmap in Fig. 2B). In addition, genes associated with hematopoietic function were not significantly expressed in late-EPCs. Interestingly, our transcriptome analysis of the 106 parental line showed that these cells exhibited high levels of KLF4 and c-MYC. Therefore, we subsequently attempted to reprogram the 106 line with 2-factors (OCT4 and SOX2) or 3-factors (OCT4, SOX2, and KLF4) and (OCT4, SOX2, and c-MYC). Transduction of the 106 EPC line with 2 or 3-factors did not yield any ES-like or ALP-positive colonies compared to 4-factor transductions (data not shown).

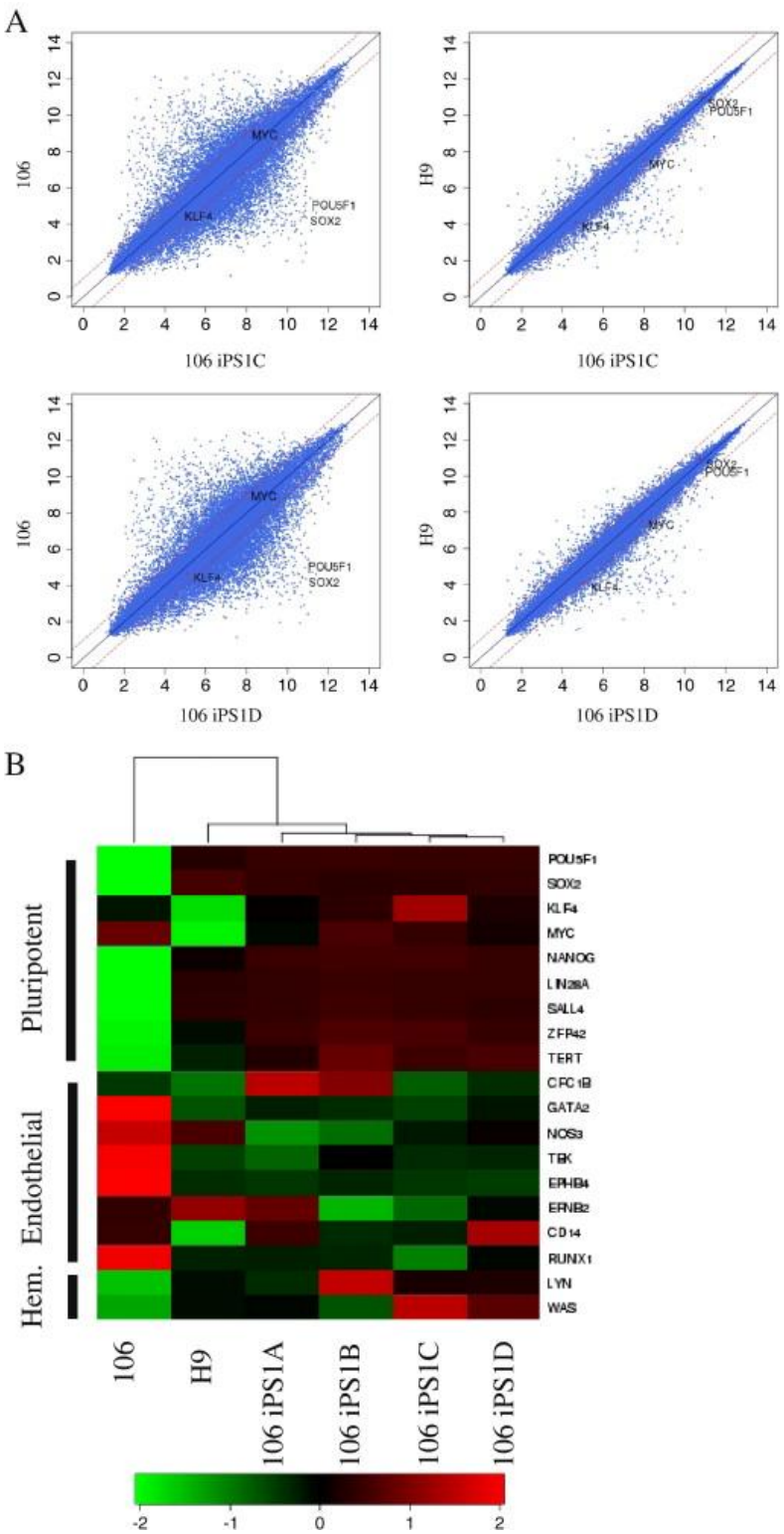

Figure 2. Global transcriptome of EPC-iPSCs are similar to hESCs. Microarray analyses were performed on EPC-iPSCs and (A) scatter-plots shows high correlation of 106-iPSCs with H9 hESCs whereas comparison with parental EPCs shows high variability. (B) We further examined the expression of specific targets associated with pluripotency, endothelial, and hematopoietic (Hem.) function, as shown in the heat map.

To determine whether EPC-iPSCs have the capacity to differentiate to cells and tissues of all three germ-layers, we performed both in vitro and in vivo differentiation assays. Embryoid bodies (EBs) (Fig. 3A and Supplemental Fig. 2) were generated from 106-iPSCs and PB1-iPSCs for 7 days and cell outgrowths were formed over 3 days. Outgrowths were then stained for markers of the three germ-layers, βIII-tubulin (ectoderm), smooth muscle actin (SMA) (mesoderm), and GATA6 (endoderm). We identified cells in our EB cultures that were positive for these markers from each EPC-iPSC line (Fig. 3B and Supplemental Fig. 2I, for example). To examine the in vivo differentiation capacity of EPC-iPSCs, we performed teratoma assays. Teratomas containing tissues from all three germ layers, such as pigmented epithelium (ectoderm), cartilage (mesoderm), and columnar epithelium reminiscent of gut or lung epithelium (endoderm), were generated from two 106-iPSC clones (Fig. 3C). Taken together, our differentiation assays demonstrate that EPC-iPSCs are pluripotent.

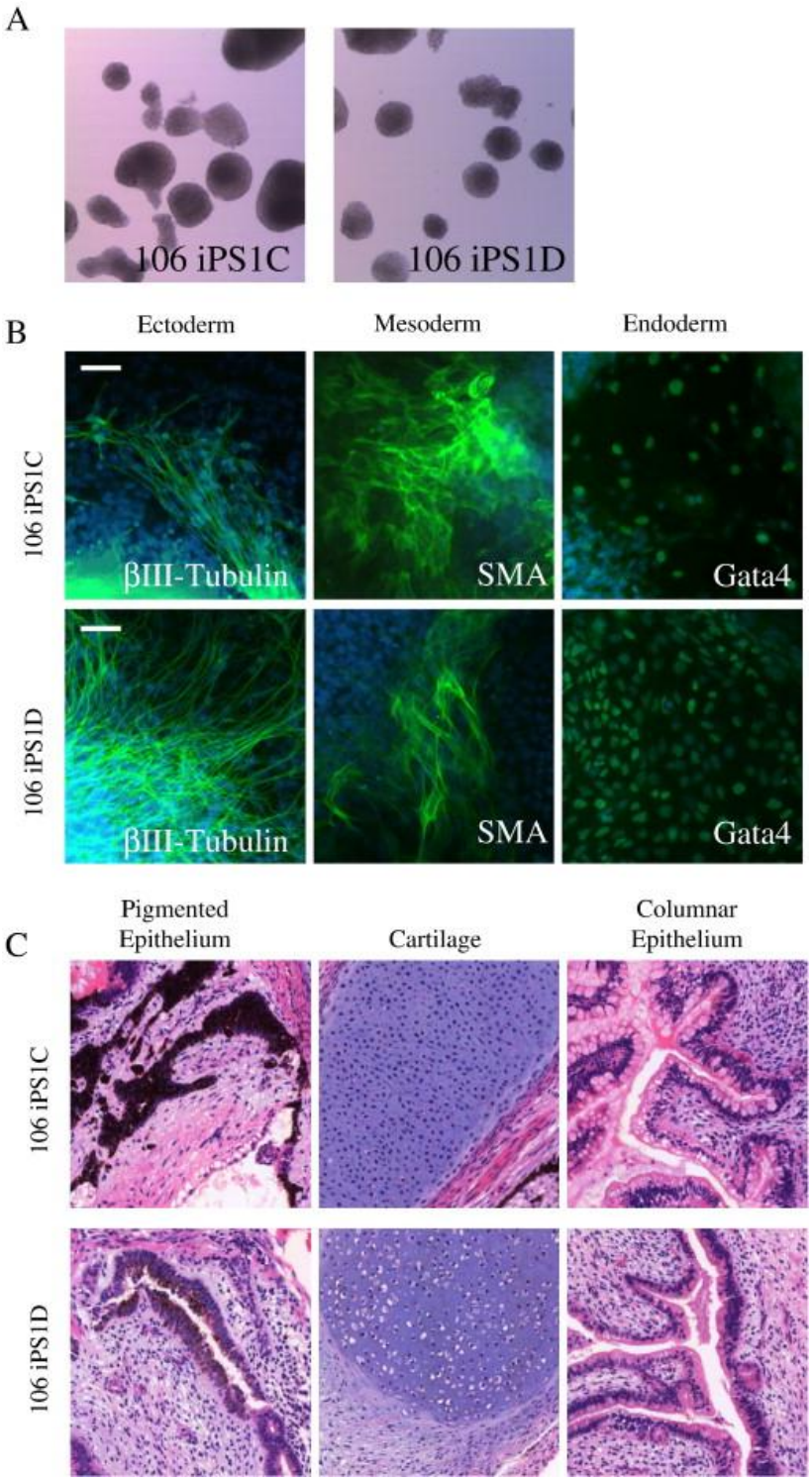

Figure 3. EPC-iPSCs have the capacity to differentiate to cells and tissues of the three germ-layers. To test the capacity of EPC-iPSCs to differentiate to cells of the three germ-layers we performed both in vitro and in vivo assays. (A) 106-iPSCs were capable of forming embryoid bodies and (B) EB outgrowths show that these cells are capable of differentiating to ectodermal (βIII-tubulin), mesodermal (smooth muscle actin), and endodermal (Gata4), scale bar = 100 μm. (C) 106-iPSCs are capable of generating tissues from the three germ-layers in teratoma assays.

Discussion

Currently, a number of cell types such as EPCs, bone marrow mononuclear cells, and mesenchymal stromal cells are being tested in clinical trials for their efficacy in treating cardiovascular diseases (O'Neill et al., 2012). Although there appears to be some benefit with adult cell therapy, this appears to be modest, and dependent primarily on paracrine mechanisms (Lasala and Minguell, 2011). Thus, the initial hypothesis that these cells would robustly differentiate into cardiac and vascular cells and directly regenerate damaged tissue has largely been unfulfilled. Human ESCs, and now iPSCs, offer potential alternative cell sources for cell therapy with much greater potential for differentiation and tissue regeneration. As well, derivation of iPSCs from patients with disease represents a valuable tool to better define underlying disease etiology and to screen for new drug therapies. However, the need for biopsy samples to derive patient-specific iPSCs is a major limitation, particularly the access to biopsies from relatives of the patients to act as genetic controls. Thus, the ability to derive iPSCs from blood enables the wider application of this technology and study of a broader range of diseases.

Collectively, our data shows that EPC-iPSCs are pluripotent. Further, we have reprogrammed late-EPCs under feeder-free and defined conditions, which should facilitate the progress of ultimately using EPC-derived iPSCs in a clinical setting. However, before this can be achieved, reprogramming of late-EPCs using non-integrating methods would be necessary. In the course of our study, we attempted to reprogram late-EPCs using several non-integrating strategies such Sendai Virus (Macarthur et al., 2012) and episomal vectors (Okita et al., 2011). Using these reprogramming methods we were not able to achieve successful reprogramming (data not shown). In fact, Sendai virus mediated reprogramming killed the late-EPCs, while

generating control iPSCs. Despite generating adult dermal fibroblast-derived iPSCs using episomal reprogramming vectors, late-EPCs transfected with these vectors did not proliferate well after switching to the hESC medium at different times post-transfection, suggesting expression of the reprogramming factors was not high enough to induce reprogramming. Thus, further optimization including the use of small molecules or the use of alternate reprogramming methodologies such as mRNA is required for successful non-integrative reprogramming of late-EPCs. Nonetheless, our study is a step forward in utilizing peripheral blood-derived late-EPCs as a cell source to derive feeder-free iPSCs in defined conditions. Late-EPCs represent an ideal cell source for reprogramming because of their accessibility from peripheral blood, their high proliferative capacity, and homogeneous population that can be frozen and thawed (Lin et al., 2011) for future genomic and proteomic analysis. Furthermore, unlike lymphoid lineages, L-EPCs do not undergo V(D)J recombination; therefore iPSCs derived from L-EPC would closer reflect other cell types from the donor which can eventually be applied to understanding diseases/disorders.

Acknowledgments

The authors would like to acknowledge the assistance from members of the Stanford and Stewart labs. This work was generously supported by the following organizations and funding agencies: the Canadian Institutes of Health Research (CIHR) to WLS for an operating grant (MOP-89910) and a CIHR Banting and Best CGS Doctoral Research Award to JLM; the Heart & Stroke Foundation of Canada for a Postdoctoral Fellowship to WYC; the Fonds de la recherché en santé du Quebec to JRL; the Ontario Research Fund (WLS); and the Canada Research Chair program which provides support to WLS through a Tier 1 Chair in Integrative Stem Cell Biology.

Supplemental Figure 1.

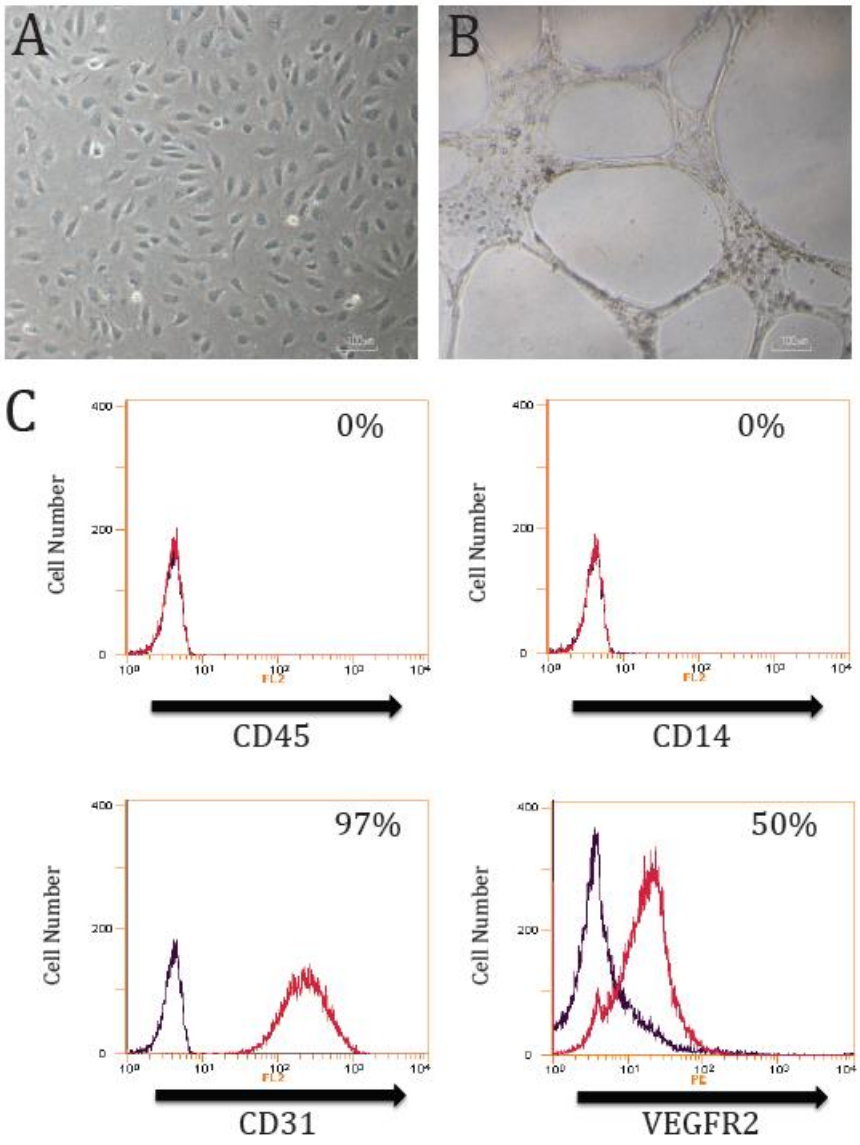

Supplemental Figure 2.

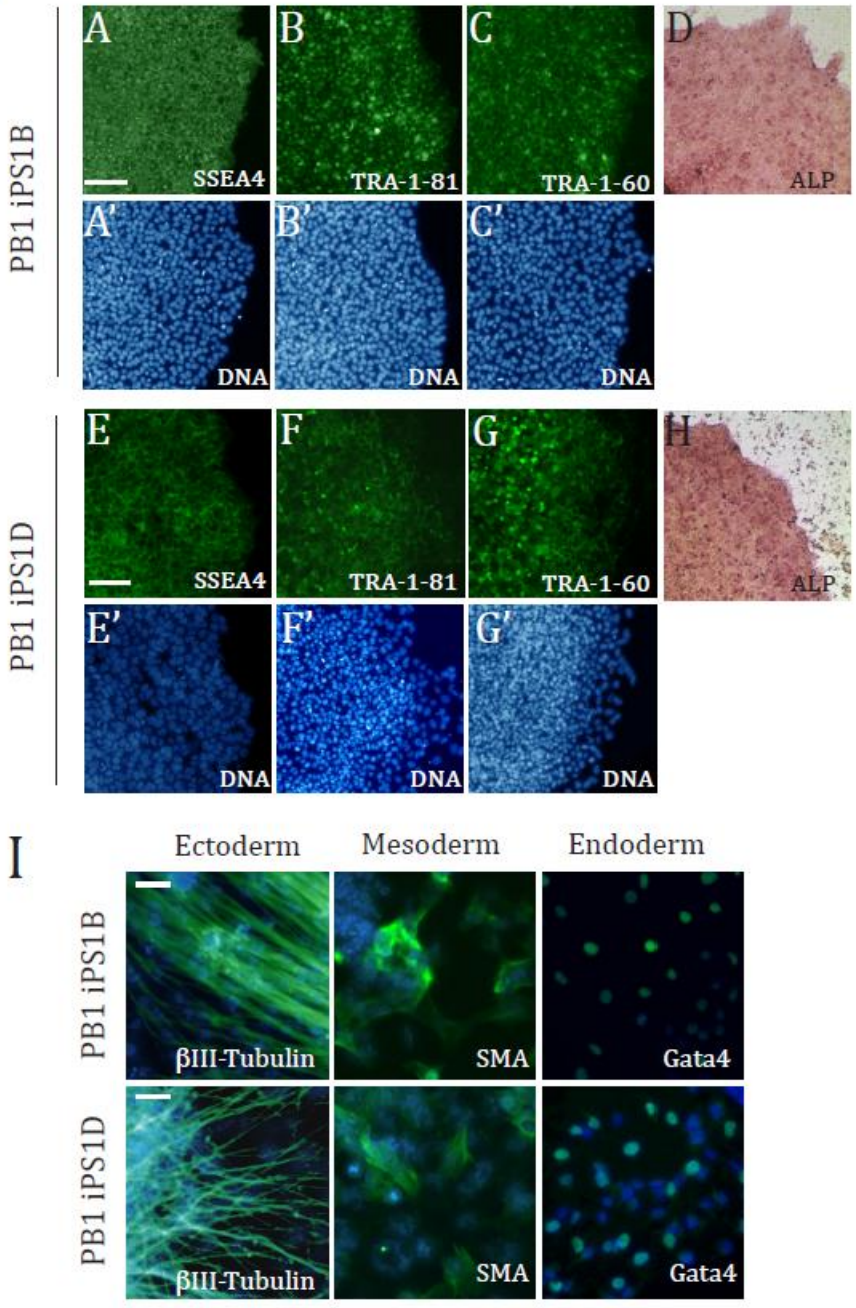

References

Brown, M.E., Rondon, E., Rajesh, D., Mack, A., Lewis, R., Feng, X., Zitur, L.J., Learish, R.D., Nuwaysir, E.F., 2010. Derivation of induced pluripotent stem cells from human peripheral blood T lymphocytes. PLoS One 5, e11373.

Chang, W.Y., Bryce, D.M., D'Souza, S.J., Dagnino, L., 2004. The DP-1 transcription factor is required for keratinocyte growth and epidermal stratification. J. Biol. Chem. 279, 51343–51353.

Chang, W.Y., Garcha, K., Manias, J.L., Stanford, W.L., 2012. Deciphering the complexities of human diseases and disorders by coupling induced-pluripotent stem cells and systems genetics.

Wiley Interdiscip. Rev. Syst. Biol. Med. 4, 339–350. Chen, G., Gulbranson, D.R., Hou, Z., Bolin, J.M., Ruotti, V., Probasco, M.D., Smuga-Otto, K., Howden, S.E., Diol, N.R.,

Propson, N.E., et al., 2011. Chemically defined conditions for human iPSC derivation and culture. Nat. Methods 8, 424–429.

Choi, S.M., Liu, H., Chaudhari, P., Kim, Y., Cheng, L., Feng, J., Sharkis, S., Ye, Z., Jang, Y.Y., 2011. Reprogramming of EBV-immortalized B-lymphocyte cell lines into induced pluripotent stem cells. Blood 118, 1801–1805.

Eminli, S., Utikal, J., Arnold, K., Jaenisch, R., Hochedlinger, K., 2008. Reprogramming of neural progenitor cells into induced pluripotent stem cells in the absence of exogenous Sox2 expression. Stem Cells 26, 2467–2474.

Grskovic, M., Javaherian, A., Strulovici, B., Daley, G.Q., 2011. Induced pluripotent stem cells–opportunities for disease modelling and drug discovery. Nat. Rev. Drug Discov. 10, 915–929.

Ho, P.J., Yen, M.L., Lin, J.D., Chen, L.S., Hu, H.I., Yeh, C.K., Peng, C.Y., Lin, C.Y., Yet, S.F., Yen, B.L., 2010. Endogenous KLF4 expression in human fetal endothelial cells allows for reprogramming to pluripotency with just OCT3/4 and SOX2– brief report. Arterioscler. Thromb. Vasc. Biol. 30, 1905–1907.

Hotta, A., Cheung, A.Y., Farra, N., Garcha, K., Chang, W.Y., Pasceri, P., Stanford, W.L., Ellis, J., 2009a. EOS lentiviral vector selection system for human induced pluripotent stem cells. Nat. Protoc. 4, 1828–1844.

Hotta, A., Cheung, A.Y., Farra, N., Vijayaragavan, K., Seguin, C.A., Draper, J.S., Pasceri, P., Maksakova, I.A., Mager, D.L., Rossant, J., et al., 2009b. Isolation of human iPS cells using EOS lentiviral vectors to select for pluripotency. Nat. Methods 6, 370-376.

Jodon de Villeroche, V., Avouac, J., Ponceau, A., Ruiz, B., Kahan, A., Boileau, C., Uzan, G., Allanore, Y., 2010. Enhanced lateoutgrowth circulating endothelial progenitor cell levels in rheumatoid arthritis and correlation with disease activity. Arthritis Res. Ther. 12, R27.

Lasala, G.P., Minguell, J.J., 2011. Vascular disease and stem celltherapies. Br. Med. Bull. 98, 187–197.

Lavoie, J.R., Stewart, D.J., 2012. Genetically modified endothelial progenitor cells in the therapy of cardiovascular disease and pulmonary hypertension. Curr. Vasc. Pharmacol. 10, 289–299.

Lin, Y., Weisdorf, D.J., Solovey, A., Hebbel, R.P., 2000. Origins of circulating endothelial cells and endothelial outgrowth from blood. J. Clin. Invest. 105, 71–77.

Lin, R.Z., Dreyzin, A., Aamodt, K., Dudley, A.C., Melero-Martin, J.M., 2011. Functional endothelial progenitor cells from cryopreserved umbilical cord blood. Cell Transplant. 20, 515–522.

Loh, Y.H., Hartung, O., Li, H., Guo, C., Sahalie, J.M., Manos, P.D., Urbach, A., Heffner, G.C., Grskovic, M., Vigneault, F., et al., 2010. Reprogramming of T cells from human peripheral blood. Cell Stem Cell 7, 15–19.

Macarthur, C.C., Fontes, A., Ravinder, N., Kuninger, D., Kaur, J., Bailey, M., Taliana, A., Vemuri, M.C., Lieu, P.T., 2012. Generation of human-induced pluripotent stem cells by a nonintegrating RNA sendai virus vector in feeder-free or xeno-free conditions. Stem Cells Int. 2012, 564612.

Martin-Ramirez, J., Hofman, M., van den Biggelaar, M., Hebbel, R.P., Voorberg, J., 2012. Establishment of outgrowth endothelial cells from peripheral blood. Nat. Protoc. 7, 1709–1715.

Okita, K., Matsumura, Y., Sato, Y., Okada, A., Morizane, A., Okamoto, S., Hong, H., Nakagawa, M., Tanabe, K., Tezuka, K., et al., 2011. A more efficient method to generate integration-free human iPS cells. Nat. Methods 8, 409–412.

O'Neill, C.L., O'Doherty, M.T., Wilson, S.E., Rana, A.A., Hirst, C.E., Stitt, A.W., Medina, R.J., 2012. Therapeutic revascularisation of ischaemic tissue: the opportunities and challenges for therapy using vascular stem/progenitor cells. Stem Cell Res. Ther. 3, 31.

Ormiston, M.L., Deng, Y., Stewart, D.J., Courtman, D.W., 2010. Innate immunity in the therapeutic actions of endothelial progenitor cells in pulmonary hypertension. Am. J. Respir. Cell Mol. Biol. 43, 546–554.

Seki, T., Yuasa, S., Oda, M., Egashira, T., Yae, K., Kusumoto, D., Nakata, H., Tohyama, S., Hashimoto, H., Kodaira, M., et al., 2010. Generation of induced pluripotent stem cells from human terminally differentiated circulating T cells. Cell Stem Cell 7, 11–14.

Sun, N., Panetta, N.J., Gupta, D.M., Wilson, K.D., Lee, A., Jia, F., Hu, S., Cherry, A.M., Robbins, R.C., Longaker, M.T., et al., 2009. Feeder-free derivation of induced pluripotent stem cells from adult human adipose stem cells. Proc. Natl. Acad. Sci. U. S. A. 106, 15720–15725.

Takahashi, K., Yamanaka, S., 2006. Induction of pluripotent stem cells from mouse embryonic and adult fibroblast cultures by defined factors. Cell 126, 663–676.

Takahashi, K., Tanabe, K., Ohnuki, M., Narita, M., Ichisaka, T., Tomoda, K., Yamanaka, S., 2007. Induction of pluripotent stem cells from adult human fibroblasts by defined factors. Cell 131, 861–872.

Thill, M., Strunnikova, N.V., Berna, M.J., Gordiyenko, N., Schmid, K., Cousins, S.W., Thompson, D.J., Csaky, K.G., 2008. Late outgrowth endothelial progenitor cells in patients with agerelated macular degeneration. Invest. Ophthalmol. Vis. Sci. 49, 2696–2708.

Walker, E., Chang, W.Y., Hunkapiller, J., Cagney, G., Garcha, K., Torchia, J., Krogan, N.J., Reiter, J.F., Stanford, W.L., 2010. Polycomb-like 2 associates with PRC2 and regulates transcriptional networks during mouse embryonic stem cell self-renewal and differentiation. Cell Stem Cell 6, 153–166.

6.3 Publication #3

Curr Vasc Pharmacol. 2012 May;10(3):289-99.

Genetically Modified Endothelial Progenitor Cells in the Therapy of Cardiovascular Disease and Pulmonary Hypertension

Jessie R. Lavoie and Duncan J. Stewart

Ottawa Hospital Research Institute, Regenerative medicine program, Ottawa, Ontario, Canada

Keywords: Endothelial progenitor cells, gene therapy, ischemic cardiovascular disease, pulmonary hypertension, vascular regeneration

Copyrights

Contributions of the Candidate

I wrote the manuscript and Dr. Duncan J. Stewart provided editing assistance and corrections.

Abstract

Since their initial discovery, endothelial progenitor cells (EPCs) have held tremendous promise for cell therapy for a variety of cardiovascular diseases including pulmonary hypertension. The clinical experience to date suggests that circulating or bone marrow mononuclear cells and EPCs can induce neovascularization, and enhance cardiac repair after myocardial function, as well as improvements in the hemodynamic and functional status of patients with idiopathic pulmonary arterial hypertension. Although these results are promising, the overall magnitude of the clinical benefits seen in these trials appear to be rather modest. Indeed, strong experimental evidence points towards a reduction in mobilization and impairment in function of EPCs in preclinical models and patients with cardiac disease or with cardiovascular risk factors such as advanced age, type I and II diabetes, hypercholesterolemia, coronary artery disease, as well as other conditions such as pulmonary hypertension. Genetic engineering of EPCs ex vivo, prior to transplantation, is a promising cell-enhancement strategy for restoring the angiogenic potential of autologous, patient-derived cells. This review provides an update of the experimental studies that have used gene-modified EPC therapy to treat ischemic cardiovascular disease and pulmonary hypertension.

1. INTRODUCTION

In 1997, Asahara et al. reported the successfully isolation of CD34 positive circulating mononuclear cells (MNC) – which they termed endothelial progenitor cells (EPCs) – from adult circulating mononuclear cells and demonstrated their ability to adopt an endothelial-like phenotype by tissue culture on fibronectin-coated wells (1). After 7 days of attached culture, these cells displayed a variety of endothelial cell lineage markers such as CD34, CD31, fetal liver kinase-1 (Flk-1), Tie-2 and E-selectin (1). The authors further showed that these EPCs had the ability to enhance blood flow recovery, and to incorporate into sites of active angiogenesis and rescue mice from induced hindlimb ischemia (1). This seminal paper introduced the concept of a rare population of circulating cells incorporating into foci of neovascularization, consistent with postnatal vasculogenesis - a process by which EPCs are recruited at the site of injury and differentiate into mature endothelial cells to give rise to de novo blood vessels (1, 2). After more than a decade of research and an ever increasing number of published reports, EPCs are seen as promising cells for the treatment of many vascular diseases. Although their regenerative potential is well described, their identity is still a matter of debate and an intense focus of investigation. Attempts to clarify the term EPC have been the subject of a recent review by Richardson and Yoder (3), in which they summarized the current lineage relationships among all cells called endothelial progenitor cells. These authors examined the commonly used methods to identify putative EPCs in human subjects, including; by adhesion to fibronectin-coated dishes with display of certain lectin and lipoprotein binding properties; by selection using cell surface phenotype (i.e. CD34, CD133, or KDR), and by colony forming assays. These methods have been thoroughly reviewed previously (3-5) and the reader is referred to these comprehensive reports for further details.

In this review, we summarize the experimental studies that have demonstrated quantitative and functional impairment of EPCs derived from patients with cardiac and vascular diseases, which have paved the way for the current research on methods to enhance progenitor cell function, including genetic modification. As well, we will review nearly all reports (as of May 2011) that have described the use of genetically engineered EPCs to treat ischemic diseases and pulmonary hypertension. We will use the term "early EPC" or "circulating angiogenic cells (CACs)" to refer endothelial-like MNCs derived by relatively brief culture (usually < 1 week; sometimes called "early outgrowth" EPCs under conditions that promote endothelial differentiation), whereas the term "late outgrowth EPC" will refer to highly differentiated endothelial-like cells that are derived after more prolonged culture (3), that are also called "endothelial colony forming cells (ECFC)". Cells identified by surface determinants will be defined using the specific markers employed.

2. EPCs AS THERAPEUTIC AGENTS

EPCs represent a very interesting source of cells for transplantation and vascular repair. They are readily available from peripheral blood, easily harvested/expanded and can be selectively differentiated in culture conditions. EPCs can also be genetically engineered ex vivo during the culture process to become vehicles for delivery of therapeutic genes to site of injury (2, 6). This allows the use of autologous EPCs, which means there are minimal potential immunogenic problems associated with the transplantation. For all these reasons, EPC-based therapies have been an intense focus of investigation in both clinical studies and experimental models of ischemic limb disease (7, 8), myocardial infarction (9, 10), and pulmonary hypertension (11-14). Based on these studies and others, a number of clinical trials have been undertaken using circulating or bone marrow mononuclear or EPCs. Although not definitive at this time, the clinical experience is

promising, suggesting improvement in cardiac repair and myocardial function post acute myocardial infarction (MI) (15-18) and in the hemodynamic and functional status of patients with idiopathic pulmonary arterial hypertension (IPAH) (19, 20). Although these results are encouraging, the overall magnitude of the clinical benefits seen in these trials appears to be rather modest. This may not be surprising in view of a number of factors which are likely to have a negative impact on the therapeutic potential of EPC therapies, including uncertainty regarding the selection of “true” EPCs, very low rates of cell survival, homing and engraftment, and a number of host factors which reduce the number and activity of autologous EPCs that will be discussed in more detail below. For these reasons, cell-enhancement strategies may be necessary in order to obtain the full therapeutic benefit, including genetic modification.

3. DISEASE-RELATED IMPAIRMENT

3.1. Quantitative assessment of EPCs in cardiovascular disease

EPCs are subjected to a variety of host and environmental factors that can affect their viability and function, thus decreasing their therapeutic potential for vascular disorders. Quantitative assessment of circulating EPCs has been suggested to be useful as a biomarker of the pathogenesis and progression of vascular diseases (Table 1). The number of early EPCs obtained from blood samples from patients with type I diabetes, characterized by acetylated low density lipoprotein (acLDL) uptake, concomitant lectin binding and CD31+ reactivity, was found to be 44% lower compared with age- and sex-matched control subjects (21). Similarly, Sibal and colleagues showed that CD34+/VE-cadherin+, CD133+/VE-cadherin+ and CD133+/VEGFR2+ EPCs are significantly lower in patients with type I diabetes (46-69%) (22). As well, flow-mediated dilatation (FMD), a measure of mature endothelial function, was reduced by 45% and carotid intima media-thickness was increased by 25% in this patient population and there was a significant

correlation between FMD and all measures of EPC numbers (r = 0.34) (22). Similarly, patients with the metabolic syndrome and type II diabetes exhibited reduced numbers of circulating EPCs, as evidenced by a decreased of 34% of circulating CD34+/KDR+ cells and of 48% in endothelial colony forming units (CFUs) in subjects with metabolic syndrome (23) and in diabetic patients compared with control subjects (9.8 ± 1.9 vs. 22.6 ± 1.7 CFUs) (24). In patients with coronary artery disease (CAD), the numbers of isolated EPCs defined by LDL/lectin-positive cells and circulating CD34/KDR-positive precursor cells were also found to be significantly reduced by 40% and 48%, respectively (25). Furthermore, Vasa et al. demonstrated an inverse relationship between the number of risk factors for atherosclerosis (including age, sex, hypertension, diabetes, smoking, positive history of CAD and LDL cholesterol levels) and the number of EPCs characterized by LDL uptake and concomitant lectin binding (r = - 0.394) or circulating CD34/KDR-positive cells (r = - 0.537) (25). Umemura et al. found that the number of CD34+/AC133+/CD45low EPCs was reduced in patients with cardiovascular disease compared to healthy subjects (1,047 ± 521 vs. 613 ± 462 cells/ml) and that the number of EPCs was significantly correlated with the number of risk factors (r = 0.424) (26). In addition, in a multivariate analysis, hypertension and age were found to be independent predictors of reduced EPC number. Heeschen et al. found that the colony-forming capacity of bone marrow mononuclear cells (BM-MNCs) from patients with chronic ischemic cardiomyopathy was significantly lower compared with healthy controls (37 ± 25 vs. 114 ± 70 CFUs) (27). In a study conducted by MacEneaney et al. it was reported that EPCs from the “high” prehypertensive group produced fewer CFUs compared with the “low” prehypertensive and normotensive adults, consistent with hypertension having an important influence of circulating EPC number (28). Likewise, Oliveras et al. found that the numbers of circulating CD34+/CD133+/CD45+ cells and early EPCs were

reduced by 56% and 77%, respectively, in patients with refractory hypertension compared with controls subjects (29).

As well, a few prospective studies have examined whether the number of circulating progenitors relates to outcomes in patients with cardiovascular diseases. During the observational period of 12 months, Werner et al. found a significantly higher incidence of death from cardiovascular causes in CAD patients with low baseline levels of EPCs (defined by the surface markers CD34+/KDR+) (30). Schmidt-Lucke et al. also observed that patients exhibiting cardiovascular events had significantly lower numbers of CD34+/KDR+ cells (31). Werner et al. performed a prospective clinical study in patients with established coronary disease in which they assessed endothelial function by quantitative coronary angiography during intracoronary acetylcholine infusion and studied the correlation with the number of either CD133+ or CD34+/KDR+ cells from each patient (32). They showed a significant correlation between endothelium-dependent vasodilatation and CD34+/KDR+ ($r = 0.427$) as well as CD133+ cell number ($r = 0.239$) (32). Similarly, Hill et al. observed a strong correlation between the number of circulating EPCs (defined as the number of CFU-EPCs) and the subjects' combined Framingham risk factor score ($r = - 0.47$) (33). The measurement of EPC levels could become a cellular marker of cardiovascular risk and essentially be a valuable tool to predict cardiovascular outcomes in patients with cardiovascular disease.

Table 1. Circulating EPC Number

CVD risk factor	N	Cell type	Result	References
Coronary artery disease	45	Early EPCs (PB)	↓ 40%	[25]
	35	$CD34^+/KDR^+$	↓ 48%	
Type II diabetes	20	Early EPCs (PB)	↓ 49%	[37]
Atherosclerosis and age	5	$CD31^+/CD45^-$	↓ 46%	[36]
		$CD34^+$	NS	
		sca-1	NS	
		c-kit^+	NS	
		$VEGFR\text{-}2^+$	NS	
Type I diabetes	20	Early EPCs (PB)	↓ 44%	[21]
Ischemic cardiomyopathy	18	$CD34^+/CD45^+$	NS	[27]
		$CD34^+/CD133^+$	NS	
		$Lin^-/CD34^+$	NS	
		$CD34^+/CXCR4^+$	NS	
		$CXCR4^+$	NS	
		CD49b	NS	
Age	20	$CD34^+/KDR^+$	NS	[34]
		$CD133^+/KDR^+$	NS	
Type II diabetes	5	CFUs	↓ 58%	[24]
Type I diabetes	7	Rat EPCs (BM)	↓ 39%	
CVD	135	$CD34^+/AC133^+/CD45^{low}$	↓ 41%	[26]
Refractory hypertension	39	$CD34^+/CD133^+/CD45^+$	↓ 56%	[29]
		Early EPCs (PB)	↓ 77%	
Type I diabetes	74	$CD34^+/VE\text{-}cadherin^+$	↓ 46-69%	[22]
		$CD133^+/VE\text{-}cadherin^+$		
		$CD133^+/VEGFR\text{-}2^+$		
Metabolic syndrome	46	$CD34^+/KDR^+$	↓ 34%	[23]
Prehypertension and hypertension	36	$CD34^+/KDR^+$	NS	[39]

BM indicates bone marrow; CFU, colony forming units; CVD, cardiovascular disease; NS, result not significant; PB, peripheral blood

3.2. Assessment of EPC activity in cardiovascular disease

A number of studies have been conducted to assess the functionality of the cells derived from patients with cardiovascular risk factors to examine the effect of host factors in EPC activity (Table 2). Assessing the functionality of the cells is of paramount importance when the aim is to use the cells in clinical settings. Heiss et al. observed no quantitative differences in the number of circulating EPCs from older but otherwise healthy subjects, defined as CD34/KDR or CD133/KDR double-positive cells in peripheral blood, but observed that fundamental functional parameters such as proliferation, survival and migration were impaired in cultured-selected EPCs from older compared with young subjects (34). The authors argue that reduced activity rather than number of certain vascular progenitor cells may be responsible for age-related vascular conditions. They reasoned that their results are in line with the findings of Hill et al. (33) which have observed an inverse correlation between the subject's age and levels of circulating EPCs by assessing the number of colonies by the CFU assay (although not statistically significant) (33) because this assay also relies on the functional properties of the cells; specifically, their ability to adhere, survive and proliferate during culture. A study conducted by Edelberg et al. (35) provided pre-clinical evidence to support an age-dependent impairment in neovascularization that is heavily influenced by the EPC phenotype. They showed that transplantation of young, but not old, genetically marked syngeneic bone marrow cells into intact, unirradiated aging mice were able to populate the senescent murine bone marrow and incorporate into the neovasculature of subsequently transplanted syngeneic neonatal myocardium (35). Similarly, Rauscher et al. reported that the atheroprotective effect of the bone marrow cells was "exhausted" with aging and prolonged exposure to cardiac risk factors (36). Indeed, they found significantly less atherosclerotic burden in mice that had received bone marrow-derived EPCs from young ApoE-/- donors than in those that had received the same cells from old

ApoE-/- donors (36). They suggest that the significant reduction in CD31+/CD45- cells in bone marrow from old ApoE-/- mice (3.79 ± 2.02% for 6-month-old ApoE-/- mice compared with 7.03 ± 2.81% for 1-month-old ApoE-/- mice and 6.36 ± 1.02% for 1-month-old wild-type mice) could explain, in part, the loss of the anti-atherosclerotic effect of the older ApoE-/- BM cells (36).

Other studies have suggested that type II diabetes may alter EPC biology and reduce their capacity to participate in new blood vessel growth. Tepper et al. showed decreased proliferation of diabetic EPCs relative to control subjects by 48%, that was inversely correlated with levels of hemoglobin A1C (37). They further showed that, although diabetic EPCs adhered normally to fibronectin, collagen, or mature endothelial cells, they had decreased ability to adhere to human umbilical vein endothelial cells (HUVECs) activated by tumor necrosis factor-alpha (TNF-α) (37). Furthermore, in a Matrigel assay, diabetic EPCs were 2.5 times less likely to participate in tubule formation compared with control cells (37). This latter finding is consistent with the results of a later report (21) which showed that conditioned media (CM) from type I diabetic EPCs exhibited reduced capacity to support endothelial tube formation in comparison to CM from control EPCs. An impairment in migratory capacity of EPCs from type II diabetic patients compared with nondiabetic control subjects was also shown by Thum et al. (24). Likewise, Heeschen et al. demonstrated that the migratory response to stromal cell-derived factor-1 alpha (SDF-1α) and vascular endothelial growth factor (VEGF) was significantly reduced in BM-MNCs derived from patients with chronic ischemic heart disease compared with cells from healthy controls (SDF-1α, 46 ± 26 vs. 109 ± 40 cells/microscopic field; VEGF, 34 ± 24 vs. 55 ± 29 cells/microscopic field) (27). They further tested the ability of BM-MNCs to improve neovascularization in a hindlimb

ischemia model using nude mice; blood flow recovery in mice treated with BM-MNCs from patients with ischemic cardiomyopathy was significantly lower compared with mice treated with cells from healthy controls (0.45 ± 0.14 versus 0.68 ± 0.15). Reduced migratory capacity was also demonstrated by Vasa et al. using EPCs from patients with CAD; and the impairment in migratory response was found to be inversely correlated with the number of atherosclerosis risk factors (r = - 0.484) (25). By multivariate analysis, Vasa et al. found that hypertension was identified as a major independent predictor for impaired EPC migration (25). Ward et al. obtained similar results than the Dimmeler group in a recent report where they showed that circulating angiogenic cells (CACs) from high-risk subjects exhibited reduced migration compared with cells from healthy controls to both VEGF-A (74 ± 9 vs. 121 ± 15 cells/high power field) and SDF-1 (80 ± 11 vs. 119 ± 13 cells/high power field, respectively), and reported a significant inverse relationship between the Framingham risk score and the migratory capacity toward both chemotactic agents (R2 = 0.205 and R2 = 0.191, VEGF-A and SDF-1, respectively) (38). Furthermore, they showed in vivo that cells from the high-risk factor group failed to enhance ischemic limb perfusion when compared to healthy cells (38). Giannotti et al. have examined in vivo endothelial repair of early EPCs isolated from healthy subjects and newly diagnosed prehypertensive and hypertensive patients after transplantation into a nude mouse carotid injury model (39). They found that in vivo endothelial repair capacity of EPCs from prehypertensive and hypertensive patients was substantially impaired as compared with cells from healthy subjects (re-endothelialized area: 15 ± 3%/13 ± 2% vs. 28 ± 3%, respectively) (39).

Table 2. EPC Function

CVD risk factor	Cell type	N	Main results	References
Human studies				
Coronary artery disease	Early EPCs (PB)	28	↓ Migration	[25]
Type II diabetes	Early EPCs (PB)	20	↓ Adherence to HUVECs (TNF-α activated); ↓ tube formation	[37]
Type I diabetes	Early EPCs (PB)	10	↓ Ability of CM to support endothelial tube formation	[21]
Ischemic cardiomyopathy	BM-MNCs	18	↓ CFU; ↓ migration; ↓ ability to restore ischemic limb perfusion; ↓ ability to incorporate into blood vessels	[27]
Age	Early EPCs (PB)	20	↓ Survival; ↓ migration; ↓ proliferation	[34]
Type II diabetes	Early EPCs (PB)	5	↑ ROS formation; ↓ migration	[24]
Type I diabetes	$CD34^+$/VE-cadherin$^+$ $CD133^+$/VEGFR-2^+ $CD34^+$	74	↓ FMD; ↑ CIMT	[22]
Metabolic syndrome	Early EPCs (PB)	15-43	↓ CFU; ↓ ability to incorporate into tubular structures	[23]
Prehypertension and hypertension	Early EPCs (PB)	36	Impairment in vivo endothelial repair capacity (re-endothelization); ↑ senescence; ↓ NO production	[39]
Coronary artery disease	CACs (PB)	9-12	↓ Migration; ↓ ability to restore ischemic limb perfusion	[38]
Prehypertension	CFUs	16	↓ CFU in high prehypertensive group	[28]
Animal studies				
Age	Murine EPCs (BM)	6-16	No effect on aging-associated decline in cardiac angiogenic function	[35]
Atherosclerosis and age	Murine EPCs (BM)	6	Loss of the anti-atherosclerotic effect	[36]
Type I diabetes	Rat BM-MNCs	7	↓ Differentiation; ↓ ability to restore ischemic limb perfusion; ↓ capillary density; ↓ neovascularization	[71]
Type II diabetes	Rat EPCs (BM)	7	↑ O_2^- production; ↑ t-eNOS; ↓ p-eNOS; ↓ eNOS dimer-to-monomer ratio	[24]

BM-MNC indicates bone marrow-derived mononuclear cells; CACs, circulating angiogenic cells; CVD, cardiovascular disease; CFU, colony forming units; CIMT, carotid intima–media thickness; CM, conditioned media; t-eNOS, total endothelial nitric oxide synthase; p-eNOS, phospho endothelial nitric oxide synthase; FMD, flow-mediated dilation; HUVECs, human umbilical vein endothelial cells; NO, nitric oxide; O_2^-, superoxide; PB, peripheral blood; ROS, reactive oxygen species; TNF-α, tumor necrosis factor-alpha

3.3. Quantitative and functional cell assessment in pulmonary hypertension

There is mounting interest in the use of EPCs in the treatment of pulmonary arterial hypertension (PAH), a progressive disease that involves vascular remodelling of the small pulmonary arteries resulting in elevated pulmonary artery pressure, subsequently right heart failure and death. However, there is controversy about whether circulating progenitor cells are beneficial or may participate in the pathogenesis of this disease, in particular the pulmonary vascular remodelling as suggested by a number of recent observational studies (40-43). Few studies have looked at the baseline number of circulating EPCs in patients with PAH but conflicting results were reported: some studies have shown a decreased in circulating EPC number in PAH patients (44-46) and others have shown an increase (47, 48) or no significant difference (49). This confusion likely results from lack of clarity about the definition of EPCs versus other progenitor cell types that have been implicated in the pathology of PAH, such as fibrocytes (50, 51). Functional studies have provided more consistent results, and seem to point towards reduced activity of EPCs from patients with PAH. Most of the studies have reported a reduction in migratory capacity (44, 52), impairment in the ability to form vascular networks (45, 48, 52), an increase in susceptibility to apoptosis (53), and a failure to reverse pulmonary hypertension (52) (for more details the reader is referred to a review by Diller et al.) (40). Since the seminal discovery of mutations in the bone morphogenetic protein receptor-2 (Bmpr-2) gene, a member of the transforming growth factor beta superfamily, in patients with heritable PAH (54-56), there have been only a few studies examining the effects of these mutations on the endothelial or progenitor cell function. For example, Morrell's group has used late outgrowth EPCs (as a surrogate for mature endothelial cells) to investigate the impact of the Bmpr-2 mutations on their functionality and has shown that the patient-derived cells have a hyperproliferative phenotype with impaired ability to form vascular structures compared to control subjects (48). This

finding is in line with other reports describing phenotypic alterations in endothelial cells derived from patients with PAH (53, 57). Bmpr-2 gene delivery may be seen as an attractive therapeutic approach to overcome the decreased signalling activity in the pathway in patients with heritable PAH, as well as for patients with sporadic IPAH with reduced pulmonary vascular expression of Bmpr-2 (58) and has been reviewed recently elsewhere (59).

4. CELL-BASED GENE THERAPY

The above studies provide strong evidence that host factors and cardiovascular diseases have a profound impact on EPC number and function, which could compromise their therapeutic usefulness. It follows that more effective autologous EPC therapies will require the development of novel approaches to restore angiogenic/vasculogenic function. The following sections will review reports that have used the gene transfer to enhance the therapeutic efficacy of EPCs (Table 3). This approach is based both on the use of EPCs as vectors for local delivery of vasculoprotective genes to effect revascularization of ischemic foci in a paracrine manner as well to augment EPC activity in a cell autonomous manner.

4.1. Gene-modified EPC for the treatment of ischemic diseases

4.1.1. Single-gene modification

In the last decade, various reports have demonstrated the superiority of stem and progenitor cells combined with gene transfer over either approach alone for therapeutic angiogenesis and vasculogenesis (60). Significant improvements in therapeutic effects have been reported when using EPCs genetically modified to overexpress angiogenic growth factors in order to improve EPC viability and biological activity. A few years after the initial discovery of the EPCs, the Asahara group investigated the consequences of

VEGF-transduced EPCs on certain EPC properties in vitro and on neovascularization in vivo (1, 61). In vitro, they found that VEGF gene transfer enhanced EPC proliferation, adhesion, and incorporation into endothelial cell monolayers. In a murine model of hindlimb ischemia, they showed that gene-modified EPCs enhanced neovascularization and blood flow recovery, and reduced limb necrosis and autoamputation. Yi et al. further explored the effect of combining EPC cell therapy with VEGF gene transfer and its impact on the vascular regeneration of ischemic flaps (62). Using human umbilical cord blood-derived EPCs they found a statistically significant increase in flap survival for the VEGF-transduced EPC group as compared with that of the non-transduced EPC group ($68 \pm 7\%$ vs. $59 \pm 5\%$), whereas both EPC groups were superior to the EBM-2 media group ($41 \pm 2\%$) (62). This was supported by the increase in capillary density and improvement in blood flow recovery of flaps in VEGF-transduced EPCs group as compared to controls (62). In another study, human cord blood-derived EPCs transfected with VEGF yielded greater improvements in blood flow in a rat model of chronic hindlimb ischemia compared to the control rats transplanted with no cells or with non-genetically modified cells (63). “Rejuvenating” EPCs via enhanced telomerase reverse transcriptase (TERT) expression is another strategy to overcome EPC dysfunction in the context of aging and cardiovascular diseases (64). Murasawa et al. argued that since EPCs are lineage-committed progenitors, and thus subject to replicative senescence, the human TERT (hTERT) gene would delay cell senescence and restore their regenerative properties (64). TERT gene transfer resulted in enhanced regenerative properties including EPC mitogenesis, migration and survival, and in improved reparative neovascularisation, with limb salvage increased by 4-fold (64). Limb perfusion and capillary density were also improved in the genetically modified EPCs in comparison with GFP-transduced EPCs (64).

Increasing glycogen synthase kinase-3 beta (GSK3-β) activity represents another possible strategy for augmenting EPC vasculogenic properties (65), since it controls several downstream transcription factors (b-catenin, heat shock protein-1), that are crucial in cell survival and function (66). In a study conducted by Choi et al., both early and the late outgrowth EPCs, obtained from the peripheral blood, were transduced with catalytically inactive GSK3-β (65). Survival and secretion of angiogenic cytokines (VEGF and interleukin-8) were increased in both cell types; whereas, proliferation was increased in early EPCs and endothelial differentiation was enhanced in late EPCs (65). Notably, transplantation of either these genetically modified human EPCs into the ischemic hindlimb of athymic nude mice significantly improved blood flow, limb salvage, and tissue capillary density compared with non-transduced EPCs (65). Cho et al. chose integrin-linked kinase (ILK) as another attractive target for gene modified cell-based therapy (67), based on the role of ILK in mediating anchorage-dependent prosurvival signalling in endothelial cells and EPCs. Indeed, Cho et al. demonstrated that not only did systemic injection of ILK-transduced EPCs result in a better outcome (capillary density, tissue perfusion, final limb fate were improved) in hindlimb ischemia model compared to the delivery of GFP-EPCs, but the transfected EPCs were effective at a 20-fold lower cell "dose" (1x104 ILK-EPCs vs. 2x105 GFP-EPCs) (67). Human recombinant hepatocyte growth factor (HGF) has been reported to increase therapeutic angiogenesis in a rabbit hindlimb ischemic model (68) and to be an important angiogenic factor involved in endothelial cell migration and growth (69, 70). Based on these findings, the potential of cell-based HGF gene therapy was tested in a murine hindlimb ischemia model. Notably, they found that HGF-transduced adherent mononuclear cells reduced the cell requirement 30-fold for the recovery of blood flow when compared with non-transduced cells or saline (71). These two latter studies indicate that cell-based gene therapy with

ILK and HGF genes decreased the number of cells required for neovascularization, an interesting outcome for autologous cell therapy.

Hypoxia inducible factor-1 alpha (HIF-1α) is another attractive target for cell therapy. Hypoxia plays an important role in pathophysiological responses induced by ischemia. HIF-1α, has been shown to be a key hypoxia sensing mechanism, regulating genes encoding for numerous angiogenic cyokines including VEGF and SDF-1α to promote greater perfusion to hypoxic cells (72). Jiang et al. demonstrated that HIF-1α overexpression enhanced hypoxia-induced EPC differentiation, proliferation and migration, and produced higher revascularization potential as shown by increased capillary density (72). Based on these results, the same group published a subsequent report showing that HIF-1α-transfected EPCs reduced limb and toe necrosis in the mouse hindlimb ischemia model compared to GFP-EPC group and medium control group at 14 days after transplantation, and a significant difference was still observed in the HIF-1α group at 1 and 2 months of follow-up (73). The authors also investigated the fate of transplanted EPCs by using human leukocyte antigen staining of the human donor cells and found that exogeneous EPCs homed to the injury site in the ischemic region on day 7 after transplantation. Interestingly, they proposed that the homing was enhanced in HIF-1α transduced cells due to the expression of genes downstream of HIF-1α such as SDF-1α and its receptor CXCR4.

Kong et al. evaluated the feasibility and therapeutic potential of genetically modified autologous rabbit EPCs overexpressing vasculoprotective genes such as endothelial nitric oxide synthase (eNOS) and heme oxygenase-1 (HO-1) in balloon-denuded carotid arteries (74). They showed that endothelization was enhanced in the EPC-transplanted

vessels relative to the saline control (74). Neointima size was further reduced in vessels treated with eNOS-transfected EPCs and thrombosis was reduced to ~ 50% of the saline-treated vessels by EPC administration, and was virtually absent in all transfected EPC groups (eNOS- and HO-1-transfected) (74). Improving therapeutic potential of angiogenic cells by increasing nitric oxide bioavailability by direct overexpression of eNOS was the approach undertaken by our group. We showed that CAC dysfunction seen in high-risk patients could be partially reversed by eNOS overexpression (38). When using lentiviral eNOS-transduced cells from CAD patients, chemotactic migration was significantly improved compared with sham transduction, and their ability to induce angiogenic tube formation when cocultured with HUVECs on Matrigel was increased (38). In vivo, eNOS-transduction enhanced the ability of patient-derived CACs to induce neovascularization and improve ischemic hindlimb perfusion (38). Chen et al. examined the effects of late outgrowth EPCs modified with the secreted version of fibroblast growth factor-1 (sp-FGF1) gene in a porcine model of chronic myocardial ischemia (75). In vitro, the gene modified EPCs displayed enhanced survival, migration and tube formation (75). Following autologous transplantation, the genetically modified cells reduced the myocardial perfusion defect compared to the non-transduced EPC group (5.2 $\pm$ 3.7% vs. 12.6 $\pm$ 4.5%) and the PBS control group (14.3 $\pm$ 3.1%) (75). The genetically modified EPCs also promoted neovascularization as shown by the increase in vascular density (as recognized by tubular structures positive for α-actin) compared to the non-transduced EPC group (148.5 $\pm$ 34.6 vs 102.3 $\pm$ 30.8/mm2) and the PBS control group (98.8 $\pm$ 25.4/mm2) (75).

Experimental studies using models of diabetes have also shown impaired EPC function and supported the need to develop enhanced cell therapies for diabetic patients (76, 77).

The Chen group showed that murine EPCs derived from a type II diabetic model (db/db mouse) were less effective than normal, wild-type EPCs in accelerating wound closure (76). Transfection with manganese superoxide dismutase (MnSOD), an antioxidant enzyme which confers protection against oxidative stress, improved the ability of diabetic EPCs to form tube networks on Matrigel and enhanced wound angiogenesis and closure, to a level similar to that achieved by an higher number of nontransfected diabetic EPCs (76).

Table 3. Studies using genetically-modified EPCs

Gene	Cell type	Model	Main results	References
Single genes				
VEGF	Early EPCs, human (PB)	Hindlimb ischemia, murine	Enhanced ability to restore ischemic limb perfusion; ↑ capillary density; ↓ limb necrosis/autoamputation	[55]
TERT	Early EPCs, human (PB)	Hindlimb ischemia, murine	Improved limb salvage; ↑ ability to restore ischemic limb perfusion; ↑ capillary density	[58]
AM	Early EPCs, human (UCB)	MCT-induced rat model of PAH	Improved hemodynamics (↓ PAP; ↓ PVR; ↓ RVSP); ↓ RV weight; ↓ remodeling; ↑ survival	[11]
eNOS or HO-1	Late outgrowth EPCs, rabbit (PB)	Arterial balloon-injury, rabbit	↑ Re-endothelization of arteries for both genes; ↓ neointima size in eNOS-EPCs	[68]
VEGF	Early EPCs, human (UCB)	Hindlimb ischemia, rat	Enhanced ability to restore ischemic limb perfusion; ↑ capillary density	[57]
GSK-3β	Early and late outgrowth EPCs, human (PB)	Hindlimb ischemia, murine	↑ Survival and proliferation of early EPCs; ↑ survival and differentiation of late EPCs; ↑ ability to restore ischemic limb perfusion; ↑ limb salvage; ↑ capillary density in early & late EPCs	[59]
ILK	Early EPCs, human (PB)	Hindlimb ischemia, murine	Enhanced ability to restore ischemic limb perfusion; prevented limb loss; ↑ capillary density	[61]
VEGF	Early EPCs, human (UCB)	Random flap, murine	Improved flap pedicle perfusion; ↑ capillary density; ↑ ability to restore ischemic limb perfusion	[56]
eNOS	Rat EPCs (BM)	MCT-induced PAH, rat	↓ RVSP; ↓ RV-hypertrophy; ↑ perfusion; ↑ survival; ↓ arteriolar muscularization	[12]
CGRP	Early EPCs, human (PB)	Shunt-induced PH, rat	↓ PAP; ↓ PVR; ↓ remodeling; ↑ survival	[75]
HIF-1α	Early EPCs, human (PB)	Hindlimb ischemia, murine	↑ Hypoxia-induced EPC differentiation; ↑ proliferation; ↑ migration; ↑ VEGF & NO secretion; ↑ capillary density	[66]
HIF-1α	Early EPCs, human (PB)	Hindlimb ischemia, murine	↑ Proliferation in vivo; ↓ limb & toe necrosis; ↑ ability to restore ischemic limb perfusion	[67]
sp-FGF1	Late outgrowth EPCs, porcine (PB)	Chronic myocardial ischemia, pig	↑ Migration; ↑ tube formation; ↑ survival; ↓ myocardial perfusion defects; ↑ vascular density in ischemic myocardium	[69]
HGF	Murine EPCs (BM)	Hindlimb ischemia, murine	↓ Apoptosis; ↑ migration; ↓ cell requirement 30-fold; ↑ capillary & arterioles	[65]
MnSOD	Murine EPCs (BM)	Type II diabetes, murine	↑ Wound repair; ↑ tube formation; ↑ capillary formation	[70]
eNOS	CACs, human (PB)	Hindlimb ischemia, murine	↑ Migration; ↑ tube formation; ↑ ability to restore ischemic limb perfusion; ↑ muscle perfusion; ↑ vessel branching	[38]
Multiple genes				
VEGF + Ang1	Cultured $CD34^+$ (UCB)	Acute MI, murine	Reduced infarct size; ↑ capillary density; ↑ FS; ↓ LVED; ↑ LVEF; ↑ LVEDd	[54]
VEGF + Ang1	Late outgrowth EPCs, rabbit (BM)	Hindlimb ischemia, rabbit	↑ Survival; ↑ SMA-positive vessel density	[72]
VEGF + rSDF-1α	Early EPCs, human (PB)	Hindlimb ischemia, murine	↑ Migration; ↓ apoptosis; ↑ ability to restore ischemic limb perfusion; ↑ capillary density; ↑ EPC recruitment	[73]
VEGF + PDGF	Cultured $CD133^+/CD34^+$ (UCB)	Acute MI, rat	Improved cardiac function (↑ FS; ↑ anterior wall tissue velocity; ↓ wall motion score index; ↑ strain & strain rates)	[74]

Ang1 indicates angiopoietin 1; AM, adrenomedullin; BM, bone marrow; CACs, circulating angiogenic cells; CGRP, calcitonin gene-related peptide; eNOS, endothelial nitric oxide synthase; EC, endothelial cells; GSK-3β, glycogen synthase kinase-3 beta; FS, fractional shortening; HGF, hepatocye growth factor; HIF-1α, hypoxia inducible factor-1 alpha; HO-1, heme oxygenase-1; ILK, integrin-linked kinase; LVEF, left ventricular ejection fraction; LVEDd, left ventricular end-diastolic diameter; LVED, left ventricular end-systolic diameter; MCT, monocrotaline; MI, myocardial infarction; MnSOD, maganese superoxide dismutase; NO, nitric oxide; PAH, pulmonary artery hypertension; PAP, pulmonary artery pressure; PB, peripheral blood; PDGF, platelet-derived growth factor; PH, pulmonary hypertension; PVR, pulmonary vascular resistance; RV, right ventricular; RVSP, right ventricular systolic pressure; rSDF-1α, recombinant stromal cell-derived factor-1 alpha; SMA, smooth muscle actin; sp-FGF1, secreted vesion of acidic fibroblast growth factor; TERT, telomerase reverse transcriptase; UCB, umbilical cord blood; VEGF, vascular endothelial growth factor

4.1.2. Combinatorial enhancement strategies

Based on the premise that a combination of therapeutic genes would be more effective than the use of any single transgene for enhancing therapeutic angiogenesis, a number of research groups have studied the additive or synergistic effects of engineering EPCs to overexpress multiple growth factors. Because VEGF acts in concert with angiopoietin-1 (Ang1) to produce a stable and functional microvasculature, the effect of combined gene transfer on human umbilical cord blood CD34+ cells was investigated (60). The combination was found to be more effective than single gene transfer alone, or nontransfected CD34+ cells, in reducing infarct size, improving cardiac function and increasing capillary density in acute myocardial infarction in mice (60). Not long after, another group (78) tested the therapeutic effect of an adeno-associated virus-2 (AAV-2) vector simultaneously encoding human VEGF and Ang1 (AAV-Ang1/VEGF). In a rabbit ischemic hindlimb model, co-transduced bone marrow-derived EPCs with Ang1 and VEGF showed higher cell survival in the ischemic tissues than nontransduced EPCs; similar to levels achieved by injection of AAV-Ang1/VEGF directly into the ischemic muscle prior to EPCs transplantation (78). AAV-Ang1/VEGF-transduced EPCs were as efficient as EPCs alone and more than the vector alone for increasing blood flow recovery; however, pre-intramuscular injection of AAV-Ang1/VEGF followed by EPCs injection led to the greatest degree of blood flow recovery (78). Altogether, the authors demonstrated that the EPCs co-transduced with Ang 1 and VEGF are superior than EPCs alone for EPC survival and α-SMA positive arteriolar density; however, intramuscularly pre-injection of the AAV-Ang1/VEGF vector followed by EPCs transplantation resulted in the greatest therapeutic effect (78). This finding led other groups to explore the therapeutic value of local preconditioning of the target organ by administration followed by the transplantation of transduced or nontransduced EPCs for treating ischemic diseases. In 2009, the Wang's group administered SDF-1α, a key

cytokine for EPC homing, into the ischemic hindlimb muscle in a nude mouse model in combination with the systemic delivery of humanVEGF165-transduced EPCs (79). They found that over-expression of human VEGF165 increased SDF-1α-mediated EPC migration in vitro, and SDF-1α combined with VEGF reduced EPC apoptosis induced by serum starvation more than SDF-1α or VEGF alone (79). In vivo, SDF-1α preconditioning increased in the accumulation of exogenous EPCs in the ischemic muscle, and the greatest improvement in blood flow recovery and capillary density was seen with the combined use of preconditioning and transduced EPCs (79). Das et al. have studied the feasibility and efficacy of overexpression of the angiogenic growth factors, VEGF and platelet derived growth factor (PDGF), in nanofiber expanded CD133+/CD34+ haematopoietic stem cells in a rat model of myocardial infarction (80). This strategy promoted a significant improvement in cardiac function shown by an increased in fractional shortening and anterior wall tissue velocity, an increased in both the strain and strain rates and a decreased in wall motion score index compared to controls (80).

To date, there has been no clinical trial that has used genetically modified cells in the therapy of cardiac diseases. The Enhanced Angiogenic Cell Therapy (ENACT) trial is planned to begin before the end of 2011, and will be the world's first trial to assess the potential value of cell-based gene therapy in patients post acute MI (Clinicaltrials.gov NCT00936819). This multicentre study will enrol 100 patients within 30 days post MI randomized to receive an intracoronary injection of one of three treatments in a blinded fashion: placebo (saline), autologous early EPCs alone or autologous EPCs transfected to overexpress eNOS, based on the demonstrated ability of this transgene to restore EPC activity from patients with cardiovascular disease.

4.2. Gene-modified EPCs for the treatment of pulmonary hypertension

EPC therapy is an attractive approach for the treatment of pulmonary arterial hypertension (PAH), presumably by contributing to repair and regeneration of lung microvasculature, thus improving the pulmonary hemodynamics. Already, there are some encouraging data from early clinical trials suggesting modest benefits of autologous EPCs in patients with PAH. However, as discussed above, the activity of EPCs appears to be reduced in patients with PAH and therefore it may be necessary to find effective strategies to enhance their function in order to develop a truly effective cell-based therapy. Nagaya et al. reported a novel hybrid cell and gene therapy based on the phagocytosis action of umbilical cord-derived EPCs (11). EPCs transfected with adrenomedullin (AM), a potent vasodilator, significantly showed greater improvement in pulmonary hypertension in MCT rats in a prevention protocol compared with nontransfected EPCs, which had only a modest but significant effect in this model (11). Although non-transduced EPCs also attenuated hypertrophy of the pulmonary vessel wall after MCT injection, quantitative analysis demonstrated a significantly greater reduction of wall thickness with AM-transduced cells (11). Furthermore, MCT rats transplanted with AM-expressing EPCs had a significant higher survival rate than those given culture medium (control group) or EPCs alone (11). Zhao et al. evaluated the therapeutic effect of calcitonin gene-related peptide (CGRP)-expressing early EPCs on left-to-right shunt-induced pulmonary hypertension in rats (81). CGRP has a strong pulmonary vasodilator activity and was therefore a good candidate to use in the treatment of pulmonary hypertension. Indeed, four weeks after CGRP-EPC injection, pulmonary artery pressure, and total pulmonary vascular resistance were both reduced, and pulmonary vascular remodelling was remarkably attenuated by this gene-enhanced EPC therapy (81). Our group reported that the administration of EPCs 3 days after MCT nearly completely prevented the increase in right ventricular systolic pressure seen at 3 weeks with MCT alone (12). However, when cell therapy was delayed until to 3 weeks

after MCT administration only animals receiving EPCs transduced with human eNOS exhibited significant reversal of established disease at day 35 (31 $\pm$ 2 mm Hg) compared with day 21 (50 $\pm$ 3 mm Hg) (12). This improvement was associated with evidence of restoration of distal arteriolar continuity and improved perfusion of alveolar capillaries in their model, and this effect was dependent of the delivery of “regenerative” cells because the injection of skin fibroblast had no effect on microvasculature structure or function (12). Moreover, the delivery of EPCs to rats with established PAH resulted in marked improvement in survival, which was greatest in the group receiving eNOS-transduced cells (12).

Wang and colleagues have performed a clinical trial of cell therapy for idiopathic PAH using nontransduced, early EPCs derived by attached cell culture of peripheral blood MNCs (20). In a randomized but nonblinded design, they showed that there were modest but significant improvements in pulmonary hemodynamics and functional capacity in patients receiving cell therapy compared to those receiving only standard therapies at 3 months (20). In addition, the same group conducted a small pilot study to assess the effect of transplantation of autologous EPCs in children with IPAH (19). Intravenous infusion of autologous EPCs in children with IPAH was associated with significant improvements in exercise capacity, New York Heart Association (NYHA) functional class, and pulmonary hemodynamics (19). These promising results have led our group to initiate the first clinical study of gene-enhanced cell therapy in PAH (Pulmonary Hypertension: Assessment of Cell Therapy, PHACeT; NCT00469027). The aim of this study is to establish the safety of autologous progenitor cell-based gene therapy of human eNOS in patients with severe PAH refractory to conventional treatment. At the time of writing, this trial was over half way complete in patient accrual, and it is hoped that we will be able to report on the findings within the next year.

5. MOLECULAR TARGETS UNDER INVESTIGATION

Current strategies for designing gene-enhanced cell therapies are based mainly on candidate gene approaches, using targets that have been demonstrated to improve EPC activity or a logical choice to enhance cell homing and survival. However, underlying mechanisms of EPC dysfunction in aging and various cardiovascular diseases are still uncertain, and it can be argued that the most effective strategies to restore their regenerative activity will come from a full understanding of pathogenic basis of this process. Therefore, unbiased genomic and proteomic profiling of EPCs derived from patients with cardiovascular disease and/or vascular risk factors and other conditions such as pulmonary hypertension will be necessary to dissect the regulatory pathways that control the phenotype of EPCs, which are not yet clearly defined. Two groups have recently employed such strategy to uncover the genes that are involved in the disease-impairment of the patient-derived EPCs. Van Oostrom et al. used genome-wide profiling to elucidate the effect of type I diabetes on EPC gene expression (82). They reported that 1591 genes are differentially expressed between type I diabetic patients and healthy controls (82). Seeger et al. performed DNA-protein binding arrays and found that one major signalling pathway involved in the vasculogenic progenitor cell reduction in type II diabetes is the activation of two transcription factors, namely ETS1 and ETS2 (E26 transformation-specific DNA binding domain) (83). They further showed that ablation of ETS1 expression by siRNA rescued high glucose-induced reduction of progenitor cell number (83). Our lab, in collaboration with Morrell's group from United Kingdom, is currently working on elucidating the effects of bone morphogenetic protein receptor-2 (Bmpr-2) mutations on the activation of proteins in the BMP signaling pathway in blood-derived late outgrowth endothelial cells using an unbiased proteomic approach. These high-throughput studies will help to shed light on the intrinsic defects of the EPCs derived

from patients in need of cellular therapy. The angiogenic targets described in the published reports and the novel targets soon to be discovered from unbiased genomic and proteomic studies will shape future therapies.

6. CONCLUSIONS

Endothelial progenitor cell therapy provides a promising therapeutic option for patients with ischemic disease and other vascular conditions such as pulmonary hypertension who do not respond well to conventional treatments. Clearly, the angiogenic and reparative activity of patient-derived cells is reduced in the context of these diseases, and thus we need effective strategies to enhance autologous EPC function and restore their full therapeutic potential. As discussed in the previous sections, autologous cell therapy will be hampered by the patient conditions, which affect the quantity and quality of the cells transplanted. The superiority of the genetically-modified EPCs over non-transduced cells to restore the angiogenic potential of patient-derived cells before autologous transplantation has been demonstrated in a number reports using not only a single but also a combination of angio- or vasculogenic genes. So far, researchers have targeted pathways with well-described angiogenic properties and obtained a superior effect with genetically modified EPCs compared with non-modified cells. At this point, future studies directed at understanding the cellular and molecular mechanisms leading to the numerical and functional impairment of EPCs are urgently needed to enhance the treatments for clinical applications.

REFERENCES

1. Asahara T, Murohara T, Sullivan A, Silver M, van der Zee R, Li T, et al. Isolation of putative progenitor endothelial cells for angiogenesis. Science. 1997 Feb 14;275(5302):964-7.

2. Asahara T. Cell therapy and gene therapy using endothelial progenitor cells for vascular regeneration. Handb Exp Pharmacol. 2007(180):181-94.

3. Richardson MR, Yoder MC. Endothelial progenitor cells: quo vadis? J Mol Cell Cardiol. 2011 Feb;50(2):266-72.

4. Yoder MC. Defining human endothelial progenitor cells. J Thromb Haemost. 2009 Jul;7 Suppl 1:49-52.

5. Hirschi KK, Ingram DA, Yoder MC. Assessing identity, phenotype, and fate of endothelial progenitor cells. Arterioscler Thromb Vasc Biol. 2008 Sep;28(9):1584-95.

6. Alessandri G, Emanueli C, Madeddu P. Genetically engineered stem cell therapy for tissue regeneration. Ann N Y Acad Sci; 2004. p. 271-84.

7. Kalka C, Masuda H, Takahashi T, Kalka-Moll WM, Silver M, Kearney M, et al. Transplantation of ex vivo expanded endothelial progenitor cells for therapeutic neovascularization. Proc Natl Acad Sci U S A. 2000 Mar 28;97(7):3422-7.

8. Shintani S, Murohara T, Ikeda H, Ueno T, Sasaki K, Duan J, et al. Augmentation of postnatal neovascularization with autologous bone marrow transplantation. Circulation. 2001 Feb 13;103(6):897-903.

9. Kawamoto A, Gwon HC, Iwaguro H, Yamaguchi JI, Uchida S, Masuda H, et al. Therapeutic potential of ex vivo expanded endothelial progenitor cells for myocardial ischemia. Circulation. 2001 Feb 6;103(5):634-7.

10. Kocher AA, Schuster MD, Szabolcs MJ, Takuma S, Burkhoff D, Wang J, et al. Neovascularization of ischemic myocardium by human bone-marrow-derived angioblasts prevents cardiomyocyte apoptosis, reduces remodeling and improves cardiac function. Nat Med. 2001 Apr;7(4):430-6.

11. Nagaya N, Kangawa K, Kanda M, Uematsu M, Horio T, Fukuyama N, et al. Hybrid cell-gene therapy for pulmonary hypertension based on phagocytosing action of endothelial progenitor cells. Circulation. 2003 Aug 19;108(7):889-95.

12. Zhao YD, Courtman DW, Deng Y, Kugathasan L, Zhang Q, Stewart DJ. Rescue of monocrotaline-induced pulmonary arterial hypertension using bone marrow-derived endothelial-like progenitor cells: efficacy of combined cell and eNOS gene therapy in established disease. Circ Res. 2005 Mar 4;96(4):442-50.

13. Ormiston ML, Deng Y, Stewart DJ, Courtman DW. Innate immunity in the therapeutic actions of endothelial progenitor cells in pulmonary hypertension. Am J Respir Cell Mol Biol. 2010 Nov;43(5):546-54.

14. Takahashi M, Nakamura T, Toba T, Kajiwara N, Kato H, Shimizu Y. Transplantation of endothelial progenitor cells into the lung to alleviate pulmonary hypertension in dogs. Tissue Eng. 2004 May-Jun;10(5-6):771-9.

15. Assmus B, Honold J, Schachinger V, Britten MB, Fischer-Rasokat U, Lehmann R, et al. Transcoronary transplantation of progenitor cells after myocardial infarction. N Engl J Med. 2006 Sep 21;355(12):1222-32.

16. Assmus B, Rolf A, Erbs S, Elsasser A, Haberbosch W, Hambrecht R, et al. Clinical outcome 2 years after intracoronary administration of bone marrow-derived progenitor cells in acute myocardial infarction. Circ Heart Fail. 2010 Jan;3(1):89-96.

17. Janssens S, Dubois C, Bogaert J, Theunissen K, Deroose C, Desmet W, et al. Autologous bone marrow-derived stem-cell transfer in patients with ST-segment elevation myocardial infarction: double-blind, randomised controlled trial. Lancet. 2006 Jan 14;367(9505):113-21.

18. Schachinger V, Erbs S, Elsasser A, Haberbosch W, Hambrecht R, Holschermann H, et al. Intracoronary bone marrow-derived progenitor cells in acute myocardial infarction. N Engl J Med. 2006 Sep 21;355(12):1210-21.

19. Zhu JH, Wang XX, Zhang FR, Shang YP, Tao QM, Zhu JH, et al. Safety and efficacy of autologous endothelial progenitor cells transplantation in children with idiopathic pulmonary arterial hypertension: open-label pilot study. Pediatr Transplant. 2008 Sep;12(6):650-5.

20. Wang XX, Zhang FR, Shang YP, Zhu JH, Xie XD, Tao QM, et al. Transplantation of autologous endothelial progenitor cells may be beneficial in patients with idiopathic pulmonary arterial hypertension: a pilot randomized controlled trial. J Am Coll Cardiol. 2007 Apr 10;49(14):1566-71.

21. Loomans CJ, de Koning EJ, Staal FJ, Rookmaaker MB, Verseyden C, de Boer HC, et al. Endothelial progenitor cell dysfunction: a novel concept in the pathogenesis of vascular complications of type 1 diabetes. Diabetes. 2004 Jan;53(1):195-9.

22. Sibal L, Aldibbiat A, Agarwal SC, Mitchell G, Oates C, Razvi S, et al. Circulating endothelial progenitor cells, endothelial function, carotid intima-media thickness and circulating markers of endothelial dysfunction in people with type 1 diabetes without macrovascular disease or microalbuminuria. Diabetologia. 2009 Aug;52(8):1464-73.

23. Jialal I, Devaraj S, Singh U, Huet BA. Decreased number and impaired functionality of endothelial progenitor cells in subjects with metabolic syndrome: implications for increased cardiovascular risk. Atherosclerosis. 2010 Jul;211(1):297-302.

24. Thum T, Fraccarollo D, Schultheiss M, Froese S, Galuppo P, Widder JD, et al. Endothelial nitric oxide synthase uncoupling impairs endothelial progenitor cell mobilization and function in diabetes. Diabetes. 2007 Mar;56(3):666-74.

25. Vasa M, Fichtlscherer S, Aicher A, Adler K, Urbich C, Martin H, et al. Number and migratory activity of circulating endothelial progenitor cells inversely correlate with risk factors for coronary artery disease. Circ Res. 2001 Jul 6;89(1):E1-7.

26. Umemura T, Soga J, Hidaka T, Takemoto H, Nakamura S, Jitsuiki D, et al. Aging and hypertension are independent risk factors for reduced number of circulating endothelial progenitor cells. Am J Hypertens. 2008 Nov;21(11):1203-9.

27. Heeschen C, Lehmann R, Honold J, Assmus B, Aicher A, Walter DH, et al. Profoundly reduced neovascularization capacity of bone marrow mononuclear cells derived from patients with chronic ischemic heart disease. Circulation. 2004 Apr 6;109(13):1615-22.

28. MacEneaney OJ, DeSouza CA, Weil BR, Kushner EJ, Van Guilder GP, Mestek ML, et al. Prehypertension and endothelial progenitor cell function. J Hum Hypertens. 2011 Jan;25(1):57-62.

29. Oliveras A, Soler MJ, Martinez-Estrada OM, Vazquez S, Marco-Feliu D, Vila JS, et al. Endothelial progenitor cells are reduced in refractory hypertension. J Hum Hypertens. 2008 Mar;22(3):183-90.

30. Werner N, Kosiol S, Schiegl T, Ahlers P, Walenta K, Link A, et al. Circulating endothelial progenitor cells and cardiovascular outcomes. N Engl J Med. 2005 Sep 8;353(10):999-1007.

31. Schmidt-Lucke C, Rossig L, Fichtlscherer S, Vasa M, Britten M, Kamper U, et al. Reduced number of circulating endothelial progenitor cells predicts future cardiovascular events: proof of concept for the clinical importance of endogenous vascular repair. Circulation. 2005 Jun 7;111(22):2981-7.

32. Werner N, Wassmann S, Ahlers P, Schiegl T, Kosiol S, Link A, et al. Endothelial progenitor cells correlate with endothelial function in patients with coronary artery disease. Basic Res Cardiol. 2007 Nov;102(6):565-71.

33. Hill JM, Zalos G, Halcox JP, Schenke WH, Waclawiw MA, Quyyumi AA, et al. Circulating endothelial progenitor cells, vascular function, and cardiovascular risk. N Engl J Med. 2003 Feb 13;348(7):593-600.

34. Heiss C, Keymel S, Niesler U, Ziemann J, Kelm M, Kalka C. Impaired progenitor cell activity in age-related endothelial dysfunction. J Am Coll Cardiol. 2005 May 3;45(9):1441-8.

35. Edelberg JM, Tang L, Hattori K, Lyden D, Rafii S. Young adult bone marrow-derived endothelial precursor cells restore aging-impaired cardiac angiogenic function. Circ Res. 2002 May 31;90(10):E89-93.

36. Rauscher FM, Goldschmidt-Clermont PJ, Davis BH, Wang T, Gregg D, Ramaswami P, et al. Aging, progenitor cell exhaustion, and atherosclerosis. Circulation. 2003 Jul 29;108(4):457-63.

37. Tepper OM, Galiano RD, Capla JM, Kalka C, Gagne PJ, Jacobowitz GR, et al. Human endothelial progenitor cells from type II diabetics exhibit impaired proliferation, adhesion, and incorporation into vascular structures. Circulation. 2002 Nov 26;106(22):2781-6.

38. Ward MR, Thompson KA, Isaac K, Vecchiarelli J, Zhang Q, Stewart DJ, et al. Nitric Oxide Synthase Gene Transfer Restores Activity of Circulating Angiogenic Cells From Patients With Coronary Artery Disease. Mol Ther. 2011 Apr 26.

39. Giannotti G, Doerries C, Mocharla PS, Mueller MF, Bahlmann FH, Horvath T, et al. Impaired endothelial repair capacity of early endothelial progenitor cells in prehypertension: relation to endothelial dysfunction. Hypertension. 2010 Jun;55(6):1389-97.

40. Diller GP, Thum T, Wilkins MR, Wharton J. Endothelial progenitor cells in pulmonary arterial hypertension. Trends Cardiovasc Med. 2010 Jan;20(1):22-9.

41. Satoh K, Kagaya Y, Nakano M, Ito Y, Ohta J, Tada H, et al. Important role of endogenous erythropoietin system in recruitment of endothelial progenitor cells in hypoxia-induced pulmonary hypertension in mice. Circulation. 2006 Mar 21;113(11):1442-50.

42. Davie NJ, Crossno JT, Jr., Frid MG, Hofmeister SE, Reeves JT, Hyde DM, et al. Hypoxia-induced pulmonary artery adventitial remodeling and neovascularization: contribution of progenitor cells. Am J Physiol Lung Cell Mol Physiol. 2004 Apr;286(4):L668-78.

43. Hayashida K, Fujita J, Miyake Y, Kawada H, Ando K, Ogawa S, et al. Bone marrow-derived cells contribute to pulmonary vascular remodeling in hypoxia-induced pulmonary hypertension. Chest. 2005 May;127(5):1793-8.

44. Junhui Z, Xingxiang W, Guosheng F, Yunpeng S, Furong Z, Junzhu C. Reduced number and activity of circulating endothelial progenitor cells in patients with idiopathic pulmonary arterial hypertension. Respir Med. 2008 Jul;102(7):1073-9.

45. Diller GP, van Eijl S, Okonko DO, Howard LS, Ali O, Thum T, et al. Circulating endothelial progenitor cells in patients with Eisenmenger syndrome and idiopathic pulmonary arterial hypertension. Circulation. 2008 Jun 10;117(23):3020-30.

46. Fadini GP, Schiavon M, Rea F, Avogaro A, Agostini C. Depletion of endothelial progenitor cells may link pulmonary fibrosis and pulmonary hypertension. Am J Respir Crit Care Med. 2007 Oct 1;176(7):724-5; author reply 5.

47. Asosingh K, Aldred MA, Vasanji A, Drazba J, Sharp J, Farver C, et al. Circulating angiogenic precursors in idiopathic pulmonary arterial hypertension. Am J Pathol. 2008 Mar;172(3):615-27.

48. Toshner M, Voswinckel R, Southwood M, Al-Lamki R, Howard LS, Marchesan D, et al. Evidence of dysfunction of endothelial progenitors in pulmonary arterial hypertension. Am J Respir Crit Care Med. 2009 Oct 15;180(8):780-7.

49. Smadja DM, Gaussem P, Mauge L, Israel-Biet D, Dignat-George F, Peyrard S, et al. Circulating endothelial cells: a new candidate biomarker of irreversible pulmonary hypertension secondary to congenital heart disease. Circulation. 2009 Jan 27;119(3):374-81.

50. Frid MG, Brunetti JA, Burke DL, Carpenter TC, Davie NJ, Reeves JT, et al. Hypoxia-induced pulmonary vascular remodeling requires recruitment of circulating mesenchymal precursors of a monocyte/macrophage lineage. Am J Pathol. 2006 Feb;168(2):659-69.

51. Nikam VS, Schermuly RT, Dumitrascu R, Weissmann N, Kwapiszewska G, Morrell N, et al. Treprostinil inhibits the recruitment of bone marrow-derived circulating fibrocytes in chronic hypoxic pulmonary hypertension. Eur Respir J. 2010 Dec;36(6):1302-14.

52. Marsboom G, Pokreisz P, Gheysens O, Vermeersch P, Gillijns H, Pellens M, et al. Sustained endothelial progenitor cell dysfunction after chronic hypoxia-induced pulmonary hypertension. Stem Cells. 2008 Apr;26(4):1017-26.

53. Teichert-Kuliszewska K, Kutryk MJ, Kuliszewski MA, Karoubi G, Courtman DW, Zucco L, et al. Bone morphogenetic protein receptor-2 signaling promotes pulmonary arterial endothelial cell survival: implications for loss-of-function mutations in the pathogenesis of pulmonary hypertension. Circ Res. 2006 Feb 3;98(2):209-17.

54. Lane KB, Machado RD, Pauciulo MW, Thomson JR, Phillips JA, 3rd, Loyd JE, et al. Heterozygous germline mutations in BMPR2, encoding a TGF-beta receptor, cause familial primary pulmonary hypertension. Nat Genet. 2000 Sep;26(1):81-4.

55. Thomson JR, Machado RD, Pauciulo MW, Morgan NV, Humbert M, Elliott GC, et al. Sporadic primary pulmonary hypertension is associated with germline mutations of the gene encoding BMPR-II, a receptor member of the TGF-beta family. J Med Genet. 2000 Oct;37(10):741-5.

56. Machado RD, Pauciulo MW, Thomson JR, Lane KB, Morgan NV, Wheeler L, et al. BMPR2 haploinsufficiency as the inherited molecular mechanism for primary pulmonary hypertension. Am J Hum Genet. 2001 Jan;68(1):92-102.

57. Tuder RM, Groves B, Badesch DB, Voelkel NF. Exuberant endothelial cell growth and elements of inflammation are present in plexiform lesions of pulmonary hypertension. Am J Pathol. 1994 Feb;144(2):275-85.

58. Atkinson C, Stewart S, Upton PD, Machado R, Thomson JR, Trembath RC, et al. Primary pulmonary hypertension is associated with reduced pulmonary vascular expression of type II bone morphogenetic protein receptor. Circulation. 2002 Apr 9;105(14):1672-8.

59. Reynolds PN. Gene therapy for pulmonary hypertension: prospects and challenges. Expert Opin Biol Ther. 2011 Feb;11(2):133-43.

60. Chen HK, Hung HF, Shyu KG, Wang BW, Sheu JR, Liang YJ, et al. Combined cord blood stem cells and gene therapy enhances angiogenesis and improves cardiac performance in mouse after acute myocardial infarction. Eur J Clin Invest. 2005 Nov;35(11):677-86.

61.Iwaguro H, Yamaguchi J, Kalka C, Murasawa S, Masuda H, Hayashi S, et al. Endothelial progenitor cell vascular endothelial growth factor gene transfer for vascular regeneration. Circulation. 2002 Feb 12;105(6):732-8.

62. Yi C, Xia W, Zheng Y, Zhang L, Shu M, Liang J, et al. Transplantation of endothelial progenitor cells transferred by vascular endothelial growth factor gene for vascular regeneration of ischemic flaps. J Surg Res. 2006 Sep;135(1):100-6.

63. Ikeda Y, Fukuda N, Wada M, Matsumoto T, Satomi A, Yokoyama S, et al. Development of angiogenic cell and gene therapy by transplantation of umbilical cord blood with vascular endothelial growth factor gene. Hypertens Res. 2004 Feb;27(2):119 28.

64.Murasawa S, Llevadot J, Silver M, Isner JM, Losordo DW, Asahara T. Constitutive human telomerase reverse transcriptase expression enhances regenerative properties of endothelial progenitor cells. Circulation. 2002 Aug 27;106(9):1133-9.

65. Choi JH, Hur J, Yoon CH, Kim JH, Lee CS, Youn SW, et al. Augmentation of therapeutic angiogenesis using genetically modified human endothelial progenitor cells with altered glycogen synthase kinase-3beta activity. J Biol Chem. 2004 Nov 19;279(47):49430-8.

66. Jope RS, Johnson GV. The glamour and gloom of glycogen synthase kinase-3. Trends Biochem Sci. 2004 Feb;29(2):95-102.

67. Cho HJ, Youn SW, Cheon SI, Kim TY, Hur J, Zhang SY, et al. Regulation of endothelial cell and endothelial progenitor cell survival and vasculogenesis by integrin-linked kinase. Arterioscler Thromb Vasc Biol. 2005 Jun;25(6):1154-60.

68. Morishita R, Nakamura S, Hayashi S, Taniyama Y, Moriguchi A, Nagano T, et al. Therapeutic angiogenesis induced by human recombinant hepatocyte growth factor in rabbit hind limb ischemia model as cytokine supplement therapy. Hypertension. 1999 Jun;33(6):1379-84.

69. Bussolino F, Di Renzo MF, Ziche M, Bocchietto E, Olivero M, Naldini L, et al. Hepatocyte growth factor is a potent angiogenic factor which stimulates endothelial cell motility and growth. J Cell Biol. 1992 Nov;119(3):629-41.

70. Comoglio PM, Trusolino L. Invasive growth: from development to metastasis. J Clin Invest. 2002 Apr;109(7):857-62.

71. Yamamoto Y, Matsuura T, Narazaki G, Sugitani M, Tanaka K, Maeda A, et al. Synergistic effects of autologous cell and hepatocyte growth factor gene therapy for neovascularization in a murine model of hindlimb ischemia. Am J Physiol Heart Circ Physiol. 2009 Oct;297(4):H1329-36.

72. Jiang M, Wang B, Wang C, He B, Fan H, Guo TB, et al. Angiogenesis by transplantation of HIF-1 alpha modified EPCs into ischemic limbs. J Cell Biochem. 2008 Jan 1;103(1):321-34.

73. Jiang M, Wang B, Wang C, He B, Fan H, Shao Q, et al. In vivo enhancement of angiogenesis by adenoviral transfer of HIF-1alpha-modified endothelial progenitor cells (Ad-HIF-1alpha-modified EPC for angiogenesis). Int J Biochem Cell Biol. 2008;40(10):2284-95.

74. Kong D, Melo LG, Gnecchi M, Zhang L, Mostoslavsky G, Liew CC, et al. Cytokine-induced mobilization of circulating endothelial progenitor cells enhances repair of injured arteries. Circulation. 2004 Oct 5;110(14):2039-46.

75. Chen SY, Wang F, Yan XY, Zhou Q, Ling Q, Ling JX, et al. Autologous transplantation of EPCs encoding FGF1 gene promotes neovascularization in a porcine model of chronic myocardial ischemia. Int J Cardiol. 2009 Jun 26;135(2):223-32.

76. Marrotte EJ, Chen DD, Hakim JS, Chen AF. Manganese superoxide dismutase expression in endothelial progenitor cells accelerates wound healing in diabetic mice. J Clin Invest. 2010 Dec 1;120(12):4207-19.

77. Tamarat R, Silvestre JS, Le Ricousse-Roussanne S, Barateau V, Lecomte-Raclet L, Clergue M, et al. Impairment in ischemia-induced neovascularization in diabetes: bone marrow mononuclear cell dysfunction and therapeutic potential of placenta growth factor treatment. Am J Pathol. 2004 Feb;164(2):457-66.

78. Chen F, Tan Z, Dong CY, Li X, Xie Y, Wu Y, et al. Combination of VEGF(165)/Angiopoietin-1 gene and endothelial progenitor cells for therapeutic neovascularization. Eur J Pharmacol. 2007 Jul 30;568(1-3):222-30.

79. Yu JX, Huang XF, Lv WM, Ye CS, Peng XZ, Zhang H, et al. Combination of stromal-derived factor-1alpha and vascular endothelial growth factor gene-modified endothelial progenitor cells is more effective for ischemic neovascularization. J Vasc Surg. 2009 Sep;50(3):608-16.

80. Das H, George JC, Joseph M, Das M, Abdulhameed N, Blitz A, et al. Stem cell therapy with overexpressed VEGF and PDGF genes improves cardiac function in a rat infarct model. PLoS One. 2009;4(10):e7325.

81. Zhao Q, Liu Z, Wang Z, Yang C, Liu J, Lu J. Effect of prepro-calcitonin gene-related peptide-expressing endothelial progenitor cells on pulmonary hypertension. Ann Thorac Surg. 2007 Aug;84(2):544-52.

82. van Oostrom O, de Kleijn DP, Fledderus JO, Pescatori M, Stubbs A, Tuinenburg A, et al. Folic acid supplementation normalizes the endothelial progenitor cell transcriptome of patients with type 1 diabetes: a case-control pilot study. Cardiovasc Diabetol. 2009;8:47.

83. Seeger FH, Chen L, Spyridopoulos I, Altschmied J, Aicher A, Haendeler J. Downregulation of ETS rescues diabetes-induced reduction of endothelial progenitor cells. PLoS One. 2009;4(2):e4529.

6.4 Publication #4

J. Proteome Res., 2011, 10 (5), pp 2465–2478

Quantitative Proteomic Analysis of Dystrophic Dog Muscle

Laetitia Guevel,[*,†] **Jessie R. Lavoie**,[‡,#] Carolina Perez-Iratxeta,[‡,#] Karl Rouger,[||] Laurence Dubreil,[||] Marie Feron,[†] Sophie Talon,[†] Marjorie Brand,[‡,§,#] and Lynn A. Megeney[‡,§,#]

[†]CNRS UMR6204, Faculte des Sciences et des Techniques, F-44322 Nantes Cedex 3, France

[‡]Sprott Center for Stem Cell Research, Ottawa Hospital Research Institute, Ottawa, ON Canada K1H 8L6

[§]Department of Medicine and Cellular and Molecular Medicine, University of Ottawa, Ottawa, ON K1H 8M5

[||]INRA UMR703, Ecole Nationale Veterinaire, Oniris, F-44307 Nantes Cedex 3, France

Keywords: Duchenne muscular dystrophy; GRMD dog; PGC1-α; quantitative proteomic; ICAT/MS/MS

Copyrights

Contributions of the Candidate

The work described in the manuscript is the result of a collaboration established between senior scientists at my Institute, Drs. Lynn Megeney and Marjorie Brand, and a scientist from the University of Nantes, Dr. Laetitia Guével. I was principally involved in the design and execution of the experiments related to the proteomics (2-D gel electrophoresis and Western blotting), as well as in the acquisition and analysis of the related data. I was also involved in drafting and editing the manuscript.

Abstract

Duchenne muscular dystrophy (DMD) is caused by null mutations in the dystrophin gene, leading to progressive and unrelenting muscle loss. Although the genetic basis of DMD is well resolved, the cellular mechanisms associated with the physiopathology remain largely unknown. Increasing evidence suggests that secondary mechanisms, as the alteration of key signaling pathways, may play an important role. In order to identify reliable biomarkers and potential therapeutic targets, and taking advantage of the clinically relevant Golden Retriever Muscular Dystrophy (GRMD) dog model, a proteomic study was performed. Isotope-coded affinity tag (ICAT) profiling was used to compile quantitative changes in protein expression profiles of the *vastus lateralis* muscles of 4-month old GRMD vs healthy dogs. Interestingly, the set of under-expressed proteins detected appeared primarily composed of metabolic proteins, many of which have been shown to be regulated by the transcriptional peroxisome proliferator-activated receptor-gamma co-activator 1 alpha (PGC-1α). Subsequently, we were able to showed that PGC1-α expression is dramatically reduced in GRMD compared to healthy muscle. Collectively, these results provide novel insights into the molecular pathology of the clinically relevant animal model of DMD, and indicate that defective energy metabolism is a central hallmark of the disease in the canine model.

Introduction

Duchenne muscular dystrophy (DMD) is a recessive X-linked neuromuscular disorder affecting one newborn boy in 3500.(1) DMD is caused by mutations in the dystrophin gene,(2-4) and is characterized by severe degeneration of muscle fibers, progressive paralysis, and ultimately, death. The dystrophin protein is localized under the sarcolemma of muscle fibers and is integrated within a large multiprotein complex (the dystrophin−glycoprotein complex, DGC), which provides a strong physical link between the actin cytoskeleton network and the extracellular matrix.(5-8) The absence of dystrophin in dystrophic muscles, which is associated with the subsequent loss of the DGC at the sarcolemma, leads to altered myofiber integrity, perturbed calcium homeostasis, activation of the calcium-dependent calpain proteases, and necrosis.(9, 10)

In addition to the increased structural fragility of DMD myofibers, accumulating evidence suggests that nonmechanical processes also contribute to pathology progression. First, the DGC is associated with several signaling molecules.(11-13) Second, studies performed in the mdx mouse, the murine model of DMD,(14) revealed changes in the MAPK and PI3K/Akt signaling cascades in dystrophic muscles.(15-18) More recently, the phosphorylation status of Akt was also shown to be altered in human dystrophic biopsies,(17) and we revealed that the PTEN phosphatase was differentially activated in dystrophic dog muscle, leading to the deregulation of the PI3K/Akt signaling pathway.(19) Collectively, these studies suggest that alterations in signal transduction pathways are significant contributing factors to the progression of DMD. Importantly, some recent studies have also suggested that the modulation of signaling molecules could affect the disease outcome.(20, 21)

However, despite the compelling evidence demonstrating the alteration of individual signaling proteins in dystrophic muscle, little is known regarding the involvement of the

corresponding signaling pathways in the development of the disease. In addition, only limited knowledge is available regarding the impact of dystrophin loss on the muscle proteome. Interestingly, proteomic profiling studies of the mdx mouse model revealed that the expression level of numerous proteins involved in the maintenance of sarcolemmal integrity (i.e., Fbxo11, adenylate kinase, the Ca2+ binding protein regucalin, and cvHSP) was altered in dystrophin−deficient fibers.(22-24) One of the most interesting aspects of the mdx mouse is that it contains subtypes of skeletal muscle that exhibit very different degrees of fiber wasting despite the fact that they all contain the same disease-associated mutation in exon 23.(25) In mature limb muscle, the murine model is characterized by successive degeneration/regeneration processes and does not exhibit the progressive muscle wasting and accumulation of connective tissue observed during development of the human disease.(26-28) However, aged mdx muscles and the mdx diaphragm show a severe dystrophic phenotype and histological alterations closely resembling those of the DMD phenotype.(25, 29-31) Another animal model of DMD, the canine Golden Retriever Muscular Dystrophy (GRMD), reflects both the genotype and phenotype of DMD. Affected dogs represents an accurate clinical phenocopy of DMD patients, as they are characterized by rapid progressive clinical dysfunction, severe muscle weakness, and abundant fiber necrosis.(32, 33)

We have recently shown that the perturbations detected within the PI3K/Akt and MAPK signaling pathways in dystrophic dog muscle could differ from the observations made in the mdx mouse model, which supports the importance of studying cell signaling events and secondary changes in the clinically relevant animal model.(19) Since there is an urgent need for the establishment of reliable biomarkers of secondary changes in muscular dystrophy, the proteomic study on GRMD muscle is crucial to completed previous proteomic profiling from the dystrophin-deficient mdx mouse. We studied the proteome variations between vastus lateralis muscle of 4-month old GRMD and healthy

dogs. At this stage, skeletal muscles are severely dystrophic and are characterized by high fiber-size variation, individual necrotic fibers, centrally nucleated fibers and fibrosis.(32, 33) We used isotope-coded affinity tag (ICAT) labeling followed by LC−MS/MS to analyzed the quantitative variations of the proteome in both a cytoplasmic fraction and a phospho-enriched fraction prepared from total extracts.(34) We chose to analyze the phospho-enriched fraction since protein phosphorylation plays a key role in regulating most cellular processes including proliferation, migration, apoptosis, and metabolic pathways. ICAT experiments revealed a significant alteration of the abundance of 85 proteins. Functional annotation of these proteins indicated a dysregulation in glycolytic and oxidative metabolism. In addition, we discovered that a significant number of proteins expressed at lower levels in the dystrophic samples are coded by genes whose expression is responsive to the peroxisome proliferator-activated receptor-gamma co-activator 1 alpha (PGC-α) a master switch for the transcriptional control of energy metabolism.(35) Accordingly, we showed that PGC-1α level is substantially reduced in GRMD muscle. Taken together, our results provide compelling new evidence that defects in energy metabolism are a hallmark of the disease in the canine model, and that in turn, these defects may contribute to the disease progression.

Experimental Procedures

Products

Ammonium bicarbonate (NH4HCO3), dibasic sodium phosphate (Na2HPO4), monobasic sodium phosphate (NaH2PO4), sodium chloride (NaCl), Tris, Triton X-100, and bicinchoninic acid (BCA) protein assay reagents were purchased from Sigma-Aldrich (St. Louis, MO). Trifluoroacetic acid and formic acid were obtained from Fluka (Milwaukee, WI). High-performance liquid chromatography grade acetonitrile (ACN: CH3CN) and methanol (CH3OH) were obtained from Fisher Scientific (Fair Lawn, NJ). Cleavable

ICAT reagents, monomeric avidin, and SCX cartridges were purchased from Applied Biosystems, Inc. (Foster City, CA).

Animals

Animals were part of a GRMD dog breeding colony established in Nantes (France). They were housed and cared for at the Boisbonne Center for Gene Therapy of the National Veterinary School of Nantes, following protocols compliant with the principles outlined in the French National Institute for Agronomic Research (INRA) Guide for the care and use of laboratory animals in biological experimentation. Affected dogs were identified during the first days of life by polymerase chain reaction genotyping using appropriate oligonucleotide primers and immunohistochemical localization of dystrophin. Four-month old GRMD dogs from Nantes colony are less active than normal littermates. They are defined by a decreased mobility and appear tired during minimal exercise.(32, 36) Their body weight is lower than that of unaffected littermates. While normal littermates display coordinated gait, GRMD dogs are characterized by an abnormal, stiff-limbed, shuffling gait and a marked weight transfer. Another prominent sign characteristic of muscular dystrophy is palmigrade/plantigrade stances.

Muscles

GRMD and healthy littermates (GRMD dog#1, #2, #3; healthy dog#1, #2, #3) from 4-month old dogs were sacrificed by intravenous sodium pentobarbital administration after general anesthesia and small 1 cm3 pieces of vastus lateralis muscle were cut and immediately frozen in liquid nitrogen during 2 min. Then, tissues were stored at −80 °C until processing. For protein extraction, the adipose portions of biopsies were carefully removed manually under a binocular microscope. Muscles were then powdered in liquid nitrogen, and homogenized in modified RIPA lysis buffer containing 150 mM NaCl, 50

mM Tris-HCl, pH 7.4, 1% (v/v) Nonidet-P40, 1% (v/v) glycerol, 1 mM EDTA, protease inhibitors cocktail (Sigma-Aldrich), and 10 mM of the tyrosine phosphatase inhibitor sodium orthovanadate. Homogenates were centrifuged at 1000g to pellet debris, and supernatants were centrifuged at 37 000g for 20 min at 4 °C to fractionate cytosolic proteins. Protein concentration was determined using a BCA protein assay. For ICAT/MS/MS analysis, a total of 80 µg of cytosolic proteins (GRMD dog#1; healthy dog#1) was subjected to buffer-exchange in TE pH 8.3 containing 50 mM NaCl. For the histopathological analysis, the sectioned blocks were embedded in Tissue-Tek 0.C.T. compound (Sakura Finetek, Torrance, CA), and frozen in isopentane cooled with liquid nitrogen. Transverse vastus lateralis muscle cryosections (8 µm) were prepared using a Leica CM 3050S cryostat. Hematoxylin & eosin (H&E) was performed as per standard histological protocols.(37)

Phosphoprotein Enrichment

Phosphoprotein enriched fractions were prepared from healthy and dystrophic muscles (GRMD dog#2; healthy dog#2) using a commercially available PhosphoProtein Purification Kit (Qiagen; Missisauga, CA).(38) The eluate was precipitated with TCA/acetone and the pellet was dissolved in ICAT labeling buffer (0.05% (w/v) SDS, 20 mM Tris-HCl, pH 8.3, 5 mM EDTA, 6 M urea). Protein concentration was measured using a BCA assay and a total of 30 µg of proteins was used for the ICAT/MS/MS analysis.

cICAT Labeling and Mass Spectrometry

Healthy and dystrophic cytosolic and phospho-enriched proteins (80 and 30 µg, respectively, n = 1 for each fraction) were labeled with the acid-cleavable ICAT reagent (cICAT) (Applied Biosystems, Framingham, MA) and analyzed by mass spectrometry as

previously described,(39) with the following modifications. Proteins from the healthy and dystrophic muscle were labeled with the isotopically light form of cICAT [12C9] and the isotopically heavy form of cICAT [13 C9], respectively. Labeled proteins were combined and proteolyzed with trypsin (Promega, Madison, WI). Resulting peptides were separated into 4 fractions by cation-exchange chromatography, and cICAT-labeled peptides were purified from each fraction by avidin-affinity chromatography.(39) Labeled peptides from the 4 fractions were analyzed by microcapillary reverse phase liquid chromatography electrospray ionization, followed by tandem mass spectrometry (μLC−ESI−MS/MS) using an ion trap mass spectrometer (LTQ, Thermofinnigan). Briefly, peptides were dried under vacuum, dissolved in a buffer containing 10% (v/v) ACN and 0.1% (v/v) trifluoroacetic acid (TFA), and pressure loaded onto an in-house prepared 10-cm × 75 μm fused silica microcapillary column packed with 5 μm Magic C18 beads. Peptides were resolved using an 80 min separation gradient from 2 to 50% HPLC Buffer (100% (v/v) ACN, 0.1% (v/v) HCOOH) at a 300 nL/min flow rate. The mass spectrometer was set to scan from 400 to 1800 m/z followed by two data-dependent MS/MS scans on the two most abundant ions. Dynamic exclusion was set to exclude ions that have been selected for MS/MS analysis for 2 min with a mass window of 2 Da.

ICAT Data Analysis

Raw data was converted to mzXML using ReAdW. MS/MS spectra were then exported as data files and searched against the ENSEMBL49 dog database, which contains 25 559 protein entries. The search was performed using SEQUEST (v 3.3.1 SP1), a data analysis program used for protein identification.(40) The mass of cysteine was statically modified by 227.13 Da (light cICAT) and differentially modified by 9.03 Da (heavy cICAT). Methionine was differentially modified as well with 16 Da to account for its oxidized form. Peptides identified by SEQUEST were analyzed using the Trans

Proteomics Pipeline (TPP) (version 3.4) mirroring the TPP at the Seattle Proteome Center. This pipeline uses the PeptideProphet(41) and ProteinProphet(42) algorithms to, respectively, validate the peptide and protein assignments to the MS/MS spectra made by SEQUEST, and to compute the probability that the assignments are correct. For the peptides database searches, we used a probability cutoff of 0.9 that corresponds to an overall false positive error rate below 0.6% for the cytoplasmic proteins, and 0.8% for the phospho-enriched proteins.(43)

Relative quantification of proteins (Light-labeled vs Heavy-labeled) was performed within the TPP using the ASAP ratio program,(44) an algorithm evaluating protein abundance ratios (i.e., ICAT ratios). For quantification of cytoplasmic proteins, 90% of the proteins with 2 or more quantified peptide ions have a relative error smaller than 22%. For quantification of phospho-enriched proteins, 62% of the proteins with 2 or more quantified peptide ions have a relative error smaller than 22%. The quality of each spectrum used for identification and quantification was verified manually. A value of ±0.5 for the log2 transformed and centered ASAP ratios was chosen as the cutoff threshold for significantly over/under represented proteins. We considered the proteins with a relative level between healthy and dystrophic muscles comprised outside the interval [0.7-fold; 1.42-fold] as significantly over/under represented.

Immunoblot Assays

To validate the protein changes detected by proteomic analyses, immunoblotting experiments were performed on a representative range of protein types. Cytosolic protein extracts (GRMD dog#1, #2, #3; healthy dog#1, #2, #3) were resolved by sodium dodecyl sulfate−polyacrylamide gel electrophoresis (SDS−PAGE) on 10% polyacrylamide gels and electroblotted onto immobilon-P membranes (Millipore Corp., Bedford, MA). Blots were blocked with PBS containing 0.1% (v/v) Tween-20, 2.5% (w/v)

BSA at room temperature for 1 h, and then incubated with sufficiently diluted primary antibodies against DJ-1, protein phosphatase 1 (PP1), alpha tubulin, lactate dehydrogenase (LDHA), cofilin 2, and pyruvate kinase type M2 (PKM2). Anti-DJ-1, anti-PP1, anti-LDHA, and anti-PKM2 were obtained from Cell Signaling Technology (Beverly, MA). Anti-cofilin 2 was obtained from Abcam (Cambridge, MA). The incubation was performed for 2 h at room temperature in PBS containing 0.1% Tween-20 and 1% BSA. Immunoreactivity was visualized by peroxidase-conjugated secondary antibodies and by SuperSignal West Pico chemiluminescence substrate (Pierce, Rockford, IL). Equal protein loading was verified through a Ponceau red staining of the membranes. The Western blot analyses were conducted using biopsies removed from three different dogs and the average value was calculated.

PGC-1α Immunohistological Analysis

To determine the location of PGC-1α, a double labeling directed against PGC-1α and β-dystroglycan (β-DG), which is expressed in the plasma membrane of healthy muscles (while it is highly reduced in the dystrophic ones(45)) was performed, in association with nuclei staining. Transverse vastus lateralis muscle cryosections (GRMD dog#1, #2, #3; healthy dog#1, #2) (8 µm) were prepared using a Leica CM 3050S cryostat. Sections were fixed with methanol and acetone at −20 °C and permeabilized by an incubation in PBS containing 0.3% TX-100 at room temperature for 5 min. They were then blocked with 10% goat serum in PBS containing 0.3% TX-100 for 30 min, and finally incubated in blocking solution at 4 °C with a rabbit polyclonal antibody against PGC-1α (1:50; Santa Cruz Biotechnology, Santa Cruz, CA). After washing with PBS, the sections were incubated 1 h at room temperature with a goat anti-rabbit secondary antibody labeled with Alexa fluor 488 (1:400; Invitrogen Life Technologies, CA). After washing, the samples were incubated for 1 h at 37 °C with a mouse monoclonal antibody against β-

dystroglycan (1/50, Novocastra), a plasma membrane component. Sections were then washed and incubated for 1 h at room temperature with an Alexa fluor 555 goat anti-mouse antibody (1/400, Invitrogen Life Technologies, CA). Nuclei were stained with Topro-3 (1/1000, Invitrogen Life Technologies). Slides were finally coverslipped and mounted with Mowiol Medium (Calbiochem EMD Biosciences, San Diego, CA). The immunolabeled sections were serially scanned with a confocal microscope (Nikon C1, Champigny-sur-Marne, France) using the argon ion laser (488 nm) to observe PGC-1α immunolabeling, a 543 nm helium neon laser to observe β-dystroglycan immunolabeling, and a 633 nm helium neon laser to observe nuclei stained.

Real-Time Reverse Transcription PCR

The genes coding for the PGC-1alpha protein (PPARGC1alpha) and its putative altered downstream targets (ACADS, FABP3, CYC1 and PFKM), chosen in the list presented in Figure 3A were analyzed by real-time RT-PCR. The LDHA gene was used as an internal reference gene, owing to its poor variation (based on our proteomic and transcriptional analysis) among different replicates and conditions. Primers were generated by the oligo 4.0 S software (National Biosciences, Plymouth, MN) and then submitted to BLASTn analysis (NCBI) to confirm their specificity. All primers were synthesized by Eurofins MWG GmBh (Germany) with the following sequences: for PPARGC1alpha, forward, 5′-ATGTGCTGCTCTGGTTGGTG-3′; reverse, 5′-AGCAAGTTCGCCTCGTTCTC-3′; for ACADS, forward, 5′-TGAACCAGGGAACGGCAG-3′; reverse, 5′-CTTCCTTCTTCCCCAGCGT-3′; for FABP3, forward, 5′-ATCAGCTTCAAGTTAGGGGTGG-3′; reverse, 5′-CCATCAACTAGCTCCCGCA-3′; for CYC1, forward, 5′-AGTGATGCTGTCGGCGTTG-3′; reverse, 5′-CCGTCCTGAACCTCCACCT-3′; for PFKM, forward, 5′-GTGGGGCTGACTGGGTTTT-3′; reverse, 5′-ATCACTGCTTCCACACCCATC-3′; for

LDHA, forward, 5′-GCTGGTTATTATCACGGC-3′; reverse, 5′-TCCCAACCTTTCCCCCA-3′. Total RNA extraction was performed from muscular biopsies of GRMD and healthy dogs (GRMD dog#1, #2, #3; healthy dog#2, #3) by using the RNeasy Fibrous Tissue Mini Kit (Qiagen) according to manufacturer's instructions. For the real-time PCR, 0.5 μg of total RNA was first reverse-transcribed using the Superscript II reverse transcriptase (Invitrogen) according the manufacturer's recommendations. Then, cDNA targets were amplified in triplicate wells using the MESABlue qPCR MasterMix Plus for SYBR Assay w/fluorescein kit (Eurogentec) according to the manufacturer's protocol and run on the iCycler iQ detection system (Bio-Rad SA, Marnes-la-Coquette, France) with the following thermal profile: an initial step of 3 min at 95 °C, followed by 40 cycles each consisting of 15 s at 95 °C and 1 min at 60 °C in a volume of 25 μL. PCR products were checked by monitoring melting curves. For data analysis, the fluorescent signals were normalized using the reference gene, LDHA. Relative quantification, following the ΔΔCt method(46) was applied to compare amounts of mRNA in healthy and dystrophic muscles. The average of gene level ratios in healthy conditions was normalized to 1. The average of gene level ratios in dystrophic muscles was expressed relatively to healthy conditions. Then, for each target gene, a statistical analysis was performed using Student's t test between healthy and dystrophic conditions.

Gene Ontology Annotation

Proteins identified as deregulated by the ICAT analyses were annotated using terms from the Gene Ontology (GO).(47) ENSEMBL protein identifiers, validated output from SEQUEST, were mapped to NCBI RefSeq identifiers and then to their corresponding Entrez Gene identifiers.(48) Because of the lack of systematic functional annotation for

dog proteins, the annotations were transferred from the corresponding human orthologs, as determined by using the Homologene database.(49)

Results

In this study, the GRMD dog model was used to profile changes in protein abundance associated with DMD. Histological analysis of a 4-month old GRMD dog based on H&E staining revealed classical pathological changes of DMD including fiber size variation, fiber splitting, and central nucleation (Figure 1). Given the importance of protein phosphorylation in signaling pathways, it is not surprising that dysregulation of protein kinases and phosphatases had been linked to a vast number of pathologies, including neuromuscular disorders. To eliminate the structural and contractile proteins that are overabundant in crude protein extracts prepared from skeletal muscle, and to enrich the samples for signaling proteins,(19, 50) we restricted our analysis to the cytosolic and phospho-enriched proteins. A proteomic study, consisting of isotope-coded affinity tagging, was conducted separately on these two fractions.

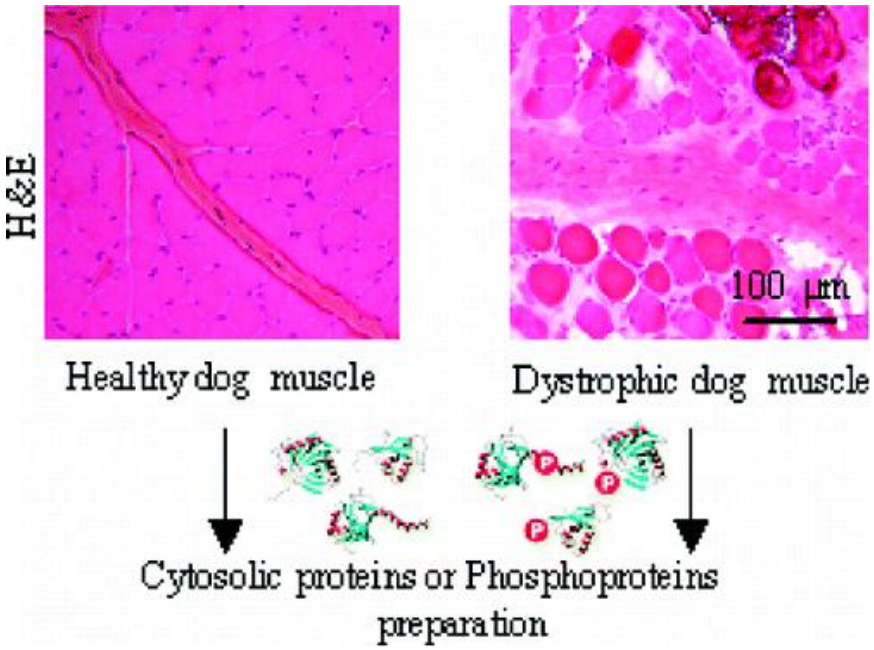

Figure 1. H&E (hematoxylin and eosin) staining showing classical pathological changes of DMD, including fiber size variation, fiber splitting, and central nucleation in skeletal muscle.

Quantitative Analysis of Dystrophic Muscle Protein Profile Using cICAT Technology

To identify global protein perturbations present in GRMD dog muscle, cytosolic and phosphoprotein-enriched protein extracts from dystrophic and healthy muscles were prepared, labeled with cICAT reagents (12C9 and 13C9), and submitted to cICAT-MS/MS analysis. From the cytosolic extracts, 337 unique cICAT-labeled peptides were identified. After database searching (SEQUEST(40)), validation (PeptideProphet & ProteinProphet(51)), and quantification (ASAP(44)) followed by manual correction, a total of 88 cytosolic proteins were identified with a probability higher than 0.9 of being true positives (Supplementary Tables 1a and 2). Among these, 61 appeared to be differentially expressed in dystrophic muscle, with 30 proteins being overrepresented (Table 1a) and 31 underrepresented (Table 2a). The experiment with the phosphoprotein-enriched fractions led to the identification of a total of 122 unique peptides, corresponding to 63 different proteins, of which 40 had not been identified in the cytosolic extract (see Supplementary Tables 1b and 3 for additional details). Among these 63 proteins, 36 display quantitative changes in the dystrophic muscle, with 18 being overrepresented (Table 1b) and 18 being underrepresented (Table 2b) compared to healthy muscle. The PhosphoProtein Purification Kit enables a separation of the phosphorylated from the nonphosphorylated protein fraction. The affinity chromatography procedure reduces sample complexity and greatly facilitates analyses of low-abundance proteins. The experiment performed with the phospho-enriched samples led to the identification of 36 proteins differentially regulated between healthy and GRMD muscles (Tables 1b and 2b). Among these proteins, 31 had been previously described as phosphoproteins (Swiss-Prot and PhosphoSite databases), giving a good indication of the efficiency and the reliability of the purification method applied. For the other five, CSRP3, MYBPH, MYL6B, CYC1, CA3, no information relative to phosphorylation have

been reported to date. It should be noted that a quantitative changes in the phospho-enriched fractions can result either from a difference in the amount of a protein or in its phosphorylation status.

Interestingly, 5 proteins identified by ICAT were also detected by 2-D/MS approach (Supplemental Figure 1). Moreover, among the proteins identified in the ICAT experiment, 6 were chosen for an analysis by Western immunoblot: LDHA, COF-2, DJ-1 (PARK7), PKM2, TUB and PP1 (Figure 2A,B). These six proteins displayed expression patterns similar to the ICAT ratios (Figure 2C). Indeed, we could confirm that PP1 and the tubulin α are overrepresented in dystrophic muscle, and that cofilin 2 and DJ-1 (PARK7) are underrepresented, while the level of LDHA remains similar between the two samples. In addition, we also confirmed by Western blot that PKM2, a protein with a ICAT log2 ratio (GRMD/Healthy) of −0.33 (ICAT and Western blot ratios GRMD/Healthy, respectively, 0.79 and 0.65) is detected at lower levels in GRDM muscle (Supplemental Table 1a,b, and Figure 2). While we have chosen a stringent cutoff of log2 ratio ±0.5 to identify proteins that are differentially represented in dystrophic muscle, proteins described in Tables 1 and 2 can be considered as potential candidates for quantitative changes between healthy and GRMD muscle.

Table 1. Overrepresented Proteins in Dystrophic versus Healthy Dog Muscle Protein Extract[a]

symbol	protein name	log2 ratio GRMD/Healthy
	(a) Cytosolic Protein Sample	
MTPN	Myotrophin	Only detected in GRMD sample
TPM4	Tropomyosin 4	Only detected in GRMD sample
CKMT2	Creatine kinase, mitochondrial 2	3.06
A1AG1	similar to Alpha-1 acid glycoprotein	2.25
CSRP3	Cysteine and glycine-rich protein 3	1.72
CLIC4	Chloride intracellular channel 4	1.66
A1BG	Alpha-1-B glycoprotein	1.43
AHSG	Alpha-2-HS-glycoprotein	1.33
HSP90AA4P	Putative heat shock protein HSP 90-alpha A4	1.28
GSTP1	Glutathione S-transferase PI isozyme YD1-2YD1-2(IV-HB)	1.24
ANP32A	Acidic leucine-rich nuclear phosphoprotein 32 family	1.19
ALB	Serum albumin (allergen Can f 3)	1.10
CALR	Calreticulin	1.06
FETUB	Fetuin B	1.06
TUBA2	similar to tubulin, alpha 2 isoform 2	1.06
PDLIM3	PDZ and LIM domain 3	1.02
ANXA1	Annexin I	0.94
HPX	Hemopexin	0.90
ACTC	Cardiac actin	0.90
TPM2	Tropomyosin beta chain (Tropomyosin-2)	0.83
LGALS1	Lectin, galactoside-binding, soluble, 1 (galectin 1)	0.83
GOT1	aspartate aminotransferase 1	0.76
PLIN4	perilipin 4	0.76
MYL1	Myosin, light chain 1, alkali; skeletal, fast	0.76
ANXA2	Annexin A2	0.66
PFN1	profilin 1	0.63
TTN	Cardiac titin	0.63
PP1	Serine/threonine-protein phosphatase PP1-beta catalytic subunit	0.60
PGAM2	Phosphoglycerate mutase 2 (muscle)	0.57
TUBB2C	Tubulin, beta 2C	0.54
	(b) Phospho-Enriched Protein Sample	
TPM4	* Tropomyosin 4	Only detected in GRMD sample
MYL3	Myosin, light chain 3, alkali; ventricular, skeletal, slow	2.82
VIM	Vimentin-like protein	2.06
TUBB6	Tubulin, beta 6	1.66
TUBB2C	* Tubulin, beta 2C	1.52
LGALS1	* Lectin, galactoside-binding. soluble, 1 (galectin 1)	1.39
ALB	* Serum albumin (allergen Can f 3)	1.35
PCYT1A	Phosphate cytidylyltransferase 1, choline. alpha	1.12
CSRP3	* Cysteine and glycine-rich protein 3 (cardiac LIM protein)	1.12
MYBPH	Myosin binding protein H	0.99
MYH3	Developmental myosin heavy chain embryonic	0.96
TUBA2	* similar to tubulin, alpha 2 isoform 2	0.87
MYPN	Myopalladin	0.84
PTGES3	Prostaglandin E synthase 3 (cytosolic)	0.84
TPM2	Tropomyosin beta chain (Tropomyosin-2)	0.76
EEF1B2	Eukaryotic translation elongation factor 1 beta 2	0.68
MYL6B	Myosin, light chain 6B	0.66
BIN1	Bridging integrator 1	0.66

[a] Proteins were identified by ICAT-MS/MS in two experiments using *vastus lateralis* muscle from 4 month-old healthy and GRMD dogs. Two different experiments were performed, one with the cytosolic fraction (Healthy dog#1; GRMD dog#1: Table 1a), and the other one with a phospho-enriched protein sample (Healthy dog#2; GRMD dog#2: Table 1b). Shown here are the centered log2 ASAP ratios (GRMD/Healthy) of the 48 proteins (30 for the cytosolic protein sample and 18 for the phospho-enriched protein sample) that display changes in their abundance between healthy and dystrophic muscle. Asterisks (*) denote proteins identified in both experiment (cytosolic and phospho-protein enriched fractions). GRMD, Golden Retriever Muscular Dystrophy.

Table 2. Underrepresented Proteins in Dystrophic versus Healthy Dog Muscle[a]

symbol	name	log2 ratio GRMD/Healthy
	(a) Cytosolic Protein Sample	
PGK1	Phosphoglycerate kinase 1	−0.61
ACADS	Acyl-Coenzyme A dehydrogenase, C-2 to C-3 short chain	−0.62
ENO3	Enolase 3 (beta, muscle)	−0.70
GAPDH	Glyceraldehyde-3-phosphate dehydrogenase (GAPDH) (EC 1.2.1.12)	−0.70
ACO2	Aconitase 2, mitochondrial	−0.72
MYH3	Developmental myosin heavy chain embryonic	−0.72
UQCRC1	Ubiquinol-cytochrome c reductase core protein I	−0.74
ALDOA	Aldolase A	−0.74
ACADVL	Acyl-Coenzyme A dehydrogenase, very long chain	−0.77
MYH2	Myosin-2 (Myosin heavy chain 2)	−0.77
MYH7	Myosin-7 (Myosin heavy chain 7)	−0.77
MYH8	Myosin-8 (Myosin heavy chain 8)	−0.77
PGM1	Phosphoglucomutase 1	−0.79
CA3	Carbonic anhydrase III, muscle specific	−0.86
FABP4	Fatty acid binding protein 4, adipocyte	−0.88
FABP3	Fatty acid binding protein 3, muscle and heart	−0.92
MDH2	Malate dehydrogenase (EC 1.1.1.37)	−0.95
AK1	Adenylate kinase 1	−0.97
PRDX3	Peroxiredoxin 3	−1.00
PARK7	Parkinson disease (autosomal recessive, early onset) 7	−1.06
UQCRH	Ubiquinol-cytochrome c reductase hinge protein	−1.07
HSPB6	Heat shock protein, alpha-Crystallin-related. B6	−1.11
ATP2A2	Sarcoplasmic/endoplasmic reticulum calcium ATPase 2	−1.16
ATP5A1	similar to ATP synthase alpha chain, mitochondrial precursor	−1.19
MYLPF	Myosin regulatory light chain 2, skeletal muscle isoform	−1.22
GOT2	aspartate aminotransferase 2	−1.38
VDAC1	voltage-dependent anion channel 1	−1.51
CAMK2D	Calcium/calmodulin-dependent protein kinase (CaM kinase) II delta	−1.99
CKM	Creatine kinase M-type	−2.05
HP	Haptoglobin	−2.76
PFKM	6-phosphofructokinase, muscle type (Phosphofructokinase 1)	Only detected in Healthy sample
	(b) Phospho-Enriched Protein Sample	
PSMA3	Proteasome (prosome, macropain) subunit, alpha type, 3	−0.56
FLNC	* Filamin C, gamma (actin binding protein 280)	−0.60
CYC1	Cytochrome c-1	−0.61
CA3	* Carbonic anhydrase III, muscle specific	−0.62
TOMM70A	Translocase of outer mitochondrial membrane 70 homologue	−0.63
PRKAR2A	Protein kinase, cAMP-dependent. regulatory, type II, alpha	−0.79
ATP2A1	ATPase, Ca++ transporting, cardiac muscle, fast twitch 1	−0.80
PFKM	* 6-phosphofructokinase, muscle type (Phosphofructokinase 1)	−1.02
PRKAR1A	Protein kinase, cAMP-dependent, regulatory, type I, alpha	−1.15
MYH2	* Myosin-2	−1.21
ENO1	ENO1 enolase 1	−1.36
CKM	* Creatine kinase M-type	−1.47
PDHB	Pyruvate dehydrogenase (lipoamide) beta	−1.54
UQCRC1	* Ubiquinol-cytochrome c reductase core protein I	−1.59
MYOM3	Myomesin-3	−1.82
MYOT	Myotilin (Titin immunoglobulin domain protein)	−1.85
CFL2	Cofilin 2	−2.64
AMPD2	adenosine monophosphate deaminase 2	Only detected in Healthy sample

[a] Proteins were identified by ICAT-MS/MS in two experiments using *vastus lateralis* muscle from 4-month old healthy and GRMD dogs. Two different experiments were performed, one with the cytosolic fraction (Healthy dog#1; GRMD dog#1: Table 2a), and the other one with a phospho-enriched protein sample (Healthy dog#1; GRMD dog#1: Table 2b). Shown here are the centered log2 ASAP ratios (GRMD/Healthy) of the 49 identified proteins (31 in the cytosolic protein sample and 18 in the phospho-enriched protein sample) that display abundance changes between healthy and dystrophic muscle. Asterisks (*) denote proteins identified in both experiment (in the cytosolic and in the phopho-protein enriched fractions). GRMD, Golden Retriever Muscular Dystrophy.

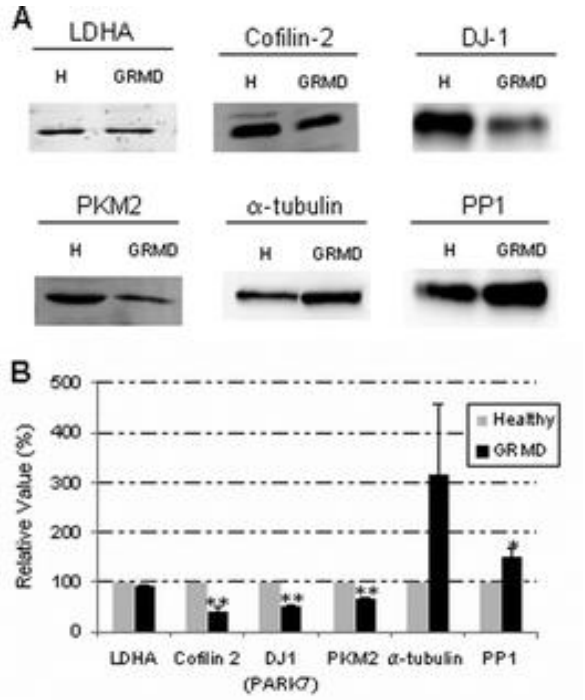

C

Protein Name Symbol	ICAT ratio GRMD/Healthy	WB ratio GRMD/Healthy
LDHA	1.11	0.92 ± 0.03
Cofilin-2	0.16	0.41± 0.09
DJ-1 (PARK7)	0.48	0.51 ± 0.04
PKM2	0.79	0.65± 0.04
α-tubulin	2.08	3.17±1.39
PP1	1.52	1.51±0.15

Figure 2. (A) Western immunoblot analyses. Representative images of immunoblots have been shown. Cytosolic proteins were separated by SDS-PAGE and the blotted proteins were revealed with specific antibodies. The results obtained confirm the increased expression level detected in dystrophic muscle for PP1 and the α-tubulin, and the decreased expression level detected for cofilin 2 and DJ-1 (no significant difference for LDHA and a low decreased expression for PKM2,). H, healthy; GRMD, Golden Retriever Muscular Dystrophy. (B) Graphical representation of the immunoblot analysis of proteins in dystrophic tissue. The histogram represents the relative level of LDHA, Cofilin 2, DJ-1, PKM2, α-tubulin, and PP1 in healthy and GRMD *vastus lateralis* muscle. The mean variation (n = 3) was calculated and the GRMD value was represented as a percentage of the healthy level taken as 100%; Statistical significance from t test analysis (StatELsoftware ; Excel, Microsoft): *$p < 0.05$; **$p < 0.02$ vs healthy conditions. (C) Quantitative MS and Western blot data Comparison of ICAT ratio and quantification of proteins described by Western blotting experiment.

Functional Annotation Analysis of Protein Changes between Healthy and Dystrophic Muscles

Proteins that are differentially represented between healthy and dystrophic muscle were grouped in functional classes according to the Gene Ontology (GO) terms of their human homologues according to “biological process” categories (Table 3). A background list of nonchanging proteins is presented in Supplementary Table 4. Through this functional annotation, the 84 proteins identified as significantly dysregulated in dystrophic muscle by the ICAT experiments (namely 61 proteins from the cytosolic fraction and 36 proteins from the phospho-enriched fraction, with an overlap of 13 proteins) were classified into 7 major categories including: (i) muscle development and contraction (31), (ii) glycolytic metabolism (14), (iii) oxidative metabolism (19), (iv) calcium ion homeostasis (6), (v) intracellular signaling (12), (vi) regulation of apoptosis (13), and (vii) other functions (15). GO annotation of the altered proteome led to several key findings which might reflect ongoing muscle regeneration taking place within dystrophic muscle. Importantly, our quantitative study using healthy and dystrophic samples allowed us to reveal important changes in the abundance of key proteins involved in these major metabolic pathways. The list of the GO categories obtained was similar to the list found in a study concerning the characterization of the human skeletal muscle proteome.(52) In this study, the authors identified all the enzymes participating in the major pathways of glucose and lipid metabolisms, a large number of proteins involved in mitochondrial oxidative phosphorylation and calcium homeostasis, and isoforms of the proteins that constitute the myofibrillar apparatus.

Table 3. Classification of the Proteins Identified by ICAT as Differentially Represented in the Healthy and Dystrophic Dog *Vastus Lateralis* Muscles, According to Their "Biological Process" GO Terms[a]

	lower expression in GRMD dog		higher expression in GRMD dog	
GO term biological process	cytosolic fraction	phospho-enriched fraction	cytosolic fraction	phospho-enriched fraction
muscle development and contraction	ALDOA, CAMK2D, MYH2, MYH7, MYH8, MYH3, MYLPF, CA3	ATP2A1, CA3, CFL2, FLNC, MYH2, MYOT,	ACTC, CKMT2, CSRP3, MYL1, PDLIM3, PFN1, PGAM2, TPM2, TPM4, TTN, TUBA2, TUBB2C	BIN1, CSRP3, MYBPH, MYH3, MYL3, MYL6B, MYPN, TPM2, TPM4, TUBB6, TUBB2C, TUBA2, VIM
glycolytic metabolism	ALDOA, AK1, CKM, ENO3, GAPDH, MDH2, PFKM, PGK1, PGM1, AK1,	CKM, ENO1, PDHB, PFKM	PGAM2, PP1	
oxidative metabolism	ACADS, ACADVL, GAPDH, MDH2, PARK7, PRDX3, UQCRC1, UQCRH, ACO2, ALDOA, ATP5A1, FABP3, FABP4	CYC-1, PDHB, PRKAR1A, PRKAR2A, UQCRC1	PGAM2, PP1	
calcium ion homeostasis	ATP2A2, CAMK2	ATP2A1	CALR, CSRP3, CLIC4	CSRP3
intracellular signaling	ATP2A2, PARK7	PRKAR1A, PRKAR2A	ANP32A, CALR, HPX, LGALS1, TTN, PP1, AHSG, FETUB	LGALS1
regulation of apoptosis	HSPB6, PRDX3, VDAC1,	ATP2A1	ACTC, ALB, ANXA1, ANXA2, CALR, GSTP1, LGALS1, HSP90, TUBB2C	ALB, LGALS1, TUBB2C
Other	GOT2, HP, NDUFAB1	AMPD2, PSMA3, TOMM70A,	MTPN, A1AG1, A1BG, AHSG, GOT1, PLIN4	PCYT1A, PTGES3, EEF1B2,

[a] Through this functional annotation, the 84 proteins identified as significantly dysregulated in dystrophic muscle by the ICAT experiments (namely 61 proteins from the cytosolic fraction and 36 proteins from the phospho-enriched fraction, with an overlap of 13 proteins) were classified into 7 major categories. A large proportion of these dysregulated proteins belong to muscle development and muscle metabolism including glycolytic and oxidative elements.

We detected a number of cytoskeletal microtubules components as being overrepresented in dystrophic muscle, such as myosin light chains (MYL6B, MYL1, MYL3). Other muscle structure and regeneration proteins were also overrepresented including, tubulin, tropomyosin, filamin, and titin (Table 3). Our study identified 5 key proteins of the glycolytic metabolic pathway as being underrepresented in dystrophic muscle: the pyruvate dehydrogenase, the phosphoglycerate kinase, the phosphoglucomutase, the enolase and the adenylate kinase (Table 3). Moreover, we identified alterations in the level of several proteins involved in Ca2+ homeostasis (Table 3). The ATPase Ca2+ transporting protein (ATP2A2) appeared under represented in dystrophic muscle, while proteins involved in Ca2+ translocation from the cytosol to the sarcoplasmic reticulum, and in Ca2+ homeostasis during muscle contraction, were found to be overrepresented (namely, chloride intracellular channel, calcium/calmodulin-dependent protein kinase and calreticulin) (Table 3). In addition, we observed an increased level of annexins A1 and A2 in healthy muscle (Table 3), suggesting a possible pathogenic contribution of these calcium-binding proteins.

Among the 12 proteins that are altered in dystrophic muscle and involved in intracellular signaling (Table 3), the protein phosphatase 1 (PP1) and the Parkinson's disease protein, DJ-1 (PARK7) appear particularly interesting. The PP1 phosphatase, present in skeletal muscle, is activated by the glycogen synthase kinase 3 (GSK3β) and DJ-1 has been recently described as a regulator of the tumor suppressor PTEN.(53, 54) The ICAT experiment revealed a higher abundance of PP1 in dystrophic muscle that could be confirmed by Western immunoblot analysis (Table 3, Figure 2). The drastic underrepresentation of DJ-1 detected by ICAT was later confirmed by Western immunoblot analysis (Table 3, Figure 2).

Decreased Protein Level and Altered Transcriptional Regulation of PGC-1α Targets

Interestingly, 30% of the proteins we found underrepresented in dystrophic muscle are coded by genes reported to be induced by the peroxisome proliferator-activated receptor-gamma coactivator-1 alpha (PGC-1α) in murine myoblasts(55) (data compiled from the Molecular Signature Database(56)) (Figure 3A). In the same study,(55) a modest reduction in the expression of PGC-1α in diabetic muscle was shown to be responsible for the mitochondrial deregulation observed in diabetes. Next, our hypothesis of an altered transcriptional regulation of PGC-1α and its downstream putative targets in dystrophic dog muscle was investigated by real-time RT-PCR. The expression of PGC-1α gene and of 4 downstream putative targets genes (ACADS, FABP3, CYC1 and PFKM) randomly chosen in the list of PGC-1α targets down-regulated at the protein level (Table 2, Figure 3A) were analyzed in RNA extracts from healthy and dystrophic dog muscles. As shown in Figure 3B, the down-expression of the PGC-1α gene (0.54 ± 0.08, p = 0.010) and its four target genes, ACADS (0.63 ± 0.17, p = 0.059), FABP3 (0.42 ± 0.10, p = 0.004), CYC1 (0.53 ± 0.11, p = 0.011) and PFKM (0.48 ± 0.18, p = 0.039) is significantly validated.

A

Gene Symbol	Description
PGK1	phosphoglycerate kinase 1
PFKM	phosphofructokinase, muscle
PKM2	pyruvate kinase, muscle
MDH2	malate dehydrogenase 2
PGM1	phosphoglucomutase 1
PRDX3	peroxiredoxin 3
ACO2	aconitase 2, mitochondrial
ATP5A1	ATP synthase, H+ transporting
CYC1	cytochrome c-1
FABP3	fatty acid binding protein 3
UQCRC1	ubiquinol-cytochrome c reductase
ACADS	acyl-Coenzyme A dehydrogenase
AK1	adenylate kinase 1

Putative PGC 1alpha related genes

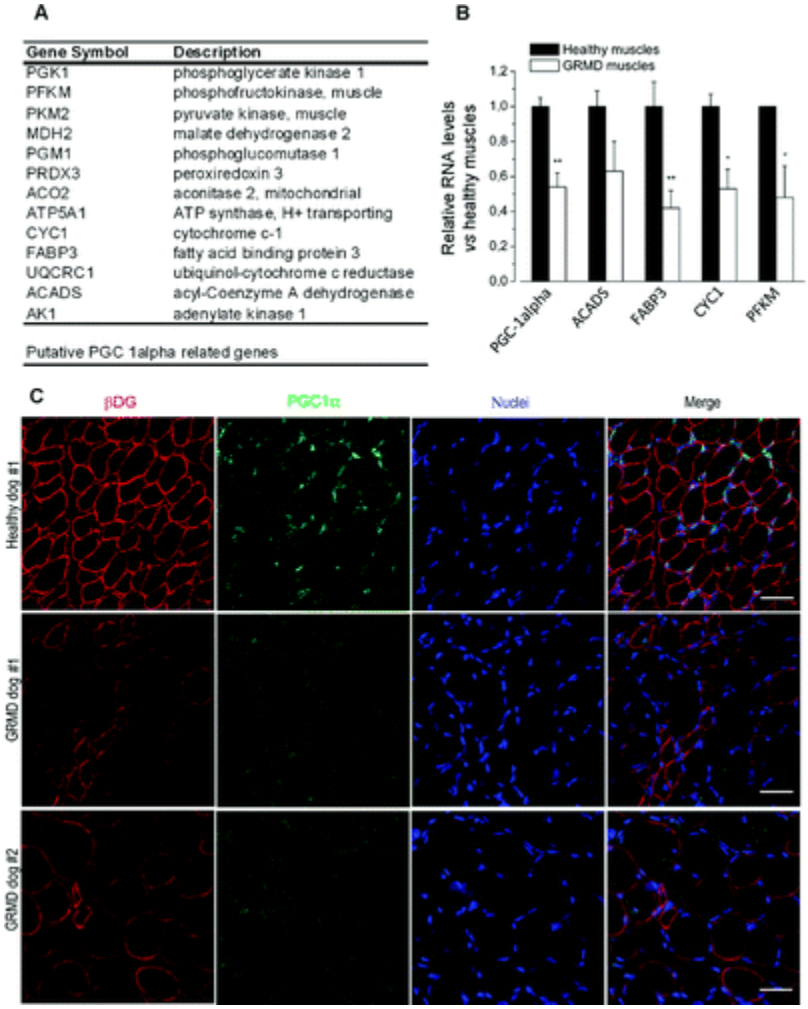

Figure 3. Decrease protein level and altered transcriptional regulation of PGC-1α targets in GRMD dog muscle. (A) Set of proteins underrepresented in dystrophic muscle identified as PGC-1α targets. (B) Relative level of PGC-1α gene and of selected target genes in healthy and dystrophic dog muscles by quantitative RT-PCR. Data are means ± SEM of 2 individual healthy and 3 individual GRMD dogs. Statistical significance from *t* test analysis: **p* < 0.05; ***p* < 0.01 vs healthy conditions. The LDHA gene was used as an internal reference gene. (C) Immunofluorescence analysis of PGC-1α for muscle sections from healthy and GRMD dogs. β-Dystroglycan, plasma membrane marker (red fluorescence); PGC-1α (green fluorescence); nuclei stained (blue fluorescence); and merge. Scale bar: 40 µm. A strong fluorescent labeling is visible in healthy muscle at the periphery of muscle fibers, whereas a fall in the intensity for PGC-1α staining was observed in the dystrophic dogs sample.

This suggested to us that PGC-1α might as well be down-regulated in the dystrophic dog muscle. To test this hypothesis, we chose to perform an immunofluorescence experiment because of the low basal levels of this protein. In healthy dog muscle section, PGC-1α labeling was observed in subsarcolemmal as well as endomysial nuclei. In dystrophic muscle, the same expression profile was observed albeit with a lower intensity (Figure 3C), confirming that the PGC-1α protein is underrepresented in dystrophic muscle. The immunolocalization data (Figure 3C) show that hypertrophied and large fibers do not display subsarcolemmal expression for PGC-1α. This label seems to concern cluster of small fibers.

Taken together, these results strongly indicate that the decreased protein levels of PGC-1α and of its downstream targets in dystrophic muscles arise from a transcriptional alteration (Figure 3). This alteration could play an important role in DMD and, as such, might represent a potential therapeutic target.(35, 57, 58)

Discussion

The precise molecular mechanisms that define the pathogenesis of DMD are not yet fully understood, hampering the development of palliative treatments and interventions that may slow down disease progression. In this perspective, high-throughput technologies, such as microarray-based gene expression profiling, have been recently applied to human biopsies.(52, 59, 60) These studies revealed that the expression level of genes involved in key metabolic pathways differ significantly between healthy and DMD muscles (105 and 618 genes were, respectively, identified). On the other hand, proteomic studies performed during the past few years have demonstrated that mass-spectrometry-based technologies can be employed to study skeletal muscle proteins. Recently, 1D-gel electrophoresis and HPLC−ESI−MS/MS was used to characterize the proteome of healthy human skeletal muscle.(52) This study provides the most comprehensive proteome coverage of human skeletal muscle. Protein expression profiling thus appears as an effective approach to define the biochemical cascades that underlie the progressive pathophysiology of DMD. The proteomic analysis that we performed using the clinically relevant GRMD dog model indeed allowed us to gain additional insight into the biochemical basis of the disease. Of the 127 proteins identified in the present study using vastus lateralis canine muscle, 101 were also detected in the Hojlund study.(52) Studies using 2D-gel electrophoresis and MS had already been applied to the proteomic profiling of young and aged mdx versus healthy skeletal muscle and diaphragm.(22, 24, 31) The proteomics findings resulting from these studies support the pathobiochemical concept that deficiency in dystrophin results in abnormalities in glycolysis, fatty acid oxidation and ion homeostasis pathways. Many proteins involved in mitochondrial function and energy metabolism were found to be altered. Of interest, our data indicated that several proteins such as adenylate kinase, PP1 phosphatase, annexin, carbonic anhydrase, and aldolase were also differentially expressed in

dystrophic versus healthy dog muscle, suggesting that generalized mitochondrial dysfunction and metabolism crisis are a characteristic common to dystrophic muscles from different animal model. More recently, the combination of proteomics, metabolomics, and fluoximics has confirmed the existence in the mdx mouse model of DMD of perturbations that reflect mitochondrial energetic alterations.(61) The broad aim of these studies has been twofold, first the identification of cofounding factors that promote or limit the disease progression and second, the identification of new biomarkers that could be used to more accurately define disease status. Our study is in keeping with this perspective, and the results obtained are discussed in details hereafter.

Glycolytic and Oxidative Metabolism

The most striking observation made during this study was the dramatic alteration of metabolic proteins in dystrophic dog muscle. Several key enzymes of energy metabolism appeared underrepresented in dystrophic versus healthy dog muscle, including proteins that control both glycolytic and oxidative metabolism. The altered glycolytic enzymes included adenylate kinase, a change previously noted in the mdx mouse model(62) and in human patients.(63) Nevertheless, the most profound alterations were noted for a cohort of mitochondrial proteins, which again reinforces the concept that basal metabolic function is perturbed in the dystrophic muscle environment. In an interesting manner, it has been estimated that 22% of the proteins detected in human skeletal muscle could be attributed to the mitochondrion(52) and decreased energy production, mitochondrial swelling, and abnormalities were described as a secondary feature of muscular dystrophy in the mdx mouse model.(64, 65)

Among the 45 proteins that we identified as underrepresented in dystrophic dog muscle (4 proteins are identified in both cytosolic and phospho-enriched protein samples), 13 has been described as regulated at the transcriptional level by the co-activator PGC-1α

(Figure 3A and ref 56). We were able to show that PGC-1α itself was present at a lower level in dystrophic dog muscle, strongly suggesting that the reduction in the PGC-1α-regulated transcriptome may originate from a reduction in its expression level (Figure 3C). Of interest, among the PGC-1α targets that we identified as underrepresented in dystrophic dog muscle (Figure 3A), 5 (namely, PFKM, PGM1, ACO2, CYC1, and FABP3) had already been identified in a transcriptomic study as expressed at lower level in DMD versus healthy human biopsies.(60) PGC-1α has been described as a potent regulator of mitochondrial biogenesis and oxidative metabolism in skeletal muscle.(66, 67) In addition, activation of the peroxysome proliferator-activated receptor (PPAR)/PGC-1α pathway has been shown, by preventing the bioenergetic deficit observed, to efficiently improve a mitochondrial myopathy phenotype,(68) suggesting that PGC-1α mediated improvement of dystrophic muscle may rely (in part) on the restoration of PGC-1α mitochondrial targets.(69) Interestingly, a recent study has shown that pharmacologic activation of peroxisome proliferator-activated receptor (PPAR) β/δ also leads to an upregulation in the expression of utrophin A, which was concurrent with a partial correction of the dystrophic phenotype.(70) As such, enhancing the expression of PGC-1α may present a multilevel advantage to improve the dystrophic muscle phenotype.

Calcium Signaling and Trafficking

We found that a number of proteins involved in Ca2+ translocation and homeostasis, namely, chloride intracellular channel, calcium/calmodulin-dependent protein kinase, and calreticulin as well as some forms of annexins were overrepresented in dystrophic versus healthy dog muscle (Table 3). The increased expression of calcium-handling proteins is likely to be a compensatory response to the altered calcium dynamics observed in dystrophic muscle fibers. Indeed, when dystrophin is absent from muscle, a

natural membrane resealing process occurs; Ca2+ leak channels are introduced into the sarcolemma, causing an elevation of cytosolic Ca2+.(23) The elevation of proteins involved in calcium homeostasis and trafficking observed in dystrophic dog muscle could be part of this mechanism. As far as the annexins are concerned, a study performed in the mouse model of dysferlinopathy, another muscular pathology that includes the Limb Girdle Muscular Dystrophy type 2B, had already shown that annexin A1 and A2 interact with dysferlin and the proteins had been described as potential muscular dystrophy genes.(71) Annexins form a diverse family of Ca2+-dependent phospholipid binding proteins widely distributed that are involved in a variety of processes, including membrane scaffolding, trafficking and organization of vesicles, exocytosis, endocytosis, and calcium ion channel formation. The increased level of annexins detected in dystrophic versus healthy dog muscle may reflect an adaptation to the altered calcium concentrations and the continual sarcolemmal disruptions observed in these circumstances.

Intracellular Signaling

Lastly, we identified alterations in a number of key signaling proteins in dystrophic muscle. Notably, our ICAT analysis revealed a strong increase in the level of the PP1 protein in dystrophic dog muscle, which was confirmed by Western immunoblot (Table 1 and Figure 2). In skeletal muscle, PP1 is known to regulate both glycogen and fatty metabolism,(72) while promoting the dephosphorylation of myosin.(73) Interestingly, a constitutive activation of PP1 had been reported previously in mdx skeletal muscle, and attributed to the enhanced protein turnover that occurs during ongoing muscle damage,(31, 54) suggesting that the increased level of PP1 that we also observed in dystrophic dog muscle may represent a conserved feature in DMD animal model. We also detected a drastic underrepresentation of the DJ-1 protein in dystrophic versus

healthy dog muscle (also called PARK7). This Parkinson's disease-associated protein was recently described as a negative regulator of the tumor suppressor PTEN, a phosphatase involved in the regulation of the PI3K/Akt pathway.(53) In a previous study,(19) we showed that PTEN is overrepresented and more active in dystrophic versus healthy dog muscle, leading to a decreased phosphorylation of Akt and the downstream kinases GSK3β and p70S6K. Other studies performed in the mdx mouse model and in human biopsies had already described an alteration of the PI3K/Akt signaling pathway in the dystrophic muscle,(17, 74, 75) and it has been shown that increasing Akt activity by transgenic overexpression of the activated kinase itself can reverse the dystrophic phenotype.(20, 76) Given the role of DJ-1 in the regulation of the PTEN phosphatase, the results presented here suggest that PTEN activation in dystrophic dog muscle may originate from the underexpression of DJ-1. Noteworthy, in addition to its role in PTEN's regulation, DJ-1 also promotes the activity of PGC-1α.(77) As such, DJ-1 sensitive signaling pathways may provide high priority targets for the development of novel drug therapies for DMD.

Summary

We used the ICAT/MS technology to map and identify clinically relevant alterations in the proteomic signature of dystrophic dog muscle. We were able to identify differences in the representation of key proteins between healthy and GRMD skeletal muscles, supporting the hypothesis that secondary changes may play an active role in muscular dystrophy. Our observations provide the first evidence of a dysregulation of the co-activator PGC-1α in dystrophic dog muscle, an alteration that may be at the origin of the general metabolic crisis that characterizes the disease. Taken together, these results suggest that the restoration of metabolic control may offer a novel treatment regime to attenuate dystrophic muscle damage.

Acknowledgment

We gratefully acknowledge Dr. Lawrence Puente, from the Stem Core Facility for his technical support, Gareth Palidwor for bioinformatics support on the TPP and Gwenina Cueff for technical assistance in mRNA extraction. This work was supported by funding from the AFM (Association Française contre les Myopathies), No. 14033 to L.G. and by funding from The Muscular Dystrophy Association USA to L.A.M. L.A.M. holds the Mach-Gaensslen Chair in Cardiac Research. M.B. holds the Canadian Research Chair in the Regulation of Gene Expression.

Supporting Information

Supplementary tables and figures. This material is available free of charge via the Internet at http://pubs.acs.org.proxy.bib.uottawa.ca.

Supplemental data

Experimental procedure

Two-dimensional gels and mass spectrometry. Samples were diluted in isoelectric focusing buffer (7M urea, 2M thiourea, 4% CHAPS, 1% DTT), absorbed into 17 cm ReadyStrip™ IPG strips (Bio-Rad Laboratories, Hercules, CA), and separated with a pH range of 4 to 7 following the manufacturer's instructions. Amounts of 200 mg of cytosolic proteins and 30 mg of phosphoproteins were used. Isoelectric focusing was performed on a Protean IEF Cell (Bio-Rad Laboratories) with the following program: 200 V for 1 hour, 500 V for 1 hour, 5000 V ramp for 5 hours and 5000 V until it rate up to 80,000 VH. For the second dimension, IPG strips were overlaid onto 10% SDS-PAGE gels and electrophoresed with the Protean II apparatus (Bio-Rad Laboratories). SDS-PAGE gels were fixed in a 10% methanol and 7% acetic acid solution for 30 minutes, before being stained with Sypro Ruby protein gel stain (Sigma-Aldrich) overnight at room temperature under agitation. Thereafter, gels were washed in a fixing solution for 30 min, and imaged on an AlphaImagerTM (AlphaInnotech, San Leandro, CA). Each experiments samples (healthy and GRMD) were ran independently repeated 3 times for the cytosolic experiment and 2 times for the phosphoprotein experiment due to sample availability, and representative 2-D gels were used for the figure 2 and to excise protein spots. In-gel digests were performed using a standard method 33. Briefly, sample cleanup was performed using ZipTip (Millipore Corporation, Billerica, MA). Tandem mass spectra were collected on an Applied Biosystems/SciEX QSTAR XL with oMALDI2 ion source. Spectra were analyzed using Mascot 2.0 (Matrix Science, UK) and the NCBI non-redundant protein sequence dog database (release 2008.03.28; 34217 sequences). MS/MS tolerance was ±0.2 Da. SYPRO Ruby-stained gels were analyzed with PDQuest software (Version 8.0, Bio-Rad Laboratories) for gel-to-gel matching and identifying

differences between dystrophic and healthy dog muscle samples. The gel images were normalized in the PDQuest software using the local regression model to even out differences in staining intensities between gels. Each matched protein spot was assigned a unique SSP (sample spot protein) number in the PDQuest software. A minimum of 1.42-fold change was considered for the up-regulated proteins and 0.7-fold for down-regulated proteins.

Result

2-D gel-based proteomic analysis revealed differentially expressed proteins in canine dystrophic muscle. To identify protein changes associated with DMD, two-dimensional (2-D) gel analysis coupled with mass spectrometry was performed on the *Vastus lateralis* muscle removed from 4-month-old healthy and dystrophic dogs. In the experiment using the crude cytosolic fraction of muscle (Figure 1A), 146 protein spots were detected by PDQuest, of which 95 corresponded to differentially expressed proteins. Among these, 5 were chosen (spots 1-5, Figure 2A-top panel), according to their high level of dysregulation, for further identification by mass spectrometry (Figure 1B). Peptides were searched against the protein database using SEQUEST. Among the 5 proteins identified, 2 are involved in contractile function (a-tubulin 1 and 2; spots 1 and 5, respectively), 2 are serum proteins (haptoglobin and serum albumin; spots 2 and 4, respectively) and 1 is a mitochondrial protein involved in energy metabolism (ubiquinol cytochrome c reductase, spot 3). Following the same procedure, 36 protein spots were detected in the phospho-enriched samples, among which 20 showed a differential abundance in dystrophic *vs* healthy dog muscle (Figure 1A-bottom panel). Three spots that showed consistent dysregulation between the 2 experiments and had a great fold-change difference between healthy and GRMD were further processed for identification

by mass spectrometry (Figure 1B). This led to the identification of another skeletal muscle marker involved in the contractile function
(tropomyosin 4, spot 8), and 2 proteins involved in chaperone functions (heat shock proteins 70 and 27; spots 6 and 7, respectively). Of interest, these 3 proteins (TPM4, HSP70, HSP27) have been described in the literature as phosphoproteins (PhosphoSite database).

Figure legend

Supplemental figure 1: Two-dimensional gel electrophoretic comparison between normal and GRMD dog muscles

A- 2-D gel analysis of cytosolic- and phospho-proteins. Spots excised and identified by MS are encircled. Proteins were detected by Sypro Ruby protein gel staining. Isoelectric focusing was performed over a pH range of 4-7. Healthy and dystrophic samples are represented on the left and right panels, respectively. Top panel: cytosolic-proteins; bottom panel: phosphoproteins. **B-** MS identification of proteins differentially expressed in dystrophic dog muscle. Stained gels were matched and analyzed with the PDQuest software. Eight proteins detected as differentially expressed in dystrophic dog muscle were then identified by MS. Spectra were analyzed using Mascot and the NCBI non-redundant protein sequence database. MS/MS tolerance was ±0.8 Da. * protein identified by 2D gels and ICAT analysis.

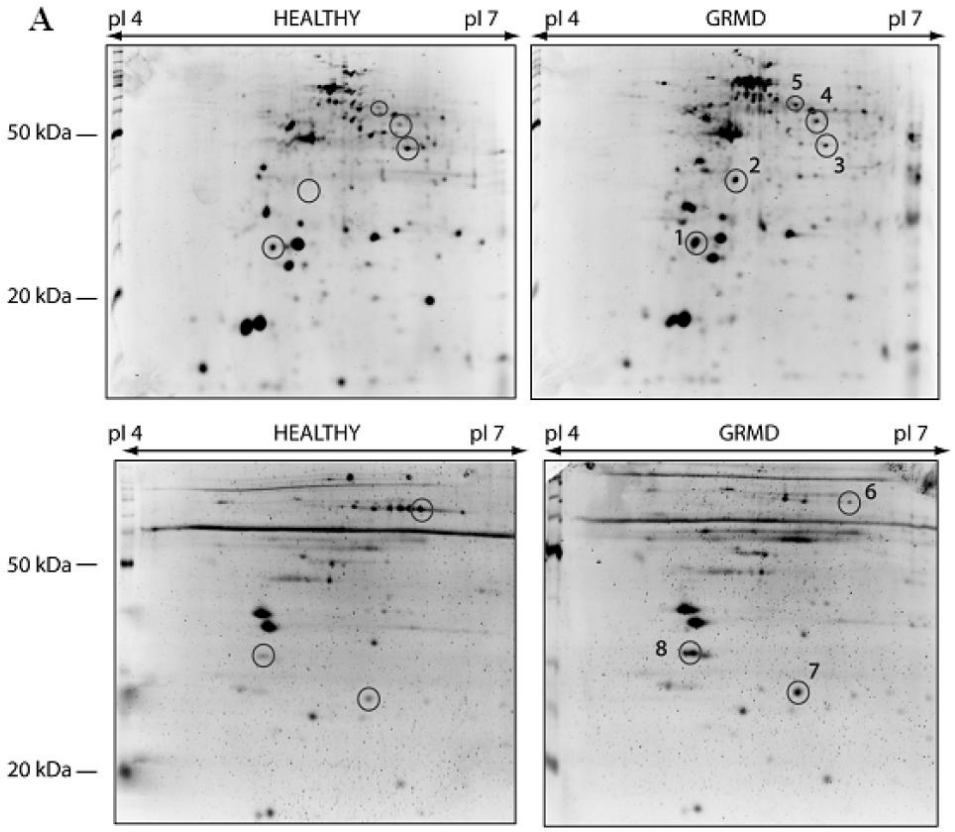

B

Spot no.	Identity	accession no.	Score/ No.uniq peptides matched	Coverage (%)	Theoretical pI/molecular mass(Da)	Normalized spotquantitation ratio H/G	ICAT data ratio H/G	ICAT data log2 ratio H/G
1	similarto Tubulin alpha 1isoform	XP_849601	173/5	13	6.8/20.5	0.42	n.d	
2*	Haptoglobinprecursor isoform 2	XP_850996	325/7	25	5.8/38.3	Only in healthy	4.49	6.18
3*	similarto ubiquinol cytochrome creductase	XP_851209	173/7	19	6.04/52.7	1.35	1.49	2.10
4*	Serumalbumin	XP_855557	464/11	16	5.51/68.5	0.49	0.36	0.47
5*	Tubulinalpha 2	XP_851095	5443/13	33	5.04/57.4	0.36	0.5	0.48
6	Heatshock70kDa protein1B	Q27965	101/5	9	5.68/70.1	0.2	n.d	
7	Heatshock27kDa protein1	NP_001007519	143/4	16	6.23/22.9	0.71	n.d	
8*	Tropomyosin4	NP_003281	104/3	14	4.67/28.5	0.19	Only in GRMD	

Supplementary Table 1: Quantitative pattern of proteins identified in the ICAT experiment. Relative quantification of proteins (Light-labelled *versus* Heavy-labelled) was performed within the TPP using the ASAP ratio program. Shown here are the ICPL abundance ratio (dystrophic *versus* healthy dog muscle) of the 88 cytosolic proteins (a) and 63 phosphoenriched proteins (b) that were identified. For additional data, see supplementary Tables 2 and 3.* proteins identified in both experiment (cytosolic and phopho-protein enriched fractions).

References

(1) Emery, A. Duchenne Muscular Dystrophy: Oxford University Press: Oxford, 1993; Vol. 24.

(2) Hoffman, E. P.; Brown, R. H., Jr.; Kunkel, L. M. Dystrophin: the protein product of the Duchenne muscular dystrophy locus. Cell 1987, 51 (6), 919–928.

(3) Koenig, M.; Hoffman, E. P.; Bertelson, C. J.; Monaco, A. P.; Feener, C.; Kunkel, L. M. Complete cloning of the Duchenne muscular

(42) Nesvizhskii, A. I.; Aebersold, R. Analysis, statistical validation and dissemination of large-scale proteomics datasets generated by tandem MS. Drug Discovery Today 2004, 9 (4), 173–181.

(43) von Haller, P. D.; Yi, E.; Donohoe, S.; Vaughn, K.; Keller, A.; Nesvizhskii, A. I.; Eng, J.; Li, X. J.; Goodlett, D. R.; Aebersold, R.; Watts, J. D. The application of new software tools to quantitative protein profiling via isotope-coded affinity tag (ICAT) and tandem mass spectrometry: II. Evaluation of tandem mass spectrometry methodologies for large-scale protein analysis, and the application of statistical tools for data analysis and interpretation. Mol. Cell. Proteomics 2003, 2 (7), 428–442.

(44) Li, X. J.; Zhang, H.; Ranish, J. A.; Aebersold, R. Automated statistical analysis of protein abundance ratios from data generated by stable-isotope dilution and tandem mass spectrometry. Anal. Chem. 2003, 75 (23), 6648–6657.

(45) Matsumura, K.; Tome, F. M.; Collin, H.; Leturcq, F.; Jeanpierre, M.; Kaplan, J. C.; Fardeau, M.; Campbell, K. P. Expression of dystrophin-associated proteins in dystrophin-positive muscle fibers (revertants) in Duchenne muscular dystrophy. Neuromuscular Disord. 1994, 4 (2), 115–120.

(46) Yuan, J. S.; Reed, A.; Chen, F.; Stewart, C. N., Jr. Statistical analysis of real-time PCR data. BMC Bioinf. 2006, 7, 85.

(47) Ashburner, M.; Ball, C. A.; Blake, J. A.; Botstein, D.; Butler, H.; Cherry, J. M.; Davis, A. P.; Dolinski, K.; Dwight, S. S.; Eppig, J. T.; Harris, M. A.; Hill, D. P.; Issel-Tarver, L.; Kasarskis, A.; Lewis, S.; Matese, J. C.; Richardson, J. E.; Ringwald, M.; Rubin, G. M.; Sherlock, G. Gene ontology: tool for the unification of biology. The Gene Ontology Consortium. Nat. Genet. 2000, 25 (1), 25–29.

(48) Maglott, D.; Ostell, J.; Pruitt, K. D.; Tatusova, T. Entrez Gene: gene-centered information at NCBI. Nucleic Acids Res. 2007, 35 (Database issue), D26–31.

(49) Sayers, E. W.; Barrett, T.; Benson, D. A.; Bryant, S. H.; Canese, K.; Chetvernin, V.; Church, D. M.; DiCuccio, M.; Edgar, R.; Federhen, S.; Feolo, M.; Geer, L. Y.; Helmberg, W.; Kapustin, Y.; Landsman, D.; Lipman, D. J.; Madden, T. L.; Maglott, D. R.; Miller, V.; Mizrachi, I.; Ostell, J.; Pruitt, K. D.; Schuler, G. D.; Sequeira, E.; Sherry, S. T.; Shumway, M.; Sirotkin, K.; Souvorov, A.; Starchenko, G.; Tatusova, T. A.; Wagner, L.; Yaschenko, E.; Ye, J. Database resources of the National Center for Biotechnology Information. Nucleic Acids Res. 2009, 37 (Database issue), D5–15.

(50) Puente, L. G.; Borris, D. J.; Carriere, J. F.; Kelly, J. F.; Megeney, L. A. Identification of candidate regulators of embryonic stem cell differentiation by comparative phosphoprotein affinity profiling. Mol Cell Proteomics 2006, 5 (1), 57–67.
(51) Han, X.; Gross, R. W. Quantitative analysis and molecular species fingerprinting of triacylglyceride molecular species directly from lipid extracts of biological samples by electrospray ionization tandem mass spectrometry. Anal. Biochem. 2001, 295 (1), 88 100.

(52) Hojlund, K.; Yi, Z.; Hwang, H.; Bowen, B.; Lefort, N.; Flynn, C. R.; Langlais, P.; Weintraub, S. T.; Mandarino, L. J. Characterization of the human skeletal muscle proteome by one-dimensional gel electrophoresis and HPLC-ESI-MS/MS. Mol. Cell. Proteomics 2008, 7 (2), 257–267.

(53) Kim, R. H.; Peters, M.; Jang, Y.; Shi, W.; Pintilie, M.; Fletcher, G. C.; DeLuca, C.; Liepa, J.; Zhou, L.; Snow, B.; Binari, R. C.; Manoukian, A. S.; Bray, M. R.; Liu, F. F.; Tsao, M. S.; Mak, T. W. DJ-1, a novel regulator of the tumor suppressor PTEN. Cancer Cell 2005, 7 (3), 263–273.

(54) Villa-Moruzzi, E.; Puntoni, F.; Marin, O. Activation of protein phosphatase-1 isoforms and glycogen synthase kinase-3 beta in muscle from mdx mice. Int. J. Biochem. Cell Biol. 1996, 28 (1), 13–22.

(55) Mootha, V. K.; Lindgren, C. M.; Eriksson, K. F.; Subramanian, A.; Sihag, S.; Lehar, J.; Puigserver, P.; Carlsson, E.; Ridderstrale, M.; Laurila, E.; Houstis, N.; Daly, M. J.; Patterson, N.; Mesirov, J. P.; Golub, T. R.; Tamayo, P.; Spiegelman, B.; Lander, E. S.; Hirschhorn, J. N.; Altshuler, D.; Groop, L. C. PGC-1alpha-responsive genes involved in oxidative phosphorylation are coordinately downregulated in human diabetes. Nat. Genet. 2003, 34 (3), 267–273.
(56) Subramanian, A.; Tamayo, P.; Mootha, V. K.; Mukherjee, S.; Ebert, B. L.; Gillette, M. A.; Paulovich, A.; Pomeroy, S. L.; Golub, T. R.; Lander, E. S.; Mesirov, J. P. Gene set enrichment analysis: a knowledgebased approach for interpreting genome-wide expression profiles. Proc. Natl. Acad. Sci. U.S.A. 2005, 102 (43), 15545–15550.

(57) Arany, Z. PGC-1 coactivators and skeletal muscle adaptations in health and disease. Curr. Opin. Genet. Dev. 2008, 18 (5), 426–434.

(58) Arnold, A. S. [PGC-1alpha controls neuromuscular junction and offers a novel therapeutic target in Duchenne dystrophy?]. Med. Sci. (Paris) 2007, 23 (11), 1034–1036.

(59) Haslett, J. N.; Sanoudou, D.; Kho, A. T.; Bennett, R. R.; Greenberg, S. A.; Kohane, I. S.; Beggs, A. H.; Kunkel, L. M. Gene expression comparison of biopsies from Duchenne muscular dystrophy (DMD) and normal skeletal muscle. Proc. Natl. Acad. Sci. U.S.A. 2002, 99 (23), 15000–15005.

(60) Pescatori, M.; Broccolini, A.; Minetti, C.; Bertini, E.; Bruno, C.; D'Amico, A.; Bernardini, C.; Mirabella, M.; Silvestri, G.; Giglio, V.; Modoni, A.; Pedemonte, M.; Tasca, G.; Galluzzi, G.; Mercuri, E.; Tonali, P. A.; Ricci, E. Gene expression profiling in the early phases of DMD: a constant molecular signature characterizes DMD muscle from early postnatal life throughout disease progression. FASEB J. 2007, 21 (4), 1210–1226.

(61) Griffin, J. L.; Des Rosiers, C. Applications of metabolomics and proteomics to the mdx mouse model of Duchenne muscular dystrophy: lessons from downstream of the transcriptome. Genome Med. 2009 1 (3), 32.

(62) Ge, Y.; Molloy, M. P.; Chamberlain, J. S.; Andrews, P. C. Proteomic analysis of mdx skeletal muscle: Great reduction of adenylate kinase 1 expression and enzymatic activity. Proteomics 2003, 3 (10), 1895–1903.

(63) Chen, Y. W.; Zhao, P.; Borup, R.; Hoffman, E. P. Expression profiling in the muscular dystrophies: identification of novel aspects of molecular pathophysiology. J. Cell Biol. 2000, 151 (6), 1321–1336.

(64) Kuznetsov, A. V.; Winkler, K.; Wiedemann, F. R.; von Bossanyi, P.; Dietzmann, K.; Kunz, W. S. Impaired mitochondrial oxidative phosphorylation in skeletal muscle of the dystrophin-deficient mdx mouse. Mol. Cell. Biochem. 1998, 183 (1 2), 87–96.

(65) Millay, D. P.; Sargent, M. A.; Osinska, H.; Baines, C. P.; Barton, E. R.; Vuagniaux, G.; Sweeney, H. L.; Robbins, J.; Molkentin, J. D. Genetic and pharmacologic inhibition of mitochondrial-dependent necrosis attenuates muscular dystrophy. Nat Med 2008, 14 (4), 442–447.

(66) Wu, Z.; Puigserver, P.; Andersson, U.; Zhang, C.; Adelmant, G.; Mootha, V.; Troy, A.; Cinti, S.; Lowell, B.; Scarpulla, R. C.; Spiegelman, B. M. Mechanisms controlling mitochondrial biogenesis and respiration through the thermogenic coactivator PGC-1. Cell 1999, 98 (1), 115–124.

(67) Lin, J.; Wu, H.; Tarr, P. T.; Zhang, C. Y.; Wu, Z.; Boss, O.; Michael, L. F.; Puigserver, P.; Isotani, E.; Olson, E. N.; Lowell, B. B.; Bassel-Duby, R.; Spiegelman, B. M. Transcriptional co-activator PGC-1 alpha drives the formation of slow-twitch muscle fibres. Nature 2002, 418 (6899), 797–801.

(68) Wenz, T.; Diaz, F.; Spiegelman, B. M.; Moraes, C. T. Activation of the PPAR/PGC-1alpha pathway prevents a bioenergetic deficit and effectively improves a mitochondrial myopathy phenotype. Cell Metab. 2008, 8 (3), 249–256.

(69) Handschin, C.; Kobayashi, Y. M.; Chin, S.; Seale, P.; Campbell, K. P.; Spiegelman, B. M. PGC-1alpha regulates the neuromuscular junction program and ameliorates Duchenne muscular dystrophy. Genes Dev. 2007, 21 (7), 770–783.

(70) Miura, P.; Chakkalakal, J. V.; Boudreault, L.; Belanger, G.; Hebert, R. L.; Renaud, J. M.; Jasmin, B. J. Pharmacological activation of PPAR stimulates utrophin A expression in skeletal muscle fibers and restores sarcolemmal integrity in mature mdx mice. Hum. Mol. Genet. 2009, 18, 4640–4649.

(71) Lennon, N. J.; Kho, A.; Bacskai, B. J.; Perlmutter, S. L.; Hyman, B. T.; Brown, R. H., Jr. Dysferlin interacts with annexins A1 and A2 and mediates sarcolemmal wound-healing. J. Biol. Chem. 2003, 278 (50), 50466–50473.

(72) Hubbard, M. J.; Cohen, P. On target with a new mechanism for the regulation of protein phosphorylation. Trends Biochem. Sci. 1993, 18 (5), 172–177.

(73) Dent, P.; MacDougall, L. K.; MacKintosh, C.; Campbell, D. G.; Cohen, P. A myofibrillar protein phosphatase from rabbit skeletal muscle contains the beta isoform of protein phosphatase-1 complexed to a regulatory subunit which greatly enhances the dephosphorylation of myosin. Eur. J. Biochem. 1992, 210 (3), 1037–1044.

(74) Dogra, C.; Changotra, H.; Wergedal, J. E.; Kumar, A. Regulation of phosphatidylinositol 3-kinase (PI3K)/Akt and nuclear factorkappa B signaling pathways in dystrophin-deficient skeletal muscle in response to mechanical stretch. J. Cell Physiol. 2006, 208 (3), 575–585.

(75) Lang, J. M.; Esser, K. A.; Dupont-Versteegden, E. E. Altered activity of signaling pathways in diaphragm and tibialis anterior muscle of dystrophic mice. Exp. Biol. Med. (Maywood, NJ, U.S.) 2004, 229 (6), 503–511.

(76) Blaauw, B.; Canato, M.; Agatea, L.; Toniolo, L.; Mammucari, C.; Masiero, E.; Abraham, R.; Sandri, M.; Schiaffino, S.; Reggiani, C. Inducible activation of Akt increases skeletal muscle mass and force without satellite cell activation. FASEB J. 2009, 23, 3896–3905.

(77) Zhong, N.; Xu, J. Synergistic activation of the human MnSOD promoter by DJ-1 and PGC-1alpha: regulation by SUMOylation and oxidation. Hum. Mol. Genet. 2008, 17 (21), 3357–3367.

6.5 Publication #5

Circulation Research. 2008; 103: 1202-1203

"B2 or not B2?"Kinin Receptors and Endothelial Progenitor Cell Dysfunction

Michael R. Ward, **Jessie Lavoie**, Duncan J. Stewart

From the St. Michael's Hospital (M.R.W.), University of Toronto; and Ottawa Health Research Institute (J.L., D.J.S.), University of Ottawa, Ontario, Canada.

Key Words: endothelial progenitor cells**,** myocardial infarction**,** cell therapy**,** bradykinin**,** risk factors

Copyrights

Contributions of the Candidate

I participated in the writing of this editorial.

The field of progenitor cell therapy appears to be poised to transform the management of many cardiovascular diseases. In particular, the use of bone marrow-derived mononuclear cells (BM-MNCs) and endothelial progenitor cells (EPCs) have shown indications of improved cardiac function post–myocardial infarction (MI), with a recent metaanalysis showing a highly significant mean improvement in global ejection fraction of 3% compared to control.1 The overall positive results from these early trials raise 2 important questions. The first is whether cell therapy really works, in other words, whether the results of these smaller trials, which generally enrolled less than 100 patients, will be reproducible in larger pivotal studies. A study currently being planned by Zeiher and colleagues (A.M. Zeiher, personal communication) will help answer this question. The second question is whether we can do better, either by selecting a more active subset of highly regenerative progenitor cells, or by enhancing progenitor cell activity before delivery. Several clinical studies exploring these strategies are already planned or underway, including our own ENACT-AMI (eNOS and Cell Therapy Ð Acute MI) trial. To inform further clinical studies, it is also critical to better understand progenitor cell biology, including the mechanisms by which they exert their function in vivo, as well as the genomic and proteomic interactions that underlie their survival, homing, and differentiation.

In this issue of Circulation Research, Kränkel et al2 demonstrate a novel pathway that may contribute importantly to EPC function and provide a potential marker of regenerative activity. They report that the kinin B2 receptor (B2R) was highly expressed by CD34+ and CD133+ MNCs, as well as in culture-selected “early growth” EPCs. Bradykinin (BK), a natural agonist for B2R, was shown to be a potent chemoattractant for the EPCs, and BK-responsive cells exhibited a more pronounced angiogenic phenotype. These effects of B2R activation involved signaling via the PI3K/Akt/eNOS pathway,

because B2R blockade led to a similar reduction in migration as with inhibition of either PI3K or eNOS. Kränkel et al also showed a reduction in the number of B2R-positive EPCs from patients with stable angina and acute MI, with an associated reduction in their migration toward BK. Finally, they showed that EPCs from B2R-deficient mice had a reduced ability to stimulate neovascularization in a mouse hindlimb ischemia model.

The finding that B2R expression and BK-responsiveness predicted progenitor cell function has potentially important experimental and clinical relevance. Kränkel et al2 showed that cells selected by their ability to migrate to BK had higher expression of endothelial markers, greater in vitro angiogenesis and greater secretion of paracrine factors compared to those not responding to BK. However, they did not test whether BK-migrating cells indeed exhibited greater efficacy in the in vivo hindlimb ischemia model and, although they demonstrated that BM-MNCs from transgenic mice deficient in B2R had impaired neovascularization capacity, the authors were unable to show a sustained increase in perfusion past 1 week in response to the wild-type cells.

If differences in the regenerative capacity between the BK-responsive and -nonresponsive EPCs are confirmed in further preclinical studies, B2R might represent a useful selection marker for a more highly regenerative cell. With a recent study demonstrating the critical influence of cell processing procedures on the clinical benefit of cell therapy post-MI,3 investigators are acutely aware of the importance of verifying viability and functionality of administered cells in the design of clinical trials of autologous cell therapy. Currently, the relatively high prevalence of CD34/KDR- or CD133/KDR-positive EPCs in the administered BM-MNC population is being proposed as a potential explanation for the apparent clinical benefit. Similarly, selection of cells based on migration to BK and/or B2R expression might improve our ability to identify highly

effective cell populations. However, this might be confounded by the presence of cardiac disease or risk factors, because EPCs from patients with acute MI or stable angina showed reduced expression of B2R compared to those of healthy controls in the present study. Thus, it remains to be confirmed to what degree these factors impact on BK-responsiveness or neovascularization capacity.

One of the caveats of autologous cell therapy is that the EPCs are derived from the very same patients with cardiovascular disease who need to be treated, and there is an inverse relationship between the number and function of the EPCs and the cardiac risks of the patients (based on age, cholesterol, diabetes, etc).4,5 Oxidative stress has been suggested to be at least partially responsible for progenitor cell dysfunction, likely through disruption of the PI3K/Akt/eNOS signaling pathway.6,7 Strategies aimed at enhancing this pathway have shown some promising results. Culturing cells in the presence of 3-hydroxy-3-methylglutaryl-coenzyme A (HMG-CoA) reductase inhibitors (statins)8 or a PPAR-γ agonist (pioglitazone),9 agents that activate Akt through different mechanisms, have been shown to improve EPC function. In addition, increasing the bioavailability of NO, either exogenously10 or by eNOS overexpression11 has led to improved migration, neovascularization, or endothelial repair. No doubt there are other unknown pathways that may be critical to the regenerative function of these cells and that may be uncovered only by using unbiased genomic or proteomic approaches, for example, by assessment of differential phosphoproteomic signatures in cells from patients with vascular disease. Nonetheless, a better understanding of the underlying mechanisms responsible for EPC dysfunction will provide the basis to develop better strategies to improve the efficacy of autologous cell therapy.

The study of EPC function as a surrogate for cardiovascular risk has generated much interest,5,12 although the complexity of EPC definitions and isolation techniques have impeded the evaluation of this as a diagnostic test. Because progenitor cell B2R expression can easily be measured by flow cytometry, this could potentially be evaluated as a marker of cardiovascular risk, either for the management of modifiable cardiac risk factors or for toxicity screening following therapeutic or experimental pharmacological administration. Although it might be possible to improve the therapeutic potential of these cells by the upregulation of B2R expression or signaling, the mechanisms responsible for reduced B2R expression and BK responsiveness in cardiovascular disease are still unknown, and their elucidation will be important to better understand how this might be overcome.

In addition to showing a novel role for the kinin–kinogen pathway, the results of Kränkel et al2 further highlight the importance of NO production for EPC activity. Although PI3K or eNOS inhibitors were not used in their in vivo studies, both agents reduced the EPC migratory response to BK in vitro to a similar degree as did B2R blockade, suggesting that this response was primarily mediated through eNOS activation. This is reminiscent of the results of earlier studies showing a degree of NO dependency for the actions of VEGF,13 statins,14 and PPAR-γ agonists15; and thus, eNOS may be a common signaling pathway through which all of these various mediators converge. In this regard, it would also be of interest to study whether pretreatment with VEGF or statins would enhance EPC migration in response to BK or whether selection by migration to another agent (ie, VEGF or SDF-1) would result in similar (or greater) enrichment for angiogenic activity.

The findings of Kränkel et al2 are exciting additions to our emerging understanding of the biology and therapeutic potential of EPCs. The ability to identify and select a more regenerative progenitor population could improve the efficacy of cell therapy for cardiovascular disease. Moreover, an improved surface marker of progenitor cell function could advance our understanding of cardiac risk factors and provide a better diagnostic tool for clinical risk stratification for our patients. Although the importance of the kinin–kinogen pathway for EPC activity needs to be confirmed in clinically relevant models of cardiovascular disease, the work of Kränkel et al highlights the importance of host factors and cell selection in the optimization of therapeutic strategies, which may be critical for enhancing the potential benefit of cell therapy in future trials.

Acknowledgments

Sources of Funding

This work was supported by Canadian Institutes of Health Research and the Krembil Foundation. MRW is supported by a Canadian Institutes of Health Research Jessie Boyd and Charles Scriver MD/PhD Student Award.

References

Abdel-Latif A, Bolli R, Tleyjeh IM, Montori VM, Perin EC, Hornung CA, Zuba-Surma EK, Al-Mallah M, Dawn B. Adult bone marrow-derived cells for cardiac repair: a systematic review and meta-analysis. Arch Intern Med. 2007; 167: 989–997.

Kränkel N, Katare RG, Siragusa M, Barcelos LS, Campagnolo P, Mangialardi G, Fortunato O, Spinetti G, Tran N, Zacharowski K, Wojakowski W, Mroz I, Herman A, Manning Fox JE, MacDonald PE, Schanstra JP, Bascands JL, Ascione R, Angelini G, Emanueli C, Madeddu P. Role of Kinin B2 receptor signaling in the recruitment of circulating progenitor cells with neovascularization potential. Circ Res. 2008; 103: 1335–1343.

Seeger FH, Tonn T, Krzossok N, Zeiher AM, Dimmeler S. Cell isolation procedures matter: a comparison of different isolation protocols of bone marrow mononuclear cells used for cell therapy in patients with acute myocardial infarction. Eur Heart J. 2007; 28: 766–772.
Vasa M, Fichtlscherer S, Aicher A, Adler K, Urbich C, Martin H, Zeiher AM, Dimmeler S. Number and migratory activity of circulating endothelial progenitor cells inversely correlate with risk factors for coronary artery disease. Circ Res. 2001; 89: e1–e7.

Hill JM, Zalos G, Halcox JP, Schenke WH, Waclawiw MA, Quyyumi AA, Finkel T. Circulating endothelial progenitor cells, vascular function, and cardiovascular risk. N Engl J Med. 2003; 348: 593–600.

Thum T, Fraccarollo D, Schultheiss M, Froese S, Galuppo P, Widder JD, Tsikas D, Ertl G, Bauersachs J. Endothelial nitric oxide synthase uncoupling impairs endothelial progenitor cell mobilization and function in diabetes. Diabetes. 2007; 56: 666–674.

Urbich C, Dimmeler S. Risk factors for coronary artery disease, circulating endothelial progenitor cells, and the role of HMG-CoA reductase inhibitors. Kidney Int. 2005; 67: 1672–1676.

Assmus B, Urbich C, Aicher A, Hofmann WK, Haendeler J, Rossig L, Spyridopoulos I, Zeiher AM, Dimmeler S. HMG-CoA reductase inhibitors reduce senescence and increase proliferation of endothelial progenitor cells via regulation of cell cycle regulatory genes. Circ Res. 2003; 92: 1049–1055.

Werner C, Kamani CH, Gensch C, Bohm M, Laufs U. The peroxisome proliferator-activated receptor-gamma agonist pioglitazone increases number and function of endothelial progenitor cells in patients with coronary artery disease and normal glucose tolerance. Diabetes. 2007; 56: 2609–2615.

Li Calzi S, Purich DL, Chang KH, Afzal A, Nakagawa T, Busik JV, Agarwal A, Segal MS, Grant MB. Carbon monoxide and nitric oxide mediate cytoskeletal reorganization in microvascular cells via vasodilator-stimulated phosphoprotein phosphorylation: evidence for blunted responsiveness in diabetes. Diabetes. 2008; 57: 2488–2494.

Sasaki K, Heeschen C, Aicher A, Ziebart T, Honold J, Urbich C, Rossig L, Koehl U, Koyanagi M, Mohamed A, Brandes RP, Martin H, Zeiher AM, Dimmeler S. Ex vivo pretreatment of bone marrow mononuclear cells with endothelial NO synthase enhancer

AVE9488 enhances their functional activity for cell therapy. Proc Natl Acad Sci U S A. 2006; 103: 14537–14541.

Fadini GP, Coracina A, Baesso I, Agostini C, Tiengo A, Avogaro A, de Kreutzenberg SV. Peripheral blood CD34+KDR+ endothelial progenitor cells are determinants of subclinical atherosclerosis in a middle-aged general population. Stroke. 2006; 37: 2277–2282.

Dimmeler S, Dernbach E, Zeiher AM. Phosphorylation of the endothelial nitric oxide synthase at ser-1177 is required for VEGF-induced endothelial cell migration. FEBS Lett. 2000; 477: 258–262.

Dimmeler S, Aicher A, Vasa M, Mildner-Rihm C, Adler K, Tiemann M, Rutten H, Fichtlscherer S, Martin H, Zeiher AM. HMG-CoA reductase inhibitors (statins) increase endothelial progenitor cells via the PI 3-kinase/Akt pathway. J Clin Invest. 2001; 108: 391–397.

Gensch C, Clever YP, Werner C, Hanhoun M, Bohm M, Laufs U. The PPAR-gamma agonist pioglitazone increases neoangiogenesis and prevents apoptosis of endothelial progenitor cells. Atherosclerosis. 2007; 192: 67–74.

CHAPTER 7: REFERENCES

Abdalla, S.A., Gallione, C.J., Barst, R.J., Horn, E.M., Knowles, J.A., Marchuk, D.A., Letarte, M., Morse, J.H., 2004. Primary pulmonary hypertension in families with hereditary haemorrhagic telangiectasia. Eur Respir J 23, 373-377.

Abdul-Salam, V.B., Paul, G.A., Ali, J.O., Gibbs, S.R., Rahman, D., Taylor, G.W., Wilkins, M.R., Edwards, R.J., 2006. Identification of plasma protein biomarkers associated with idiopathic pulmonary arterial hypertension. Proteomics 6, 2286-2294.

Abdul-Salam, V.B., Wharton, J., Cupitt, J., Berryman, M., Edwards, R.J., Wilkins, M.R., 2010. Proteomic analysis of lung tissues from patients with pulmonary arterial hypertension. Circulation 122, 2058-2067.

Abe, K., Toba, M., Alzoubi, A., Ito, M., Fagan, K.A., Cool, C.D., Voelkel, N.F., McMurtry, I.F., Oka, M., 2010. Formation of plexiform lesions in experimental severe pulmonary arterial hypertension. Circulation 121, 2747-2754.

Adachi-Yamada, T., Nakamura, M., Irie, K., Tomoyasu, Y., Sano, Y., Mori, E., Goto, S., Ueno, N., Nishida, Y., Matsumoto, K., 1999. p38 mitogen-activated protein kinase can be involved in transforming growth factor beta superfamily signal transduction in Drosophila wing morphogenesis. Mol Cell Biol 19, 2322-2329.

Aldred, M.A., Machado, R.D., James, V., Morrell, N.W., Trembath, R.C., 2007. Characterization of the BMPR2 5'-untranslated region and a novel mutation in pulmonary hypertension. Am J Respir Crit Care Med 176, 819-824.

Altieri, D.C., 2003. Validating survivin as a cancer therapeutic target. Nat Rev Cancer 3, 46-54.

Altman, R., Scazziota, A., Rouvier, J., Gurfinkel, E., Favaloro, R., Perrone, S., Fareed, J., 1996. Coagulation and fibrinolytic parameters in patients with pulmonary hypertension. Clin Cardiol 19, 549-554.

Ameshima, S., Golpon, H., Cool, C.D., Chan, D., Vandivier, R.W., Gardai, S.J., Wick, M., Nemenoff, R.A., Geraci, M.W., Voelkel, N.F., 2003. Peroxisome proliferator-activated receptor gamma (PPARgamma) expression is decreased in pulmonary hypertension and affects endothelial cell growth. Circ Res 92, 1162-1169.

Amson, R., Pece, S., Lespagnol, A., Vyas, R., Mazzarol, G., Tosoni, D., Colaluca, I., Viale, G., Rodrigues-Ferreira, S., Wynendaele, J., Chaloin, O., Hoebeke, J., Marine, J.C., Di Fiore, P.P., Telerman, A., 2012. Reciprocal repression between P53 and TCTP. Nat Med 18, 91-99.

Amzallag, N., Passer, B.J., Allanic, D., Segura, E., Thery, C., Goud, B., Amson, R., Telerman, A., 2004. TSAP6 facilitates the secretion of translationally controlled tumor

protein/histamine-releasing factor via a nonclassical pathway. J Biol Chem 279, 46104-46112.

Andree, H., Thiele, H., Fahling, M., Schmidt, I., Thiele, B.J., 2006. Expression of the human TPT1 gene coding for translationally controlled tumor protein (TCTP) is regulated by CREB transcription factors. Gene 380, 95-103.

Arcuri, F., Papa, S., Carducci, A., Romagnoli, R., Liberatori, S., Riparbelli, M.G., Sanchez, J.C., Tosi, P., del Vecchio, M.T., 2004. Translationally controlled tumor protein (TCTP) in the human prostate and prostate cancer cells: expression, distribution, and calcium binding activity. Prostate 60, 130-140.

Atkinson, C., Stewart, S., Upton, P.D., Machado, R., Thomson, J.R., Trembath, R.C., Morrell, N.W., 2002. Primary pulmonary hypertension is associated with reduced pulmonary vascular expression of type II bone morphogenetic protein receptor. Circulation 105, 1672-1678.

Balabanian, K., Foussat, A., Dorfmuller, P., Durand-Gasselin, I., Capel, F., Bouchet-Delbos, L., Portier, A., Marfaing-Koka, A., Krzysiek, R., Rimaniol, A.C., Simonneau, G., Emilie, D., Humbert, M., 2002. CX(3)C chemokine fractalkine in pulmonary arterial hypertension. Am J Respir Crit Care Med 165, 1419-1425.

Barradeau, S., Imaizumi-Scherrer, T., Weiss, M.C., Faust, D.M., 2002. Intracellular targeting of the type-I alpha regulatory subunit of cAMP-dependent protein kinase. Trends Cardiovasc Med 12, 235-241.

Barst, R.J., Rubin, L.J., Long, W.A., McGoon, M.D., Rich, S., Badesch, D.B., Groves, B.M., Tapson, V.F., Bourge, R.C., Brundage, B.H., Koerner, S.K., Langleben, D., Keller, C.A., Murali, S., Uretsky, B.F., Clayton, L.M., Jobsis, M.M., Blackburn, S.D., Shortino, D., Crow, J.W., 1996. A comparison of continuous intravenous epoprostenol (prostacyclin) with conventional therapy for primary pulmonary hypertension. N Engl J Med 334, 296-301.

Baudet, C., Perret, E., Delpech, B., Kaghad, M., Brachet, P., Wion, D., Caput, D., 1998. Differentially expressed genes in C6.9 glioma cells during vitamin D-induced cell death program. Cell Death Differ 5, 116-125.

Beppu, H., Ichinose, F., Kawai, N., Jones, R.C., Yu, P.B., Zapol, W.M., Miyazono, K., Li, E., Bloch, K.D., 2004. BMPR-II heterozygous mice have mild pulmonary hypertension and an impaired pulmonary vascular remodeling response to prolonged hypoxia. Am J Physiol Lung Cell Mol Physiol 287, L1241-1247.

Beppu, H., Kawabata, M., Hamamoto, T., Chytil, A., Minowa, O., Noda, T., Miyazono, K., 2000. BMP type II receptor is required for gastrulation and early development of mouse embryos. Dev Biol 221, 249-258.

Betel, D., Koppal, A., Agius, P., Sander, C., Leslie, C., 2010. Comprehensive modeling of microRNA targets predicts functional non-conserved and non-canonical sites. Genome Biol 11, R90.

Bini, L., Magi, B., Marzocchi, B., Arcuri, F., Tripodi, S., Cintorino, M., Sanchez, J.C., Frutiger, S., Hughes, G., Pallini, V., Hochstrasser, D.F., Tosi, P., 1997. Protein expression profiles in human breast ductal carcinoma and histologically normal tissue. Electrophoresis 18, 2832-2841.

Bohm, H., Benndorf, R., Gaestel, M., Gross, B., Nurnberg, P., Kraft, R., Otto, A., Bielka, H., 1989. The growth-related protein P23 of the Ehrlich ascites tumor: translational control, cloning and primary structure. Biochem Int 19, 277-286.

Bommer, U.A., Borovjagin, A.V., Greagg, M.A., Jeffrey, I.W., Russell, P., Laing, K.G., Lee, M., Clemens, M.J., 2002. The mRNA of the translationally controlled tumor protein P23/TCTP is a highly structured RNA, which activates the dsRNA-dependent protein kinase PKR. Rna 8, 478-496.

Bommer, U.A., Thiele, B.J., 2004. The translationally controlled tumour protein (TCTP). Int J Biochem Cell Biol 36, 379-385.

Boutet, K., Montani, D., Jais, X., Yaici, A., Sitbon, O., Simonneau, G., Humbert, M., 2008. Therapeutic advances in pulmonary arterial hypertension. Ther Adv Respir Dis 2, 249-265.

Budhiraja, R., Tuder, R.M., Hassoun, P.M., 2004. Endothelial dysfunction in pulmonary hypertension. Circulation 109, 159-165.

Bull, T.M., Coldren, C.D., Moore, M., Sotto-Santiago, S.M., Pham, D.V., Nana-Sinkam, S.P., Voelkel, N.F., Geraci, M.W., 2004. Gene microarray analysis of peripheral blood cells in pulmonary arterial hypertension. Am J Respir Crit Care Med 170, 911-919.

Campbell, A.I., Zhao, Y., Sandhu, R., Stewart, D.J., 2001. Cell-based gene transfer of vascular endothelial growth factor attenuates monocrotaline-induced pulmonary hypertension. Circulation 104, 2242-2248.

Cans, C., Passer, B.J., Shalak, V., Nancy-Portebois, V., Crible, V., Amzallag, N., Allanic, D., Tufino, R., Argentini, M., Moras, D., Fiucci, G., Goud, B., Mirande, M., Amson, R., Telerman, A., 2003. Translationally controlled tumor protein acts as a guanine nucleotide dissociation inhibitor on the translation elongation factor eEF1A. Proc Natl Acad Sci U S A 100, 13892-13897.

Chan, T.H., Chen, L., Liu, M., Hu, L., Zheng, B.J., Poon, V.K., Huang, P., Yuan, Y.F., Huang, J.D., Yang, J., Tsao, G.S., Guan, X.Y., 2012. Translationally controlled tumor protein induces mitotic defects and chromosome missegregation in hepatocellular carcinoma development. Hepatology 55, 491-505.

Chang, W.Y., Lavoie, J.R., Kwon, S.Y., Chen, Z., Manias, J.L., Behbahani, J., Ling, V., Kandel, R.A., Stewart, D.J., Stanford, W.L., 2013. Feeder-independent derivation of induced-pluripotent stem cells from peripheral blood endothelial progenitor cells. Stem Cell Res 10, 195-202.

Chaouat, A., Coulet, F., Favre, C., Simonneau, G., Weitzenblum, E., Soubrier, F., Humbert, M., 2004. Endoglin germline mutation in a patient with hereditary haemorrhagic telangiectasia and dexfenfluramine associated pulmonary arterial hypertension. Thorax 59, 446-448.

Chen, H.B., Shen, J., Ip, Y.T., Xu, L., 2006. Identification of phosphatases for Smad in the BMP/DPP pathway. Genes Dev 20, 648-653.

Chen, S.H., Wu, P.S., Chou, C.H., Yan, Y.T., Liu, H., Weng, S.Y., Yang-Yen, H.F., 2007. A knockout mouse approach reveals that TCTP functions as an essential factor for cell proliferation and survival in a tissue- or cell type-specific manner. Mol Biol Cell 18, 2525-2532.

Chen, Y.F., Oparil, S., 2000. Endothelial dysfunction in the pulmonary vascular bed. Am J Med Sci 320, 223-232.

Chida, A., Shintani, M., Nakayama, T., Furutani, Y., Hayama, E., Inai, K., Saji, T., Nonoyama, S., Nakanishi, T., 2012. Missense mutations of the BMPR1B (ALK6) gene in childhood idiopathic pulmonary arterial hypertension. Circ J 76, 1501-1508.

Chitpatima, S.T., Makrides, S., Bandyopadhyay, R., Brawerman, G., 1988. Nucleotide sequence of a major messenger RNA for a 21 kilodalton polypeptide that is under translational control in mouse tumor cells. Nucleic Acids Res 16, 2350.

Cho, Y., Maeng, J., Ryu, J., Shin, H., Kim, M., Oh, G.T., Lee, M.Y., Lee, K., 2012. Hypertension resulting from overexpression of translationally controlled tumor protein increases the severity of atherosclerosis in apolipoprotein E knock-out mice. Transgenic Res 21, 1245-1254.

Choi, S., Min, H.J., Kim, M., Hwang, E.S., Lee, K., 2009. Proton pump inhibitors exert anti-allergic effects by reducing TCTP secretion. PLoS One 4, e5732.

Christman, B.W., 1998. Lipid mediator dysregulation in primary pulmonary hypertension. Chest 114, 205S-207S.

D'Alonzo, G.E., Barst, R.J., Ayres, S.M., Bergofsky, E.H., Brundage, B.H., Detre, K.M., Fishman, A.P., Goldring, R.M., Groves, B.M., Kernis, J.T., et al., 1991. Survival in patients with primary pulmonary hypertension. Results from a national prospective registry. Ann Intern Med 115, 343-349.

David, L., Mallet, C., Keramidas, M., Lamande, N., Gasc, J.M., Dupuis-Girod, S., Plauchu, H., Feige, J.J., Bailly, S., 2008. Bone morphogenetic protein-9 is a circulating vascular quiescence factor. Circ Res 102, 914-922.

Deng, Z., Morse, J.H., Slager, S.L., Cuervo, N., Moore, K.J., Venetos, G., Kalachikov, S., Cayanis, E., Fischer, S.G., Barst, R.J., Hodge, S.E., Knowles, J.A., 2000. Familial primary pulmonary hypertension (gene PPH1) is caused by mutations in the bone morphogenetic protein receptor-II gene. Am J Hum Genet 67, 737-744.

Dorfmuller, P., Zarka, V., Durand-Gasselin, I., Monti, G., Balabanian, K., Garcia, G., Capron, F., Coulomb-Lhermine, A., Marfaing-Koka, A., Simonneau, G., Emilie, D., Humbert, M., 2002. Chemokine RANTES in severe pulmonary arterial hypertension. Am J Respir Crit Care Med 165, 534-539.

Drake, K.M., Zygmunt, D., Mavrakis, L., Harbor, P., Wang, L., Comhair, S.A., Erzurum, S.C., Aldred, M.A., 2011. Altered MicroRNA processing in heritable pulmonary arterial hypertension: an important role for Smad-8. Am J Respir Crit Care Med 184, 1400-1408.

Eglen, R.M., Bosse, R., Reisine, T., 2007. Emerging concepts of guanine nucleotide-binding protein-coupled receptor (GPCR) function and implications for high throughput screening. Assay Drug Dev Technol 5, 425-451.

El Chami, H., Hassoun, P.M., 2012. Immune and inflammatory mechanisms in pulmonary arterial hypertension. Prog Cardiovasc Dis 55, 218-228.

Farber, H.W., Loscalzo, J., 2004. Pulmonary arterial hypertension. N Engl J Med 351, 1655-1665.

Farh, K.K., Grimson, A., Jan, C., Lewis, B.P., Johnston, W.K., Lim, L.P., Burge, C.B., Bartel, D.P., 2005. The widespread impact of mammalian MicroRNAs on mRNA repression and evolution. Science 310, 1817-1821.

Frumkin, L.R., 2012. The pharmacological treatment of pulmonary arterial hypertension. Pharmacol Rev 64, 583-620.

Fujioka, S., Shomori, K., Nishihara, K., Yamaga, K., Nosaka, K., Araki, K., Haruki, T., Taniguchi, Y., Nakamura, H., Ito, H., 2009. Expression of minichromosome maintenance 7 (MCM7) in small lung adenocarcinomas (pT1): Prognostic implication. Lung Cancer 65, 223-229.

Fujiwara, M., Yagi, H., Matsuoka, R., Akimoto, K., Furutani, M., Imamura, S., Uehara, R., Nakayama, T., Takao, A., Nakazawa, M., Saji, T., 2008. Implications of mutations of activin receptor-like kinase 1 gene (ALK1) in addition to bone morphogenetic protein receptor II gene (BMPR2) in children with pulmonary arterial hypertension. Circ J 72, 127-133.

Gachet, Y., Tournier, S., Lee, M., Lazaris-Karatzas, A., Poulton, T., Bommer, U.A., 1999. The growth-related, translationally controlled protein P23 has properties of a tubulin binding protein and associates transiently with microtubules during the cell cycle. J Cell Sci 112 (Pt 8), 1257-1271.

Gaine, S., 2000. Pulmonary hypertension. Jama 284, 3160-3168.

Gaine, S.P., Rubin, L.J., 1998. Primary pulmonary hypertension. Lancet 352, 719-725.

Galie, N., Brundage, B.H., Ghofrani, H.A., Oudiz, R.J., Simonneau, G., Safdar, Z., Shapiro, S., White, R.J., Chan, M., Beardsworth, A., Frumkin, L., Barst, R.J., 2009a. Tadalafil therapy for pulmonary arterial hypertension. Circulation 119, 2894-2903.

Galie, N., Ghofrani, H.A., Torbicki, A., Barst, R.J., Rubin, L.J., Badesch, D., Fleming, T., Parpia, T., Burgess, G., Branzi, A., Grimminger, F., Kurzyna, M., Simonneau, G., 2005. Sildenafil citrate therapy for pulmonary arterial hypertension. N Engl J Med 353, 2148-2157.

Galie, N., Hoeper, M.M., Humbert, M., Torbicki, A., Vachiery, J.L., Barbera, J.A., Beghetti, M., Corris, P., Gaine, S., Gibbs, J.S., Gomez-Sanchez, M.A., Jondeau, G., Klepetko, W., Opitz, C., Peacock, A., Rubin, L., Zellweger, M., Simonneau, G., 2009b. Guidelines for the diagnosis and treatment of pulmonary hypertension. Eur Respir J 34, 1219-1263.

Galie, N., Hoeper, M.M., Humbert, M., Torbicki, A., Vachiery, J.L., Barbera, J.A., Beghetti, M., Corris, P., Gaine, S., Gibbs, J.S., Gomez-Sanchez, M.A., Jondeau, G., Klepetko, W., Opitz, C., Peacock, A., Rubin, L., Zellweger, M., Simonneau, G., 2009c. Guidelines for the diagnosis and treatment of pulmonary hypertension: the Task Force for the Diagnosis and Treatment of Pulmonary Hypertension of the European Society of Cardiology (ESC) and the European Respiratory Society (ERS), endorsed by the International Society of Heart and Lung Transplantation (ISHLT). Eur Heart J 30, 2493-2537.

Galie, N., Manes, A., Branzi, A., 2002. Emerging medical therapies for pulmonary arterial hypertension. Prog Cardiovasc Dis 45, 213-224.

Galie, N., Manes, A., Negro, L., Palazzini, M., Bacchi-Reggiani, M.L., Branzi, A., 2009d. A meta-analysis of randomized controlled trials in pulmonary arterial hypertension. Eur Heart J 30, 394-403.

Gambichler, T., Shtern, M., Rotterdam, S., Bechara, F.G., Stucker, M., Altmeyer, P., Kreuter, A., 2009. Minichromosome maintenance proteins are useful adjuncts to differentiate between benign and malignant melanocytic skin lesions. J Am Acad Dermatol 60, 808-813.

Geraci, M.W., Moore, M., Gesell, T., Yeager, M.E., Alger, L., Golpon, H., Gao, B., Loyd, J.E., Tuder, R.M., Voelkel, N.F., 2001. Gene expression patterns in the lungs of patients with primary pulmonary hypertension: a gene microarray analysis. Circ Res 88, 555-562.

Geti, I., Ormiston, M.L., Rouhani, F., Toshner, M., Movassagh, M., Nichols, J., Mansfield, W., Southwood, M., Bradley, A., Rana, A.A., Vallier, L., Morrell, N.W., 2012. A practical and efficient cellular substrate for the generation of induced pluripotent stem cells from adults: blood-derived endothelial progenitor cells. Stem Cells Transl Med 1, 855-865.

Giaid, A., Saleh, D., 1995. Reduced expression of endothelial nitric oxide synthase in the lungs of patients with pulmonary hypertension. N Engl J Med 333, 214-221.

Giaid, A., Yanagisawa, M., Langleben, D., Michel, R.P., Levy, R., Shennib, H., Kimura, S., Masaki, T., Duguid, W.P., Stewart, D.J., 1993. Expression of endothelin-1 in the lungs of patients with pulmonary hypertension. N Engl J Med 328, 1732-1739.

Gilboa, L., Nohe, A., Geissendorfer, T., Sebald, W., Henis, Y.I., Knaus, P., 2000. Bone morphogenetic protein receptor complexes on the surface of live cells: a new oligomerization mode for serine/threonine kinase receptors. Mol Biol Cell 11, 1023-1035.

Gnanasekar, M., Thirugnanam, S., Zheng, G., Chen, A., Ramaswamy, K., 2009. Gene silencing of translationally controlled tumor protein (TCTP) by siRNA inhibits cell growth and induces apoptosis of human prostate cancer cells. Int J Oncol 34, 1241-1246.

Gross, B., Gaestel, M., Bohm, H., Bielka, H., 1989. cDNA sequence coding for a translationally controlled human tumor protein. Nucleic Acids Res 17, 8367.

Guillaume, E., Pineau, C., Evrard, B., Dupaix, A., Moertz, E., Sanchez, J.C., Hochstrasser, D.F., Jegou, B., 2001. Cellular distribution of translationally controlled tumor protein in rat and human testes. Proteomics 1, 880-889.

Guo, Y., Xiao, P., Lei, S., Deng, F., Xiao, G.G., Liu, Y., Chen, X., Li, L., Wu, S., Chen, Y., Jiang, H., Tan, L., Xie, J., Zhu, X., Liang, S., Deng, H., 2008. How is mRNA expression predictive for protein expression? A correlation study on human circulating monocytes. Acta Biochim Biophys Sin (Shanghai) 40, 426-436.

Gygi, S.P., Rochon, Y., Franza, B.R., Aebersold, R., 1999. Correlation between protein and mRNA abundance in yeast. Mol Cell Biol 19, 1720-1730.

Hanahan, D., Weinberg, R.A., 2000. The hallmarks of cancer. Cell 100, 57-70.

Harrison, R.E., Berger, R., Haworth, S.G., Tulloh, R., Mache, C.J., Morrell, N.W., Aldred, M.A., Trembath, R.C., 2005. Transforming growth factor-beta receptor mutations and pulmonary arterial hypertension in childhood. Circulation 111, 435-441.

Harrison, R.E., Flanagan, J.A., Sankelo, M., Abdalla, S.A., Rowell, J., Machado, R.D., Elliott, C.G., Robbins, I.M., Olschewski, H., McLaughlin, V., Gruenig, E., Kermeen, F., Halme, M., Raisanen-Sokolowski, A., Laitinen, T., Morrell, N.W., Trembath, R.C., 2003. Molecular and functional analysis identifies ALK-1 as the predominant cause of pulmonary hypertension related to hereditary haemorrhagic telangiectasia. J Med Genet 40, 865-871.

Hassoun, P.M., Mouthon, L., Barbera, J.A., Eddahibi, S., Flores, S.C., Grimminger, F., Jones, P.L., Maitland, M.L., Michelakis, E.D., Morrell, N.W., Newman, J.H., Rabinovitch, M., Schermuly, R., Stenmark, K.R., Voelkel, N.F., Yuan, J.X., Humbert, M., 2009. Inflammation, growth factors, and pulmonary vascular remodeling. J Am Coll Cardiol 54, S10-19.

Hata, A., Lagna, G., Massague, J., Hemmati-Brivanlou, A., 1998. Smad6 inhibits BMP/Smad1 signaling by specifically competing with the Smad4 tumor suppressor. Genes Dev 12, 186-197.

Hong, K.H., Lee, Y.J., Lee, E., Park, S.O., Han, C., Beppu, H., Li, E., Raizada, M.K., Bloch, K.D., Oh, S.P., 2008. Genetic ablation of the BMPR2 gene in pulmonary endothelium is sufficient to predispose to pulmonary arterial hypertension. Circulation 118, 722-730.

Huang, Z., Wang, D., Ihida-Stansbury, K., Jones, P.L., Martin, J.F., 2009. Defective pulmonary vascular remodeling in Smad8 mutant mice. Hum Mol Genet 18, 2791-2801.

Humbert, M., Monti, G., Brenot, F., Sitbon, O., Portier, A., Grangeot-Keros, L., Duroux, P., Galanaud, P., Simonneau, G., Emilie, D., 1995. Increased interleukin-1 and interleukin-6 serum concentrations in severe primary pulmonary hypertension. Am J Respir Crit Care Med 151, 1628-1631.

Humbert, M., Morrell, N.W., Archer, S.L., Stenmark, K.R., MacLean, M.R., Lang, I.M., Christman, B.W., Weir, E.K., Eickelberg, O., Voelkel, N.F., Rabinovitch, M., 2004a. Cellular and molecular pathobiology of pulmonary arterial hypertension. J Am Coll Cardiol 43, 13S-24S.

Humbert, M., Sitbon, O., Chaouat, A., Bertocchi, M., Habib, G., Gressin, V., Yaici, A., Weitzenblum, E., Cordier, J.F., Chabot, F., Dromer, C., Pison, C., Reynaud-Gaubert, M., Haloun, A., Laurent, M., Hachulla, E., Simonneau, G., 2006. Pulmonary arterial hypertension in France: results from a national registry. Am J Respir Crit Care Med 173, 1023-1030.

Humbert, M., Sitbon, O., Simonneau, G., 2004b. Treatment of pulmonary arterial hypertension. N Engl J Med 351, 1425-1436.

Hur, J., Yoon, C.H., Kim, H.S., Choi, J.H., Kang, H.J., Hwang, K.K., Oh, B.H., Lee, M.M., Park, Y.B., 2004. Characterization of two types of endothelial progenitor cells and their different contributions to neovasculogenesis. Arterioscler Thromb Vasc Biol 24, 288-293.

Ingram, D.A., Mead, L.E., Tanaka, H., Meade, V., Fenoglio, A., Mortell, K., Pollok, K., Ferkowicz, M.J., Gilley, D., Yoder, M.C., 2004. Identification of a novel hierarchy of endothelial progenitor cells using human peripheral and umbilical cord blood. Blood 104, 2752-2760.

Jackson, A.L., Linsley, P.S., 2010. Recognizing and avoiding siRNA off-target effects for target identification and therapeutic application. Nat Rev Drug Discov 9, 57-67.

Jeffery, T.K., Morrell, N.W., 2002. Molecular and cellular basis of pulmonary vascular remodeling in pulmonary hypertension. Prog Cardiovasc Dis 45, 173-202.

Jeffery, T.K., Wanstall, J.C., 2001. Pulmonary vascular remodeling: a target for therapeutic intervention in pulmonary hypertension. Pharmacol Ther 92, 1-20.

Jiang, B., Deng, Y., Taha, M., Li, G., Stewart, D., 2012. Inhibition of vegfr2 is sufficient to produce severe plexogenic pulmonary arterial hypertension in rats, Canadian Cardiovascular Congress 2012: 65th Annual Meeting of the Canadian Cardiovascular Society. Canadian Journal of Cardiology, pp. S121-S122.

Jiang, L., Huang, Q., Zhang, S., Zhang, Q., Chang, J., Qiu, X., Wang, E., 2010. Hsa-miR-125a-3p and hsa-miR-125a-5p are downregulated in non-small cell lung cancer and have inverse effects on invasion and migration of lung cancer cells. BMC Cancer 10, 318.

Jung, J., Kim, H.Y., Kim, M., Sohn, K., Lee, K., 2011. Translationally controlled tumor protein induces human breast epithelial cell transformation through the activation of Src. Oncogene 30, 2264-2274.

Jung, J., Kim, M., Kim, M.J., Kim, J., Moon, J., Lim, J.S., Lee, K., 2004. Translationally controlled tumor protein interacts with the third cytoplasmic domain of Na,K-ATPase alpha subunit and inhibits the pump activity in HeLa cells. J Biol Chem 279, 49868-49875.

Jurasz, P., Courtman, D., Babaie, S., Stewart, D.J., 2010. Role of apoptosis in pulmonary hypertension: from experimental models to clinical trials. Pharmacol Ther 126, 1-8.

Kashiwakura, J.C., Ando, T., Matsumoto, K., Kimura, M., Kitaura, J., Matho, M.H., Zajonc, D.M., Ozeki, T., Ra, C., MacDonald, S.M., Siraganian, R.P., Broide, D.H., Kawakami, Y., Kawakami, T., 2012. Histamine-releasing factor has a proinflammatory role in mouse models of asthma and allergy. J Clin Invest 122, 218-228.

Kim, J.E., Koo, K.H., Kim, Y.H., Sohn, J., Park, Y.G., 2008a. Identification of potential lung cancer biomarkers using an in vitro carcinogenesis model. Exp Mol Med 40, 709-720.

Kim, M., Min, H.J., Won, H.Y., Park, H., Lee, J.C., Park, H.W., Chung, J., Hwang, E.S., Lee, K., 2009. Dimerization of translationally controlled tumor protein is essential for its cytokine-like activity. PLoS One 4, e6464.

Kim, M.J., Kwon, J.S., Suh, S.H., Suh, J.K., Jung, J., Lee, S.N., Kim, Y.H., Cho, M.C., Oh, G.T., Lee, K., 2008b. Transgenic overexpression of translationally controlled tumor protein induces systemic hypertension via repression of Na+,K+-ATPase. J Mol Cell Cardiol 44, 151-159.

Konishi, T., Sasaki, S., Watanabe, T., Kitayama, J., Nagawa, H., 2005. Overexpression of hRFI (human ring finger homologous to inhibitor of apoptosis protein type) inhibits death receptor-mediated apoptosis in colorectal cancer cells. Mol Cancer Ther 4, 743-750.

Kwapiszewska, G., Wilhelm, J., Wolff, S., Laumanns, I., Koenig, I.R., Ziegler, A., Seeger, W., Bohle, R.M., Weissmann, N., Fink, L., 2005. Expression profiling of laser-microdissected intrapulmonary arteries in hypoxia-induced pulmonary hypertension. Respir Res 6, 109.

Kwapiszewska, G., Wygrecka, M., Marsh, L.M., Schmitt, S., Trosser, R., Wilhelm, J., Helmus, K., Eul, B., Zakrzewicz, A., Ghofrani, H.A., Schermuly, R.T., Bohle, R.M., Grimminger, F., Seeger, W., Eickelberg, O., Fink, L., Weissmann, N., 2008. Fhl-1, a new key protein in pulmonary hypertension. Circulation 118, 1183-1194.

Lane, K.B., Machado, R.D., Pauciulo, M.W., Thomson, J.R., Phillips, J.A., 3rd, Loyd, J.E., Nichols, W.C., Trembath, R.C., 2000. Heterozygous germline mutations in BMPR2, encoding a TGF-beta receptor, cause familial primary pulmonary hypertension. Nat Genet 26, 81-84.

Langdon, J.M., Vonakis, B.M., MacDonald, S.M., 2004. Identification of the interaction between the human recombinant histamine releasing factor/translationally controlled tumor protein and elongation factor-1 delta (also known as eElongation factor-1B beta). Biochim Biophys Acta 1688, 232-236.

Laudi, S., Steudel, W., Jonscher, K., Schoning, W., Schniedewind, B., Kaisers, U., Christians, U., Trump, S., 2007. Comparison of lung proteome profiles in two rodent models of pulmonary arterial hypertension. Proteomics 7, 2469-2478.

Lavoie, J.R., Stewart, D.J., 2012. Genetically modified endothelial progenitor cells in the therapy of cardiovascular disease and pulmonary hypertension. Curr Vasc Pharmacol 10, 289-299.

Levy, M., Maurey, C., Celermajer, D.S., Vouhe, P.R., Danel, C., Bonnet, D., Israel-Biet, D., 2007. Impaired apoptosis of pulmonary endothelial cells is associated with intimal proliferation and irreversibility of pulmonary hypertension in congenital heart disease. J Am Coll Cardiol 49, 803-810.

Li, F., Zhang, D., Fujise, K., 2001. Characterization of fortilin, a novel antiapoptotic protein. J Biol Chem 276, 47542-47549.

Li, S.S., Xue, W.C., Khoo, U.S., Ngan, H.Y., Chan, K.Y., Tam, I.Y., Chiu, P.M., Ip, P.P., Tam, K.F., Cheung, A.N., 2005. Replicative MCM7 protein as a proliferation marker in endometrial carcinoma: a tissue microarray and clinicopathological analysis. Histopathology 46, 307-313.

Liu, C., Chen, J., Gao, Y., Deng, B., Liu, K., 2009. Endothelin receptor antagonists for pulmonary arterial hypertension. Cochrane Database Syst Rev, CD004434.

Liu, H., Peng, H.W., Cheng, Y.S., Yuan, H.S., Yang-Yen, H.F., 2005. Stabilization and enhancement of the antiapoptotic activity of mcl-1 by TCTP. Mol Cell Biol 25, 3117-3126.

Liu, Y.Z., Jiang, Y.Y., Hao, J.J., Lu, S.S., Zhang, T.T., Shang, L., Cao, J., Song, X., Wang, B.S., Cai, Y., Zhan, Q.M., Wang, M.R., 2012. Prognostic significance of MCM7 expression in the bronchial brushings of patients with non-small cell lung cancer (NSCLC). Lung Cancer 77, 176-182.

Lo, W.Y., Wang, H.J., Chiu, C.W., Chen, S.F., 2012. miR-27b-regulated TCTP as a novel plasma biomarker for oral cancer: from quantitative proteomics to post-transcriptional study. J Proteomics 77, 154-166.

Ma, Q., Geng, Y., Xu, W., Wu, Y., He, F., Shu, W., Huang, M., Du, H., Li, M., 2010. The role of translationally controlled tumor protein in tumor growth and metastasis of colon adenocarcinoma cells. J Proteome Res 9, 40-49.

Macchia, A., Marchioli, R., Marfisi, R., Scarano, M., Levantesi, G., Tavazzi, L., Tognoni, G., 2007. A meta-analysis of trials of pulmonary hypertension: a clinical condition looking for drugs and research methodology. Am Heart J 153, 1037-1047.

Macdonald, S.M., 2012. Potential role of histamine releasing factor (HRF) as a therapeutic target for treating asthma and allergy. J Asthma Allergy 5, 51-59.

MacDonald, S.M., Rafnar, T., Langdon, J., Lichtenstein, L.M., 1995. Molecular identification of an IgE-dependent histamine-releasing factor. Science 269, 688-690.

Machado, R.D., Eickelberg, O., Elliott, C.G., Geraci, M.W., Hanaoka, M., Loyd, J.E., Newman, J.H., Phillips, J.A., 3rd, Soubrier, F., Trembath, R.C., Chung, W.K., 2009. Genetics and genomics of pulmonary arterial hypertension. J Am Coll Cardiol 54, S32-42.

Machado, R.D., Pauciulo, M.W., Thomson, J.R., Lane, K.B., Morgan, N.V., Wheeler, L., Phillips, J.A., 3rd, Newman, J., Williams, D., Galie, N., Manes, A., McNeil, K., Yacoub, M., Mikhail, G., Rogers, P., Corris, P., Humbert, M., Donnai, D., Martensson, G., Tranebjaerg, L., Loyd, J.E., Trembath, R.C., Nichols, W.C., 2001. BMPR2

haploinsufficiency as the inherited molecular mechanism for primary pulmonary hypertension. Am J Hum Genet 68, 92-102.

Maclean, M.R., Johnston, E.D., McCulloch, K.M., Pooley, L., Houslay, M.D., Sweeney, G., 1997. Phosphodiesterase isoforms in the pulmonary arterial circulation of the rat: changes in pulmonary hypertension. J Pharmacol Exp Ther 283, 619-624.

Massague, J., 2003. Integration of Smad and MAPK pathways: a link and a linker revisited. Genes Dev 17, 2993-2997.

Massague, J., Seoane, J., Wotton, D., 2005. Smad transcription factors. Genes Dev 19, 2783-2810.

Mattson, M.P., 1997. Cellular actions of beta-amyloid precursor protein and its soluble and fibrillogenic derivatives. Physiol Rev 77, 1081-1132.

McDonald, J., Bayrak-Toydemir, P., Pyeritz, R.E., 2011. Hereditary hemorrhagic telangiectasia: an overview of diagnosis, management, and pathogenesis. Genet Med 13, 607-616.

McMurtry, M.S., Archer, S.L., Altieri, D.C., Bonnet, S., Haromy, A., Harry, G., Puttagunta, L., Michelakis, E.D., 2005. Gene therapy targeting survivin selectively induces pulmonary vascular apoptosis and reverses pulmonary arterial hypertension. J Clin Invest 115, 1479-1491.

Medina, R.J., O'Neill, C.L., Sweeney, M., Guduric-Fuchs, J., Gardiner, T.A., Simpson, D.A., Stitt, A.W., 2010. Molecular analysis of endothelial progenitor cell (EPC) subtypes reveals two distinct cell populations with different identities. BMC Med Genomics 3, 18.

Meyrick, B.O., Friedman, D.B., Billheimer, D.D., Cogan, J.D., Prince, M.A., Phillips, J.A., 3rd, Loyd, J.E., 2008. Proteomics of transformed lymphocytes from a family with familial pulmonary arterial hypertension. Am J Respir Crit Care Med 177, 99-107.

Michel, R.P., Langleben, D., Dupuis, J., 2003. The endothelin system in pulmonary hypertension. Can J Physiol Pharmacol 81, 542-554.

Miyazono, K., Maeda, S., Imamura, T., 2005. BMP receptor signaling: transcriptional targets, regulation of signals, and signaling cross-talk. Cytokine Growth Factor Rev 16, 251-263.

Mizuno, S., Bogaard, H.J., Kraskauskas, D., Alhussaini, A., Gomez-Arroyo, J., Voelkel, N.F., Ishizaki, T., 2011. p53 Gene deficiency promotes hypoxia-induced pulmonary hypertension and vascular remodeling in mice. Am J Physiol Lung Cell Mol Physiol 300, L753-761.

Mizuno, S., Farkas, L., Al Husseini, A., Farkas, D., Gomez-Arroyo, J., Kraskauskas, D., Nicolls, M.R., Cool, C.D., Bogaard, H.J., Voelkel, N.F., 2012. Severe pulmonary arterial hypertension induced by SU5416 and ovalbumin immunization. Am J Respir Cell Mol Biol 47, 679-687.

Morrell, N.W., 2006. Pulmonary hypertension due to BMPR2 mutation: a new paradigm for tissue remodeling? Proc Am Thorac Soc 3, 680-686.

Morrell, N.W., Adnot, S., Archer, S.L., Dupuis, J., Jones, P.L., MacLean, M.R., McMurtry, I.F., Stenmark, K.R., Thistlethwaite, P.A., Weissmann, N., Yuan, J.X., Weir, E.K., 2009. Cellular and molecular basis of pulmonary arterial hypertension. J Am Coll Cardiol 54, S20-31.

Muesch, A., Hartmann, E., Rohde, K., Rubartelli, A., Sitia, R., Rapoport, T.A., 1990. A novel pathway for secretory proteins? Trends Biochem Sci 15, 86-88.

Murray, F., Patel, H.H., Suda, R.Y., Zhang, S., Thistlethwaite, P.A., Yuan, J.X., Insel, P.A., 2007. Expression and activity of cAMP phosphodiesterase isoforms in pulmonary artery smooth muscle cells from patients with pulmonary hypertension: role for PDE1. Am J Physiol Lung Cell Mol Physiol 292, L294-303.

Nagano-Ito, M., Ichikawa, S., 2012. Biological effects of Mammalian translationally controlled tumor protein (TCTP) on cell death, proliferation, and tumorigenesis. Biochem Res Int 2012, 204960.

Nasim, M.T., Ogo, T., Ahmed, M., Randall, R., Chowdhury, H.M., Snape, K.M., Bradshaw, T.Y., Southgate, L., Lee, G.J., Jackson, I., Lord, G.M., Gibbs, J.S., Wilkins, M.R., Ohta-Ogo, K., Nakamura, K., Girerd, B., Coulet, F., Soubrier, F., Humbert, M., Morrell, N.W., Trembath, R.C., Machado, R.D., 2011. Molecular genetic characterization of SMAD signaling molecules in pulmonary arterial hypertension. Hum Mutat 32, 1385-1389.

Nickel, W., 2003. The mystery of nonclassical protein secretion. A current view on cargo proteins and potential export routes. Eur J Biochem 270, 2109-2119.

Nishihara, K., Shomori, K., Fujioka, S., Tokuyasu, N., Inaba, A., Osaki, M., Ogawa, T., Ito, H., 2008. Minichromosome maintenance protein 7 in colorectal cancer: implication of prognostic significance. Int J Oncol 33, 245-251.

Nohe, A., Keating, E., Knaus, P., Petersen, N.O., 2004. Signal transduction of bone morphogenetic protein receptors. Cell Signal 16, 291-299.

Ormiston, M.L., Deng, Y., Stewart, D.J., Courtman, D.W., 2010. Innate immunity in the therapeutic actions of endothelial progenitor cells in pulmonary hypertension. Am J Respir Cell Mol Biol 43, 546-554.

Park, J.E., Tan, H.S., Datta, A., Lai, R.C., Zhang, H., Meng, W., Lim, S.K., Sze, S.K., 2010. Hypoxic tumor cell modulates its microenvironment to enhance angiogenic and metastatic potential by secretion of proteins and exosomes. Mol Cell Proteomics 9, 1085-1099.

Peacock, A.J., Murphy, N.F., McMurray, J.J., Caballero, L., Stewart, S., 2007. An epidemiological study of pulmonary arterial hypertension. Eur Respir J 30, 104-109.

Porter, A.G., Janicke, R.U., 1999. Emerging roles of caspase-3 in apoptosis. Cell Death Differ 6, 99-104.

Rai, P.R., Cool, C.D., King, J.A., Stevens, T., Burns, N., Winn, R.A., Kasper, M., Voelkel, N.F., 2008. The cancer paradigm of severe pulmonary arterial hypertension. Am J Respir Crit Care Med 178, 558-564.

Rajkumar, R., Konishi, K., Richards, T.J., Ishizawar, D.C., Wiechert, A.C., Kaminski, N., Ahmad, F., 2010. Genomewide RNA expression profiling in lung identifies distinct signatures in idiopathic pulmonary arterial hypertension and secondary pulmonary hypertension. Am J Physiol Heart Circ Physiol 298, H1235-1248.

Rho, S.B., Lee, J.H., Park, M.S., Byun, H.J., Kang, S., Seo, S.S., Kim, J.Y., Park, S.Y., 2011. Anti-apoptotic protein TCTP controls the stability of the tumor suppressor p53. FEBS Lett 585, 29-35.

Rhodes, C.J., Wharton, J., Boon, R.A., Roexe, T., Tsang, H., Wojciak-Stothard, B., Chakrabarti, A., Howard, L.S., Gibbs, J.S., Lawrie, A., Condliffe, R., Elliot, C.A., Kiely, D.G., Huson, L., Ghofrani, H.A., Tiede, H., Schermuly, R., Zeiher, A.M., Dimmeler, S., Wilkins, M.R., 2013. Reduced MicroRNA-150 Is Associated with Poor Survival in Pulmonary Arterial Hypertension. Am J Respir Crit Care Med 187, 294-302.

Riazi, A.M., Kwon, S.Y., Stanford, W.L., 2009. Stem cell sources for regenerative medicine. Methods Mol Biol 482, 55-90.

Rich, S., Dantzker, D.R., Ayres, S.M., Bergofsky, E.H., Brundage, B.H., Detre, K.M., Fishman, A.P., Goldring, R.M., Groves, B.M., Koerner, S.K., et al., 1987. Primary pulmonary hypertension. A national prospective study. Ann Intern Med 107, 216-223.

Richardson, M.R., Yoder, M.C., 2011. Endothelial progenitor cells: quo vadis? J Mol Cell Cardiol 50, 266-272.

Rubin, L.J., Badesch, D.B., Fleming, T.R., Galie, N., Simonneau, G., Ghofrani, H.A., Oakes, M., Layton, G., Serdarevic-Pehar, M., McLaughlin, V.V., Barst, R.J., 2011. Long-term treatment with sildenafil citrate in pulmonary arterial hypertension: the SUPER-2 study. Chest 140, 1274-1283.

Sage-Ono, K., Ono, M., Harada, H., Kamada, H., 1998. Dark-induced accumulation of mRNA for a homolog of translationally controlled tumor protein (TCTP) in Pharbitis. Plant Cell Physiol 39, 357-360.

Sakao, S., Taraseviciene-Stewart, L., Lee, J.D., Wood, K., Cool, C.D., Voelkel, N.F., 2005. Initial apoptosis is followed by increased proliferation of apoptosis-resistant endothelial cells. Faseb J 19, 1178-1180.

Scharpfenecker, M., van Dinther, M., Liu, Z., van Bezooijen, R.L., Zhao, Q., Pukac, L., Lowik, C.W., ten Dijke, P., 2007. BMP-9 signals via ALK1 and inhibits bFGF-induced endothelial cell proliferation and VEGF-stimulated angiogenesis. J Cell Sci 120, 964-972.

Schroeder, J.T., Lichtenstein, L.M., MacDonald, S.M., 1996. An immunoglobulin E-dependent recombinant histamine-releasing factor induces interleukin-4 secretion from human basophils. J Exp Med 183, 1265-1270.

Shevchenko, A., Tomas, H., Havlis, J., Olsen, J.V., Mann, M., 2006. In-gel digestion for mass spectrometric characterization of proteins and proteomes. Nat Protoc 1, 2856-2860.

Shi, W., Chen, H., Sun, J., Chen, C., Zhao, J., Wang, Y.L., Anderson, K.D., Warburton, D., 2004. Overexpression of Smurf1 negatively regulates mouse embryonic lung branching morphogenesis by specifically reducing Smad1 and Smad5 proteins. Am J Physiol Lung Cell Mol Physiol 286, L293-300.

Shintani, M., Yagi, H., Nakayama, T., Saji, T., Matsuoka, R., 2009. A new nonsense mutation of SMAD8 associated with pulmonary arterial hypertension. J Med Genet 46, 331-337.

Simonneau, G., Barst, R.J., Galie, N., Naeije, R., Rich, S., Bourge, R.C., Keogh, A., Oudiz, R., Frost, A., Blackburn, S.D., Crow, J.W., Rubin, L.J., 2002. Continuous subcutaneous infusion of treprostinil, a prostacyclin analogue, in patients with pulmonary arterial hypertension: a double-blind, randomized, placebo-controlled trial. Am J Respir Crit Care Med 165, 800-804.

Simonneau, G., Galie, N., Rubin, L.J., Langleben, D., Seeger, W., Domenighetti, G., Gibbs, S., Lebrec, D., Speich, R., Beghetti, M., Rich, S., Fishman, A., 2004. Clinical classification of pulmonary hypertension. J Am Coll Cardiol 43, 5S-12S.

Simonneau, G., Robbins, I.M., Beghetti, M., Channick, R.N., Delcroix, M., Denton, C.P., Elliott, C.G., Gaine, S.P., Gladwin, M.T., Jing, Z.C., Krowka, M.J., Langleben, D., Nakanishi, N., Souza, R., 2009. Updated clinical classification of pulmonary hypertension. J Am Coll Cardiol 54, S43-54.

Sirois, I., Raymond, M.A., Brassard, N., Cailhier, J.F., Fedjaev, M., Hamelin, K., Londono, I., Bendayan, M., Pshezhetsky, A.V., Hebert, M.J., 2011. Caspase-3-

dependent export of TCTP: a novel pathway for antiapoptotic intercellular communication. Cell Death Differ 18, 549-562.

Stenmark, K.R., Mecham, R.P., 1997. Cellular and molecular mechanisms of pulmonary vascular remodeling. Annu Rev Physiol 59, 89-144.

Stewart, D.J., Levy, R.D., Cernacek, P., Langleben, D., 1991. Increased plasma endothelin-1 in pulmonary hypertension: marker or mediator of disease? Ann Intern Med 114, 464-469.

Stoeber, K., Tlsty, T.D., Happerfield, L., Thomas, G.A., Romanov, S., Bobrow, L., Williams, E.D., Williams, G.H., 2001. DNA replication licensing and human cell proliferation. J Cell Sci 114, 2027-2041.

Susini, L., Besse, S., Duflaut, D., Lespagnol, A., Beekman, C., Fiucci, G., Atkinson, A.R., Busso, D., Poussin, P., Marine, J.C., Martinou, J.C., Cavarelli, J., Moras, D., Amson, R., Telerman, A., 2008. TCTP protects from apoptotic cell death by antagonizing bax function. Cell Death Differ 15, 1211-1220.

Taraseviciene-Stewart, L., Kasahara, Y., Alger, L., Hirth, P., Mc Mahon, G., Waltenberger, J., Voelkel, N.F., Tuder, R.M., 2001. Inhibition of the VEGF receptor 2 combined with chronic hypoxia causes cell death-dependent pulmonary endothelial cell proliferation and severe pulmonary hypertension. Faseb J 15, 427-438.

Teichert-Kuliszewska, K., Kutryk, M.J., Kuliszewski, M.A., Karoubi, G., Courtman, D.W., Zucco, L., Granton, J., Stewart, D.J., 2006. Bone morphogenetic protein receptor-2 signaling promotes pulmonary arterial endothelial cell survival: implications for loss-of-function mutations in the pathogenesis of pulmonary hypertension. Circ Res 98, 209-217.

Telerman, A., Amson, R., 2009. The molecular programme of tumour reversion: the steps beyond malignant transformation. Nat Rev Cancer 9, 206-216.

Thaw, P., Baxter, N.J., Hounslow, A.M., Price, C., Waltho, J.P., Craven, C.J., 2001. Structure of TCTP reveals unexpected relationship with guanine nucleotide-free chaperones. Nat Struct Biol 8, 701-704.

Thery, C., Ostrowski, M., Segura, E., 2009. Membrane vesicles as conveyors of immune responses. Nat Rev Immunol 9, 581-593.

Thiele, H., Berger, M., Skalweit, A., Thiele, B.J., 2000. Expression of the gene and processed pseudogenes encoding the human and rabbit translationally controlled tumour protein (TCTP). Eur J Biochem 267, 5473-5481.

Thomas, G., Luther, H., 1981. Transcriptional and translational control of cytoplasmic proteins after serum stimulation of quiescent Swiss 3T3 cells. Proc Natl Acad Sci U S A 78, 5712-5716.

Thomas, M.K., Francis, S.H., Corbin, J.D., 1990. Characterization of a purified bovine lung cGMP-binding cGMP phosphodiesterase. J Biol Chem 265, 14964-14970.

Thomson, J.R., Machado, R.D., Pauciulo, M.W., Morgan, N.V., Humbert, M., Elliott, G.C., Ward, K., Yacoub, M., Mikhail, G., Rogers, P., Newman, J., Wheeler, L., Higenbottam, T., Gibbs, J.S., Egan, J., Crozier, A., Peacock, A., Allcock, R., Corris, P., Loyd, J.E., Trembath, R.C., Nichols, W.C., 2000. Sporadic primary pulmonary hypertension is associated with germline mutations of the gene encoding BMPR-II, a receptor member of the TGF-beta family. J Med Genet 37, 741-745.

Toshner, M., Voswinckel, R., Southwood, M., Al-Lamki, R., Howard, L.S., Marchesan, D., Yang, J., Suntharalingam, J., Soon, E., Exley, A., Stewart, S., Hecker, M., Zhu, Z., Gehling, U., Seeger, W., Pepke-Zaba, J., Morrell, N.W., 2009. Evidence of dysfunction of endothelial progenitors in pulmonary arterial hypertension. Am J Respir Crit Care Med 180, 780-787.

Trembath, R.C., Thomson, J.R., Machado, R.D., Morgan, N.V., Atkinson, C., Winship, I., Simonneau, G., Galie, N., Loyd, J.E., Humbert, M., Nichols, W.C., Morrell, N.W., Berg, J., Manes, A., McGaughran, J., Pauciulo, M., Wheeler, L., 2001. Clinical and molecular genetic features of pulmonary hypertension in patients with hereditary hemorrhagic telangiectasia. N Engl J Med 345, 325-334.

Tsai, E.J., Kass, D.A., 2009. Cyclic GMP signaling in cardiovascular pathophysiology and therapeutics. Pharmacol Ther 122, 216-238.

Tuder, R.M., Cool, C.D., Geraci, M.W., Wang, J., Abman, S.H., Wright, L., Badesch, D., Voelkel, N.F., 1999. Prostacyclin synthase expression is decreased in lungs from patients with severe pulmonary hypertension. Am J Respir Crit Care Med 159, 1925-1932.

Tuder, R.M., Cool, C.D., Yeager, M., Taraseviciene-Stewart, L., Bull, T.M., Voelkel, N.F., 2001. The pathobiology of pulmonary hypertension. Endothelium. Clin Chest Med 22, 405-418.

Tuder, R.M., Groves, B., Badesch, D.B., Voelkel, N.F., 1994. Exuberant endothelial cell growth and elements of inflammation are present in plexiform lesions of pulmonary hypertension. Am J Pathol 144, 275-285.

Tuder, R.M., Marecki, J.C., Richter, A., Fijalkowska, I., Flores, S., 2007. Pathology of pulmonary hypertension. Clin Chest Med 28, 23-42, vii.

Tuder, R.M., Voelkel, N.F., 1998. Pulmonary hypertension and inflammation. J Lab Clin Med 132, 16-24.

Tuynder, M., Fiucci, G., Prieur, S., Lespagnol, A., Geant, A., Beaucourt, S., Duflaut, D., Besse, S., Susini, L., Cavarelli, J., Moras, D., Amson, R., Telerman, A., 2004. Translationally controlled tumor protein is a target of tumor reversion. Proc Natl Acad Sci U S A 101, 15364-15369.

Tuynder, M., Susini, L., Prieur, S., Besse, S., Fiucci, G., Amson, R., Telerman, A., 2002. Biological models and genes of tumor reversion: cellular reprogramming through tpt1/TCTP and SIAH-1. Proc Natl Acad Sci U S A 99, 14976-14981.

Upton, P.D., Davies, R.J., Trembath, R.C., Morrell, N.W., 2009. Bone morphogenetic protein (BMP) and activin type II receptors balance BMP9 signals mediated by activin receptor-like kinase-1 in human pulmonary artery endothelial cells. J Biol Chem 284, 15794-15804.

Valdimarsdottir, G., Goumans, M.J., Rosendahl, A., Brugman, M., Itoh, S., Lebrin, F., Sideras, P., ten Dijke, P., 2002. Stimulation of Id1 expression by bone morphogenetic protein is sufficient and necessary for bone morphogenetic protein-induced activation of endothelial cells. Circulation 106, 2263-2270.

Ventetuolo, C.E., Klinger, J.R., 2012. WHO Group 1 pulmonary arterial hypertension: current and investigative therapies. Prog Cardiovasc Dis 55, 89-103.

Voelkel, N.F., Cool, C., Lee, S.D., Wright, L., Geraci, M.W., Tuder, R.M., 1998. Primary pulmonary hypertension between inflammation and cancer. Chest 114, 225S-230S.

Wang, Z., Rao, P.J., Castresana, M.R., Newman, W.H., 2005. TNF-alpha induces proliferation or apoptosis in human saphenous vein smooth muscle cells depending on phenotype. Am J Physiol Heart Circ Physiol 288, H293-301.

Warton, K., Tonini, R., Fairlie, W.D., Matthews, J.M., Valenzuela, S.M., Qiu, M.R., Wu, W.M., Pankhurst, S., Bauskin, A.R., Harrop, S.J., Campbell, T.J., Curmi, P.M., Breit, S.N., Mazzanti, M., 2002. Recombinant CLIC1 (NCC27) assembles in lipid bilayers via a pH-dependent two-state process to form chloride ion channels with identical characteristics to those observed in Chinese hamster ovary cells expressing CLIC1. J Biol Chem 277, 26003-26011.

West, J., Cogan, J., Geraci, M., Robinson, L., Newman, J., Phillips, J.A., Lane, K., Meyrick, B., Loyd, J., 2008. Gene expression in BMPR2 mutation carriers with and without evidence of pulmonary arterial hypertension suggests pathways relevant to disease penetrance. BMC Med Genomics 1, 45.

Widlitz, A., Barst, R.J., 2003. Pulmonary arterial hypertension in children. Eur Respir J 21, 155-176.

Wu, D., Guo, Z., Min, W., Zhou, B., Li, M., Li, W., Luo, D., 2012. Upregulation of TCTP expression in human skin squamous cell carcinoma increases tumor cell viability through anti-apoptotic action of the protein. Exp Ther Med 3, 437-442.

Xue, C., Johns, R.A., 1995. Endothelial nitric oxide synthase in the lungs of patients with pulmonary hypertension. N Engl J Med 333, 1642-1644.

Yamaguchi, A., Komori, T., Suda, T., 2000. Regulation of osteoblast differentiation mediated by bone morphogenetic proteins, hedgehogs, and Cbfa1. Endocr Rev 21, 393-411.

Yang, J., Davies, R.J., Southwood, M., Long, L., Yang, X., Sobolewski, A., Upton, P.D., Trembath, R.C., Morrell, N.W., 2008. Mutations in bone morphogenetic protein type II receptor cause dysregulation of Id gene expression in pulmonary artery smooth muscle cells: implications for familial pulmonary arterial hypertension. Circ Res 102, 1212-1221.

Yang, J., Li, X., Al-Lamki, R.S., Southwood, M., Zhao, J., Lever, A.M., Grimminger, F., Schermuly, R.T., Morrell, N.W., 2010. Smad-dependent and smad-independent induction of id1 by prostacyclin analogues inhibits proliferation of pulmonary artery smooth muscle cells in vitro and in vivo. Circ Res 107, 252-262.

Yang, X., Long, L., Reynolds, P.N., Morrell, N.W., 2011. Expression of mutant BMPR-II in pulmonary endothelial cells promotes apoptosis and a release of factors that stimulate proliferation of pulmonary arterial smooth muscle cells. Pulm Circ 1, 103-110.

Yang, X., Long, L., Southwood, M., Rudarakanchana, N., Upton, P.D., Jeffery, T.K., Atkinson, C., Chen, H., Trembath, R.C., Morrell, N.W., 2005. Dysfunctional Smad signaling contributes to abnormal smooth muscle cell proliferation in familial pulmonary arterial hypertension. Circ Res 96, 1053-1063.

Yarm, F.R., 2002. Plk phosphorylation regulates the microtubule-stabilizing protein TCTP. Mol Cell Biol 22, 6209-6221.

Yeager, M.E., Halley, G.R., Golpon, H.A., Voelkel, N.F., Tuder, R.M., 2001. Microsatellite instability of endothelial cell growth and apoptosis genes within plexiform lesions in primary pulmonary hypertension. Circ Res 88, E2-E11.

Yenofsky, R., Bergmann, I., Brawerman, G., 1982. Messenger RNA species partially in a repressed state in mouse sarcoma ascites cells. Proc Natl Acad Sci U S A 79, 5876-5880.

Yu, M., Wang, X.X., Zhang, F.R., Shang, Y.P., Du, Y.X., Chen, H.J., Chen, J.Z., 2007. Proteomic analysis of the serum in patients with idiopathic pulmonary arterial hypertension. J Zhejiang Univ Sci B 8, 221-227.

Yu, P.B., Beppu, H., Kawai, N., Li, E., Bloch, K.D., 2005. Bone morphogenetic protein (BMP) type II receptor deletion reveals BMP ligand-specific gain of signaling in pulmonary artery smooth muscle cells. J Biol Chem 280, 24443-24450.

Yuditskaya, S., Tumblin, A., Hoehn, G.T., Wang, G., Drake, S.K., Xu, X., Ying, S., Chi, A.H., Remaley, A.T., Shen, R.F., Munson, P.J., Suffredini, A.F., Kato, G.J., 2009. Proteomic identification of altered apolipoprotein patterns in pulmonary hypertension and vasculopathy of sickle cell disease. Blood 113, 1122-1128.

Zhao, Y.D., Campbell, A.I., Robb, M., Ng, D., Stewart, D.J., 2003. Protective role of angiopoietin-1 in experimental pulmonary hypertension. Circ Res 92, 984-991.